



UNIVERSITY OF  
LIVERPOOL

# Invariants of Lagrangian Maps between 3-manifolds

Thesis submitted in accordance with the requirements of the  
University of Liverpool for the degree of Doctor in Philosophy

by

Gregory James Roberts

August 2020

# Abstract

Let  $\mathcal{L}$  be the space of all Lagrangian maps  $M \looparrowright T^*N \rightarrow N$  between two 3-manifolds, both oriented and without boundaries, and  $M$  being compact. Let  $\Sigma \subset \mathcal{L}$  be the discriminantal hypersurface, that is, the set of all maps whose singularities are not stable under small perturbations. The aim of this thesis is to classify local invariants of generic elements of  $\mathcal{L}$ . The locality means here that the increments of the invariants along generic paths in  $\mathcal{L}$  should be defined completely by the equivalence classes of local bifurcations at  $\Sigma$ .

Local invariants are completely defined by codimension 1 discriminantal cycles in  $\mathcal{L}$ , that is, those lying in  $\Sigma$ . In addition, these cycles must be trivial. Respectively, the main results of this thesis describe the spaces of the discriminantal cycles, possibly non-trivial: we prove that the dimension of the space of rational cycles turns out to be 15, and it is 20 in the *mod*2 case. We have also been able to establish that the trivial cycles form the subspaces of codimension at most 1 over  $\mathbb{Q}$  for any  $N$  and at most 2 over  $\mathbb{Z}_2$  for  $N = \mathbb{R}^3$ . The codimension estimates come from the number of linearly independent local geometric invariants we have been able to observe and construct: over the rationals, they are mostly the numbers of points of the caustics of various isolated singularity types, while over  $\mathbb{Z}_2$  we also have a few interesting linking numbers.

The main tool to obtain our main results is analysis of generic 1- and

2-parameter bifurcations of Lagrangian maps which generalises a rather constrained approach taken in [9].

At the end, we investigate the effects on the spaces of discriminantal cycles and local invariants of an assumption of non-orientability of the source or/and target manifolds.

# Acknowledgements

I would like to thank my supervisor Professor Victor Goryunov for his encouragement and guidance over the past four years. I am extremely grateful for his invaluable help, without which, this thesis would not have been possible. I would also like to thank my second supervisor Dr Oleg Karpenkov for his support.

I am grateful to everyone in the Department of Mathematical Sciences at the University of Liverpool for your friendship and encouragement. Particularly to those I taught with as a graduate teaching assistant as well as those I had the joy of sharing Office 208 with. I won't list you all as I would certainly miss people out so I would like to thank you all collectively.

I must also thank Joel Haddley for helping me install the computer programmes required for my work as well as for his guidance and kind words of support.

Finally, I would like to thank my family and friends. A special thanks to my boyfriend, Adam, as without his support I could not have achieved this work. I owe my parents, Linda and Paul, a debt of thanks for financially supporting me during my PhD and thank them for all the help and encouragement they both provided.

# Contents

<b>0</b>	<b>Introduction</b>	<b>1</b>
0.1	Knot invariants . . . . .	3
0.2	Local invariants . . . . .	6
0.3	Planar curves invariants . . . . .	7
0.4	Lagrangian maps between surfaces . . . . .	9
0.5	Smooth maps between 3-manifolds . . . . .	12
0.5.1	General information about the invariants . . . . .	12
0.5.2	Framing invariants in $\mathbb{R}^3$ . . . . .	14
0.6	Lagrangian maps between 3-manifolds . . . . .	16
0.7	Results of the thesis . . . . .	22
<b>1</b>	<b>Basic Concepts</b>	<b>28</b>
1.1	Local invariants . . . . .	28
1.2	Lagrangian maps . . . . .	30
<b>2</b>	<b>Local invariants of Lagrangian maps between 3-manifolds</b>	<b>33</b>
2.1	Singularities of a generic caustic in three dimensions . . . . .	34

2.2	Examples of invariants of generic Lagrangian maps . . . . .	36
2.3	Bifurcations in generic 1-parameter families of caustics . . . . .	37
2.3.1	Corank 1 bifurcations . . . . .	38
2.3.1.1	Uni-germs . . . . .	38
2.3.1.2	Multi-germs . . . . .	39
2.3.2	Corank 2 bifurcations . . . . .	43
2.3.2.1	Uni-germs . . . . .	43
2.3.2.2	Multi-germs . . . . .	44
2.4	Derivatives of the basic invariants . . . . .	47
2.5	Ranks of spaces of the discriminantal cycles . . . . .	54
2.6	Bifurcations in 2-parameter families . . . . .	55
2.6.1	Corank 1 bifurcations . . . . .	56
2.6.1.1	Extra $A_2$ component . . . . .	57
2.6.1.1.1	Example: Gluing up the $A_3^{s,\sigma} A_2^2$ strata.	58
2.6.1.1.2	Passing a smooth $A_2$ sheet through $A_5^{s,\sigma,-}$ and $A_3^{2,e;s,+,s',-}$ . . . . .	60
2.6.1.2	Cubic bifurcations . . . . .	62
2.6.1.3	Multi-germ families: Non-transversal interactions with a cuspidal edge . . . . .	64
2.6.1.4	Multi-germ families: Interaction with a swallowtail . . . . .	67
2.6.1.5	Uni-germs of codimension 2 . . . . .	71
2.6.2	Corank 2 bifurcations . . . . .	74

2.6.2.1	Uni-germs: $D_4$ . . . . .	75
2.6.2.2	Uni-germs: $D_5$ . . . . .	80
2.6.2.3	Extra $A_2$ component . . . . .	97
2.6.2.4	Interaction of a purse and a pyramid with other local components $C$ . . . . .	99
2.6.2.4.1	Extra cuspidal edge . . . . .	100
2.6.2.4.2	Extra $A_2^2$ component . . . . .	102
2.6.2.4.3	Tangent $A_2$ component . . . . .	105
2.6.2.5	$D_6$ and $E_6$ bifurcations . . . . .	110
<b>3</b>	<b>Proofs of Theorems 2.5.1 and 2.5.3</b>	<b>112</b>
<b>4</b>	<b><math>D_6^+</math> bifurcations</b>	<b>123</b>
4.1	1-dimensional strata in $\mathcal{C}(D_6^+)$ and their straight projection . .	125
4.2	2-dimensional strata in $\mathcal{C}(D_6^+)$ and their straight projection . .	128
4.3	Tilting the 2-dimensional strata . . . . .	130
4.3.1	The $A_2^3$ stratum . . . . .	130
4.3.2	The $A_3A_2$ stratum . . . . .	135
<b>5</b>	<b><math>D_6^-</math> bifurcations</b>	<b>145</b>
5.1	1-dimensional strata in $\mathcal{C}(D_6^-)$ and their straight projection . .	146
5.2	2-dimensional strata in $\mathcal{C}(D_6^-)$ and their straight projection . .	149
5.3	Complete bifurcation diagram for $D_6^-$ . . . . .	161
<b>6</b>	<b><math>E_6</math> bifurcations</b>	<b>162</b>

6.1	$E_6^+$ bifurcations . . . . .	165
6.1.1	Stratification of $\mathcal{C}(E_6^+)$ . . . . .	165
6.1.1.1	The $A_3$ stratum in $\mathcal{C}(E_6^+)$ . . . . .	165
6.1.1.1.1	2-dimensional strata in the closure of the $A_3$ stratum in $\mathcal{C}(E_6^+)$ . . . . .	166
6.1.1.1.2	1-dimensional strata in the closure of the $A_3$ stratum in $\mathcal{C}(E_6^+)$ . . . . .	168
6.1.1.2	The $A_2^3$ stratum in $\mathcal{C}(E_6^+)$ . . . . .	170
6.1.2	The closure of the $A_3$ stratum in $\mathcal{C}(E_6^+)$ . . . . .	171
6.1.2.1	The straight projection of the $A_3$ stratum . . . . .	174
6.1.2.2	Tilted projections of strata in the closure of the $A_3$ stratum . . . . .	176
6.1.2.2.1	The $A_4$ stratum in $\mathcal{C}(E_6^+)$ . . . . .	177
6.1.2.2.2	The $D_4$ stratum in $\mathcal{C}(E_6^+)$ . . . . .	179
6.1.2.2.3	The $A_3A_2$ stratum in $\mathcal{C}(E_6^+)$ . . . . .	183
6.1.3	The closure of the $A_2^3$ stratum in $\mathcal{C}(E_6^+)$ . . . . .	186
6.1.4	The $E_6^+$ cyclic equation . . . . .	189
6.2	$E_6^-$ equations . . . . .	189

**7 Geometric interpretations of additional mod2 discriminantal cycles** **190**

7.1	The number of components and self-linking of the cuspidal edge ( $I_{fe}$ ) . . . . .	192
-----	--	-----



7.2	Framed link formed by positive cuspidal edges and self-intersection lines ( $I_{dc^+}$ ) . . . . .	203
7.3	Framing negative cuspidal edges and self-intersection lines ( $I_{dc^-}$ )	225
7.4	Linking invariant ( $I_\lambda$ ) . . . . .	234
7.5	<i>mod</i> 2 degrees of generic singularities in $\mathbb{R}^3$ . . . . .	248
7.6	Summary of the extra <i>mod</i> 2 invariants . . . . .	255
<b>8</b>	<b>Non-oriented source or target</b>	<b>257</b>
8.1	Non-oriented source . . . . .	258
8.2	Non-oriented target . . . . .	266
	<b>List of Figures</b>	<b>274</b>
	<b>Bibliography</b>	<b>284</b>

# Chapter 0

## Introduction

In this thesis we study topological invariants of Lagrangian maps between 3-manifolds from a singularity theory point of view, via degenerations of the maps. The approach we are following is basically that used by Vassiliev when he introduced finite-type invariants of knots in [18]. Since then his interpretation has served as a basis for consideration of invariants of generic and special generic maps in a range of low dimensions.

Following Vassiliev's approach, Arnold studied local order 1 invariants of regular planar curves [5, 6] and planar wave fronts [7]. For the regular curves, Arnold introduced three Vassiliev-type invariants dual to the three types of local bifurcations appearing in generic 1-parameter families of planar curves: triple points, direct self-tangencies and inverse self-tangencies. Later, two of these invariants were generalised to higher order settings in [14, 15, 19]. However, these cases are the only ones in which going beyond order 1

invariants has so far been possible.

The next order 1 setting that was considered came in [13] where Goryunov classified the local invariants of maps of surfaces to  $\mathbb{R}^3$ . Ohmoto and Aicardi then progressed the study of order 1 invariants further by classifying them for maps of surfaces to  $\mathbb{R}^2$  in [16]. Later on, Goryunov and Gallagher considered in [12] and [9] the Lagrangian analogue of the Ohmoto-Aicardi setting, and found additional invariants specific to the Lagrangian situation. Another important result in the area is Yamamoto's list of order 1 invariants of smooth maps from 3-manifolds to the plane [21].

The next major development was made by Goryunov in [10] where he classified the local order 1 invariants of smooth maps between 3-manifolds. This is of particular interest to us as this thesis provides a Lagrangian analogue to his work.

Alsaeed and Goryunov considered in [11] local order 1 invariants of fronts in 3-manifolds. That paper formed a part of Alsaeed's dissertation [2]. The considerations were now in the Legendrian setting. This meant a finer classification of local singularities comparing with that in [10], which made the task of detecting the invariants more complicated.

Finally, in [9], Gallagher classified local order 1 invariants of Lagrangian maps between 3-manifolds. Her task was similar to what we are doing in this thesis, but she simplified the situation substantially by not distinguishing between certain classes of singularities. This is the last order 1 setting that has been considered so far and it is this that provides a starting point and the

main motivation for this thesis. Comparing with [9], this thesis is based on the complete classification of local singularities of Lagrangian maps between 3-manifolds, which, on the one hand, introduces further complications but, on the other hand, delivers richer results.

We recall some of these highlighted results in the next few sections. We first provide an intrinsic example of how we classify invariants of maps by looking at the way the finite-type knot invariants were introduced by Vassiliev in [18]. Afterwards, based on the ideas of Arnold and Vassiliev we provide the formal definitions required to understand what we mean by ‘local invariants’. These are necessary to discuss the works by Arnold, Goryunov and Gallagher that further developed the study of order 1 invariants of maps, all of which provide background for this thesis.

## 0.1 Knot invariants

One of the most impressive approaches in looking for topological invariants of maps was invented by Vassiliev in [18] when he introduced finite-type invariants of knots. His invariants are based on the study of the discriminant in the space of maps of the circle to  $\mathbb{R}^3$ . In general, the discriminant is the hypersurface in the space of maps which consists of maps with non-stable singularities. We now recall some of the key points from [18].

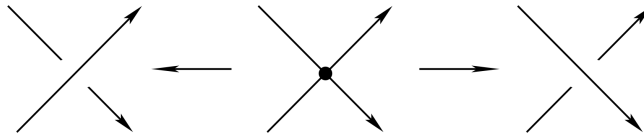
Consider the space  $\Omega$  of all smooth maps from an oriented circle to  $\mathbb{R}^3$  and let  $f : S^1 \rightarrow \mathbb{R}^3$  be a generic smooth map. If the map  $f$  is an embedding then

the image of  $f$  is a *knot*. The complement to the set of all embeddings is the discriminant  $\Sigma \subset \Omega$ . This consists of all smooth maps  $f : S^1 \rightarrow \mathbb{R}^3$  that have singularities. Here, they may be singularities where  $f' = 0$  or when  $f$  is not injective.

Using the discriminants helps us to introduce the idea of equivalence. Two knots are considered *equivalent* if they can be joined by a path in  $\Omega$  that does not cross the discriminant,  $\Sigma$ .

A generic point of  $\Sigma$  is a map whose image has exactly one singularity, a double point. So, we define a *singular knot* as an immersion  $f : S^1 \rightarrow \mathbb{R}^3$  with no singularities except a finite number of *generic double points*, that is, points at which pairs of branches meet at non-zero angles.

The definition of a ‘singular knot’ allows us to co-orient the discriminant  $\Sigma$  at its generic points. Indeed, a double point of the image may be perturbed in one of the following two ways:



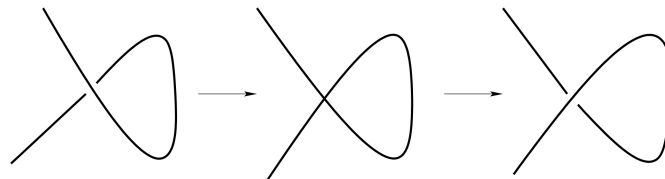
So, we call the local perturbation on the right *positive* and on the left *negative*. These names also correspond to the sides of  $\Sigma$  in  $\Omega$ .

Any knot invariant  $v$  can be extended to singular knots with one generic double point by the *Vassiliev skein relation* (see [8] or [17]):

$$v(\text{crossing with dot}) = v(\text{crossing}) - v(\text{crossing})$$

We can use this skein relation recursively to extend our knot invariant to all singular knots. Following [17], a knot invariant  $v$  is said to be a *Vassiliev invariant* of order no greater than  $n$  if it vanishes on any singular knot with more than  $n$  double points.

We should notice that in this thesis we are considering local order 1 invariants, that is, those whose increments in generic 1-parameter families of maps are completely determined by the type of the local bifurcation of a map. To demonstrate a level of complications for going beyond order 1, let us draw a comparison with what local order 1 invariants are for knots. Namely, for knots, the increment of such an invariant under any crossing change must be the same as the difference of its values on two non-singular knots differing just by the fragments shown in the left and right in the figure below. These two knots are isotopic, hence the difference is zero. Therefore, there are no local order 1 invariants of knots.



On the other hand, we will see in Chapter 2 that the number of possible bifurcations in generic 1-parameter families of Lagrangian maps between 3-

manifolds is 132. Thus, restricting attention to just local order 1 invariants is a very substantial task in our setting.

## 0.2 Local invariants

Following Vassiliev's discriminantal approach we now introduce the notion of local invariants in a generic setting.

Let  $\Omega$  be a space of maps, and  $\Sigma \subset \Omega$  a subset of non-generic maps of our choice. Consider invariants of generic maps with values in an abelian group  $G$ , that is, maps of the set of connected components of  $\Omega \setminus \Sigma$  to  $G$ . We say an invariant is *local* of order 1 if every increment of the invariant in a generic 1-parameter family of maps is completely determined by the type of the local bifurcation of the map. Since no higher order invariants are involved in this thesis, we call such invariants *local*. The discriminant  $\Sigma$  must be co-orientable if, for example, we are working with integer invariants.

Up to a choice of an additive constant (individual for each connected component of  $\Omega$ ), any local invariant  $I$  is defined by its *derivative*  $I' = \sum x_i X_i$ , where the  $X_i$  are discriminantal strata of codimension 1 in  $\Omega$ , and the  $x_i$  are the increments of  $I$  along paths crossing the  $X_i$  in the co-orienting direction.

Every discriminantal stratum of codimension 2 in  $\Omega$  provides an equation on the increments, which we will call a *cyclic equation*. A linear combination  $\sum x_i X_i$ , in which the  $x_i$  satisfy all possible cyclic equations, is a codimension 1 cycle in  $\Omega$  and is called *discriminantal*. Given a discriminantal cycle for which

similar vanishing holds on loops *non-contractible* in  $\Omega$  we can ‘integrate’ it to an invariant. In such case we call a discriminantal cycle *trivial*.

With the formal definition of local invariants in hand, we shall now give a brief overview of invariants of: planar curves, Lagrangian maps between surfaces and smooth maps between 3-manifolds. Later, we look at Gallagher’s work on invariants of Lagrangian maps between 3-manifolds in far greater detail since it provides a starting point for this thesis.

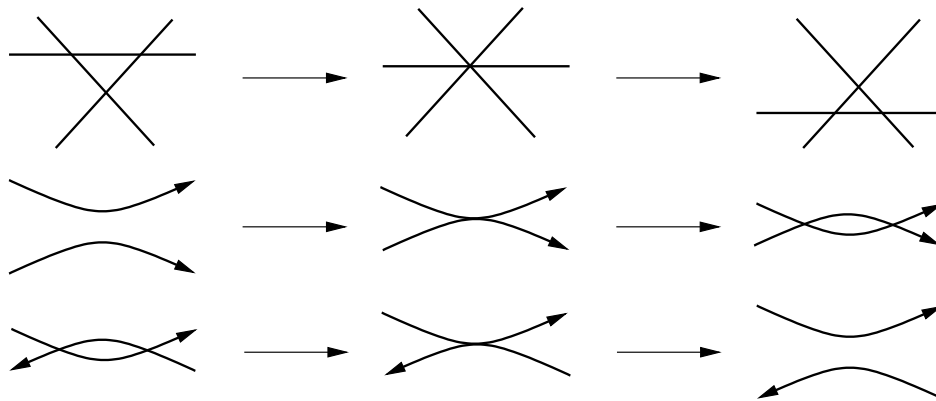
### 0.3 Planar curves invariants

In [5] and [6] Arnold studied local (order 1) invariants of planar curves. We now introduce the basic definitions and ideas which allowed him to construct the three Vassiliev-type invariants that were mentioned earlier.

We define a *curve* as a smooth immersion of an (oriented) circle into the plane. Let  $\Omega$  be the space of all such curves. A generic element of  $\Omega$  is a curve whose only singularities are transversal self-intersections. Connected components of  $\Omega$  are numbered by the Whitney winding numbers of the curves [20].

In generic 1-parameter families of planar curves, three events can occur: triple points, direct self-tangencies (a self-tangency point of an immersed curve with the tangent vectors pointing in the same direction) and inverse self-tangencies (tangent vectors pointing in different directions). They are shown below.





So, the codimension 1 discriminantal strata in  $\Omega$  correspond to triple points, direct self-tangencies and inverse self-tangencies.


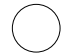


In [5] the co-orientations of the three codimension 1 discriminantal strata are defined. The positive self-tangency moves are exactly those shown in the diagram above. The co-orientation of the triple point stratum is more complicated and involves certain non-local information about the curves, and we prefer to omit it here.

Arnold's three basic invariants of generic planar curves are:

- $St$  (strangeness): which changes along generic paths in  $\Omega$  just under triple point moves, each time by a fixed amount;
- $J^+$ : which changes similarly just under direct self-tangency moves;
- $J^-$ : which changes similarly just under inverse self-tangency moves.

Arnold has also made a special choice of the 'constants of integration' on different connected components of  $\Omega$  to guarantee the additivity of his invariants under connected summation of planar curves. Arnold's normalisation of

the increments of the invariants under the positive moves and of the values of the invariants on particular representatives of the connected components of  $\Omega$  are given in the table below. We should note that the invariants do not depend on the curve orientations.

	Triple point move	Direct self-tangency move	Inverse self-tangency move					...
$St$	1	0	0	0	0	1	2	...
$J^+$	0	2	0	0	0	-2	-4	...
$J^-$	0	0	2	-1	0	-3	-6	...

As mentioned earlier, two of these invariants have been generalised to higher order settings in [14], [15] and [19]. However, since these cases are the only known ones which go beyond order 1 invariants, and since we are only considering order 1 invariants, we are not quoting these results.

## 0.4 Lagrangian maps between surfaces

The next order 1 setting whose details are essential for us is the Goryunov-Gallagher study of local invariants of Lagrangian maps from surfaces to  $\mathbb{R}^2$  carried out in [12, 9]. Their work provides a Lagrangian analogue to that by Ohmoto and Aicardi in [16], which studied ordinary smooth maps. We shall also point out the difference between the two sets of the results showing that the Lagrangian case has a richer geometry.

We use the symbol  $\looparrowright$  to denote an immersion. Let  $\mathcal{L} = \mathcal{L}(M, T^*\mathbb{R}^2, \mathbb{R}^2)$

be the space of all Lagrangian maps  $M \looparrowright T^*\mathbb{R}^2 \rightarrow \mathbb{R}^2$  between a fixed surface  $M$  and an oriented plane  $\mathbb{R}^2$ .

The only uni-germ singularities a generic Lagrangian map  $f : M \rightarrow \mathbb{R}^2$  may have are Lagrangian folds and pleats. Their generating families of functions are  $\mathcal{R}_+$ -versal deformations of isolated function singularities  $A_2$  and respectively  $A_3$  (see Section 1.2). Our notation of points of the caustic  $\mathcal{C}(f)$  will follow that of the generating families:  $A_2$  for its regular points and  $A_3$  for cusps. The only other types of points a generic caustic may have are transversal self-intersections,  $A_2^2$ . In fact, there are four types of cusps which we denote  $A_3^{s,\sigma}$ . Here the sign  $\sigma = \pm$  stays for the local degree  $\pm 1$  of the Lagrangian map, and  $s = \pm$  indicates which of the two real  $\mathcal{R}$ -types of the  $A_3$  function singularity, either  $+x^4$  or  $-x^4$ , is actually used in the local generating family.

All singularities of generic caustics are shown in Figure 1. The co-orientation of the caustic  $\mathcal{C} \subset \mathbb{R}^2$  is to the side with a higher number of local pre-images. This induces the orientations of the local branches, as shown in Figure 1. This orientation allows to lift the caustic to a Legendrian link in the projectivisation of the cotangent bundle of the plane and consider its Bennequin invariant, that is, the self-linking number of the caustic [16].

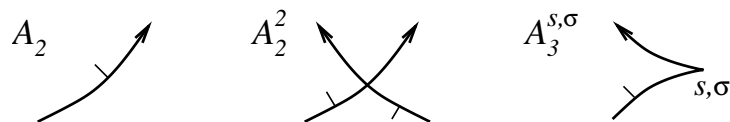


Figure 1: Singularities of generic caustics in  $\mathbb{R}^2$ .

One of the main results of [12] is

**Theorem 0.4.1.** *The space of rational discriminantal cycles in  $\mathcal{L}(M, T^*\mathbb{R}^2, \mathbb{R}^2)$  has rank 8.*

This space is spanned by the derivatives of the six invariants:

$I_d$ , the number of double points  $A_2^2$ ;

$I_{s,\sigma}^c$ ,  $s, \sigma = \pm$ , the number of  $A_3^{s,\sigma}$  points;

$I_\ell$ , the restriction to the set of Lagrangian maps of the Bennequin invariant of the critical value sets of generic smooth maps from  $M$  to the plane, defined by Ohmoto and Aicardi in [16],

and two extra discriminantal cycles related to corank 2 bifurcations.

Comparing this result to that of Ohmoto and Aicardi in [16] we see there are four types of  $A_3$  invariants compared to two. This is due to the absence of the  $s$  marking in the non-Lagrangian context. Moreover, the two extra discriminantal cycles did not appear in [16] since corank 2 bifurcations occur in generic 1-parameter families of maps only in the Lagrangian setting.

In the space of integer discriminantal cycles in [12] one of the two extra cycles is actually a non-trivial discriminantal cycle. This was proved in [12] by constructing a loop in the space  $\mathcal{L}(S^2, T^*\mathbb{R}^2, \mathbb{R}^2)$  which has a non-zero intersection number with the cycle. This loop in its turn is non-contractible. The question of whether the other cycle is trivial or not remains open.

Moving to the *mod2* analogue of Theorem 0.4.1 we have:

**Theorem 0.4.2.** *The space of  $\mathbb{Z}_2$  discriminantal cycles in  $\mathcal{L}(M, T^*\mathbb{R}^2, \mathbb{R}^2)$  has rank 9.*

We now turn our attention to invariants of maps of one dimension higher. First, we introduce the work by Goryunov which considers smooth maps between 3-manifolds. Afterwards, we consider its Lagrangian version.

## 0.5 Smooth maps between 3-manifolds

Goryunov studied local (order 1) invariants of ordinary smooth maps between 3-manifolds in [10]. In this section we first look at the paper's two main results, and then pay some special attention to *mod*2 framing invariants.

### 0.5.1 General information about the invariants

Assume the source manifold  $M$  and target  $N$  are oriented and without boundaries, and  $M$  is compact. All possible local singularities of the critical value set of a generic smooth map are shown in Figure 2.

In [10] Goryunov identified seven local invariants of generic maps:

$I_t$ , the number of triple points;

$I_{s_+}$ , the number of positive swallowtails;

$I_{s_-}$ , the number of negative swallowtails;

$I_{c_+}$ , the number of intersection points of a positive cuspidal edge with a smooth sheet;

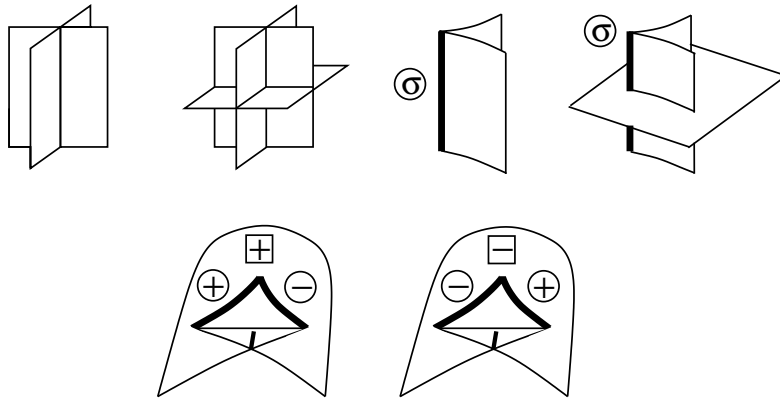


Figure 2: Local singularities of the critical value sets. The encircled values  $\sigma = \pm$  indicate the local degree  $\pm 1$  of a map at the cuspidal edge. The boxed signs are the definitions of the signs of the swallowtail points.

$I_{c-}$ , the number of intersection points of a negative cuspidal edge with a smooth sheet;

$I_{\chi}$ , half of the Euler characteristic of the critical locus of a mapping;

$I_{\Sigma^2}$ , the linking number in  $J^1(M, N)$  of the image of the 1-jet extension of a map with the set of all corank  $< 1$  1-jets.

In a bit more general sense, these local invariants may be considered up to additive constants which may be chosen arbitrarily for each connected component of the space of smooth maps between 3-manifolds. The main result from [10] is:

**Theorem 0.5.1.** *The space of integer local invariants of maps between two*

oriented 3-dimensional manifolds has rank 7. This space is generated by

$$(I_{s_+} \pm I_{s_-})/2, \quad (I_{c_+} + I_{c_-})/2, \quad I_t, \quad (I_t + I_{c_+})/2, \quad I_\chi, \quad I_{\Sigma^2}.$$

Furthermore, the *mod2* analogue of Theorem 0.5.1 with  $\mathbb{R}^3$  as the target is:

**Theorem 0.5.2.** *The space of mod2 local invariants of maps from an oriented 3-dimensional manifold to oriented  $\mathbb{R}^3$  has rank 11.*

Thus, in the *mod2* setting we have four extra linearly independent invariants, in addition to the *mod2* reduction of the invariants from Theorem 0.5.1. One of these invariants combines the number of components and the self-linking of the cuspidal edge of the critical value set. The details will come in the next subsection.

Finally, in [10] Goryunov obtained a classification of invariants, both over  $\mathbb{Z}$  and  $\mathbb{Z}_2$ , assuming that either the source, or target manifold, or both of them are not oriented. In this thesis we apply a similar analysis to our Lagrangian version in Chapter 8.

## 0.5.2 Framing invariants in $\mathbb{R}^3$

The *mod2* invariant mentioned by the end of the previous subsection is an invariant of a framed link constructed from the cuspidal edge of the critical value set according to the following procedure. The framing at a regular

point of a cuspidal edge depends on the sign of the edge as shown in Figure 3, left. Near swallowtail points the edges are smoothed and the framings along the two edge branches are joined by adding a half twist of the sign the same as that of the swallowtail as shown in Figure 3, right. After arbitrarily orienting the framed link, its writhe  $\omega$  is calculated as the algebraic number of crossings of the cores of the components of the link diagram plus the sum of the algebraic numbers of full rotations done by the framing of each of the components around its own core. The number of components of the link is denoted by  $n$ .

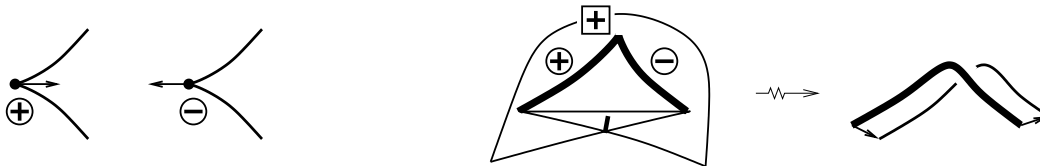


Figure 3: Making a framed link from cuspidal edges from [10].

**Theorem 0.5.3** ([10]). *The mod2 invariant  $I_{fe} = n + w/2$  is local.*

Later on, in [1], Aicardi found similar geometric interpretations for two more linearly independent additional *mod2* discriminantal cycles of Theorem 0.5.2. For that, she constructed framed links from the self-intersection sets and either positive or negative cuspidal edges of the critical value set. We leave the details of the framing construction along the self-intersection curves till our Sections 7.2 and 7.3. Denoting by  $n^\pm$  and  $w^\pm$  the number of the components and the writhes of the two links, we have



**Theorem 0.5.4** ([1]). *The mod2 invariants  $I_{dc^+} = (n^+ + w^+)/2$  and  $I_{dc^-} = (n^- + w^-)/2$  are local.*

These three framing invariants provide a starting point for some geometric interpretations of discriminantal cycles in this thesis. Of course, we will be adapting them to the Lagrangian setting as well as considering certain details differently. For example, our framing at triple points differs from that in [1].

We now move to the Lagrangian analogue of [10]. Here, the results are bifurcationally richer comparing to just ordinary smooth maps due to the presence of stable  $D_4$  points.

## 0.6 Lagrangian maps between 3-manifolds

The study of local (order 1) invariants of smooth maps between 3-manifolds in [10] was adapted to the Lagrangian setting by Gallagher in [9]. However, Gallagher did not provide a full classification in [9] since she did not distinguish between certain classes of singularities. We now look at the results from [9] in detail, as well as explain how they were obtained, since they provide the foundations for the work in this thesis.

Let  $\mathcal{L} = \mathcal{L}(M, T^*N, N)$  be the space of all Lagrangian maps  $M \looparrowright T^*N \rightarrow N$  between fixed 3-manifolds  $M$  and  $N$ . Both manifolds are oriented and without boundaries, and  $M$  is compact. We assume  $f : M \rightarrow N$  to be a generic Lagrangian map and denote its caustic by  $\mathcal{C}(f)$ .

Similar to the 2-dimensional case considered in Section 0.4,  $\mathcal{C}(f)$  is strati-

fied according to the singularities of the local generating families of functions. The caustic has regular part,  $A_2$ , and we will use its traditional co-orientation to the side with the greater number of preimages. From [5] we know that singular strata of  $\mathcal{C}(f)$  in general are cuspidal edges  $A_3$ , transversal self-intersections  $A_2^2$ , and isolated points  $A_4$ ,  $D_4^\pm$ ,  $A_3A_2$  and  $A_2^3$ . All of them are shown in Figure 4. Similar to the cusps in the 2-dimensional case, we introduce distinction of the cuspidal edges  $A_3^\sigma$ ,  $\sigma = \pm$ , by the local degree  $\pm 1$  of a Lagrangian map. However, in the 3-dimensional setting considered in [9], there is no distinction between two real  $\mathcal{R}$ -forms  $+x^4$  and  $-x^4$  of the  $A_3$  function singularities. We will call this setting *special*, and all discriminantal cycles making no distinction between  $+x^4$  and  $-x^4$  will also be called *special*. Formally, this specialisation means that we are enlarging our  $\mathcal{R}_+$ -equivalence by allowing to multiply the functions by  $-1$ . Distinguishing the two types  $A_3^\sigma$  of the cuspidal edges leads to the refinement of the types of isolated singular points of the caustics according to the sign of the participating edges  $A_3^\sigma A_2$ ,  $A_4^\sigma$  and  $D_4^{\pm, \sigma}$ . All these singularities are depicted in Figure 4. All the edges entering the  $D_4$  points there have sign  $\sigma$ .

The main result of [9] is

**Theorem 0.6.1.** *The space of rational special discriminantal cycles in  $\mathcal{L}(M, T^*N, N)$  is 10-dimensional. All these cycles are trivial, and the space is spanned by the derivatives of the following 10 invariants:*

$I_t$ , the number of triple points  $A_2^3$ ;

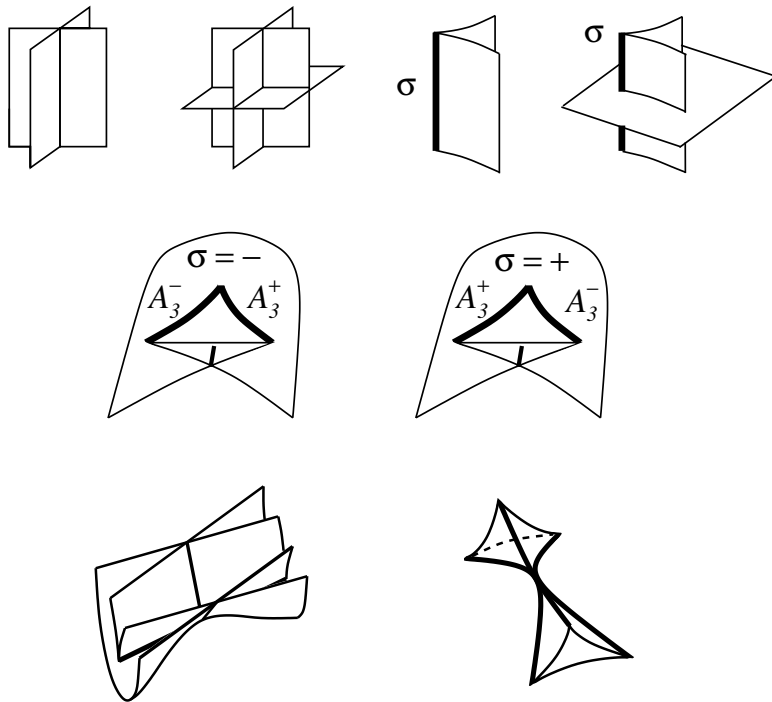


Figure 4: The top row shows  $A_2^2$ ,  $A_2^3$ ,  $A_3^\sigma$  and  $A_3^\sigma A_2$  singularities of generic caustics. The middle row shows the two different types of  $A_4^\sigma$  singularities whilst the bottom row depicts  $D_4^+$  (purse) and  $D_4^-$  (pyramid) singularities.

$I_{s_{\pm}}$ , the numbers of positive and negative swallowtails;

$I_{c_{\pm}}$ , the numbers of  $A_3^{\pm}A_2$  points;

$I_{d_{\pm}^{-}}$ , the numbers of  $D_4^{-,\pm}$  points;

$I_{d_{\pm}^{+}}$ , the numbers of  $D_4^{+,\pm}$  points;

$I_{\chi}$ , half of the Euler characteristic of the critical locus of a mapping.

Considering invariants up to an arbitrary choice of an additive constant for each connected component of the space of maps, we have

**Corollary 0.6.2.** *The dimension of the space of rational special local invariants on  $\mathcal{L}(M, T^*N, N)$  is 10. It is spanned by the 10 invariants listed in Theorem 0.6.1.*

The proof of Theorem 0.6.1 given in [9] is based on analysing generic 1-parameter families of Lagrangian maps and studying their interaction in generic 2-parameter families. In particular, the 1-parameter families allowed to immediately establish the linear independence of the ten derivatives. We shall now illustrate some other moments of the proof.

Figure 5 shows caustics of some of the 1-parameter families of maps identified in [9]. In every case the most degenerate moment corresponds to the discriminantal hypersurface  $\Sigma$  in the space  $\mathcal{L}(M, T^*N, N)$ . So, the names of the bifurcations provide the notation of the components of the discriminantal hypersurface  $\Sigma$  in  $\mathcal{L}(M, T^*N, N)$ . Each of these strata is co-oriented in the direction of the bifurcations shown in Figure 5.

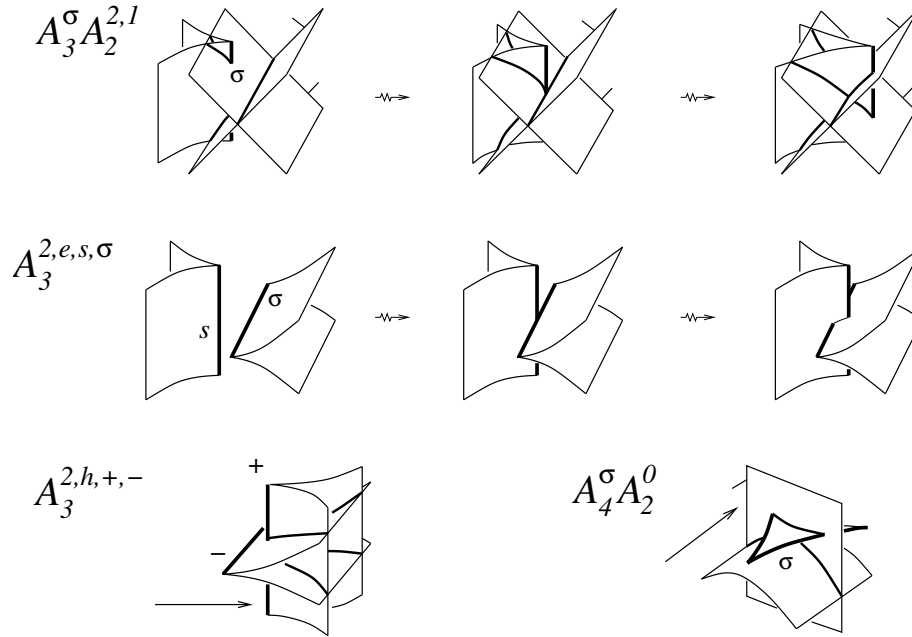


Figure 5: Examples of 1-parameter bifurcations from [9].

The derivative  $I' = \sum x_i X_i$  of a local invariant  $I$  is a trivial codimension 1 cycle in  $\mathcal{L}$ . That is, their intersection index with any loop in  $\mathcal{L}$  must be zero. Therefore, construction of such linear combinations (without an a priori knowledge of the invariants) splits into two parts:

1. establishing conditions on linear combinations of the codimension 1 strata to be cycles, and
2. checking the triviality of these cycles.

The first part was approached in [9] by analysis of local singularities and hence does not depend of the choice of  $M$ ,  $T^*N$  and  $N$  (except for the orientability) and of a particular connected component of  $\mathcal{L}(M, T^*N, N)$ .

Analysing generic 2-parameter families of maps produces bifurcation diagrams like the one shown in Figure 6. This example is produced by a swallowtail interacting with a smooth  $A_2$  sheet.

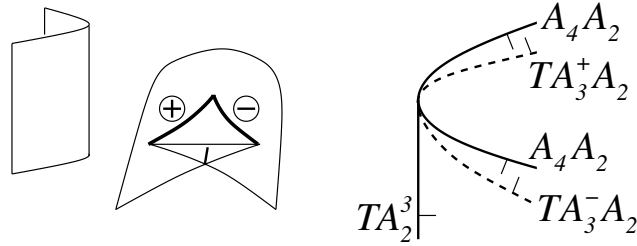


Figure 6: A codimension 2 degeneration involving a swallowtail and a smooth  $A_2$  sheet from [9]. At the most degenerate moment, the sheet is tangent to the self-intersection line at the swallowtail point.

We have already mentioned that each bifurcation diagram gives a cyclic equation on the increments of the local invariants across the codimension 1 strata. A cyclic equation represents the fact that the total increment of an invariant along a generic loop in  $\mathcal{L}(M, T^*N, N)$  must be zero. For example, the bifurcation diagram in Figure 6 gives the cyclic equation

$$ta_2^3 + ta_3^+ a_2 + ta_3^- a_2 - 2a_4 a_2 = 0.$$

After analysing all possible 2-parameter families of maps and various reductions, Gallagher obtained 13 linearly independent cyclic equations in 23 unknowns. This meant the solution space must be 10-dimensional. This proved the first claim of Theorem 0.6.1.

The second part followed from spotting integral (that is, homotopy free) interpretations of the ten invariants. This proved Corollary 0.6.2.

The dissertation [9] contains also a *mod2* version of Theorem 0.6.1:

**Theorem 0.6.3.** *The space of  $\mathbb{Z}_2$  special discriminantal cycles in  $\mathcal{L}(M, T^*N, N)$  has rank 16.*

Gallagher’s classification provides a starting point for this thesis. In our case we carry out the analysis in the spirit of [9] but we do not have the special simplification where  $A_3^+$  and  $A_3^-$  are declared the same. The bifurcations considered in [9] do cover the range we will analyse, however we introduce extra splittings of quite a few of them, which in turn makes the situation more complicated and the results richer. This allows us to substantially refine Theorems 0.6.1 and 0.6.3 — see Section 2.5.

## 0.7 Results of the thesis

In this thesis we study the space  $\mathcal{L} = \mathcal{L}(M, T^*N, N)$  of all Lagrangian maps  $M \looparrowright T^*N \rightarrow N$  between fixed 3-manifolds  $M$  and  $N$ . Both manifolds are without boundaries and  $M$  is compact. For now, we keep both manifolds oriented. Comparing to [9], we are now making difference between the  $A_3^+$  and  $A_3^-$  singularities, which also splits many other singularity strata in  $\mathcal{L}$  in smaller components. This allows us to obtain a complete description of the space of discriminantal cycles, and detect new invariants. However, we must now extract much more details about the bifurcations involved, and the

volume of the calculations rises very significantly: for example, the number of codimension 1 bifurcations (that is, the number of the unknowns in the system of cyclic equations) nearly doubles up to 132 from 68 used in [9].

The two main results of this thesis are Theorem 2.5.1 and Theorem 2.5.3. The first of them claims that the space of rational discriminantal cycles in  $\mathcal{L}(M, T^*N, N)$  is 15-dimensional. This space turns out to be generated by the derivatives of fourteen local invariants described in Lemma 2.4.1 and the cycle  $I'_{15}$  introduced in Section 2.4. Out of these fourteen local invariants, thirteen count the numbers of points of isolated singularity types on a caustic and the last is half of the Euler characteristic of the critical locus of a mapping. At the moment, the triviality of the cycle  $I'_{15}$ , that is, if there exists a genuine local invariant  $I_{15}$ , is not known. All the elements of our basis of the space of rational discriminantal cycles are actually integer, and Remark 2.4.2 points out a way to construct from them another basis, for the space of integer discriminantal cycles.

Our second result, Theorem 2.5.3, establishes that the space of *mod*2 discriminantal cycles in  $\mathcal{L}(M, T^*N, N)$  is 20-dimensional. This space is generated by the *mod*2 reduction of the basis of the space of integer discriminantal cycles, and a further five linearly independent discriminantal cycles introduced in Remark 2.4.3. For  $N = \mathbb{R}^3$ , we have found geometric interpretations for three of these five extra cycles by adapting the invariants  $I_{fe}$ ,  $I_{dc+}$  and  $I_{dc-}$  from [10] and [1]. We have also found that a fourth cycle out of the five is the derivative of the invariant counting the *mod*2 degrees of swallowtail points



in  $\mathbb{R}^3$ .

Finally, we investigate the effects of non-orientability of the source and/or target manifolds and prove corresponding versions of Theorems 2.5.1 and 2.5.3.

We set the structure of the thesis to be:

**Chapter 1:** in Section 1.1 we introduce the notion of a local invariant by recalling some basic definitions from [11] and [12]. Section 1.2 introduces Lagrangian maps by recalling key definitions, concepts and examples from [3] and [4]. Finally, we introduce the  $A$ ,  $D$ ,  $E$  function singularities.

**Chapter 2:** in Section 2.1 we list the types of singularities a caustic of a generic Lagrangian map from a 3-manifold to  $\mathbb{R}^3$  can have. We then list invariants of generic Lagrangian maps counting the numbers of isolated singularities of their caustics. Section 2.3 lists all possible bifurcations in generic 1-parameter families of caustics. In order to make it easier for the reader we have split these bifurcations into two types: corank 1 and corank 2 bifurcations. We have further split these types into uni-germs and multi-germs. In Section 2.4 we find the derivatives of the basic invariants introduced in Section 2.1. These derivatives are very helpful for our main results, Theorems 2.5.1 and 2.5.3. Finally, in Section 2.6 we analyse all bifurcations in 2-parameter families obtaining cyclic equations which we use to prove Theorems 2.5.1 and 2.5.3. At that moment we state the equations coming from the  $D_6^\pm$  and  $E_6^\pm$  bifurcations as Theorem 2.6.2 whose proof is very lengthy and, therefore, postponed to Chapters 4–6. However, we already use the result of

this theorem in Chapter 3.

**Chapter 3:** in this chapter, we derive two reduced versions – over  $\mathbb{Z}$  and over  $\mathbb{Z}_2$  – of the system of all our cyclic equations obtained in Chapter 2. This is done by elimination of all the equations which are either  $\mathbb{Z}$ - or  $\mathbb{Z}_2$ -linear combinations of the others. Expressions of the derivatives of the fourteen integer invariants from Lemma 2.4.1 help us to construct bases of the solutions spaces, that is, bases of the spaces of the rational, integer and mod2 discriminantal cycles. This proves Theorems 2.5.1 and 2.5.3.

**Chapters 4-6:** in these three chapters we prove Theorem 2.6.2, that is, we obtain the cyclic equations corresponding to the  $D_6^+$ ,  $D_6^-$  and  $E_6$  isolated function singularities. The task initially is to analyse how we can represent the ‘big’ caustics  $\mathcal{C} \subset \mathbb{R}^5$  as a collection of 2-parameter bifurcations of 3-dimensional caustics. In order to fulfill the task we study how various strata of  $\mathcal{C}$  are mapped by a generic map  $\pi : (\mathbb{R}_{\alpha,\beta,\gamma,\delta,\varepsilon}^5, \mathcal{C}) \rightarrow \mathbb{R}^2$ . Some of the information we need is already visible in the principal quasi-homogeneous part  $\pi_0$  of this map. However, detection of the behaviour of all the strata requires a more delicate analysis based on consideration of successive approximations of  $\pi$  by terms of increasing quasi-homogenous degrees. We note that the calculations of the bifurcation diagrams have already been done in [9], so we just give a brief overview of how they were obtained for the benefit of the reader. The main challenge in these chapters is to find our refined decorations of the strata.

**Chapter 7:** the main topic of this chapter is a search for  $\mathbb{Z}_2$  local invari-

ants which are not just *mod2* reductions of the integer. In Remark 2.4.3 we introduced a further five linearly independent *mod2* discriminantal cycles that along with the *mod2* reduction of the basis of the space of integer discriminantal cycles generate the space of *mod2* discriminantal cycles in  $\mathcal{L}(M, T^*N, N)$ . So, we are now trying to ‘integrate’ some of these five extra cycles, perhaps modulo the reduced integer cycles. In Sections 7.1, 7.2 and 7.3, for  $N = \mathbb{R}^3$ , we find geometric interpretations for three of the five cycles based on the invariants  $I_{fe}$ ,  $I_{dc+}$  and  $I_{dc-}$  from [10] and [1]. Here, we adapt them to the Lagrangian setting as well as consider certain details of their definitions differently. For example, we treat triple points in a way different to [1]: we resolve them and obtain genuine framed links while the links in [1] stayed with the triple point singularities. In Section 7.4 we construct one more *mod2* invariant based on the linking number of two framed links constructed from the cuspidal edges and self-intersection locus of  $\mathcal{C}$ . However, this provides an integral geometric interpretation for a linear combination of discriminantal cycles whose geometric interpretations are already known. Finally, in Section 7.5 we integrate exactly one of the five extra *mod2* cycles to the invariant counting the *mod2* degrees of swallowtail points in  $\mathbb{R}^3$ .

**Chapter 8:** in the final chapter we look at the effects of non-orientability of the source and/or target manifolds over  $\mathbb{Q}$ ,  $\mathbb{Z}$  and  $\mathbb{Z}_2$ . Here, we see invariants which count the number of isolated singularity types that only differ by the signs of the local degrees of maps merge together, whereas some other invariants completely disappear. Of course, in all cases, the number

of discriminantal cycles and invariants go down, making the classification of invariants substantially simpler.

# Chapter 1

## Basic Concepts

### 1.1 Local invariants

We first introduce the notion of local invariants of maps by stating some general definitions that can be found in [11] or [12].

Let  $\Omega$  be a space of maps, and  $\Sigma \subset \Omega$  a subset of non-generic maps of our choice. Consider invariants of generic maps with values in an abelian group  $G$ , that is, maps of the set of connected components of  $\Omega \setminus \Sigma$  to  $G$ .

**Definition 1.1.1.** *We call an invariant local if every increment of the invariant in a generic 1-parameter family of maps is completely determined by the type of the local bifurcation of the map.*

The discriminant  $\Sigma$  must be co-orientable if, for example, we are working with integer invariants.

**Definition 1.1.2.** *Up to a choice of an additive constant (individual for each connected component of  $\Omega$ ), any local invariant  $I$  is defined by its derivative  $I' = \sum x_i X_i$ , where the  $X_i$  are discriminantal strata of codimension 1 in  $\Omega$ , and the  $x_i$  are the increments of  $I$  across them.*

**Definition 1.1.3.** *Every discriminantal stratum of codimension 2 in  $\Omega$  provides an equation on the increments, called a cyclic equation.*

**Example 1.1.4.** *Figure 7 shows a discriminantal stratum of codimension 2 with its corresponding cyclic equation,  $-x_1 + x_2 - x_3 = 0$ .*

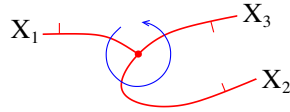


Figure 7: Transversal section of a discriminantal stratum of codimension 2 in  $\Omega$ .

**Definition 1.1.5.** *A linear combination  $\sum x_i X_i$ , in which the  $x_i$  satisfy all possible cyclic equations, is a codimension 1 cycle in  $\Omega$ . We call such cycles discriminantal.*

**Definition 1.1.6.** *Given a discriminantal cycle for which similar vanishing holds on loops non-contractible in  $\Omega$  we can ‘integrate’ it to an invariant. In such case we call a discriminantal cycle trivial.*

**Remark 1.1.7.** *If we cross a discriminant stratum in the same direction as its co-orientation we say this is a positive move.*

## 1.2 Lagrangian maps

We recall a series of standard definitions which may be found, for example, in [3] or [4].

**Definition 1.2.1.** *A symplectic form on a manifold is a non-degenerate closed differential 2-form (also called a symplectic structure).*

**Example 1.2.2.** *The linear space  $\mathbb{R}^{2n}$  with coordinates  $(p_1, \dots, p_n; q_1, \dots, q_n)$  has the standard symplectic structure  $\omega = \sum dp_i \wedge dq_i$ .*

**Definition 1.2.3.** *A Lagrangian submanifold of a symplectic manifold is a submanifold of maximal dimension on which the symplectic structure vanishes.*

**Example 1.2.4.** *In the previous example,  $q = \text{constant}$  is a Lagrangian submanifold.*

**Definition 1.2.5.** *A Lagrangian fibration  $E^{2n} \rightarrow B^n$  of a symplectic manifold is a fibration with Lagrangian fibres.*

**Example 1.2.6.**  $\mathbb{R}_{p,q}^{2n} \rightarrow \mathbb{R}_q^n$  *is a Lagrangian fibration.*

There exists a theorem in [3] which states that, locally, any Lagrangian fibration is the same as the example above.

**Definition 1.2.7.** *Consider an immersed Lagrangian submanifold  $L$  in the space of a Lagrangian fibration  $E \rightarrow B$ . The projection of  $L$  to  $B$  is called a Lagrangian map.*

Thus, a Lagrangian map is a triple  $L \hookrightarrow E \rightarrow B$ , where the left arrow is a Lagrangian immersion and the right one a Lagrangian fibration.

**Definition 1.2.8.** *The set of all critical values of a Lagrangian map is called its caustic.*

**Definition 1.2.9.** *A Lagrangian equivalence of two Lagrangian maps is a symplectomorphism (that is, an isomorphism in the category of symplectic manifolds) of the total spaces transforming the first Lagrangian fibration to the second, and the first Lagrangian immersion to the second.*

Thus, a Lagrangian equivalence is a commutative  $(3 \times 2)$  diagram

$$\begin{array}{ccccc} L_1 & \hookrightarrow & E_1 & \twoheadrightarrow & B_1 \\ \downarrow & & \downarrow & & \downarrow \\ L_2 & \hookrightarrow & E_2 & \twoheadrightarrow & B_2 \end{array}$$

**Definition 1.2.10.** *A Lagrangian singularity is a germ of a Lagrangian map, considered up to the Lagrangian equivalence.*

Now, since in this thesis we are considering Lagrangian maps to 3-manifolds, a local model for this case is the Lagrangian fibration

$$\mathbb{R}^6 \rightarrow \mathbb{R}^3, (u, v, w, U, V, W) \mapsto (u, v, w).$$

The symplectic form here is  $dU \wedge du + dV \wedge dv + dW \wedge dw$ , where  $u, v, w$  and  $U, V, W$  are coordinates respectively on the target and along the fibres of the fibration. From [3] we have,



**Definition 1.2.11.** Any Lagrangian submanifold  $L \subset \mathbb{R}^6$  is defined locally by a generating family of functions  $F(x; u, v, w)$  :

$$L = \{(u, v, w, U, V, W) | \exists x \in \mathbb{R}^3 : F_x = 0, U = F_u, V = F_v, W = F_w\}.$$

Smoothness of  $L$  is equivalent to the rank of the matrix  $(F_x)_{x,u,v,w}$  of the second derivatives being maximal, that is, equal to the dimension of  $x$ . The caustic in  $\mathbb{R}_{u,v,w}^3$  consists of those points  $(u, v, w)$  for which the member  $F(\cdot; u, v, w)$  of the generating family has non-Morse critical points.

In terms of local generating families  $F(x; u, v, w)$  Lagrangian equivalence corresponds to the stable  $\mathcal{R}_+$ -equivalence preserving the fibration  $(x; u, v, w) \mapsto (u, v, w)$  (see [3]). The stability here is in the sense of addition of non-degenerate quadratic forms in extra  $x$ -variables.

Finally, we recall the  $A$ ,  $D$ ,  $E$  function singularities (see [3]). In a neighbourhood of a simple critical point 0, every function  $f : (\mathbb{R}^n, 0) \rightarrow (\mathbb{R}, 0)$  is stably  $\mathcal{R}_+$ -equivalent to one of the following function germs:

$A_k$	$D_k$	$E_6$	$E_7$	$E_8$
$\pm x^{k+1}, k \geq 1$	$x^2 y \pm y^{k-1}, k \geq 4$	$x^3 \pm y^4$	$x^3 + xy^3$	$x^3 + y^5$

## Chapter 2

# Local invariants of Lagrangian maps between 3-manifolds

We shall consider a parallel to Gallagher's work in [9], Section 2, where she listed all singularities of a generic caustic in three dimensions, gave intrinsic examples of local invariants and introduced the bifurcations in generic 1-parameter families of caustics. In [9], Gallagher made a significant concession in the classification of singularities whereas in our setting we are going to consider the case without any. We borrow the standard notation for the bifurcations from [9], and use the figures from [10] and [9] edited for our case. Following this we then list all bifurcations in 2-parameter families from which we obtain cyclic equations. The main aim of this chapter is to see how the extra edge decoration  $s$  behaves in bifurcations and how this effects the dimensions of the equation and solution spaces over  $\mathbb{Q}$  and  $\mathbb{Z}_2$ .

## 2.1 Singularities of a generic caustic in three dimensions

Following [9], the Lagrangian fibration in nearly the whole thesis will be the cotangent bundle  $T^*N \rightarrow N$  our target manifold, and we denote by  $\mathcal{L} = \mathcal{L}(M, T^*N, N)$  the space of all Lagrangian maps  $M \looparrowright T^*N \rightarrow N$  between fixed 3-manifolds  $M$  and  $N$ . The source  $M$  will always be compact, both 3-manifolds will always be without boundaries, and till Chapter 8 we are assuming both of them oriented. All our considerations will be local, with  $N = \mathbb{R}^3$  taken for the local model, and therefore all our results, except for those in Chapter 7 obtained specifically for  $N = \mathbb{R}^3$ , are valid for any Lagrangian fibration over the target.

Let  $f$  be a generic Lagrangian map between  $M$  and  $\mathbb{R}^3$ , and  $\mathcal{C}(f)$  its caustic. We co-orient the regular part of a smooth sheet,  $A_2$ , of  $\mathcal{C}(f)$  to the side where the number of local preimages of a point is greater. From [4], a generic Lagrangian map from a 3-manifold to  $\mathbb{R}^3$  has the caustic whose singularities may locally be the following:

$A_2^2$ , transversal intersections of two smooth sheets, Figure 8;

$A_2^3$ , transversal intersections of three smooth sheets, Figure 8;

$A_3^{s,\sigma}$ , cuspidal edges, with generating families  $F(x; u, v, w) = sx^4 + vx^2 + ux$ , Figure 8. The sign  $\sigma = \pm$  denotes the local degree  $\pm 1$  of the Lagrangian

map. In our case we are differentiating between functions  $x^4$  and  $-x^4$  by introducing the extra coefficient  $s = \pm$  in the generating family. Formally, the two sign options of the  $x^4$  coefficient in the generating families are in different equivalence classes, unlike in [9];

$A_3^{s,\sigma} A_2$ , transversal intersections of a cuspidal edge with a smooth sheet, Figure 8. Again, the signs  $s$  and  $\sigma$  correspond to the signs of the cuspidal edge;

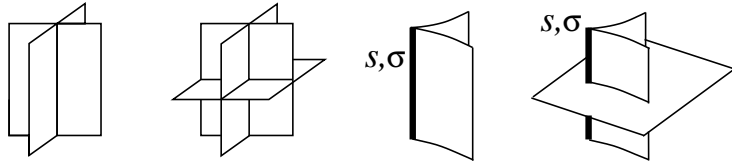


Figure 8: The  $A_2^2$ ,  $A_2^3$ ,  $A_3^{s,\sigma}$  and  $A_3^{s,\sigma} A_2$  stable singularities of generic caustics.

$A_4^{s,\sigma}$ , swallowtails, with the generating family  $F(x; u, v, w) = x^5 + wx^3 + vx^2 + ux$ . The notation  $s = \pm$ ,  $\sigma = \pm$  for the swallowtail comes from the signs of the right cuspidal edge, which can be seen in Figure 9. This is different to [9] where the notation of the swallowtail came from the sign of the left cuspidal edge;

$D_4^{\pm,\sigma}$ , the central points of the two caustics shown in Figure 10, with the generating family

$$F(x, y; u, v, w) = \pm x^2 y + y^3 + wy^2 + vy + ux. \quad (1)$$

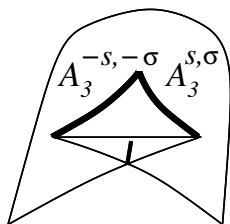


Figure 9:  $A_4^{s,\sigma}$  singularities.

The sign  $\sigma = \pm$  indicates the local degree  $\pm 1$  of the Lagrangian map along the cuspidal edges. We should note that as a cuspidal edge passes through the most degenerate point of  $D_4^{\pm,\sigma}$ , its decorations switch from  $(-, \sigma)$  to  $(+, \sigma)$ . Hence, the notation  $s$  is not needed for  $D_4^{\pm,\sigma}$ .

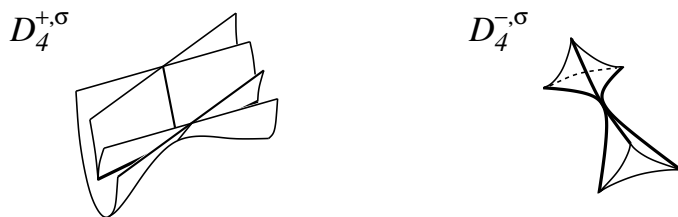


Figure 10: The  $D_4^{\pm,\sigma}$  caustics in  $\mathbb{R}^3$ , the purse and pyramid.

## 2.2 Examples of invariants of generic Lagrangian maps

One of the most intrinsic ways to define an invariant of generic Lagrangian maps is to count the numbers of points of isolated singularity types of their caustics. In our case we have thirteen such invariants, compared to nine in [9].

**Examples 2.2.1.** The number of isolated singularities of  $\mathcal{C}(f)$  of a particular type is a local invariant. We now introduce notations for such invariants:

$I_t$ , the number of triple points  $A_2^3$ ;

$I_{sw_{s\sigma}}$ , the numbers of  $(s, \sigma)$ -swallowtails,  $s, \sigma = \pm$ ;

$I_{cs\sigma}$ , the numbers of  $A_3^{s,\sigma} A_2$  points,  $s, \sigma = \pm$ ;

$I_{d\sigma^-}$ , the numbers of  $D_4^{-,\sigma}$  points,  $\sigma = \pm$ ;

$I_{d\sigma^+}$ , the numbers of  $D_4^{+,\sigma}$  points,  $\sigma = \pm$ .

Another obvious invariant is

$I_\chi$ , half of the Euler characteristic of the critical locus of a mapping.

## 2.3 Bifurcations in generic 1-parameter families of caustics

We shall now introduce bifurcations in generic 1-parameter families, which we will split into two categories: corank 1 and corank 2 bifurcations. The normal forms may be found, for example, in [4], [22] and [9]. Here we have edited the normal forms to include the extra decoration sign  $s = \pm$  in the coefficient of  $x^4$ . We depict cuspidal edges by a thicker solid line. The directions of the bifurcations shown in the figures co-orient the discriminantal strata wherever the initial and final local caustics differ. Such bifurcations will also be called

positive. In terms of the normal forms, they correspond to the sign of the bifurcation parameter  $\lambda$  changing from negative to positive. Respectively, we will also call the corresponding sides of the strata negative and positive.

### 2.3.1 Corank 1 bifurcations

First, we shall list the corank 1 bifurcations. Here we are not allowing any of the critical points to have corank 2, that is no  $D_4$  or  $D_5$  points.

#### 2.3.1.1 Uni-germs

For corank 1 uni-germs we have the following transformations of the caustics along with their normal forms. They are depicted in Figure 11. We introduce the notations  $e$  and  $h$  in order to distinguish between elliptic and hyperbolic versions of bifurcations. Again, the decorations  $s = \pm$  and  $\sigma = \pm$  correspond to the sign of the coefficient of  $x^4$  and the sign of the local degree of the Lagrangian map at the cuspidal edge. The last two decorations in the notation of  $A_3$  uni-germs are the signs of the squares in the coefficient of  $x^2$ .

$A_3^{s,\sigma,+,+}$ ,  $F = s(x^4 + (v^2 + w^2 - \lambda)x^2 + ux)$ , birth of a flying saucer.

$A_3^{s,\sigma,+,-}$ ,  $F = s(x^4 + (v^2 - w^2 + \lambda)x^2 + ux)$ , hyperbolic transformation of an edge.

$A_3^{s,\sigma,-,-}$ ,  $F = s(x^4 - (v^2 + w^2 + \lambda)x^2 + ux)$ , death of a compact component of an edge.

$A_4^{\varepsilon,e}$ ,  $F = x^5 + (w^2 - \lambda)x^3 + vx^2 + ux$ , birth of cuspidal lips. Here  $\varepsilon = s\sigma$  with the product taken along either of the two newborn edges (see Figure 9).

$A_4^{\varepsilon,h}$ ,  $F = x^5 + (\lambda - w^2)x^3 + vx^2 + ux$ , beaks bifurcation on the edge. Again,  $\varepsilon = s\sigma$ .

$A_5^{s,\sigma,\omega}$ ,  $F = s(x^6 - \lambda x^4 + vx^3 + wx^2 + ux)$ . Here  $s$  is the sign of  $x^6$  and  $\sigma$  is the local degree of the whole map. Moreover,  $\omega$  is the writhe of the cuspidal edge. We denote the sign of the swallowtails born in the bifurcation by  $(t, \tau)$ . Hence, we have the relation,  $(t, \tau) = \text{writhe} \cdot (-s, -\sigma)$ .

### 2.3.1.2 Multi-germs

For corank 1 multi-germs we have the following transformations of caustics, depicted in Figure 12. We use the notation:  $T$  for tangency between participating components, and  $e, h$  to distinguish between elliptic and hyperbolic versions of bifurcations, as before. We set  $r$  to be the number of faces of the bounded regions to be co-oriented outwards after the bifurcation.

$A_2^{4,r}$ ,  $r = 2, 3, 4$ , intersection of four smooth sheets. The pre-bifurcation tetrahedral region has  $4 - r$  faces co-oriented outwards. Therefore, the  $r = 2$  stratum  $A_2^{4,2}$  is not co-orientable in  $\mathcal{L}$  by local means.

$TA_2^{3,r}$ ,  $r = 0, 1, 2, 3$ , three smooth sheets are pairwise transversal to each other, but the line of intersection of any two of them is tangent to the third sheet at the moment of bifurcation.



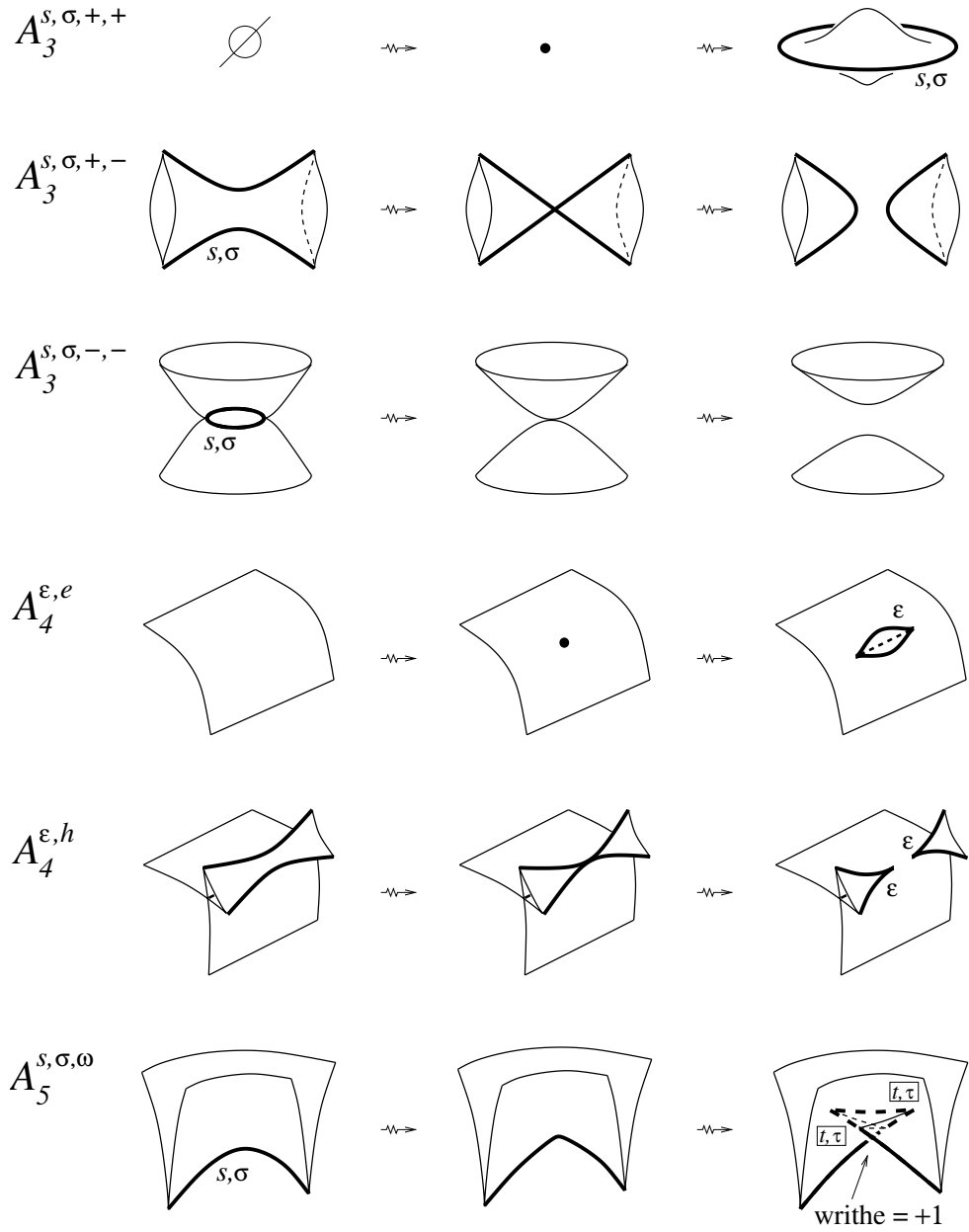


Figure 11: Positive moves in generic 1-parameter bifurcations of caustics of corank 1 maps.

$TA_2^{2,e,r}$ ,  $r = 0, 1, 2$ , elliptic tangency of two smooth sheets.

$TA_2^{2,h,r}$ ,  $r = 0, 1$ , same as above, but hyperbolic. We write  $r = 1$  if the sheets have the same co-orientation, and  $r = 0$  if the co-orientations are opposite. For  $r = 1$ , we fail to locally co-orient the stratum in  $\mathcal{L}$ .

$A_3^{s,\sigma}A_2^{2,r}$ ,  $r = 0, 1, 2$ , cuspidal edge meets the intersection of two smooth sheets.

$A_3^{2,e;s,\sigma;s',\sigma'}$ , two edges of given signs meet face-to-face. The notation is up to permutation of  $(s, \sigma)$  and  $(s', \sigma')$ .

$A_3^{2,h;s,\sigma;s',\sigma'}$ , one of the edges is overtaking the other. The notation assumes that two  $A_3^{s,\sigma}A_2$  points appear after the bifurcation instead of two  $A_3^{s',\sigma'}A_2$  points which the caustic had before. Therefore, the notation is anti-symmetric with respect to the  $(s, \sigma) \leftrightarrow (s', \sigma')$  swap:  $A_3^{2,h;s',\sigma';s,\sigma} = -A_3^{2,h;s,\sigma;s',\sigma'}$ . In particular, such strata are not co-orientable if  $(s, \sigma) = (s', \sigma')$ .

$A_4^{s,\sigma}A_2^r$ ,  $r = 0, 1$ , a smooth sheet passes through a swallowtail.

$TA_3^{s,\sigma}A_2^{e,r}$ ,  $r = 0, 1$ , cuspidal edge becomes tangent to a smooth sheet so that the two local components of the caustic do not intersect before the bifurcation.

$TA_3^{s,\sigma}A_2^{h,r}$ ,  $r = 0, 1$ , the hyperbolic version of the previous with no  $A_3A_2$  points before the bifurcation. For  $r = 1$ , the co-orientation of the  $A_2$  sheet is towards the cuspidal edge before the bifurcation. For  $r = 0$ , it is opposite.

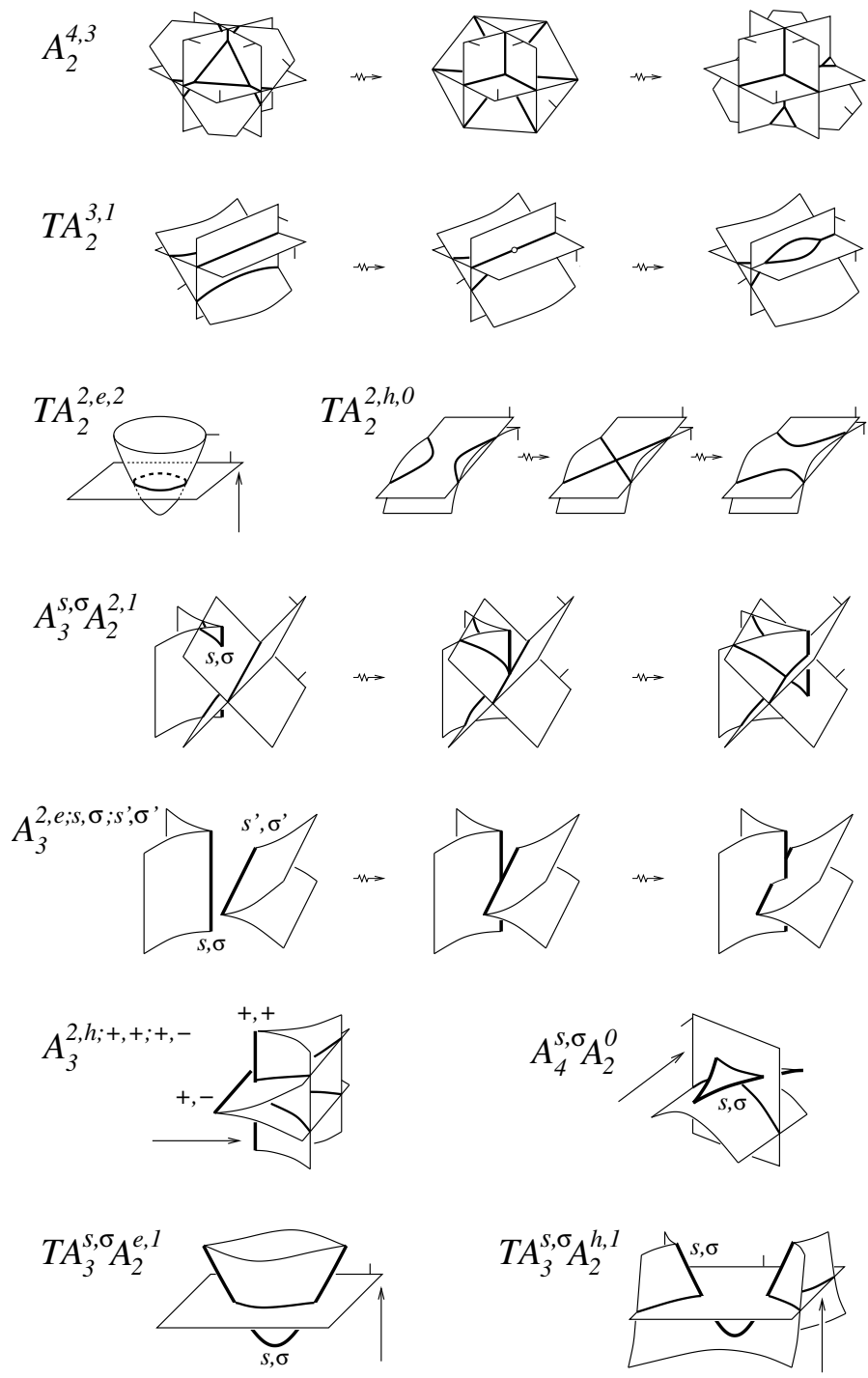


Figure 12: Positive moves in generic 1-parameter families of corank 1 multi-germs of caustics.

## 2.3.2 Corank 2 bifurcations

Now, we shall examine the corank 2 bifurcations. Here we are allowing the derivatives of individual maps to have corank 2 at some critical points, that is  $D_4$  and  $D_5$  points.

### 2.3.2.1 Uni-germs

We now use the index  $q$  in the sense of quadratic. This word relates to the features appearing in the normal forms of our singularities.

There are four  $D_{4,q}^\pm$  ‘quadratic’ bifurcations induced from the generating family

$$F = s(\pm x^2 y + \frac{1}{3} y^3 + \varphi \frac{y^2}{2} + v y + u x), \quad (2)$$

where,  $\varphi$  respectively is:

- $D_{4,q}^{-,s,\sigma}$  :  $\lambda - w^2 \pm v + \alpha u$ ;
- $D_{4,a}^{+,s,\sigma}$  :  $\lambda - w^2 + v + \alpha u$ ,  $|\alpha| < 1$ ;
- $D_{4,b}^{+,s,\sigma}$  :  $\lambda - w^2 \pm v + \alpha u$ ,  $|\alpha| > 1$ ;
- $D_{4,c}^{+,s,\sigma}$  :  $\lambda - w^2 - v + \alpha u$ ,  $|\alpha| < 1$ .

Here  $\alpha \in \mathbb{R}$  is a modulus. The quadraticity is of course in  $w$ , and we have ‘three values of  $q$ ’ in the  $D_4^+$  case. Figure 13 provides the illustrations. The signs  $s$  and  $\sigma$  correspond to the majority of the cuspidal edge after the bifurcation. The interval of the cuspidal edge between the two  $D_4$  points after the

bifurcation has signs  $(-s, \sigma)$ .

The  $D_5^{s,\sigma}$  generating family is

$$F = s(x^2y + y^4 - (\lambda \pm w + au)y^3 + wy^2 + vy + ux), \quad a \in \mathbb{R},$$

with its illustration provided in Figure 13. The sign  $\sigma = \pm$  denotes the local degree  $\pm 1$  of the Lagrangian map. We shall use the notation  $D_5^{s,\sigma}$ , where to the left of the  $D_4$  points we have the cuspidal edge decorations  $(-s, \sigma)$  and to the right  $(s, \sigma)$ .

### 2.3.2.2 Multi-germs

Now we list the multi-germ bifurcations with corank 2 points. In each of the following cases the smooth sheet passes during a positive move through a  $D_4$  point from the side with the cuspidal edge  $(-, \sigma)$  to that with  $(+, \sigma)$ . Hence we set that the  $A_3^{+,\sigma}A_2$  points appear after the bifurcation. Figures 14 and 15 provide the illustrations.

$D_4^{-,\sigma}A_2^+$ , a smooth sheet passing through a pyramid in the direction of its co-orientation.

$D_4^{-,\sigma}A_2^-$ , a smooth sheet passing through a pyramid in the direction opposite to its co-orientation.

$D_{4,0}^{+,\sigma}A_2^+$ , a smooth sheet passing through a purse so that the number of triple

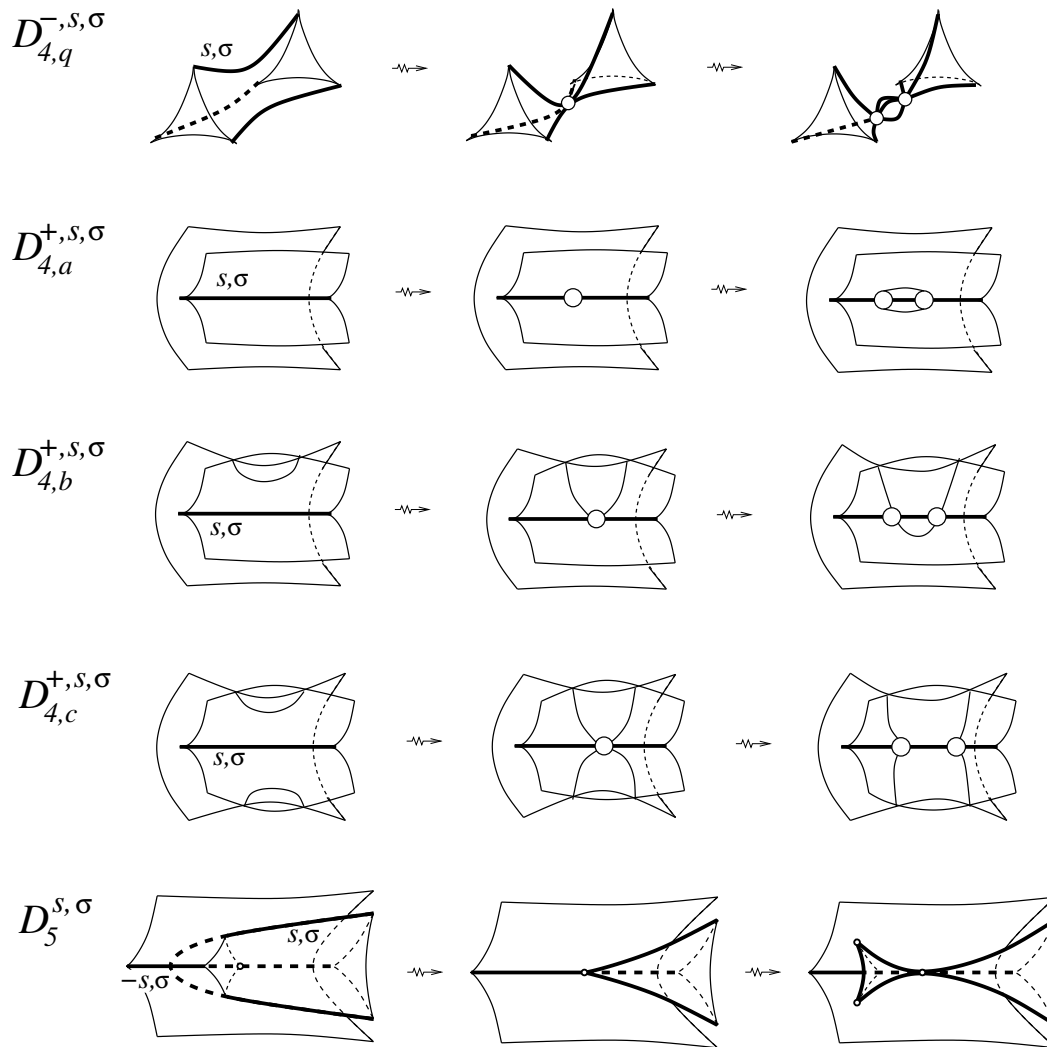


Figure 13: Positive moves in generic 1-parameter bifurcations of uni-germ caustics near corank 2 points of the maps.

points decreases. The sheet is moving in the direction of its co-orientation.

$D_{4,0}^{+,\sigma} A_2^-$ , a smooth sheet passing through a purse so that the number of triple points decreases. The sheet is moving in the direction opposite to its co-orientation.

$D_{4,2}^{+,\sigma} A_2^+$ , a smooth sheet passing through a purse so that the number of triple points increases. The sheet is moving in the direction of its co-orientation.

$D_{4,2}^{+,\sigma} A_2^-$ , a smooth sheet passing through a purse so that the number of triple points increases. The sheet is moving in the direction opposite to its co-orientation.

$D_{4,r}^{+,\sigma} A_2^+$ , a smooth sheet passing through a purse so that the triple point passes from the left to the right if we are looking in the direction of the movement which in this case coincides with the co-orientation of the sheet.

$D_{4,r}^{+,\sigma} A_2^-$ , a smooth sheet passing through a purse so that the triple point passes from the left to the right if we are looking in the direction of the movement which in this case is opposite to the co-orientation of the sheet.

$D_{4,l}^{+,\sigma} A_2^+$ , a smooth sheet passing through a purse so that the triple point passes from the right to the left if we are looking in the direction of the movement which in this case coincides with the co-orientation of the sheet.

$D_{4,l}^{+,\sigma} A_2^-$ , a smooth sheet passing through a purse so that the triple point passes from the right to the left if we are looking in the direction of the movement which is now opposite to the co-orientation of the sheet.

## 2.4 Derivatives of the basic invariants

Direct analysis of the illustrations to our lists of bifurcations in generic 1-parameter families from Section 2.3 yields

**Lemma 2.4.1.** *The derivatives of the 14 invariants introduced in Example 2.2.1 are*

$$\begin{aligned}
I'_t & : 2TA_2^3 + 2A_3A_2^2 + A_4A_2 + 2D_{4,2}^+A_2 - 2D_{4,0}^+A_2 \\
I'_{sw_{++}} & : A_4^{+,e/h} + 2A_5^{+,+,-} + 2A_5^{-,-,+} + D_5^{+,-} + D_5^{-,+} \\
I'_{sw_{+-}} & : A_4^{-,e/h} + 2A_5^{-,+,+} + 2A_5^{+,-,-} + D_5^{+,+} + D_5^{-,-} \\
I'_{sw_{-+}} & : A_4^{-,e/h} + 2A_5^{+,-,+} + 2A_5^{-,+,+} + D_5^{+,+} + D_5^{-,-} \\
I'_{sw_{--}} & : A_4^{+,e/h} + 2A_5^{+,+,+} + 2A_5^{-,-,-} + D_5^{+,-} + D_5^{-,+} \\
I'_{c_{++}} & : 2TA_3^{++}A_2 + 4A_3^{2,e,+,+,+,+} + 2A_3^{2,e,+,+,+,-} + 2A_3^{2,e,+,+,-,+} \\
& \quad + 2A_3^{2,e,+,+,-,-} + 2A_3^{2,h,+,+,+,-} + 2A_3^{2,h,+,+,-,-} + 2A_3^{2,h,+,+,-,+} \\
& \quad + A_4^+A_2 + 2A_5^{+,+,+} + 2A_5^{+,+,-} + 3D_4^{-,+}A_2 + D_{4,0}^+A_2 + D_{4,2}^+A_2 \\
& \quad + D_{4,l}^{+,+}A_2 + D_{4,r}^{+,+}A_2 - 2D_5^{+,+} \\
I'_{c_{+-}} & : 2TA_3^{+-}A_2 + 4A_3^{2,e,+,+,-,+} + 2A_3^{2,e,+,+,+,-} + 2A_3^{2,e,+,+,-,-} \\
& \quad + 2A_3^{2,e,+,+,-,-} + 2A_3^{2,h,+,+,-,-,+} + 2A_3^{2,h,+,+,-,-,-} - 2A_3^{2,h,+,+,-,+} \\
& \quad + A_4^-A_2 + 2A_5^{+,-,+} + 2A_5^{+,-,-} + 3D_4^{-,-}A_2 + D_{4,0}^+A_2 + D_{4,2}^+A_2 \\
& \quad + D_{4,l}^{+,-}A_2 + D_{4,r}^{+,-}A_2 - 2D_5^{+,-}
\end{aligned}$$



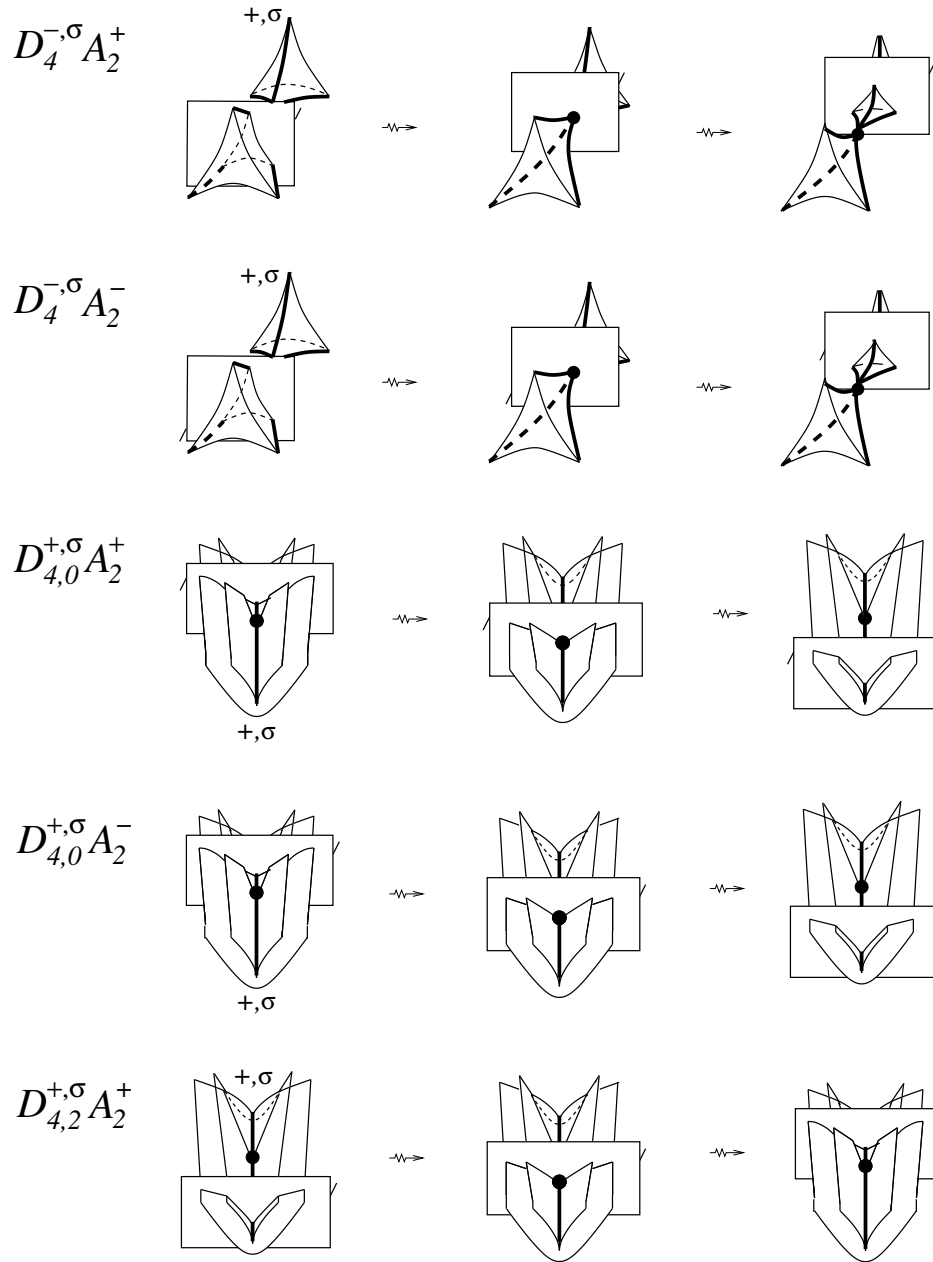


Figure 14: Positive moves in generic 1-parameter bifurcations of multi-germ caustics involving corank 2 points of the maps.

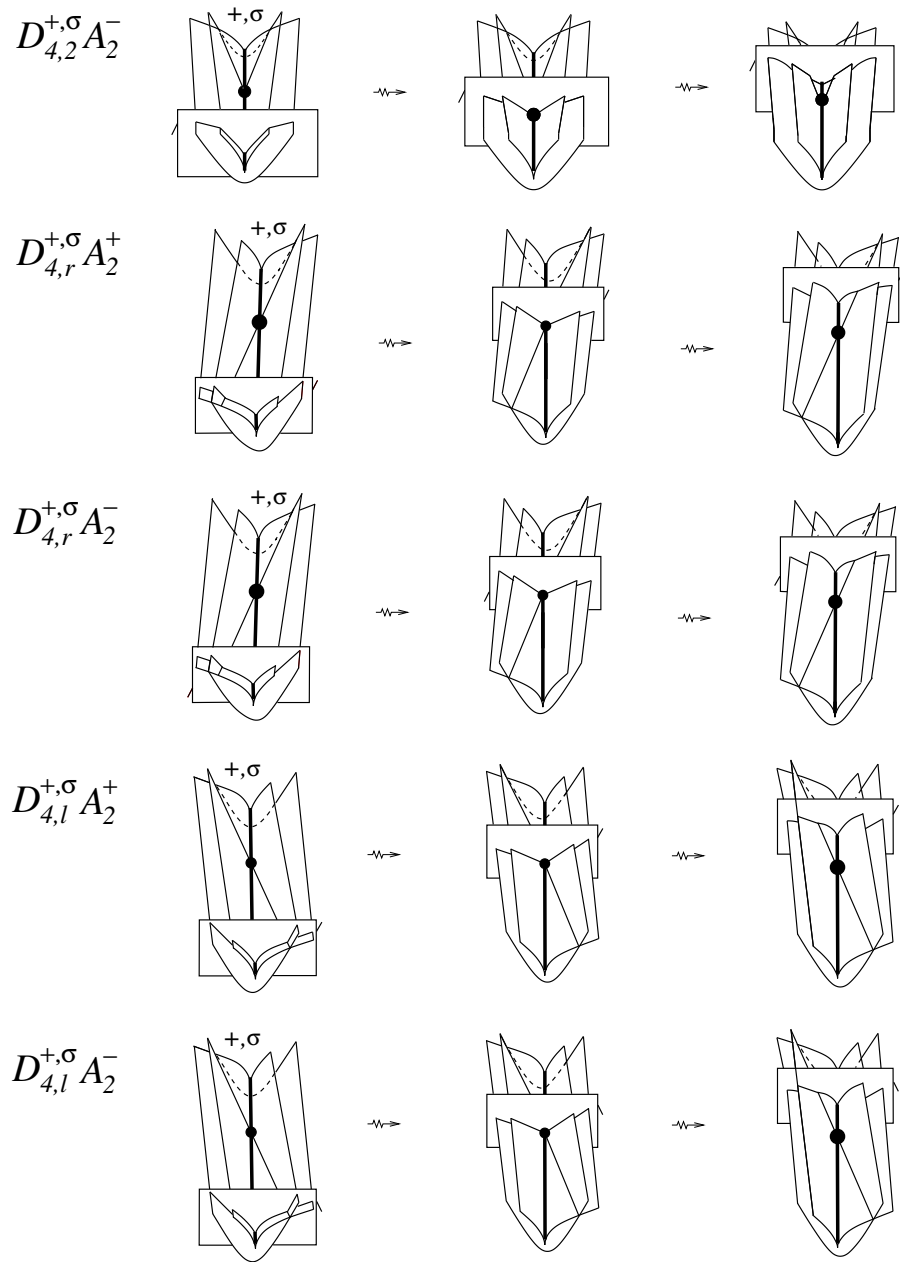


Figure 15: More positive moves in generic 1-parameter bifurcations of multi-germ caustics involving corank 2 points of the maps.

$$\begin{aligned}
I'_{c_{-+}} &: 2TA_3^{-+}A_2 + 4A_3^{2,e,-,+,-,+} + 2A_3^{2,e,+,+,-,+} + 2A_3^{2,e,+,+,-,+} \\
&\quad + 2A_3^{2,e,-,+,-,-} + 2A_3^{2,h,-,+,-,-} - 2A_3^{2,h,+,+,-,+} - 2A_3^{2,h,+,+,-,+} \\
&\quad + A_4^{-}A_2 + 2A_5^{+,+,+} + 2A_5^{+,-,+} - 3D_4^{-,+}A_2 - D_{4,0}^{+,+}A_2 - D_{4,2}^{+,+}A_2 \\
&\quad - D_{4,l}^{+,+}A_2 - D_{4,r}^{+,+}A_2 - 2D_5^{-,+} \\
I'_{c_{--}} &: 2TA_3^{--}A_2 + 4A_3^{2,e,-,-,-,-} + 2A_3^{2,e,+,+,-,-} + 2A_3^{2,e,+,+,-,-} \\
&\quad + 2A_3^{2,e,-,+,-,-} - 2A_3^{2,h,+,+,-,-} - 2A_3^{2,h,+,+,-,-} - 2A_3^{2,h,-,+,-,-} \\
&\quad + A_4^{+}A_2 + 2A_5^{-,-,+} + 2A_5^{-,-,-} - 3D_4^{-,-}A_2 - D_{4,0}^{+,-}A_2 - D_{4,2}^{+,-}A_2 \\
&\quad - D_{4,l}^{+,-}A_2 - D_{4,r}^{+,-}A_2 - 2D_5^{-,-} \\
I'_{d_{+}^{+}} &: 2D_{4,a}^{+,+} + 2D_{4,b}^{+,+} + 2D_{4,c}^{+,+} - D_5^{+,+} - D_5^{-,+} \\
I'_{d_{+}^{-}} &: 2D_{4,a}^{+,-} + 2D_{4,b}^{+,-} + 2D_{4,c}^{+,-} - D_5^{+,-} - D_5^{-,-} \\
I'_{d_{+}^{-}} &: 2D_{4,q}^{-,+} + D_5^{+,+} + D_5^{-,+} \\
I'_{d_{-}^{-}} &: 2D_{4,q}^{-,-} + D_5^{+,-} + D_5^{-,-} \\
I'_{\chi} &: -D_{4,a}^{+} - D_{4,b}^{+} - D_{4,c}^{+} + D_{4,q}^{-} + A_3^q
\end{aligned}$$

Here, omission of an index means summation along all possible values of this index. We also set  $\varepsilon = s\sigma$ , so we have  $A_4^{\varepsilon}A_2$  and  $A_4^{\varepsilon,e/h} = A_4^{\varepsilon,e} + A_4^{\varepsilon,h}$ . Finally, we set  $D_{4,q}^{+} = D_{4,a}^{+} + D_{4,b}^{+} + D_{4,c}^{+}$  and  $A_3^q = A_3^{\pm,\pm,+,+} + A_3^{\pm,\pm,+,-} + A_3^{\pm,\pm,-,-}$ .

**Proof of Lemma 2.4.1.** By inspection of the 126 co-orientable bifurcations in Section 2.3. □

In what follows we will be using the 15<sup>th</sup> linear combination

$$I'_{15} : A_3^{+,+,q} - A_3^{+,-,q} - A_3^{-,+,q} + A_3^{-,-,q},$$

which turns out to be a discriminantal cycle linearly independent from the 14 derivatives.

**Remark 2.4.2.** *There is another set of 15 integer discriminantal cycles which will be useful for us in the next subsection:*

$$\begin{aligned}
& I'_t, \quad I'_{sw_{++}}, \quad I'_{sw_{+-}}, \quad I'_{c_{++}}, \quad I'_{c_{+-}}, \quad I'_{d_+^+}, \quad I'_{d_-^+}, \quad I'_\chi, \quad I'_{15}, \\
(I'_{sw_{++}} + I'_{sw_{--}})/2 & : A_4^{+,e/h} + A_5^{+,+,-} + A_5^{-,-,+} + A_5^{+,+,+} + A_5^{-,-,-} \\
& \quad + D_5^{+,-} + D_5^{-,+} \\
(I'_{sw_{+-}} + I'_{sw_{-+}})/2 & : A_4^{-,e/h} + A_5^{-,+,+} + A_5^{+,-,-} + A_5^{+,-,+} + A_5^{-,+,+} \\
& \quad + D_5^{+,+} + D_5^{-,-} \\
(I'_{d_+^+} + I'_{d_-^+})/2 & : D_{4,a}^{+,+} + D_{4,b}^{+,+} + D_{4,c}^{+,+} + D_{4,q}^{-,+} \\
(I'_t + I'_{c_{++}} + I'_{c_{-+}})/2 & : TA_2^3 + A_3^{\pm,+}A_2^2 + A_3^{\pm,-}A_2^2 + 2A_3^{2,e;+,+,+,+} + A_3^{2,e;+,+;+,-} \\
& \quad + 2A_3^{2,e;+,+;+,-} + A_3^{2,e;+,+;+,-} + A_3^{2,e;+,+;+,-} \\
& \quad + 2A_3^{2,e;+,-;+,-} + A_3^{2,e;+,-;+,-} + A_3^{2,h;+,+;+,-} \\
& \quad + A_3^{2,h;+,+;+,-} - A_3^{2,h;+,+;+,-} + A_3^{2,h;+,-;+,-} + A_4^+A_2 \\
& \quad + A_4^-A_2 + TA_3^{+,+}A_2 + TA_3^{-,+}A_2 + A_5^{+,+,+} + A_5^{+,+,-} \\
& \quad + A_5^{-,+,+} + A_5^{-,+,+} - D_5^{+,+} - D_5^{-,+} + D_{4,2}^{+,+}A_2 \\
& \quad + D_{4,2}^{+,-}A_2 - D_{4,0}^{+,+}A_2 - D_{4,0}^{+,-}A_2
\end{aligned}$$

$$\begin{aligned}
(I'_t + I'_{c_{+-}} + I'_{c_{--}})/2 & : TA_2^3 + A_3^{\pm,+} A_2^2 + A_3^{\pm,-} A_2^2 + A_3^{2,e;+,+;+,-} \\
& + A_3^{2,e;+,+;-,-} + 2A_3^{2,e;+,-;+,-} + A_3^{2,e;+,-;-,+} \\
& + 2A_3^{2,e;+,-;-,-} + A_3^{2,e;-,+;-,-} + 2A_3^{2,e;-,-;-,-} \\
& - A_3^{2,h;+,+;+,-} - A_3^{2,h;+,+;-,-} + A_3^{2,h;+,-;-,+} \\
& - A_3^{2,h;-,-;-,-} + A_4^+ A_2 + A_4^- A_2 + TA_3^+ A_2 \\
& + TA_3^- A_2 + A_5^{+,-,+} + A_5^{+,-,-} + A_5^{-,-,+} \\
& + A_5^{-,-,-} - D_5^{+,-} - D_5^{-,-} + D_{4,2}^+ A_2 \\
& + D_{4,2}^- A_2 - D_{4,0}^+ A_2 - D_{4,0}^- A_2 \\
((I'_{d_+^+} + I'_{d_+^-} + I'_{d_-^+} + I'_{d_-^-})/2 \\
+ I'_\chi + I'_{15})/2 & : A_3^{+,+,q} + A_3^{-,-,q} + D_{4,q}^{+,-} + D_{4,q}^{-,+}
\end{aligned}$$

**Remark 2.4.3.** *In the  $\mathbb{Z}_2$  setting, we will need an extension to 20 elements of the mod2 reduction of the set of the 15 integer cycles from the previous remark. The extension is by the linear combinations  $I'_{i=16,\dots,20}$  at the end of this list:*

$$\begin{aligned}
I'_t & : A_4 A_2 \\
I'_{sw_{++}} & : A_4^{+,e/h} + D_5^{+,-} + D_5^{-,+} \\
I'_{sw_{+-}} & : A_4^{-,e/h} + D_5^{+,+} + D_5^{-,-} \\
I'_{c_{++}} & : A_4^+ A_2 + D_4^{-,+} A_2 + D_{4,0}^{+,+} A_2 + D_{4,2}^{+,+} A_2 + D_{4,l}^{+,+} A_2 + D_{4,r}^{+,+} A_2 \\
I'_{c_{+-}} & : A_4^- A_2 + D_4^{-,-} A_2 + D_{4,0}^{+,-} A_2 + D_{4,2}^{+,-} A_2 + D_{4,l}^{+,-} A_2 + D_{4,r}^{+,-} A_2 \\
I'_{d_+^+} & : D_5^{+,+} + D_5^{-,+}
\end{aligned}$$

$$\begin{aligned}
I'_{d_{\pm}^+} & : D_5^{+,-} + D_5^{-,-} \\
I'_{\chi} & : D_{4,a}^+ + D_{4,b}^+ + D_{4,c}^+ + D_{4,q}^- + A_3^q \\
I'_{15} & : A_3^{+,+,q} + A_3^{+,-,q} + A_3^{-,+,q} + A_3^{-,-,q} \\
(I'_{sw_{++}} + I'_{sw_{--}})/2 & : A_4^{+,e/h} + A_5^{+,+,-} + A_5^{-,-,+} + A_5^{+,+,+} + A_5^{-,-,-} \\
& \quad + D_5^{+,-} + D_5^{-,+} \\
(I'_{sw_{+-}} + I'_{sw_{-+}})/2 & : A_4^{-,e/h} + A_5^{-,+,+} + A_5^{+,-,-} + A_5^{+,-,+} + A_5^{-,+,+} \\
& \quad + D_5^{+,+} + D_5^{-,-} \\
(I'_{d_+^+} + I'_{d_+^-})/2 & : D_{4,a}^{+,+} + D_{4,b}^{+,+} + D_{4,c}^{+,+} + D_{4,q}^{-,+} \\
(I'_t + I'_{c_{++}} + I'_{c_{-+}})/2 & : TA_2^3 + A_3^{\pm,+} A_2^2 + A_3^{\pm,-} A_2^2 + A_3^{2,e/h;+,+;+,-} \\
& \quad + A_3^{2,e/h;+,+;-,-} + A_3^{2,e/h;+,-;-,+} + A_3^{2,e/h;-,+;-,-} \\
& \quad + A_4^+ A_2 + A_4^- A_2 + TA_3^{\pm,+} A_2 + A_5^{+,+,\pm} + A_5^{-,-,\pm} \\
& \quad + D_5^{+,+} + D_5^{-,+} + D_{4,2}^{+,+} A_2 + D_{4,2}^{+,-} A_2 + D_{4,0}^{+,+} A_2 \\
& \quad + D_{4,0}^{+,-} A_2 \\
(I'_t + I'_{c_{+-}} + I'_{c_{--}})/2 & : TA_2^3 + A_3^{\pm,+} A_2^2 + A_3^{\pm,-} A_2^2 + A_3^{2,e/h;+,+;+,-} \\
& \quad + A_3^{2,e/h;+,+;-,-} + A_3^{2,e/h;+,-;-,+} + A_3^{2,e/h;-,+;-,-} \\
& \quad + A_4^+ A_2 + A_4^- A_2 + TA_3^{\pm,-} A_2 + A_5^{+,-,\pm} + A_5^{-,-,\pm} \\
& \quad + D_5^{+,-} + D_5^{-,-} + D_{4,2}^{+,+} A_2 + D_{4,2}^{+,-} A_2 + D_{4,0}^{+,+} A_2 \\
& \quad + D_{4,0}^{+,-} A_2 \\
((I'_{d_+^+} + I'_{d_+^-} + I'_{d_-^+} + I'_{d_-^-})/2) & \\
+ I'_{\chi} + I'_{15})/2 & : A_3^{+,+,q} + A_3^{-,-,q} + D_{4,q}^{-,+} + D_{4,q}^{-,-}
\end{aligned}$$

$$\begin{aligned}
I'_{16} & : TA_2^2 + A_3^{-,+q} + A_3^{-,-q} + D_{4,b}^{+,+} + D_{4,b}^{+,-} \\
I'_{17} & : TA_2^3 + TA_3^{\pm,-}A_2 + D_4^{-,+}A_2 + D_4^{-,-}A_2 \\
& \quad + D_{4,1}^{+,+}A_2 + D_{4,1}^{+,-}A_2 \\
I'_{18} & : A_3^{2,e/h;+,+,+,+} + A_3^{2,e/h;+,+,+,-} + A_3^{2,e/h;+,+,-,+} \\
& \quad + A_3^{2,e/h;+,+,-,-} + A_3^{2,e/h;+,-,+,+} + A_3^{2,e/h;+,-,-,+} \\
& \quad + A_3^{2,e/h;+,-,-,-} + A_3^{2,e/h;-,+,-,+} + A_3^{2,e/h;-,-,-,-} \\
& \quad + A_3^{2,e/h;-,-,-,-} + A_5^{-,+,\pm} + A_5^{-,-,\pm} \\
I'_{19} & : A_2^4 + A_3^{\pm,-}A_2^2 + A_3^{2,e/h;+,-,+,+} + A_3^{2,e/h;+,-,-,-} \\
& \quad + A_3^{2,e/h;-,-,-,-} \\
I'_{20} & : A_4^+A_2
\end{aligned}$$

Along with the first 15, the last 5 expressions here turn out to be  $\mathbb{Z}_2$  discriminantal cycles. The set of all 20 is linearly independent over  $\mathbb{Z}_2$ . In Chapter 7, we will find integral geometric interpretations for 4 elements of the  $\mathbb{Z}_2$  span of the 20 which are linearly independent modulo the span of the first 15.

## 2.5 Ranks of spaces of the discriminantal cycles

We now formulate the main results of this thesis. Their proofs are given in Chapter 3. All statements in this section refer to any particular connected component of the space  $\mathcal{L}(M, T^*N, N)$ . Here,  $M$  and  $N$  are oriented

and without boundaries, and  $M$  is compact. We introduce the notation  $\mathcal{D}(M, T^*N, N; \mathbb{K})$  for the space of discriminantal cycles in  $\mathcal{L}(M, T^*N, N)$  with coefficients  $\mathbb{K} = \mathbb{Q}, \mathbb{Z}, \mathbb{Z}_2$ .

Our first main result is:

**Theorem 2.5.1.** *The space  $\mathcal{D}(M, T^*N, N; \mathbb{Q})$  has rank 15. It is spanned by the 14 derivatives from Lemma 2.4.1 and the cycle*

$$I'_{15} : A_3^{+,+,q} - A_3^{+,-,q} - A_3^{-,+,q} + A_3^{-,-,q}.$$

**Corollary 2.5.2.** *The space  $\mathcal{D}(M, T^*N, N; \mathbb{Z})$  has rank 15. It is spanned by the 15 discriminantal cycles from Remark 2.4.2.*

Our second main result is the  $\mathbb{Z}_2$  analogue of Theorem 2.5.1:

**Theorem 2.5.3.** *The space  $\mathcal{D}(M, T^*N, N; \mathbb{Z}_2)$  has rank 20. Its basis is formed by the 20 discriminantal cycles in Remark 2.4.3.*

## 2.6 Bifurcations in 2-parameter families

In this section we consider the bifurcations in 2-parameter families of Lagrangian maps from [9] with the extra decoration  $s$  in the notation of bifurcations containing cuspidal edges. Each family of bifurcations will give us a bifurcation diagram, which in turn gives a cyclic equation on the increments of our local invariants across the codimension 1 strata. We denote the increment by the lower case version of the stratum notation. If a stratum is non



co-orientable its increment will be zero over  $\mathbb{Z}$  and may be non-zero over  $\mathbb{Z}_2$ . Increments across non co-orientable strata will be put in square brackets.

Generally, these cyclic equations allow us to glue certain strata together, since we know that the increments across them are equal. We shall call glued up strata ‘big strata’. If one of the summands of the big stratum is non co-orientable, then the increment of any invariant across the big stratum is zero over  $\mathbb{Z}$ .

The general approach to the study of bifurcations in families of caustics was developed in [22]. If a local family of caustics in  $\mathbb{R}^n$  has  $p$  parameters we can collect it to one big caustic  $\tilde{\mathcal{C}} \subset \mathbb{R}^{n+p}$ . If the family is generic then  $\tilde{\mathcal{C}}$  is the caustic of a generic Lagrangian map germ to  $\mathbb{R}^{n+p}$ . If the germ is a uni-germ such a map is stable and  $\tilde{\mathcal{C}}$  is the caustic of an  $\mathcal{R}_+$ -versal deformation of one of the  $A_k, D_k, E_k$  isolated function singularities with  $k \leq n + p + 1$ . In order to understand all possible  $p$ -parameter bifurcations of uni-germ caustics we must understand all generic maps  $\pi : (\mathbb{R}^{n+p}, \tilde{\mathcal{C}}) \mapsto \mathbb{R}^p$ . Here, the critical value set of  $\pi$  on  $\tilde{\mathcal{C}}$  is the bifurcation diagram of the corresponding family of caustics in  $\mathbb{R}^n$ .

### 2.6.1 Corank 1 bifurcations

First we consider only corank 1 bifurcations in 2-parameter families, that is, bifurcations without  $D_4$  and  $D_5$  points.

### 2.6.1.1 Extra $A_2$ component

The first bifurcation type we will consider is when a smooth  $A_2$  sheet of  $\mathcal{C}$  passes through a point of a codimension 1 bifurcation  $S$  in a generic way. We list the first five bifurcations  $S$  in the table below, where the  $SA_2$  bifurcation diagrams are of the form shown in Figure 16 and only differ in decoration of strata. Here, the vertical coordinate  $\lambda$  is the parameter in the bifurcation  $S$  and the horizontal coordinate  $\mu$  measures the position of the smooth  $A_2$  sheet. These five bifurcations  $S$  result in cyclic equations of the form  $u = v$ , which are listed in the table below. Where the cyclic equations allow us to glue up certain strata together, the big strata are also listed in the table.

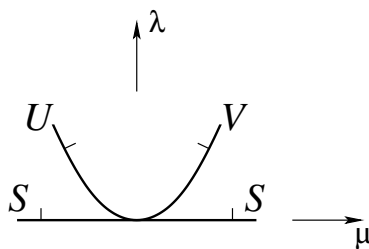


Figure 16: Bifurcation diagram of the families  $SA_2$  obtained from interaction of a smooth  $A_2$  sheet with a codimension 1 bifurcation  $S$ .

$S$	$r$	cyclic equation	big stratum
1. $TA_2^{3,r}$	2, 3	$[a_2^{4,2}] = a_2^{4,3} = a_2^{4,4}$	$[A_2^4]$
2. $TA_2^{2,e,r}$	0, 1, 2	$ta_2^{3,r+1} = ta_2^{3,r}$	$TA_2^3$
3. $TA_3^{s,\sigma} A_2^{e,r}$	0, 1	$a_3^{s,\sigma} a_2^{2,r+1} = a_3^{s,\sigma} a_2^{2,r}$	$A_3^{s,\sigma} A_2^2$
4. $A_3^{s,\sigma,+,+}$		$ta_3^{s,\sigma} a_2^{e,0} = ta_3^{s,\sigma} a_2^{e,1}$	$TA_3^{s,\sigma} A_2^e$
$A_3^{s,\sigma,-,-}$		$ta_3^{s,\sigma} a_2^{h,0} = ta_3^{s,\sigma} a_2^{h,1}$	$TA_3^{s,\sigma} A_2^h$
5. $A_4^{\varepsilon,e}$		$a_4^{s,\sigma} a_2^0 = a_4^{-s,-\sigma} a_2^1$	

#### 2.6.1.1.1 Example: Gluing up the $A_3^{s,\sigma} A_2^2$ strata.

We now explain in detail how one of the five bifurcations  $S$  produces a bifurcation diagram shown in Figure 16. Consider the third row of the table above, that is, when  $S = TA_3^{s,\sigma} A_2^{e,r}$ , setting  $r = 1$  and passing a smooth  $A_2$  sheet through it. As explained earlier we set the vertical coordinate  $\lambda$  to be the parameter in the  $TA_3^{s,\sigma} A_2^{e,1}$  bifurcation and the horizontal coordinate  $\mu$  measures the position of the smooth  $A_2$  sheet, as shown in Figure 17. By inspection of Figure 17 we see the  $A_3^{s,\sigma} A_2^2$  discriminantal stratum is a parabola since it follows the parabolic shape of the cuspidal edge in  $TA_3^{s,\sigma} A_2^{e,1}$ . The two bounded regions corresponding to the two  $A_3 A_2^2$  bifurcations are best seen at the central ( $\mu = 0$ ) position of the smooth sheet when  $\lambda > 0$ : the left has one face co-oriented outwards, and the right has two of them. Therefore,  $U = A_3^{s,\sigma} A_2^{2,1}$  and  $V = A_3^{s,\sigma} A_2^{2,2}$ .

A similar analysis can be done for the  $TA_3^{s,\sigma} A_2^{e,0}$  bifurcation. Both results

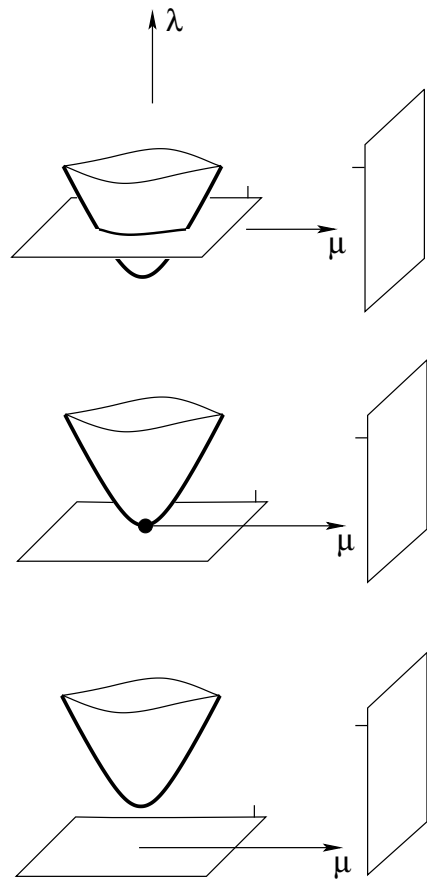


Figure 17: A  $TA_3^{s,\sigma}A_2^{e,1}$  bifurcation interacting with a smooth  $A_2$  sheet.

together give us equation **3** in the table above and create the big stratum  $A_3^{s,\sigma} A_2^2$ .

### 2.6.1.1.2 Passing a smooth $A_2$ sheet through $A_5^{s,\sigma,-}$ and $A_3^{2,e;s,+;s',-}$ .

Passing a smooth  $A_2$  sheet through  $A_5^{s,\sigma,-}$  and  $A_3^{2,e;s,+;s',-}$  yields bifurcation diagrams different from the previous cases. Therefore we consider  $A_5^{s,\sigma,-}$  in detail and state the result in the  $A_3^{2,e;s,+;s',-}$  case (see [9] or [10] for its bifurcation diagram).

Similar to the previous case, Figure 18 shows how an  $A_5^{s,\sigma,-}$  bifurcation interacts with a smooth  $A_2$  sheet. By inspection of Figure 18 we see that we will have  $A_4 A_2$  and  $A_3 A_2^2$  degenerations during the interaction. Recall  $A_5^{s,\sigma,-}$  has normal form  $F = s(x^6 - \lambda x^4 + vx^3 + wx^2 + ux)$ , and  $v$  in this formula is the horizontal coordinate in the target of our Lagrangian maps, so that the extra smooth  $A_2$  sheet in the figure is  $v = \mu$ . If we assign weights  $w_x = 1, w_u = 5, w_v = 3, w_w = 4$  and  $w_\lambda = 2$  our normal form  $F$  becomes quasi-homogeneous and our parameters have weight  $w_\lambda = 2$  and  $w_\mu = 3$ . Hence, the  $A_4 A_2$  and  $A_3 A_2^2$  strata are semicubical parabolas with the equations  $\lambda^3 = \text{const} \cdot \mu^2$ , as shown in Figure 19.

Since we are working with  $A_5^{s,\sigma,-}$  we know from the relation  $(t, \tau) = \text{writhe}(-s, -\sigma)$  that the two swallowtails have sign  $(s, \sigma)$ . Therefore, the strata in Figure 19 will have decoration  $(s, \sigma)$ . We also know the  $A_5^{s,\sigma,-}$  singularity occurs when  $\lambda = 0$ , hence in Figure 19 it is depicted as a horizontal line. Finally, the co-orientation of the strata are found by calculating the increment

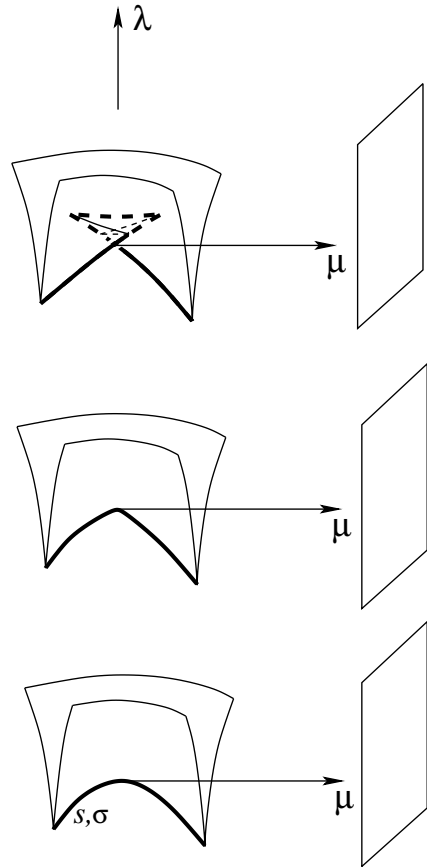


Figure 18: An  $A_5^{s,\sigma,-}$  bifurcation interacting with a smooth  $A_2$  sheet.

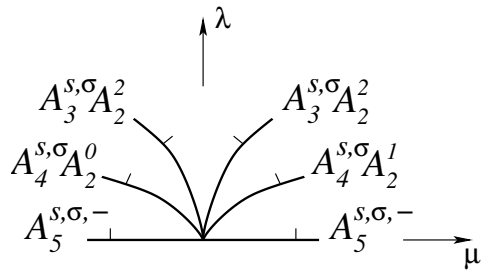


Figure 19: Bifurcations obtained from interaction of a smooth  $A_2$  sheet with  $A_5^{s,\sigma,-}$ .

of the number of  $A_3A_2$  points across the strata. Figure 19 yields the cyclic equation

$$\mathbf{6.} \quad a_4^{s,\sigma} a_2^0 = a_4^{s,\sigma} a_2^1.$$

We see that we are able to use equations **5** and **6** to create the big stratum  $A_4^\varepsilon A_2 = A_4^{s,\sigma} A_2 + A_4^{-s,-\sigma} A_2$  where  $\varepsilon = s\sigma$ .

By similar calculations the interaction of passing a smooth  $A_2$  sheet through  $A_3^{2,e;s,+;s',-}$  yields the cyclic equation

$$\mathbf{7.} \quad 2a_3^{s,+} a_2^2 = 2a_3^{s',-} a_2^2$$

which allows us to create the big stratum  $A_3A_2^2$  over  $\mathbb{Z}$ .

### 2.6.1.2 Cubic bifurcations

We now explain in detail an example of obtaining a cubic bifurcation for  $A_4^{\varepsilon,e}$ . Afterwards we will state the remaining results without explanation (see [10]) since the calculations for all the different bifurcations  $S$  are the same and only differ by the strata involved in the bifurcation diagram.

The singularity  $A_4^{\varepsilon,e}$  has generating family  $F = x^5 + (w^2 - \lambda)x^3 + vx^2 + ux$ . Writing  $w^3$  instead of  $w^2$ , we obtain a codimension 2 uni-germ, with a Lagrangian-versal deformation  $F = x^5 + (w^3 + \lambda_1 w + \lambda_2)x^3 + vx^2 + ux$ . We know the  $A_4^{\varepsilon,e}$  strata occurs when the coefficients of  $x$  and  $x^2$  equal zero

and the coefficient of  $x^3$  has a double root as a polynomial in  $w$ , that is, if  $4\lambda_1^3 + 27\lambda_2^2 = 0$ . From Figure 11 we see that at each of the two  $A_4$  points two cuspidal edges of opposite pairs of signs meet. Hence, each swallowtail has decoration  $A_4^\varepsilon$  with  $\varepsilon = s\sigma$ . We detect if the stratum is elliptic or hyperbolic by comparing our normal form to normal forms of  $A_3^{\varepsilon,e/h}$  in Section 2.3.1.1.

Finally, we co-orient the strata to the side where  $w^3 + \lambda_1 w + \lambda_2 = 0$ , that is the coefficient of  $x^3$  equaling zero, has the greater number of real roots. Hence, we obtain the bifurcation diagram in Figure 20, which yields equation 8 in the list below.

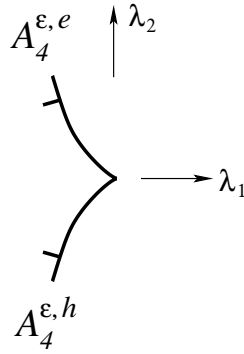


Figure 20: Bifurcation diagram of a cubic analogue of the  $A_4^{\varepsilon,e}$  bifurcation.

$S$	Equation	Big stratum
8. $A_4^{\varepsilon,e}$	$a_4^{\varepsilon,e} = a_4^{\varepsilon,h}$	$A_4^{\varepsilon,e/h} = A_4^{\varepsilon,e} + A_4^{\varepsilon,h}$
9. $A_3^{s,\sigma,+,\pm}$	$a_3^{s,\sigma,+,+} = a_3^{s,\sigma,+,-} = a_3^{s,\sigma,-,-}$	$A_3^{s,\sigma,q} = A_3^{s,\sigma,+,+} + A_3^{s,\sigma,+,-} + A_3^{s,\sigma,-,-}$
10. $TA_3^{s,\sigma} A_2^e$	$ta_3^{s,\sigma} a_2^e = ta_3^{s,\sigma} a_2^h$	$TA_3^{s,\sigma} A_2 = TA_3^{s,\sigma} A_2^e + TA_3^{s,\sigma} A_2^h$
11. $TA_2^{2,e,r}, TA_2^{2,h,r}$	$ta_2^{2,e,2} = -ta_2^{2,e,0} = ta_2^{2,h,0}$ $ta_2^{2,e,1} = [ta_2^{2,h,1}]$	$TA_2^{2,opp} = TA_2^{2,e,2} - TA_2^{2,e,0} + TA_2^{2,h,0}$ $[TA_2^{2,dir}] = TA_2^{2,e,1} + [TA_2^{2,h,1}]$



For the big strata here we have introduced a new notation. We let  $q$  stand for quadratic,  $dir$  = direct for the tangency between two sheets with coinciding co-orientations and  $opp$  for similar tangency with opposite co-orientations.

### 2.6.1.3 Multi-germ families: Non-transversal interactions with a cuspidal edge

The three codimension 2 events that occur when the plane  $\Pi$  tangent to the critical point set at its edge point is in a special position with other local components of  $\mathcal{C}$  are:

1. the plane  $\Pi$  coincides with the plane tangent to a smooth  $A_2$  sheet;
2. the plane  $\Pi$  contains the tangent direction of the line of transversal intersection of two  $A_2$  sheets;
3. the plane  $\Pi$  contains the tangent direction of another cuspidal edge curve.

Figure 21 gives an example of the bifurcation diagram for the last case, which we will study in detail (again, see [9] or [10] for the other cases' bifurcation diagrams). We can assume our cuspidal edge surface  $\Gamma$  has equation  $x^3 = y^2$  in the 3-space. We project it down to the  $xy$ -plane by the map  $(x, y, z) \mapsto (x, y)$ . We also introduce a curve that locally represents the projection of the other cuspidal edge called  $C$  with equation  $y + \alpha x + \beta = 0$  where  $\alpha$  and  $\beta$  are parameters. We now inspect diagrams in the  $xy$ -plane showing how  $\Gamma$  and  $C$  interact for various values of  $\alpha$  and  $\beta$ , see Figure 22. It is obvious from Figure

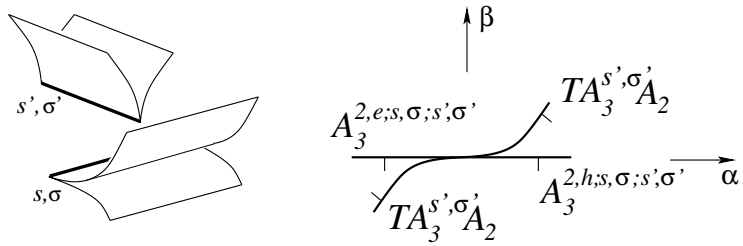


Figure 21: Codimension 2 degeneration due to special position of a cuspidal edge with respect to the tangent plane at an edge point.

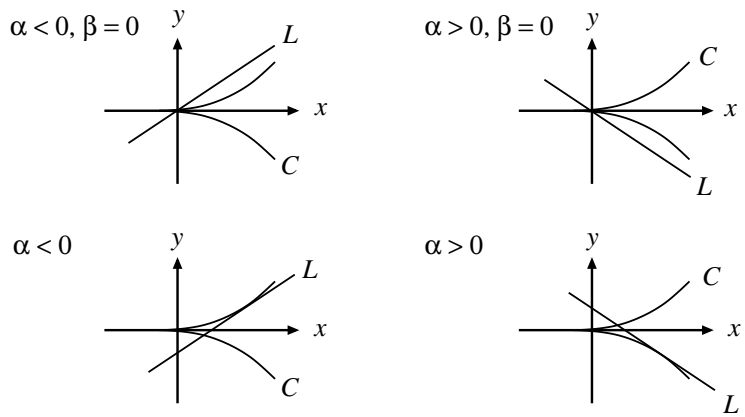


Figure 22:  $\Gamma$  and  $C$  interacting for various values of  $\alpha$  and  $\beta$  in the projected  $xy$ -plane.

22 that at the following values of  $\alpha$  and  $\beta$  we have these bifurcations:

$$\begin{aligned}
\alpha < 0, \beta = 0 & : A_3^{2,e;s,\sigma;s',\sigma'} \\
\alpha > 0, \beta = 0 & : A_3^{2,h;s,\sigma;s',\sigma'} \\
\alpha < 0, \beta & : TA_3^{s',\sigma'} \\
\alpha > 0, \beta & : TA_3^{s',\sigma'}
\end{aligned}$$

In order to determine the shape of the strata we assign weights to our parameters. The projected surface  $\Gamma$  is quasi-homogeneous if  $w_x = 2$  and  $w_y = 3$  and therefore, our parameters have weights  $w_\alpha = 1$  and  $w_\beta = 3$ . Hence, the  $TA_3^{s',\sigma'}$  strata will be a cubic curve  $\beta = \text{const} \cdot \alpha^3$  and  $A_3^{2,e;s,\sigma;s',\sigma'} / A_3^{2,h;s,\sigma;s',\sigma'}$  will be the horizontal line  $\beta = 0$ . The signs of the strata follow from the signs of the cuspidal edges participating. Finally, the co-orientations of the strata are found by looking at the increments of the number of  $A_3A_2$  points across the strata. This yields the cyclic equations **14** shown below.

Respectively cases 1. and 2. give equations **12** and **13**.

$$\begin{aligned}
\mathbf{12.} \quad ta_2^{2,opp} & = [ta_2^{2,dir}] \\
\mathbf{13.} \quad 2ta_2^3 & = 2a_3^{+,+}a_2^2 \\
& = 2a_3^{+,-}a_2^2 \\
& = 2a_3^{-,+}a_2^2 \\
& = 2a_3^{-,-}a_2^2
\end{aligned}$$

$$\begin{aligned}
14. \quad 2ta_3^{+,+}a_2 &= a_3^{2,e;+,+,+,+} - [a_3^{2,h;+,+,+,+}] \\
&= a_3^{2,e;+,-,+,+} - a_3^{2,h;+,-,+,+} \\
&= a_3^{2,e;- ,+,+,+} - a_3^{2,h;- ,+,+,+} \\
&= a_3^{2,e;-,-,+,+} - a_3^{2,h;-,-,+,+} \\
2ta_3^{+,-}a_2 &= a_3^{2,e;+,+,+,-} - a_3^{2,h;+,+,+,-} \\
&= a_3^{2,e;+,-,+, -} - [a_3^{2,h;+,-,+, -}] \\
&= a_3^{2,e;- ,+,+, -} - a_3^{2,h;- ,+,+, -} \\
&= a_3^{2,e;-,-,+, -} - a_3^{2,h;-,-,+, -} \\
2ta_3^{-,+}a_2 &= a_3^{2,e;+,+,-,+} - a_3^{2,h;+,+,-,+} \\
&= a_3^{2,e;+,-,-,+} - a_3^{2,h;+,-,-,+} \\
&= a_3^{2,e;- ,+,-,+} - [a_3^{2,h;- ,+,-,+}] \\
&= a_3^{2,e;-,-,-,+} - a_3^{2,h;-,-,-,+} \\
2ta_3^{-,-}a_2 &= a_3^{2,e;+,+,-,-} - a_3^{2,h;+,+,-,-} \\
&= a_3^{2,e;+,-,-,-} - a_3^{2,h;+,-,-,-} \\
&= a_3^{2,e;- ,+,-,-} - a_3^{2,h;- ,+,-,-} \\
&= a_3^{2,e;-,-,-,-} - [a_3^{2,h;-,-,-,-}]
\end{aligned}$$

Equation **12** enables us to create the big stratum,  $[TA_2^2] = TA_2^{2,opp} + [TA_2^{2,dir}]$  for mod2 invariants only.

#### 2.6.1.4 Multi-germ families: Interaction with a swallowtail

Now let us consider how a swallowtail interacts with other local components of  $\mathcal{C}$ . Figure 23 gives an example of its interaction with a cuspidal edge.

We consider this in detail below, which yields equations **17**. Other local components of  $\mathcal{C}$  could be a smooth sheet (Figure 24 left, equations **15**) or a transversal intersection of two smooth sheets (Figure 24 right, equations **16**).

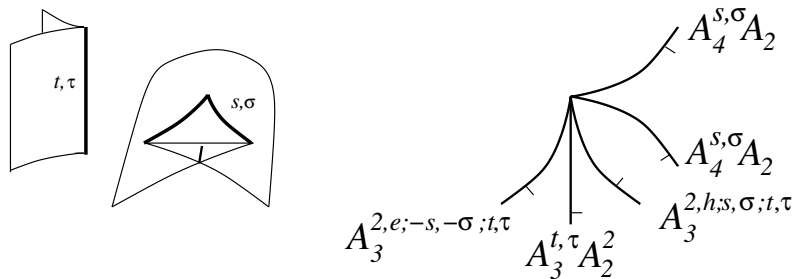


Figure 23: Codimension 2 degeneration of a swallowtail interacting with a cuspidal edge.

We explain in detail how we obtain Figure 23. We let  $\Pi$  be the plane tangent to the surface at the swallowtail point. We make a coordinate change so that the cuspidal edge curve  $C$  is straight and perpendicular to  $\Pi$ . We then project the swallowtail in the direction of  $C$  to the plane  $\Pi$ . Under this projection the swallowtail gives a semi-cubical parabola and its bisector. This semi-cubical parabola and bisector represent the special positions of  $C$  meeting the cuspidal edges and self-intersection set of the swallowtail, which give the  $A_3^{2,e/h}$  and  $A_3 A_2^2$  strata.

The  $A_4 A_2$  bifurcations have been located in Figure 23 from a slightly different perspective. We keep the same projected plane  $\Pi$  as described before but this time we are interested in what happens at the origin of the plane, that is at the projected  $A_4$  point. We consider the cuspidal edge surface as

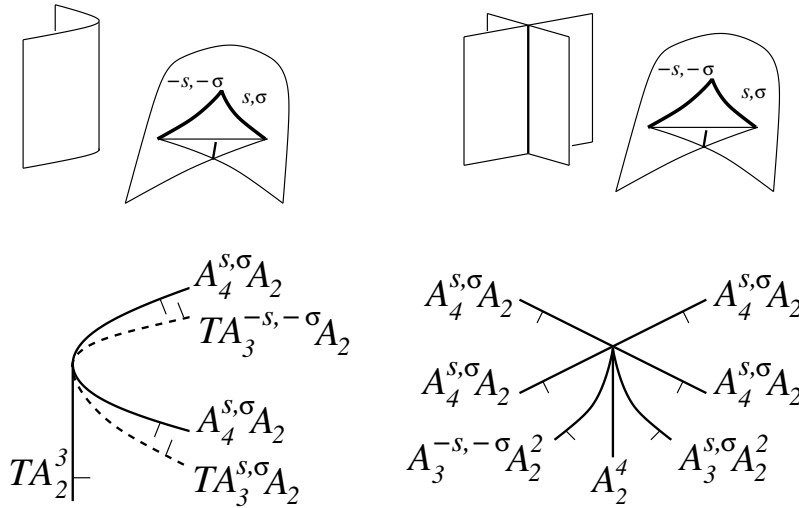


Figure 24: Codimension 2 degenerations of a swallowtail interacting with a smooth sheet and the transversal intersection of two smooth sheets.

a vertical cylinder that projects to the plane  $\Pi$  as a semi-cubical parabola,  $E$ . We then move  $E$  by parallel translations in the plane  $\Pi$  to see how it goes through the swallowtail point. This produces the extra half branches shown in Figure 23 that represents the swallowtail point and cuspidal edge folds meeting.

The decorations of the strata are from the decorations of the cuspidal edges participating in the bifurcation. Finally, the co-orientations are found by looking at the increments of the number of  $A_3A_2$  points across strata.

For the three cases listed before we obtain the cyclic equations:

$$\begin{aligned}
15. \quad 2a_4^{+,+}a_2 &= ta_3^{+,+}a_2 + ta_3^{-,-}a_2 + ta_2^3 \\
2a_4^{+,-}a_2 &= ta_3^{+,-}a_2 + ta_3^{-,+}a_2 + ta_2^3 \\
2a_4^{-,+}a_2 &= ta_3^{-,+}a_2 + ta_3^{+,-}a_2 + ta_2^3 \\
2a_4^{-,-}a_2 &= ta_3^{-,-}a_2 + ta_3^{+,+}a_2 + ta_2^3 \\
16. \quad a_3^{-,-}a_2^2 &= a_3^{+,+}a_2^2 + [a_2^4] \\
a_3^{-,+}a_2^2 &= a_3^{+,-}a_2^2 + [a_2^4] \\
a_3^{+,-}a_2^2 &= a_3^{-,+}a_2^2 + [a_2^4] \\
a_3^{+,+}a_2^2 &= a_3^{-,-}a_2^2 + [a_2^4] \\
17. \quad 2a_4^{+,+}a_2 &= a_3^{+,+}a_2^2 + a_3^{2,e;-,-;+,+} + [a_3^{2,h;+,+;+,+}] \\
&= a_3^{+,-}a_2^2 + a_3^{2,e;-,-;+,-} + a_3^{2,h;+,+;+,-} \\
&= a_3^{-,+}a_2^2 + a_3^{2,e;-,-;-,+} + a_3^{2,h;+,+;-,+} \\
&= a_3^{-,-}a_2^2 + a_3^{2,e;-,-;-,-} + a_3^{2,h;+,+;-,-} \\
2a_4^{+,-}a_2 &= a_3^{+,+}a_2^2 + a_3^{2,e;-,+;+,+} + a_3^{2,h;+,-;+,+} \\
&= a_3^{+,-}a_2^2 + a_3^{2,e;-,+;+,-} + [a_3^{2,h;+,-;+,-}] \\
&= a_3^{-,+}a_2^2 + a_3^{2,e;-,+;-,+} + a_3^{2,h;+,-;-,+} \\
&= a_3^{-,-}a_2^2 + a_3^{2,e;-,+;-,-} + a_3^{2,h;+,-;-,-} \\
2a_4^{-,+}a_2 &= a_3^{+,+}a_2^2 + a_3^{2,e;+,-;+,+} + a_3^{2,h;-,+;+,+} \\
&= a_3^{+,-}a_2^2 + a_3^{2,e;+,-;+,-} + a_3^{2,h;-,+;+,-} \\
&= a_3^{-,+}a_2^2 + a_3^{2,e;+,-;-,+} + [a_3^{2,h;-,+;-,+}] \\
&= a_3^{-,-}a_2^2 + a_3^{2,e;+,-;-,-} + a_3^{2,h;-,+;-,-}
\end{aligned}$$

$$\begin{aligned}
2a_4^{-,-}a_2 &= a_3^{+,+}a_2^2 + a_3^{2,e;+,+;+,+} + a_3^{2,h;-,+;+,+} \\
&= a_3^{+,-}a_2^2 + a_3^{2,e;+,+;+,-} + a_3^{2,h;-,+;+,-} \\
&= a_3^{-,+}a_2^2 + a_3^{2,e;+,+;-,+} + a_3^{2,h;-,+;-,+} \\
&= a_3^{-,-}a_2^2 + a_3^{2,e;+,+;-, -} + [a_3^{2,h;-,+;-, -}]
\end{aligned}$$

### 2.6.1.5 Uni-germs of codimension 2

We now consider uni-germs of codimension 2. The three 2-parameter deformations shown in Figure 25 are of generating families induced from versal deformations of  $A_5$ ,  $A_4$  and  $A_3$  function singularities. They were obtained in [10] and have been modified to the Lagrangian setting for our case. As before,  $\varepsilon = s\sigma$ . In particular, in the top diagram we set  $s = +$  and therefore  $\varepsilon = \sigma$ . The boxed signs in the bottom row of Figure 25 correspond to the choice of the signs of the coefficients of  $v^2$  and  $w^2$  in the generating family.

We now explain how to construct the bifurcation diagram in the top of Figure 25. Its generating family induced from a versal deformation of  $A_5$  is

$$F = \frac{1}{7}x^7 + \frac{1}{5}(\lambda_1 \pm w + \alpha v)x^5 + \frac{1}{4}\lambda_2x^4 + \frac{1}{3}wx^3 + \frac{1}{2}vx^2 + ux,$$

where  $\alpha \in \mathbb{R}$ . Assigning the weights  $w_x = 1, w_{\lambda_1} = 2, w_{\lambda_2} = 3, w_u = 4, w_v = 5, w_w = 6$ , gives us the principal part

$$\tilde{F} = \frac{1}{7}x^7 + \frac{1}{5}\lambda_1x^5 + \frac{1}{4}\lambda_2x^4 + \frac{1}{3}wx^3 + \frac{1}{2}vx^2 + ux,$$



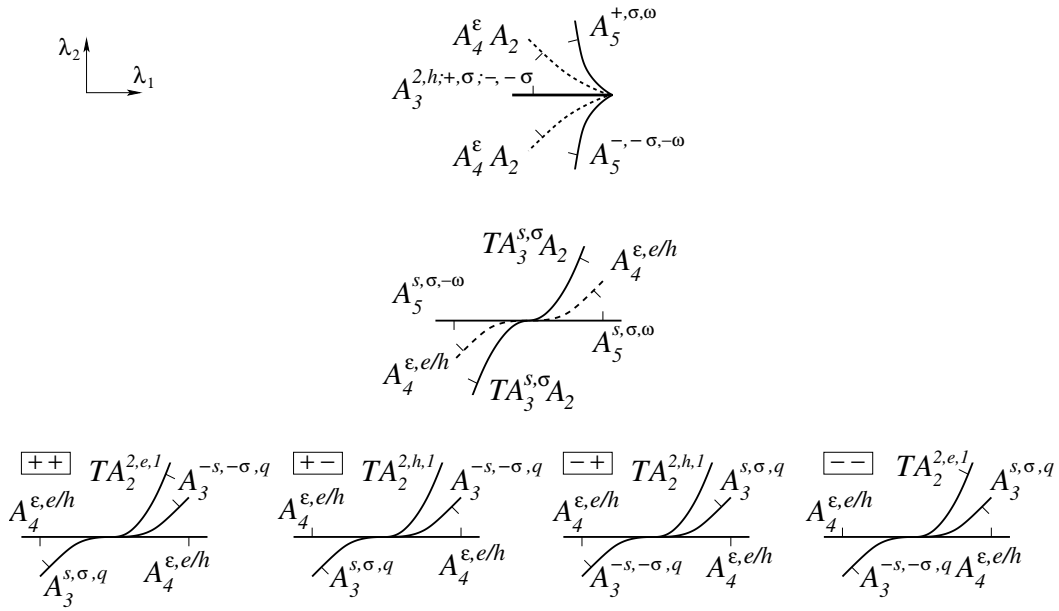


Figure 25: Discriminants of the families

$$\frac{1}{7}x^7 + \frac{1}{5}(\lambda_1 \pm w + \alpha v)x^5 + \frac{1}{4}\lambda_2 x^4 + \frac{1}{3}wx^3 + \frac{1}{2}vx^2 + ux, \quad \alpha \in \mathbb{R};$$

$$s\left(\frac{1}{6}x^6 + \frac{1}{4}wx^4 + \frac{1}{3}(\pm w^2 + \lambda_1 w + \lambda_2)x^3 + \frac{1}{2}vx^2 + ux\right);$$

$$\frac{1}{5}x^5 + \frac{1}{3}vx^3 + \frac{1}{2}(\pm v^2 + \lambda_1 v + \lambda_2 \pm w^2)x^2 + ux.$$

which is sufficient for our considerations. The equation of the source is

$$\tilde{F}_x = 0 \implies x^6 + \lambda_1 x^4 + \lambda_2 x^3 + wx^2 + vx + u = 0.$$

We now compare the coefficients of  $\tilde{F}_x$  to normal forms of certain bifurcations in order to find an equation of the discriminant in the  $\lambda_1\lambda_2$ -plane. In the following cases we assume that  $x = t$  corresponds to the root of maximal multiplicity at the singularity.

$A_5$  stratum:  $(x - t)^5(x + 5t) = x^6 - 15t^2x^4 + 40t^3x^3 - 45t^4x^2 + 24t^5x - 5t^6.$

Equating the coefficients gives us:

$$(\lambda_1, \lambda_2) = (-15t^2, 40t^3)$$

which gives the  $A_5$  stratum as a semicubical parabola in the  $\lambda_1\lambda_2$ -plane. Now, decorations of the  $A_5$  stratum are found by analysing the integral of  $(x - t)^5(x + 5t)$ , which shows us we have an  $A_5^{+, \sigma}$  point for  $t > 0$  and  $A_5^{-, -\sigma}$  for  $t < 0$ . Finally, MAPLE calculations imply that these two bifurcations have opposite writhes.

$A_4A_2$  stratum:  $(x - t)^4(x + 2t)^2 = x^6 - 6t^2x^4 + 4t^3x^3 + 9t^4x^2 - 12t^5x + 4t^6.$

Equating the coefficients:

$$(\lambda_1, \lambda_2) = (-6t^2, 4t^3)$$

which gives the  $A_4A_2$  stratum as another semicubical parabola. MAPLE

calculations show we have opposite signs of  $s$  and  $\sigma$  of the cuspidal edges at  $A_4$  for different signs of  $t$ . However, since  $\varepsilon = s\sigma$ , we decorate both strata with  $A_4^\varepsilon A_2$ .

$A_3^2$  stratum:  $(x-t)^3(x+t)^3 = x^6 - 3t^2x^4 + 3t^4x^2 - t^6$ . Equating the coefficients:

$$(\lambda_1, \lambda_2) = (-3t^2, 0)$$

which gives us the  $A_3^2$  stratum as the negative  $\lambda_1$ -axis. By the symmetry of the function it is apparent we have opposite signs  $(s, \sigma)$  in  $A_3$  for different signs of  $t$ . We also detect the stratum is hyperbolic by comparing our normal form  $F$  to the normal forms in Section 2.3.1.1.

Again, the co-orientations are found by looking at the increments of the number of  $A_3A_2$  points across strata. Respectively each row of bifurcation diagrams in Figure 25 gives the cyclic equations,

$$\begin{aligned} 18. \quad & a_3^{2,h;+,\sigma;,-,-\sigma} = a_5^{+,\sigma,\omega} - a_5^{-,-\sigma,-\omega} \\ 19. \quad & 2a_4^{\varepsilon,e/h} = a_5^{s,\sigma,\omega} + a_5^{s,\sigma,-\omega} - 2ta_3^{s,\sigma}a_2 \\ 20. \quad & a_3^{s,\sigma,q} - a_3^{-s,-\sigma,q} = [ta_2^2] \end{aligned}$$

## 2.6.2 Corank 2 bifurcations

We now consider bifurcations in 2-parameter families that contain  $D_4$  and  $D_5$  points.

### 2.6.2.1 Uni-germs: $D_4$

Consider the cubic analogues of the quadratic  $D_4^\pm$  singularities introduced in Section 2.3.2,

$$F = \pm x^2 y + \frac{1}{3} y^3 + \frac{\varphi}{2} y^2 + \beta y + \delta x \quad (3)$$

where

$$\varphi = \alpha^3 + \alpha r + t \pm \beta + a\delta, \quad a \in \mathbb{R}, a \neq \pm 1. \quad (4)$$

Here  $r, t$  are parameters that give us an  $rt$ -family of caustics in  $\mathbb{R}_{\alpha, \beta, \delta}^3$  with the big caustic in  $\mathbb{R}^5$ . According to Section 2.3.2.1 our normal form  $F$  produces three bifurcations:

1.  $D_4^-$ ;
2.  $D_4^+$  when  $|a| < 1$ ;
3.  $D_4^+$  when  $|a| > 1$ .

Now, we know a  $D_{4,q}^\pm$  singularity occurs when the coefficients of  $x, y$  are zero and the coefficient of  $y^2$  has a double root as a polynomial in  $\alpha$ , that is, if  $4r^3 + 27t^2 = 0$ . We co-orient the strata to the side where the number of  $D_4$  points of the caustic is greater. The bifurcation diagrams in the  $rt$ -plane are shown in Figure 26: the left is for  $D_4^-$ , the final two are for  $D_4^+$  with the middle when  $|a| < 1$  and the right when  $|a| > 1$ .

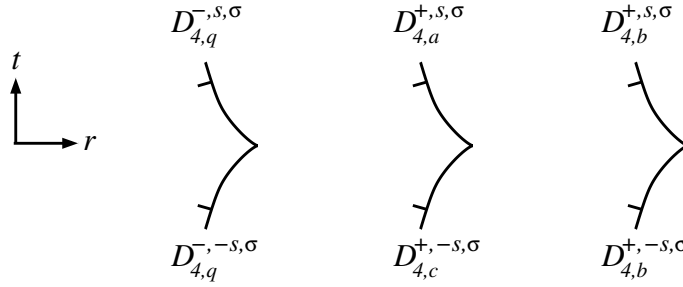


Figure 26: Bifurcations diagrams of the cubic analogues of the quadratic  $D_4^\pm$  singularities.

We now explain where the decorations of the strata come from. For all three cases let the top branch of the bifurcation diagrams have signs  $s, \sigma$  and recall the generating family

$$F = \pm x^2 y + \frac{1}{3} y^3 + \frac{1}{2} (\alpha^3 + \alpha r + t \pm \beta + a\delta) y^2 + \beta y + \delta x.$$

Setting  $(r, t) \mapsto (r, -t)$  to examine the symmetry of the bifurcation diagrams, we see that in order to preserve the generating family we set

$$F \mapsto -F, x \mapsto -x, y \mapsto -y, \alpha \mapsto -\alpha, \beta \mapsto -\beta, \delta \mapsto \delta.$$

Since  $F \mapsto -F$  the sign  $s$  changes as  $t$  changes from positive to negative. We also see that since the orientation of the source and target remain the same, so does the degree  $\sigma$ . Therefore, we conclude that if the upper branch in Figure 26 has signs  $s, \sigma$  the lower branch will have  $-s, \sigma$ .

Now, recall the normal forms of the  $D_4$  uni-germs in Section 2.3.2,

$$G = s(\pm x^2 y + \frac{1}{3} y^3 + \varphi \frac{y^2}{2} + v y + u x),$$

where,  $\varphi$  respectively is:

- $D_{4,q}^{-,s,\sigma}$  :  $\lambda - w^2 \pm v + \alpha u$ ;
- $D_{4,a}^{+,s,\sigma}$  :  $\lambda - w^2 + v + \alpha u$ ,  $|\alpha| < 1$ ;
- $D_{4,b}^{+,s,\sigma}$  :  $\lambda - w^2 \pm v + \alpha u$ ,  $|\alpha| > 1$ ;
- $D_{4,c}^{+,s,\sigma}$  :  $\lambda - w^2 - v + \alpha u$ ,  $|\alpha| < 1$ .

Comparing our  $F$  with the normal forms of the  $D_4$  uni-germs we see that  $\beta = v$  and  $\delta = u$ . Hence when we do the transformation  $\beta \mapsto -\beta$  when considering the symmetry of the bifurcation diagram under the transformation  $(r, t) \mapsto (r, -t)$  we are actually changing the sign of  $v$ . Therefore for the  $D_4^+$  case when  $|a| < 1$  one of the branches will be  $D_{4,a}^{+,s,\sigma}$  and the other  $D_{4,c}^{+,-s,-\sigma}$ . For the  $D_4^+$  case when  $|a| > 1$  both branches will be of type  $D_{4,b}^+$  since changing the sign of  $v$  does not affect the type of bifurcation.

Respectively the bifurcation diagrams produce the cyclic equations

	Equation	Big stratum
<b>21.</b>	$d_{4,q}^{-,s,\sigma} = d_{4,q}^{-,-s,\sigma}$	$D_{4,q}^{-,\sigma}$
	$d_{4,a}^{+,s,\sigma} = d_{4,c}^{+,-s,\sigma}$	
	$d_{4,b}^{+,s,\sigma} = d_{4,b}^{+,-s,\sigma}$	$D_{4,b}^{+,\sigma}$

So far we have only considered  $D_4^+$  uni-germs with the condition that  $a \neq \pm 1$ . We will now remove this constraint by considering (3) stated at the start of this section where

$$\varphi = \pm\alpha^2 \pm \beta \pm \delta + q(\beta, \delta) + t + r\ell(\beta, \delta) + \text{higher quasi-homogeneous terms.}$$

In  $\varphi$ ,  $q$  is a quadratic form that is not divisible by the  $\pm\beta \pm \delta$ , and  $\ell$  is a linear form which is not a multiple of the  $\pm\beta \pm \delta$ . Function  $\varphi$ , as described is such that for  $t = r = 0$  its restriction to one of the self-intersection lines of the purse  $\delta = \pm\beta$  in  $\alpha = 0$  has a Morse point at the origin and this point moves along this line off the origin if  $r \neq 0$ .

For example, set

$$\varphi = \alpha^2 + \beta + \delta \pm \beta^2 + 2r\beta + t. \tag{5}$$

The restriction of  $\varphi$  onto  $\beta = -\delta < 0 = \alpha$  is  $\varphi = \pm\beta^2 + 2r\beta + t$ . This restriction gives a self-intersection line in the  $D_4^+$  singularity, that is one of the arms of the ‘V’ self-intersection locus of the purse, corresponding to  $TA_2^2$ . Hence, the discriminantal stratum  $TA_2^2$  is found by looking at the critical point set of  $\varphi$  on its zero level (that is, a double root in  $\beta$ ) which gives  $r^2 = \pm t$ . Here the sign depends on the sign of  $\pm\beta^2$ . Now since we are only considering the case where  $\beta < 0$  we restrict the discriminantal stratum to  $\beta = \mp r < 0$ . The bifurcation diagrams for the sign choices of the coefficient of  $\beta$  in (5) are shown in Figure 27.

We find the equation of the  $D_{4,q}$  stratum by setting  $\beta = \delta = \psi = 0$  and  $\psi_\alpha = 0$ , giving a discriminantal strata of  $t = 0$ .

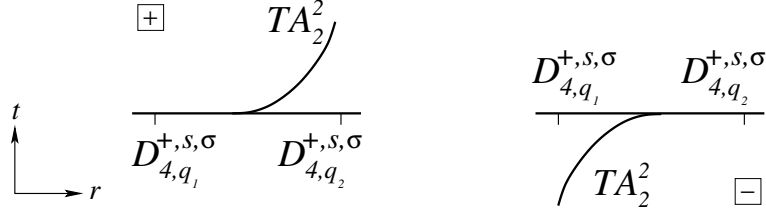


Figure 27: Bifurcation diagrams for the sign choices of the coefficient of  $\beta$  in (5).

Like we did for the other cases of  $D_4^+$  uni-germs, we set the right  $D_4^+$  branches in Figure 27 to have signs  $s, \sigma$ . Then by studying the symmetry of the bifurcation diagram under the transformation  $(r, t) \mapsto (-r, t)$  we see the other branch will be of the same signs. Again, we see that in order to preserve the normal form we do the transformation  $\beta \mapsto -\beta$  which results in a change of sign of  $v$ . Therefore one branch will be of type  $b$  and the other is  $a$  or  $c$  (see previous case for the method). However, due to the symmetry of the bifurcation diagrams we do not specify which branch is of which type.

We co-orient the strata to the side where the number of  $D_4$  points of the caustic is greater. The  $TA_2^2$  stratum does not have co-orientation (we proved its non co-orientability in equations **11** and **12**) and therefore contributes in the *mod2* setting only.



From Figure 27 we obtain the cyclic equations:

$$\begin{aligned}d_{4,a}^{+,s,\sigma} - d_{4,b}^{+,s,\sigma} + [ta_2^2] &= 0; \\d_{4,c}^{+,s,\sigma} - d_{4,b}^{+,s,\sigma} + [ta_2^2] &= 0.\end{aligned}$$

All other sign choices in  $\varphi$  (for  $\alpha^2, \beta, \delta$ ) yield the same cyclic equations. Taking their difference gives us

$$d_{4,a}^{+,s,\sigma} = d_{4,c}^{+,s,\sigma}$$

both over  $\mathbb{Z}$  and  $\mathbb{Z}_2$ . Therefore, the big strata for any coefficients are

$$\begin{aligned}D_{4,a/c}^{+,\sigma} &= D_{4,a}^{+,+,\sigma} + D_{4,a}^{+,-,\sigma} + D_{4,c}^{+,+,\sigma} + D_{4,c}^{+,-,\sigma} \\D_{4,b}^{+,\sigma} &= D_{4,b}^{+,+,\sigma} + D_{4,b}^{+,-,\sigma}\end{aligned}$$

Hence the last cyclic equations reduce to

$$\mathbf{22.} \quad d_{4,a/c}^{+,\sigma} - d_{4,b}^{+,\sigma} + [ta_2^2] = 0$$

### 2.6.2.2 Uni-germs: $D_5$

In this section we will state the basic idea of how we obtain the bifurcation diagrams for  $D_5$  uni-germs, however we will not repeat all necessary calculations of certain strata that can be found in [9]. The main aim of this section is to understand the decorations of the strata which will be explained in detail.

Consider the  $\mathcal{R}_+$ -miniversal deformation of the  $D_5$  function

$$G = s(x^2y + \frac{1}{4}y^4 + \frac{1}{3}\alpha y^3 + \frac{1}{2}\psi y^2 + \beta y + \delta x).$$

We introduce the parameters  $r$  and  $t$  that give us an  $rt$ -family of caustics in  $\mathbb{R}_{\alpha,\beta,\delta}^3$  with the big caustic in  $\mathbb{R}_{\alpha,\beta,\delta,r,t}^5$  being the product of the caustic  $D_5^{s,\sigma}$  and  $\mathbb{R}$ . Here  $\psi|_{r=t=0} := \psi_0(\alpha, \beta, \delta)$  is  $k\alpha^2$ ,  $k = \text{const} \neq 0$ , modulo terms of higher quasi-homogeneous order. We take  $\psi = k\alpha^2 + r\alpha + t$  which is sufficient for our considerations. Taking the resultant of  $G_x = 0$  and  $G_y = 0$  yields the function

$$\Psi = y^2(y^3 + \alpha y^2 + \psi y + \beta) + \frac{\delta^2}{4} \quad (6)$$

which we use to describe all degenerations in  $G$  in terms of those in  $\Psi$ . Formally, the big caustic in  $\mathbb{R}_{\alpha,\beta,\delta,r,t}^5$  corresponds to those polynomials  $\Psi$  which have either the root  $y = 0$  of multiplicity  $k > 2$  or a root  $y \neq 0$  of multiplicity  $k > 1$ . These two options result in the big caustic and its transversal sections having respectively  $D_k$  or  $A_k$  points. We should note we consider the  $D_3$  singularity in  $\mathbb{R}_{\alpha,\beta,\delta,r,t}^5$  as the  $A_3$  singularity at the origin  $x = y = 0$ .

Consider all degenerations  $X$ , that can occur in  $D_5$ . These strata are in  $\mathbb{R}_{\alpha,\psi,\beta,\delta}^4$  and parametrised in terms of  $\Psi$ . We are interested in their preimage  $\tilde{X}$  in the space  $\mathbb{R}_{\alpha,\beta,\delta,r,t}^5$  under the map

$$(\alpha, \beta, \delta, r, t) \mapsto (\alpha, \psi(\alpha, \beta, \delta, r, t), \beta, \delta),$$

where the dimension of the preimage is one higher. We then find the critical value set  $Y \subset \mathbb{R}_{r,t}^2$  of the restriction of the projection  $\pi : \mathbb{R}_{\alpha,\beta,\delta,r,t}^5 \rightarrow \mathbb{R}_{r,t}^2$  to  $\tilde{X}$ , which gives us the discriminantal stratum in the  $rt$ -plane.

The correspondence  $X \sim Y$  is:

$$\dim X = 0 : D_5 \sim D_5$$

$$\dim X = 1 : D_4^\pm \sim D_{4,q}^\pm \quad A_4 \sim A_4^{e/h} \quad A_3 A_2 \sim T A_3 A_2 \quad D_3 A_2 \sim T D_3 A_2$$

$$\dim X = 2 : A_2^2 \sim T A_2^2 \quad A_3 \sim A_3^q$$

$\dim X = 3$  :  $A_2$ , the regular part of the caustic, cannot have any critical values under  $\pi$  as long as we assume our Lagrangian submanifold  $G_x|_{r=t=0} = G_y|_{r=t=0} = 0$  smooth (and this is so for the family we are considering).

Rather than showing all strata on one bifurcation diagram we will build up a series of bifurcation diagrams in order to make the case easier to analyse.

$D_5$  and  $D_4$  strata of the big caustic, Figure 28. The  $D_5$  singularity occurs in  $\mathbb{R}_{\alpha,\beta,\delta,r,t}^5$  when  $\Psi$  has the zero root of multiplicity 5. Here we let  $\Psi = y^5$  by setting  $\alpha = \psi = \beta = \delta = 0$ . The discriminantal stratum is given by the critical value set  $t = 0$  in the  $rt$ -parameter plane.

Similarly the  $D_4$  singularity occurs when  $\Psi$  has the zero root of multiplicity 4. This time we let  $\Psi = y^5 + \alpha y^4$  by setting  $\psi = \beta = \delta = 0$  which implies  $k\alpha^2 + r\alpha + t = 0$ . Calculating the discriminant of the polynomial in  $\alpha$  yields

the critical value set  $r^2 - 4kt = 0$  which is the  $D_{4,q}^\pm$  stratum in the  $rt$ -parameter plane.

Since the big caustic is the product of the caustic  $D_5^{s,\sigma}$  and  $\mathbb{R}$  all  $D_5$  points are of the same signs. Therefore the  $D_5$  stratum in Figure 28 is  $D_5^{s,\sigma}$ . Now, by looking at the  $D_5^{s,\sigma}$  bifurcation in Figure 13 we see it contains a  $D_{4,q}$  point of signs  $s$  and  $\sigma$ . We therefore conclude that the  $D_{4,q}$  stratum in Figure 28 will have the same decorations as  $D_5^{s,\sigma}$ . However we do not include the sign  $s$  in the  $D_{4,q}^-$  stratum due to equation **21**.

We detect if the  $D_{4,q}$  branches are of type  $D_{4,q}^+$  or  $D_{4,q}^-$  by looking at the sign of the double root of  $\alpha$  in  $\psi$  for each branch and comparing it to the normal forms of  $D_{4,q}^\pm$  uni-germs in Section 2.3.2. We also find if the  $D_{4,q}^+$  branches are of type  $a$  or  $c$  by comparing our normal form for different values of  $k$  to the normal forms of  $D_{4,q}^+$ .

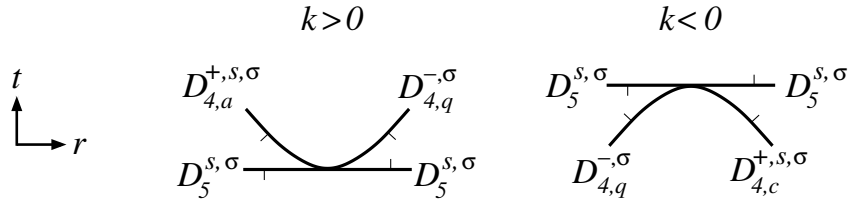


Figure 28: The  $D_5$  and  $D_{4,q}$  strata.

Finally, co-orientation of the  $D_5$  stratum will be explained in the  $A_4$  section. The  $D_{4,q}$  stratum is co-oriented towards the positivity of the discriminant.

$A_4$  stratum, Figure 29. Here we require  $\Psi$  to have the zero root of multiplicity 4. Therefore we parametrise the  $A_4$  stratum in  $\mathbb{R}_{\alpha,\psi,\beta,\delta}^4$  by

$$\Psi = (y - u)^4 \left( y + \frac{u}{4} \right).$$

Equating the coefficients with (6) gives  $(\alpha, \psi, \beta, \delta^2) = (-\frac{15}{4}u, 5u^2, -\frac{5}{2}u^3, u^5)$ . From this we obtain the surface  $k\alpha^2 + r\alpha + t = \frac{16}{45}\alpha^2$ . The critical locus of projecting this surface to  $\mathbb{R}_{rt}^2$  is  $r = -2\alpha(k - \frac{16}{45})$  with  $\alpha < 0$  and is doubled in the  $\delta$ -direction. The discriminantal stratum  $2A_4^{e/h}$  is given by the critical value set  $r^2 - 4t(k - \frac{16}{45}) = 0, \alpha < 0$  in the  $rt$ -parameter plane. Here the stratum is co-oriented towards the positivity of the discriminant.

Recall that at a positive  $D_5^{s,\sigma}$  bifurcation two swallowtails are born with signs  $(s, -\sigma)$  and  $(-s, \sigma)$ . Therefore, our stratum has decoration  $2A_4^{-\varepsilon, e/h}$  where  $\varepsilon = s\sigma$ .

We can now find the co-orientations of the  $D_5$  strata in Figure 28 by looking at the increments of the number of  $A_4$  points when crossing the  $D_5$  and  $A_4^{e/h}$  strata.

$A_3A_2$  stratum, Figure 30. We require  $\Psi$  to now have the zero roots of multiplicity 3 and 2 so we parametrise the  $A_3A_2$  stratum in  $\mathbb{R}_{\alpha,\psi,\beta,\delta}^4$  by

$$\Psi = \left( y - \frac{u}{2} \right)^3 \left( y + \frac{u}{3} \right)^2.$$

Equating the coefficients with (6) gives  $(\alpha, \psi, \beta, \delta^2) = (-\frac{5}{6}u, -\frac{5}{36}u^2, \frac{5}{24}u^3, -\frac{1}{18}u^5)$ .

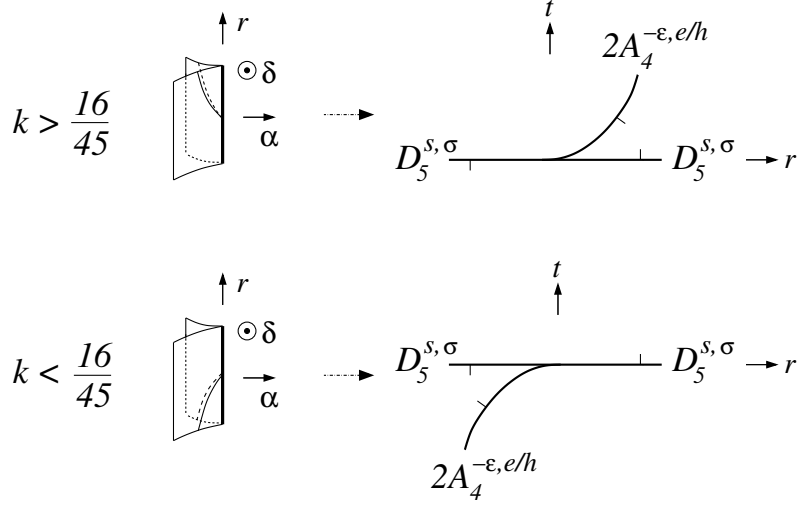


Figure 29: The  $A_4$  surface in  $\mathbb{R}_{\alpha,\beta,\delta,r,t}^5$ . Its edge is the  $D_5$  stratum. Projection to  $\mathbb{R}_{r,t}^2$  provides the bifurcational strata.

From this we obtain the surface  $\alpha^2(k + \frac{1}{5}) + r\alpha + t = 0$  with  $\alpha > 0$ . Projecting this surface to  $\mathbb{R}_{rt}^2$  has critical locus  $r = -2\alpha(k + \frac{1}{5})$  and is doubled in the  $\delta$ -direction. Hence the discriminantal stratum  $2TA_3^{s,\sigma}A_2$  is given by  $r^2 - 4(k + \frac{1}{5})t = 0$ ,  $\alpha > 0$ . Its co-orientation follows from the previous case. Since we know that at a positive  $D_5^{s,\sigma}$  bifurcation we lose two  $A_3^{s,\sigma}A_2$  points, our stratum will have decoration  $2TA_3^{s,\sigma}A_2$ .

$D_3A_2$  stratum, Figure 31. We require  $\Psi$  to have the zero root of multiplicity 3 and a non-zero root of multiplicity 2. Therefore we parametrise the  $A_3A_2$  singularity in  $\mathbb{R}_{\alpha,\psi,\beta,\delta}^4$  by

$$\Psi = y^3(y - u)^2.$$

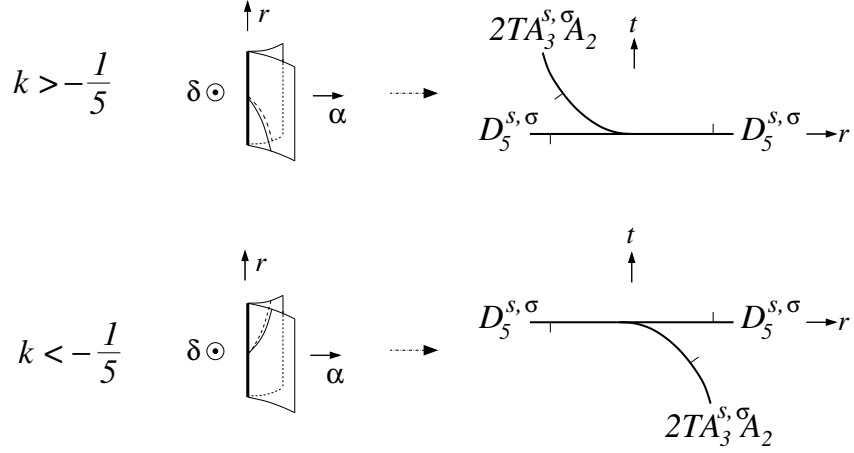


Figure 30: The  $TA_3A_2$  stratum.

Equating the coefficients with (6) gives  $(\alpha, \psi, \beta, \delta) = (-2u, u^2, 0, 0)$  and we obtain the surface

$$(k - \frac{1}{4})\alpha^2 + r\alpha + t = 0. \quad (7)$$

Projection of this surface to  $\mathbb{R}_{r,t}^2$  is a fold map, and its critical value set  $TD_3A_2$  is the zero set of the discriminant of the quadratic equation (7) in  $\alpha$ :  $r^2 - 4(k - \frac{1}{4})t = 0$ . Respectively, the co-orientation of the stratum  $TD_3A_2$  in Figure 31 is to the side where the discriminant is positive, that is, where the local caustics have two  $D_3A_2$  points. (Recall that  $D_3A_2$  is our alternative notation for  $A_3A_2$ , and see the  $TA_3A_2$  bifurcations in Figure 12). According to Figure 13, our  $D_3A_2 = A_3A_2$  points have decoration  $(-s, \sigma)$  as participants of the  $D_5^{s, \sigma}$  bifurcation.

$A_2^2$  stratum, There is no  $TA_2^2$  stratum (see [9] for details).

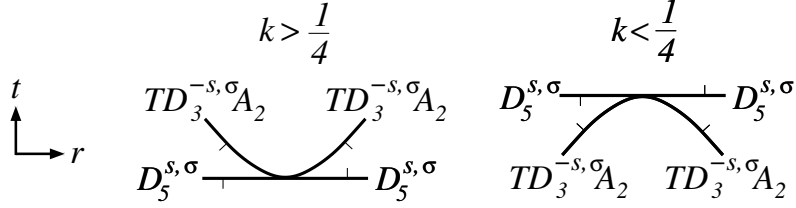


Figure 31: The  $TD_3A_2$  stratum.

$A_3$  stratum, Figure 32. In order to understand the decorations of all the  $A_3^q$  strata we first derive the equation of the discriminantal stratum in detail. The equations of the source are

$$G_x = s(2xy + \delta),$$

$$G_y = s(x^2 + y^3 + \alpha y^2 + (k\alpha^2 + r\alpha + t)y + \beta).$$

Here we have the map  $(x, y, \alpha) \mapsto (\alpha, \beta, \delta)$ . We calculate the Hessian

$$\begin{pmatrix} 2sy & 2sx \\ 2sx & s(k\alpha^2 + r\alpha + 2\alpha y + 3y^2 + t) \end{pmatrix}.$$

The critical point set is

$$H = 2s^2y(k\alpha^2 + r\alpha + 2\alpha y + 3y^2 + t) - 4s^2x^2 = 0.$$



The previous equation implies that

$$2s^2y(k\alpha^2 + r\alpha + 2\alpha y + 3y^2 + t) = 4s^2x^2.$$

Since we already know that  $x = 0$  we must find the singular points of

$$y(k\alpha^2 + r\alpha + 2\alpha y + 3y^2 + t) = 0$$

that is, of

$$y \left( 3 \left( y + \frac{\alpha}{3} \right)^2 + \left( k - \frac{1}{3} \right) \left( \alpha + \frac{r}{2 \left( k - \frac{1}{3} \right)} \right)^2 + t - \frac{r^2}{4 \left( k - \frac{1}{3} \right)} \right) = 0.$$

Therefore the  $A_3^q$  stratum is  $r^2 = 4 \left( k - \frac{1}{3} \right) t$ , while the  $D_{4,q}^\pm$  is  $r^2 = 4kt$ . This is so because the  $D_{4,q}^\pm$  events are described as non-transversalities of the zero sets of the two factors above, while the  $A_3^q$  degenerations correspond to the zero set of the long factor becoming singular. In particular, the  $A_3^q$  transitions occur at  $y + \frac{\alpha}{3} = \alpha + \frac{r}{2(k-1/3)} = 0$ .

We will now consider in detail the decorations of the  $A_3$  bifurcations. First we will consider whether we have the birth of a flying saucer, hyperbolic transformation of an edge or the death of a compact component of an edge. To calculate the type of bifurcation we extend our Hessian matrix by

$$\left( \frac{H_x}{2}, \frac{H_y}{2} \right) = (-4x, 9y^2 + 4\alpha y + \psi)$$

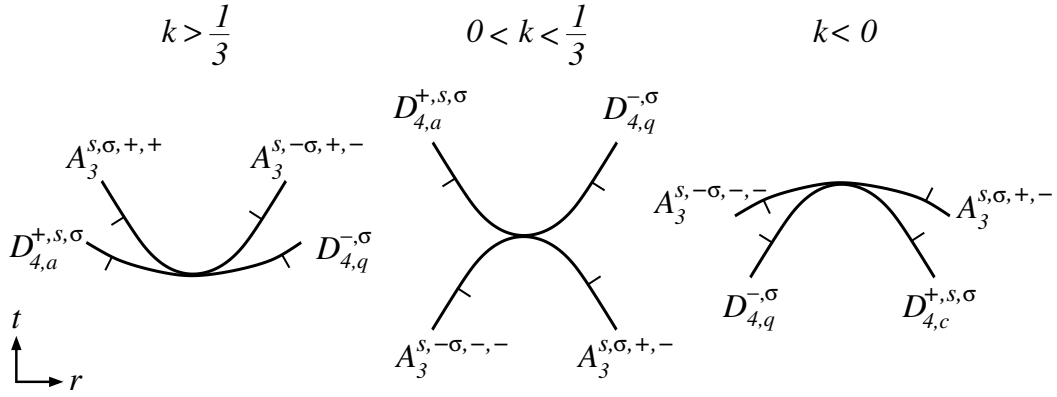


Figure 32: The  $A_3^q$  and  $D_{4,q}^\pm$  strata.

which is the same as extending the Hessian matrix by a row  $(0, 15y^2 + 8\alpha y + 3\psi)$ . We should remind the reader that here and until the end of this section  $\psi = k\alpha^2 + r\alpha + t$ .

At  $A_3$  points, the rank of this extended matrix must be 1. That is the same as

$$H = 0,$$

$$y(15y^2 + 8\alpha y + 3\psi) = 0,$$

$$x(15y^2 + 8\alpha y + 3\psi) = 0.$$

Hence we can plot  $y(3y^2 + 2\alpha y + \psi) = 0$  together with  $15y^2 + 8\alpha y + 3\psi = 0$  for an arbitrary point above and below the  $A_3^q$  half-branch in order to detect what type of bifurcation we have and to which side the half-branch is co-oriented. In the following figures the first equation is shown in red, with the second in blue. We have two cases, when  $k > 1/3$  and when  $k < 1/3$ . In both

cases we consider  $r > 0$  and  $r < 0$ .

$k > 1/3, r > 0$ : This corresponds to the left diagram in Figure 32, right  $A_3^q$  bifurcation curve. The plot of the two curves for below the  $A_3^q$  half-branch is shown in Figure 33 and for above in Figure 34. The regions covered by  $H = 0$  twice are shaded. Hence it is apparent here we have an  $A_3^{*,*,+,-}$  bifurcation.

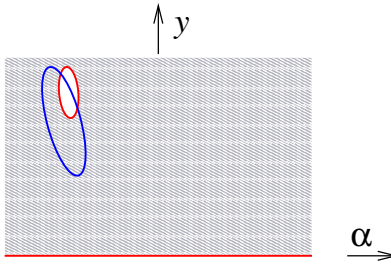


Figure 33:  $y(3y^2 + 2\alpha y + \psi) = 0$  and  $15y^2 + 8\alpha y + 3\psi = 0$  below the  $A_3^{*,*,+,-}$  half-branch.

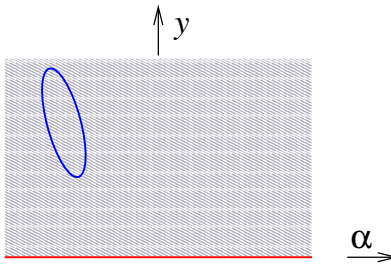


Figure 34:  $y(3y^2 + 2\alpha y + \psi) = 0$  and  $15y^2 + 8\alpha y + 3\psi = 0$  above the  $A_3^{*,*,+,-}$  half-branch.

$k > 1/3, r < 0$ : Left diagram in Figure 32, left  $A_3^q$  bifurcation curve. Figures 35 and 36 show the curves above and below the bifurcation. From this

we conclude that we have an  $A_3^{*,*,+,+}$  bifurcation.

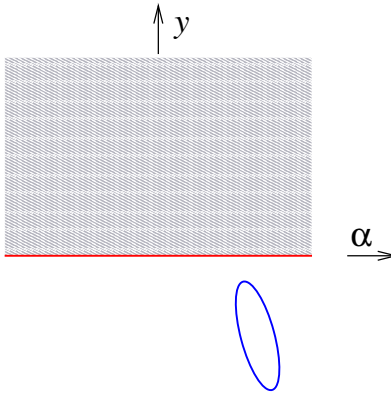


Figure 35:  $y(3y^2 + 2\alpha y + \psi) = 0$  and  $15y^2 + 8\alpha y + 3\psi = 0$  above the  $A_3^{*,*,+,+}$  half-branch.

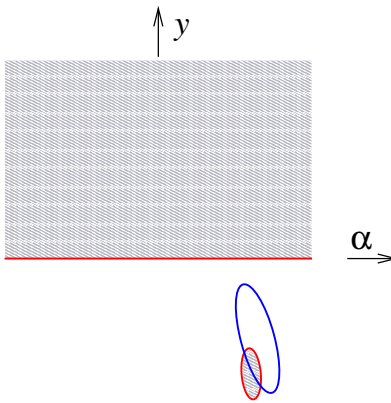


Figure 36:  $y(3y^2 + 2\alpha y + \psi) = 0$  and  $15y^2 + 8\alpha y + 3\psi = 0$  below the  $A_3^{*,*,+,+}$  half-branch.

$k < 1/3, r > 0$ : Two right diagrams in Figure 32, right  $A_3^q$  bifurcation curve. Figures 37, 38 and 39 show the transition of the two curves during

the bifurcation. Hence we have an  $A_3^{*,*,+,-}$  bifurcation.

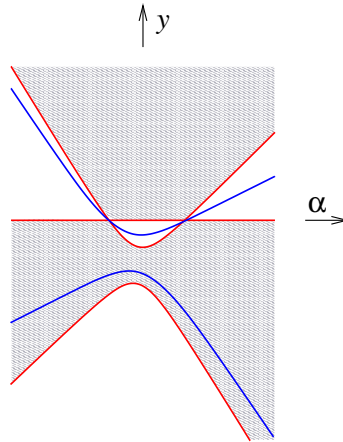


Figure 37:  $y(3y^2 + 2\alpha y + \psi) = 0$  and  $15y^2 + 8\alpha y + 3\psi = 0$  below the  $A_3^{*,*,+,-}$  half-branch.

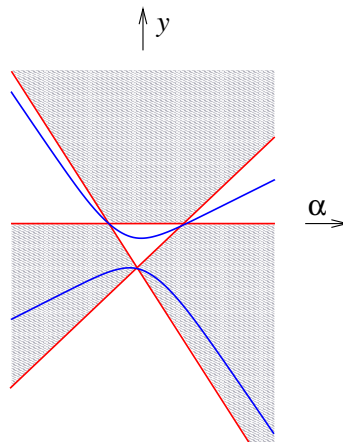


Figure 38:  $y(3y^2 + 2\alpha y + \psi) = 0$  and  $15y^2 + 8\alpha y + 3\psi = 0$  at the  $A_3^{*,*,+,-}$  half-branch.

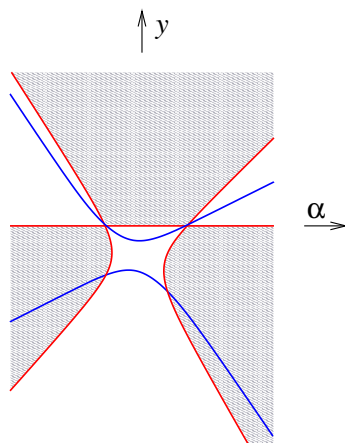


Figure 39:  $y(3y^2 + 2\alpha y + \psi) = 0$  and  $15y^2 + 8\alpha y + 3\psi = 0$  above the  $A_3^{*,*,+,-}$  half-branch.

$k < 1/3, r < 0$ : Two right diagrams in Figure 32, left  $A_3^q$  bifurcation curve. Figures 40, 41 and 42 show the transition of the two curves during the bifurcation. Hence we have an  $A_3^{*,*,-,-}$  bifurcation.

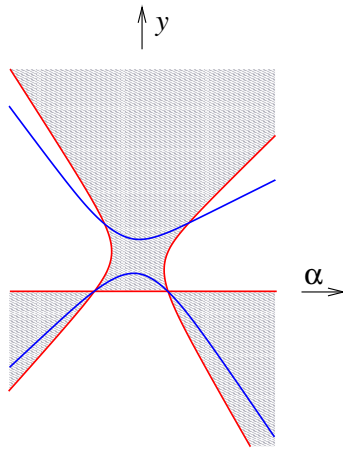


Figure 40:  $y(3y^2 + 2\alpha y + \psi) = 0$  and  $15y^2 + 8\alpha y + 3\psi = 0$  above the  $A_3^{*,*, -, -}$  half-branch.

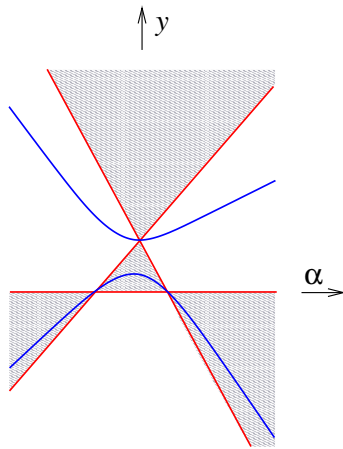


Figure 41:  $y(3y^2 + 2\alpha y + \psi) = 0$  and  $15y^2 + 8\alpha y + 3\psi = 0$  at the  $A_3^{*,*, -, -}$  half-branch.

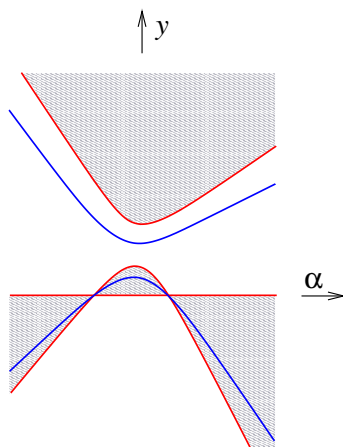


Figure 42:  $y(3y^2 + 2\alpha y + \psi) = 0$  and  $15y^2 + 8\alpha y + 3\psi = 0$  below the  $A_3^{*,*,\cdot,-}$  half-branch.

We now work out the signs  $s$  and  $\sigma$  of the  $A_3^q$  strata by comparing the coefficients of our generating family

$$G = s(x^2y + \frac{1}{4}y^4 + \frac{1}{3}\alpha y^3 + \frac{1}{2}\psi y^2 + \beta y + \delta x),$$

to the generating family

$$F = s(x^2y + y^4 - \lambda y^3 + wy^2 + vy + ux)$$

of  $D_5^{s,\sigma}$  from Section 2.3.2.1. Recall the  $D_5^{s,\sigma}$  bifurcation shown in Figure 13. We know the direction of  $\lambda$  there is the direction of the bifurcation, from left to right. We also know that the direction of  $v$  there is into the page away from the reader, the direction of  $w$  is from right to left and the direction of  $u$  does



not matter since the bifurcation is symmetric. Comparison of the coefficients tells us  $u \approx \delta$ ,  $v \approx \beta$ ,  $w \approx \psi$  and  $\lambda \approx -\alpha$ . Hence we know the directions of  $\alpha, \beta, \delta$  and  $\lambda$ .

From

$$y \left( 3 \left( y + \frac{\alpha}{3} \right)^2 + \left( k - \frac{1}{3} \right) \left( \alpha + \frac{r}{2 \left( k - \frac{1}{3} \right)} \right)^2 + t - \frac{r^2}{4 \left( k - \frac{1}{3} \right)} \right) = 0$$

at the point of bifurcation we have  $y = -\frac{\alpha}{3}$ ,  $\alpha = -\frac{r}{2 \left( k - \frac{1}{3} \right)}$ ,  $t = \frac{r^2}{4 \left( k - \frac{1}{3} \right)}$ . Since  $x = 0$  we have  $u = 0$  in  $F$  and the signs  $s$  and  $\sigma$  of the bifurcation corresponds to a cuspidal edge in the middle of the  $D_5^{s,\sigma}$  bifurcation.

- $k > 1/3, r > 0$ : Here  $\lambda > 0, w > 0 \implies A_3^{s,-\sigma}$ .
- $k > 1/3, r < 0$ : Here  $\lambda < 0, w > 0 \implies A_3^{s,\sigma}$ .
- $k < 1/3, r > 0$ : Here  $\lambda < 0, w > 0 \implies A_3^{s,\sigma}$ .
- $k < 1/3, r < 0$ : Here  $\lambda > 0, w > 0 \implies A_3^{s,-\sigma}$ .

Now, summing up the increments across the strata from all the bifurcation diagrams in this section gives us the following Lemma.

**Lemma 2.6.1.** *The 2-parameter bifurcations of the  $D_5$  uni-germs yield the cyclic equation:*

$$\mathbf{23.} \quad 2d_5^{s,\sigma} + d_{4,a/c}^{+,s,\sigma} - d_{4,q}^{-,\sigma} - 2a_4^{-\varepsilon,e/h} + 2ta_3^{s,\sigma}a_2 + a_3^{s,\sigma,q} + a_3^{s,-\sigma,q} = 0, \quad \varepsilon = s\sigma.$$

### 2.6.2.3 Extra $A_2$ component

We now consider passing a smooth  $A_2$  sheet through the corank 2 uni-germs  $S$  listed in Section 2.3.2.1. Here, we borrow the bifurcation diagrams from [9] and modify them to include the extra  $s$  decoration of the strata.

First we consider  $SA_2$  where  $S$  is one of the four  $D_{4,q}$  quadratic singularities listed in Figure 13. The bifurcation diagrams are shown in Figure 43 with the cyclic equations and big strata below. The top and bottom rows of diagrams differ only by opposite co-orientation of the smooth  $A_2$  sheet. The signs  $s$  and  $\sigma$  are inherited from the signs of the cuspidal edge in the  $D_{4,q}$  singularity. Finally, the co-orientations of the strata are found by looking at the  $S$  bifurcations in Figure 13 to see how a smooth sheet interacts with them.

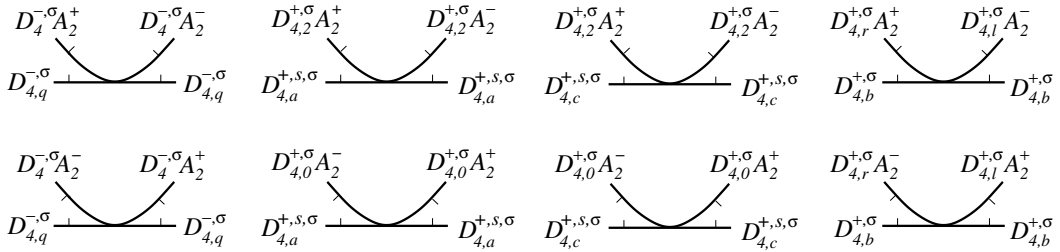


Figure 43: The bifurcation diagrams for  $SA_2$  where  $S = D_{4,q}^\pm$ .

Figure 43 yields the equations:

	$S$	equations	big stratum
24.	$D_{4,q}^{-,\sigma}$	$d_{4,2}^{-,\sigma} a_2^+ = d_{4,2}^{-,\sigma} a_2^-$	$D_{4,2}^{-,\sigma} A_2$
25.	$D_{4,a}^{+,s,\sigma}$ or $D_{4,c}^{+,s,\sigma}$	$d_{4,2}^{+,s,\sigma} a_2^+ = d_{4,2}^{+,s,\sigma} a_2^-$ $d_{4,0}^{+,s,\sigma} a_2^- = d_{4,0}^{+,s,\sigma} a_2^+$	$D_{4,2}^{+,s,\sigma} A_2$ $D_{4,0}^{+,s,\sigma} A_2$
26.	$D_{4,b}^{+,s,\sigma}$	$d_{4,r}^{+,s,\sigma} a_2^t = d_{4,l}^{+,s,\sigma} a_2^{-t}$	

Now consider  $S = D_5^{s,\sigma}$ . The bifurcation diagram of  $D_5^{s,\sigma} A_2$  is shown in Figure 44. Note that when  $s = +$ , the right horizontal branch has decoration

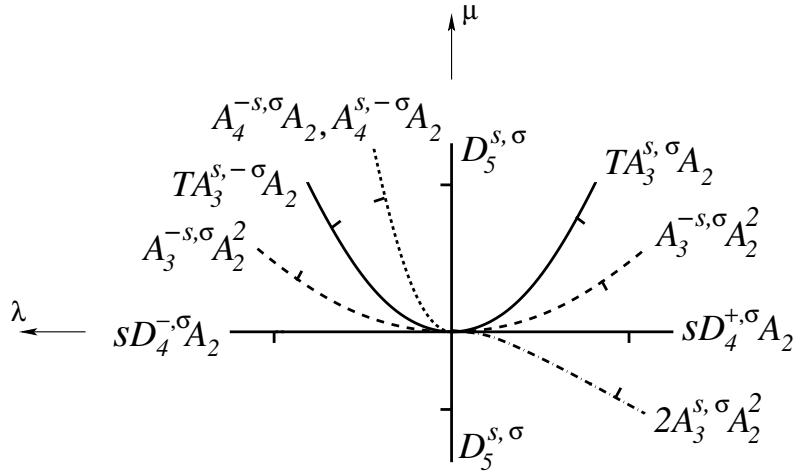


Figure 44: Bifurcation diagram of passing a smooth  $A_2$  sheet through  $D_5^{s,\sigma}$ .

$D_{4,2}^{+,\sigma} A_2$  and when  $s = -$  it has decoration  $D_{4,0}^{+,\sigma} A_2$ . We should also note that the co-orientation of the  $D_4 A_2$  stratum in Figure 44 depends on the sign of the decoration  $s$  in the  $D_5^{s,\sigma}$  singularity.

Here we obtained the bifurcation diagram by setting the horizontal coordinate  $\lambda$  to be the parameter in the  $D_5^{s,\sigma}$  bifurcation and the vertical coordinate  $\mu$  to measure the position of the smooth  $A_2$  sheet. We then determine the decoration of the strata by looking at the signs  $(s, \sigma)$  of cuspidal edges in the  $D_5$  bifurcation as shown in Figure 13. Again, co-orientations are found by looking at the increments of the numbers of  $A_3A_2$  and  $A_2^3$  points across the strata.

From Figure 44 we obtain the cyclic equation:

$$27. \quad 2a_4^{-\varepsilon}a_2 + 2a_3^{s,\sigma}a_2^2 - 2a_3^{-s,\sigma}a_2^2 - ta_3^{s,\sigma}a_2 - ta_3^{s,-\sigma}a_2 - sd_{4,2}^{+,\sigma}a_2 + sd_4^{-,\sigma}a_2 = 0$$

#### 2.6.2.4 Interaction of a purse and a pyramid with other local components $C$

In this section we consider the interaction of a purse and a pyramid with other local components  $C$ . Here  $C$  will be either a cuspidal edge, two transversal smooth  $A_2$  sheets or a tangent smooth  $A_2$  sheet.

For the bifurcations involving a pyramid we take the pyramid as it is shown in Figure 10 and assume that its ‘top’ edge is a straight flat curve. Let  $\Pi$  be the tangent plane of this edge. We also assume the additional component  $C$  is a cylinder with its generators perpendicular to  $\Pi$ . Then the bifurcation diagrams are obtained by parallel translations of  $C$ . The bifurcation diagrams are drawn in the plane  $\Pi$ . They mark the intersections of the distinguished generator of  $C$  with  $\Pi$  when the surface  $C$  is in special positions with the

pyramid.

We obtain bifurcation diagrams for the interaction of a purse with  $C$  by the same method. We take the purse as it is shown in Figure 10 and assume that its cuspidal edge is a straight flat curve. Then we let  $\Pi$  be the tangent plane containing its cuspidal edge and dividing the purse in Figure 10 into two diffeomorphic but not necessarily symmetric halves.

In each case the decorations of the strata come from the signs of the cuspidal edges participating in the bifurcation. The co-orientations are found by looking at the increment of the number of  $A_3A_2$  points across the strata. Of course, symmetric pairs of  $A_3^{2,e/h}$  branches are co-oriented in opposite ways due to the symmetry of the pyramid and the purse.

#### 2.6.2.4.1 Extra cuspidal edge

In this section we take for the extra component a cuspidal edge surface, with the edge curve  $A_3^{s,\sigma}$ . The distinguished generator in this case is the cuspidal edge curve. We have two options to place a cuspidal edge surface relative to a pyramid. Both of them are shown in Figure 45 with their respective bifurcation diagram underneath.

Respectively we obtain the cyclic equations,

$$\begin{aligned}
 \mathbf{28.} \quad & a_3^{2,e;s,\sigma;+,\tau} - a_3^{2,e;s,\sigma;-,\tau} + 2a_3^{2,h;+,\tau;s,\sigma} - 2a_3^{2,h;-,\tau;s,\sigma} - 2d_4^{-,\tau} a_2 = 0 \\
 & a_3^{2,h;s,\sigma;+,\tau} - a_3^{2,h;s,\sigma;-,\tau} - 2a_3^{2,e;s,\sigma;+,\tau} + 2a_3^{2,e;s,\sigma;-,\tau} + 2d_4^{-,\tau} a_2 = 0
 \end{aligned}$$

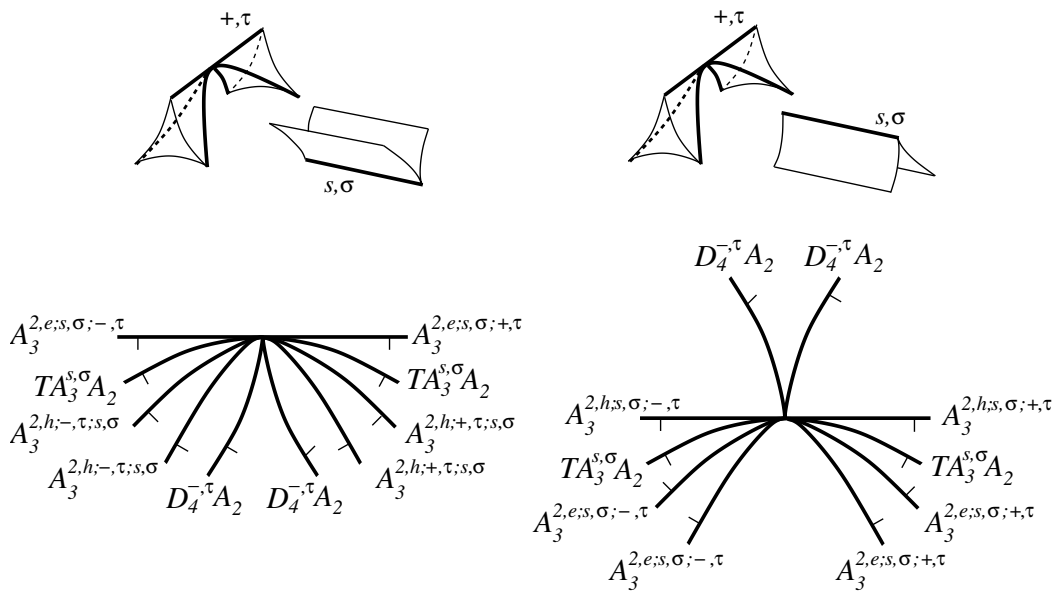


Figure 45: Bifurcation diagrams for a cuspidal edge surface interacting with a pyramid.

Now, consider the interaction of the same cuspidal edge surface with a purse. Again, we have two options to place it relative to a purse. They are shown in Figure 46 along with their respective bifurcation diagrams. For each case, we have three subcases: at the most degenerate moment, the two self-intersection rays of a purse may be either both to the left side, both to the right side or to different sides of the plane tangent to the cuspidal surface at its edge.

From Figure 46 we obtain the cyclic equations,

$$\begin{aligned}
29. \quad & -a_3^{2,h;+,\tau;s,\sigma} + 2a_3^{s,\sigma} a_2^2 + a_3^{2,h;-\,\tau;s,\sigma} + 2d_{4,0}^{+,\tau} a_2 = 0 \\
& a_3^{2,e;s,\sigma;+,\tau} - 2a_3^{s,\sigma} a_2^2 - a_3^{2,e;s,\sigma;-\,\tau} - 2d_{4,0}^{+,\tau} a_2 = 0 \\
& -a_3^{2,h;+,\tau;s,\sigma} - 2a_3^{s,\sigma} a_2^2 + a_3^{2,h;-\,\tau;s,\sigma} + 2d_{4,2}^{+,\tau} a_2 = 0 \\
& a_3^{2,e;s,\sigma;+,\tau} + 2a_3^{s,\sigma} a_2^2 - a_3^{2,e;s,\sigma;-\,\tau} - 2d_{4,2}^{+,\tau} a_2 = 0 \\
& -a_3^{2,h;+,\tau;s,\sigma} + a_3^{2,h;-\,\tau;s,\sigma} + 2d_{4,1}^{+,\tau} a_2 = 0 \\
& a_3^{2,e;s,\sigma;+,\tau} - a_3^{2,e;s,\sigma;-\,\tau} - 2d_{4,1}^{+,\tau} a_2^- = 0
\end{aligned}$$

#### 2.6.2.4.2 Extra $A_2^2$ component

We now take for  $C$  a transversal intersection of two smooth sheets and consider how it may meet a pyramid. The distinguished generator here is the self-intersection curve  $A_2^2$ . Assuming that the self-intersection curve passes through the vertex of a pyramid at the most degenerate moment, we obtain the bifurcation diagram shown in Figure 47. It yields the cyclic equation,

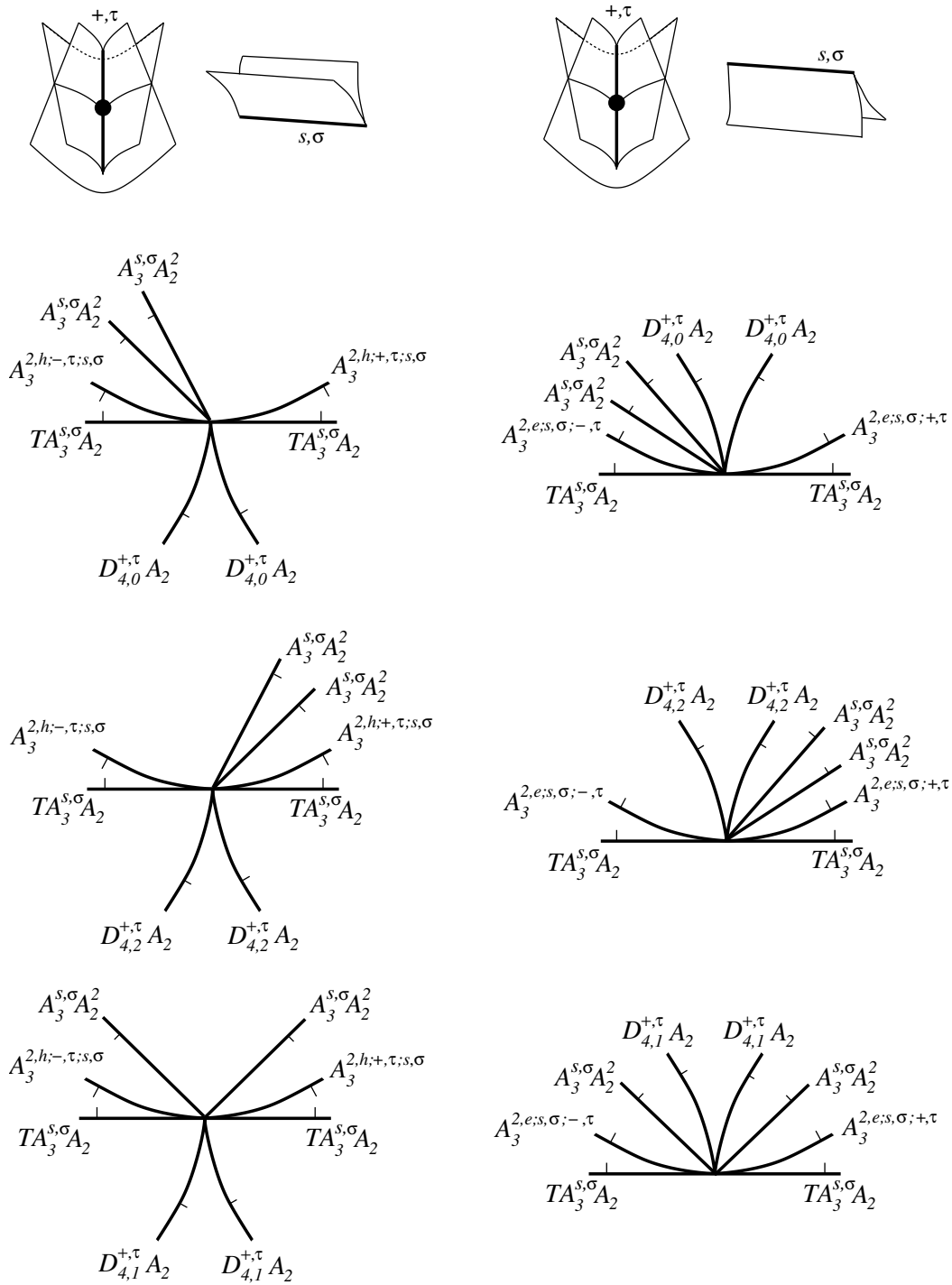


Figure 46: Bifurcations of a cuspidal surface interacting with a purse.



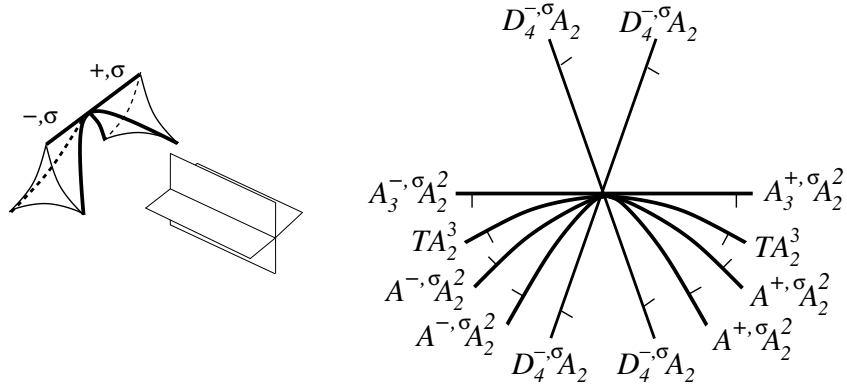


Figure 47: Bifurcations of a pair of transversal  $A_2$  sheets with a pyramid.

$$30. \quad a_3^{+, \sigma} a_2^2 - a_3^{-, \sigma} a_2^2 = 0.$$

Equation **30** gives us the big strata  $A_3^\sigma A_2^2 = A_3^{+, \sigma} A_2^2 + A_3^{-, \sigma} A_2^2$ .

Now, consider the interaction of  $C = A_2^2$  with a purse. Here we have a number of configurations due to the relative positions of a purse and the  $A_2$  sheets at the most degenerate moment. Assume that at such a moment one of the four connected components into which the two  $A_2$  sheets cut the ambient space contains both self-intersection rays of the purse and one of its cuspidal half-branches. Figure 48 shows three examples of bifurcation diagrams out of up to a possible sixteen. They all give us the cyclic equation

$$31. \quad a_3^{+, \sigma} a_2^2 - a_3^{-, \sigma} a_2^2 = 0.$$

In all sixteen possible situations we will have similar components con-

tributing in the bifurcation diagram. That is,

- two  $[A_2^4]$  branches contributing zero to the cyclic equation;
- a symmetric pair of  $TA_2^3$  branches contributing nothing;
- four  $D_{4,0/1/2}^{+\sigma}A_2$  branches contributing nothing;
- an  $A_3^{s,\sigma}A_2^2$  branch and an  $A_3^{-s,\sigma}A_2^2$  branch, of opposite co-orientations.

Hence the cyclic equation for all sixteen cases is  $a_3^{+,\sigma}a_2^2 - a_3^{-,\sigma}a_2^2 = 0$ .

### 2.6.2.4.3 Tangent $A_2$ component

We let surface  $C = A_2$  and consider the tangency of  $C$  to a pyramid at the  $D_4$  point. We consider the smooth  $A_2$  sheet as a parabolic cylinder. The distinguished generator of  $C$  this time is the line of vertices of the parabolas.

There are two ways to place the parabolic cylinder relative to a pyramid. Both are shown in Figure 49 with their respective bifurcation diagrams underneath. Both cases provide us with the cyclic equation

$$\mathbf{32.} \quad 3ta_3^{+,\sigma}a_2 - 3ta_3^{-,\sigma}a_2 - 2d_4^{-,\sigma}a_2 = 0.$$

We should note that in Figure 49 the parabolic  $A_2$  sheet is rather steep. If we reduce the steepness we will get a series of bifurcation diagrams with the  $D_4^{-,\sigma}A_2$  curve successively in pairs of the sectors between the other strata. We should also note that switching the co-orientation of the  $A_2$  sheet does

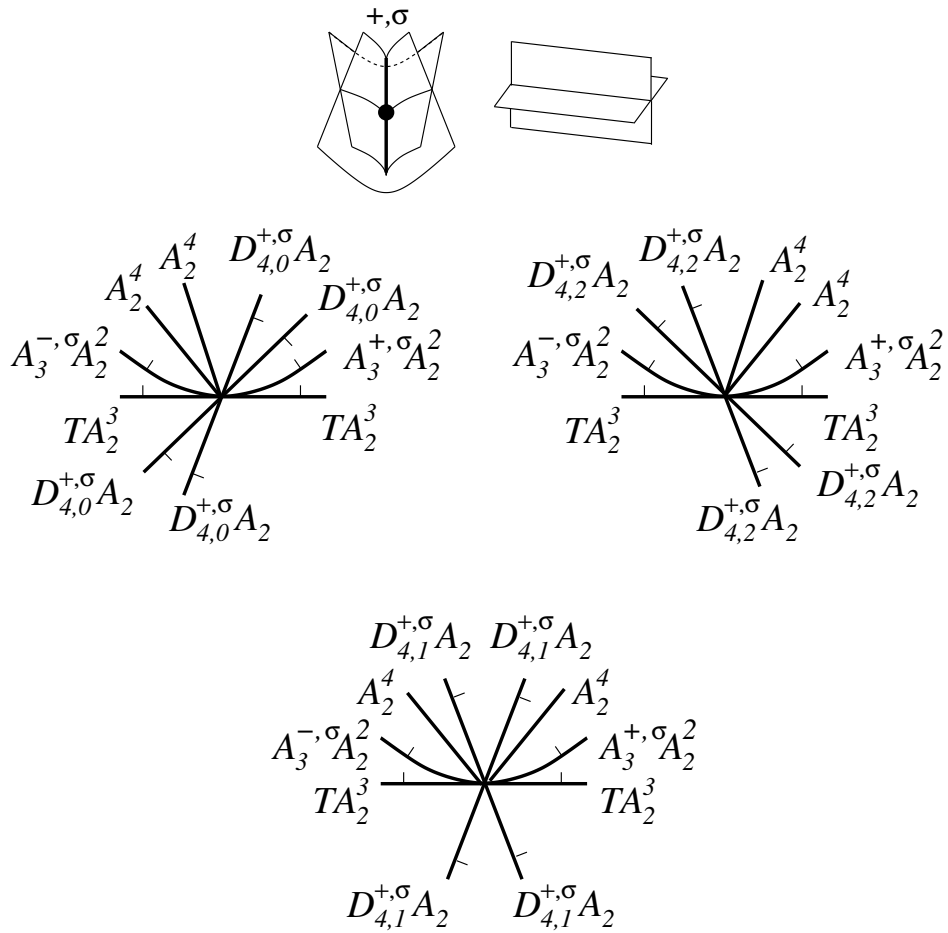


Figure 48: Three examples of bifurcations of a pair of transversal sheets with a purse out of up to a possible sixteen.

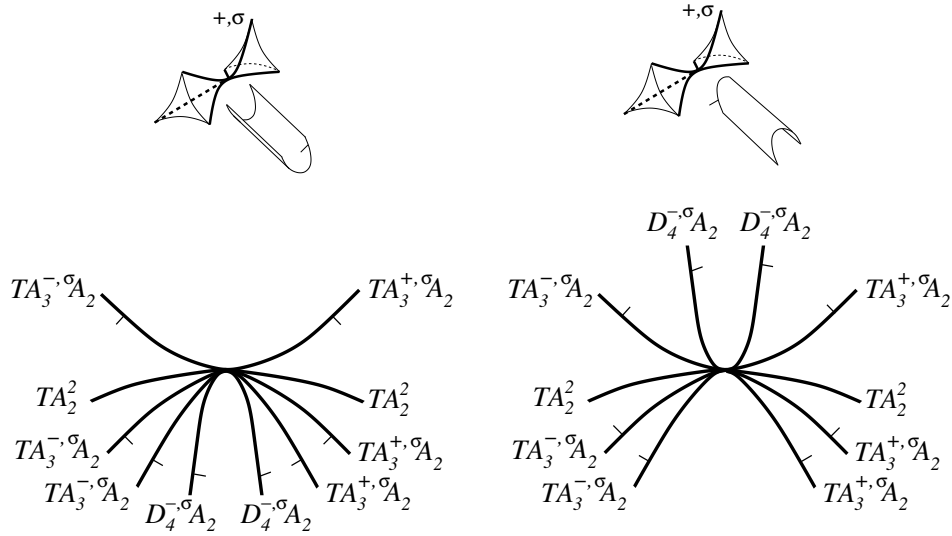


Figure 49: Bifurcations of a pyramid and a smooth  $A_2$  sheet of a caustic tangent to the cuspidal edge of the pyramid at the  $D_4^-$  point.

not affect the result.

**Remark.** All possible bifurcations of a smooth  $A_2$  surface that is tangent to an edge of the pyramid at its vertex are covered by families of surfaces

$$\delta = k\beta + m\varphi^2 + \lambda_1\varphi + \lambda_2.$$

Here

- $\varphi, \beta, \delta$  are the coordinates in the space containing the pyramid used in the generating family at the start of Section 2.6.2.1;
- $k$  and  $m$  are a pair of fixed parameters with their values chosen in a

generic way;

- $\lambda_1$  and  $\lambda_2$  are bifurcation parameters.

The  $TA_3A_2$  strata of the bifurcation diagrams in Figure 49 are formed by those points  $(\lambda_1, \lambda_2)$  for which the edges of the pyramid have double point intersections with the surfaces. The  $D_4^-A_2$  strata correspond to the surfaces passing through the origin, and the  $TA_2^2$  strata to tangencies of the surfaces to regular parts of the pyramid. All options of choosing  $k$  and  $m$  in a generic way yield the same equation **32**.

Now consider the tangency of a smooth sheet to the purse at the  $D_4$  point. Again, there are two ways to place a steep parabolic  $A_2$  sheet relative to a purse. They are shown in Figure 50 with their respective bifurcation diagrams underneath. Both bifurcation diagrams give us the cyclic equation

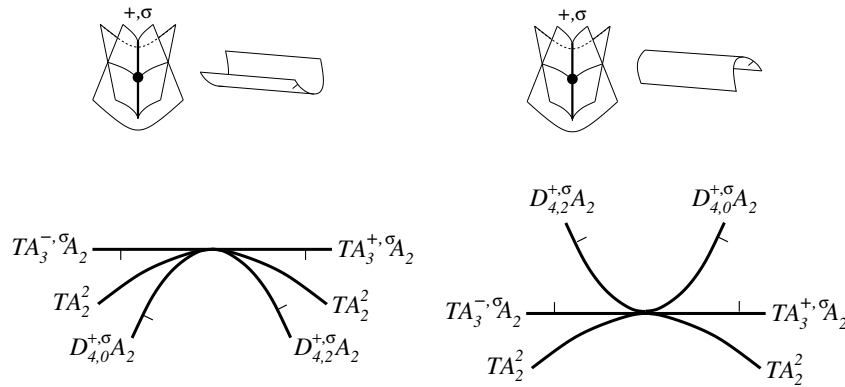


Figure 50: Bifurcations of a purse and a smooth  $A_2$  sheet of a caustic tangent to the cuspidal edge of the purse at the  $D_4^+$  point.

$$\mathbf{33.} \quad ta_3^{-,\sigma} a_2 - ta_3^{+,\sigma} a_2 + d_{4,0}^{+,\sigma} a_2 + d_{4,2}^{+,\sigma} a_2 = 0.$$

Again, switching the co-orientation of the  $A_2$  sheet does not affect the result. Consideration of the families of surfaces mentioned in the remark about the pyramid yields the same equation **33** in all the cases.

Finally, consider the tangency of  $C = A_2$  to one of the self-intersection rays at a  $D_4^+$  point. We obtain four bifurcation diagrams which are shown in Figure 51 and the cyclic equations

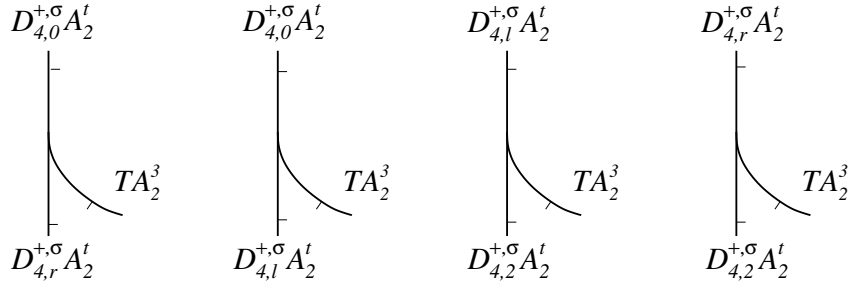


Figure 51: Bifurcation diagrams of an  $A_2$  sheet of a caustic tangent to a self-intersection ray of a purse at its  $D_4^+$  point.

$$d_{4,0}^{+,\sigma} a_2^t - d_{4,r}^{+,\sigma} a_2^t + ta_2^3 = 0$$

$$d_{4,0}^{+,\sigma} a_2^t - d_{4,l}^{+,\sigma} a_2^t + ta_2^3 = 0$$

$$d_{4,l}^{+,\sigma} a_2^t - d_{4,2}^{+,\sigma} a_2^t + ta_2^3 = 0$$

$$d_{4,r}^{+,\sigma} a_2^t - d_{4,2}^{+,\sigma} a_2^t + ta_2^3 = 0$$

where  $t$  is positive if the  $A_2$  sheet is moving in the direction of its co-orientation and negative otherwise.

The difference of the first equations above gives

$$d_{4,r}^{+,\sigma} a_2^t = d_{4,l}^{+,\sigma} a_2^t$$

for  $t = \pm$ . Hence we introduce the big strata

$$D_{4,1}^{+,\sigma} A_2 = D_{4,r}^{+,\sigma} A_2^+ + D_{4,r}^{+,\sigma} A_2^- + D_{4,l}^{+,\sigma} A_2^+ + D_{4,l}^{+,\sigma} A_2^-$$

This yields the equations (in terms of the big strata)

$$\begin{aligned} \mathbf{34.} \quad & d_{4,0}^{+,\sigma} a_2 - d_{4,1}^{+,\sigma} a_2 + ta_2^3 = 0 \\ & d_{4,1}^{+,\sigma} a_2 - d_{4,2}^{+,\sigma} a_2 + ta_2^3 = 0 \end{aligned}$$

### 2.6.2.5 $D_6$ and $E_6$ bifurcations

The three remaining big caustics of generic 2-parameter families we must consider are  $D_6^+$ ,  $D_6^-$  and  $E_6$ . We claim

**Theorem 2.6.2.** *Generic 2-parameter families of 3-dimensional caustics making up the big caustics  $D_6^+$ ,  $D_6^-$  and  $E_6$  provide equations **35-37**, **38** and **39-40***

respectively (the  $E_6$  equations **39-40** are mod2 only):

$$35. \quad a_3^{2,e;+,\sigma;+,-\sigma} - a_3^{2,e;-\sigma;-, -\sigma} + 2a_4^{-\sigma}a_2 + 2a_4^{\sigma}a_2 - 2ta_3^{+,-\sigma}a_2 - 2ta_3^{+,\sigma}a_2 - 2d_{4,2}^{+,\sigma}a_2 + a_4^{-\sigma,e/h} - a_4^{\sigma,e/h} + d_5^{-,\sigma} - d_5^{+,\sigma} = 0$$

$$36. \quad a_3^{2,e;+,\sigma;+,-\sigma} - a_3^{2,e;-\sigma;-, -\sigma} - ta_3^{+,-\sigma}a_2 - ta_3^{+,\sigma}a_2 + ta_3^{-,\sigma}a_2 + ta_3^{-,-\sigma}a_2 - 2d_{4,1}^{+,\sigma}a_2 + a_4^{-\sigma,e/h} - a_4^{\sigma,e/h} + d_5^{-,\sigma} - d_5^{+,\sigma} = 0$$

$$37. \quad a_3^{2,e;+,\sigma;+,-\sigma} - a_3^{2,e;-\sigma;-, -\sigma} - 2a_4^{-\sigma}a_2 - 2a_4^{\sigma}a_2 + 2ta_3^{-,\sigma}a_2 + 2ta_3^{-,-\sigma}a_2 - 2d_{4,0}^{+,\sigma}a_2 + a_4^{-\sigma,e/h} - a_4^{\sigma,e/h} + d_5^{-,\sigma} - d_5^{+,\sigma} = 0$$

$$38. \quad d_5^{+,\sigma} - d_5^{-,\sigma} + a_4^{-\sigma,e/h} - a_4^{\sigma,e/h} + a_5^{+,\sigma,+} + a_5^{+,\sigma,-} - a_5^{-,\sigma,+} - a_5^{-,\sigma,-} - 2d_4^{-,\sigma}a_2 + 2a_3^{2,h;+,\sigma;-, \sigma} + [a_3^{2,h;+,\sigma;+,\sigma}] + [a_3^{2,h;-, \sigma;-, \sigma}] = 0$$

$$39. \quad a_3^{2,e/h;+,\sigma;+,-\sigma} + a_3^{2,e/h;+,-\sigma;-, \sigma} = 0$$

$$40. \quad a_3^{2,e/h;-, \sigma;-, -\sigma} + a_3^{2,e/h;-, -\sigma;+,\sigma} = 0$$

Since the proof of Theorem 2.6.2 is lengthy we delay it to be the main subject of Chapters 4, 5 and 6. However, for now we use the equations from this theorem in Chapter 3.



# Chapter 3

## Proofs of Theorems 2.5.1 and 2.5.3

In this chapter we prove our main Theorems 2.5.1 and 2.5.3.

Recall from Section 2.5 that  $\mathcal{D}(M, T^*N, N; \mathbb{K})$  is the space of discriminantal cycles in  $\mathcal{L}(M, T^*N, N)$  with coefficients  $\mathbb{K} = \mathbb{Q}, \mathbb{Z}, \mathbb{Z}_2$ . We also introduce the notation  $\mathcal{E}(M, T^*N, N; \mathbb{Q})$  and  $\mathcal{E}(M, T^*N, N; \mathbb{Z}_2)$  for the spaces spanned over  $\mathbb{Q}$  and  $\mathbb{Z}_2$  by the cyclic equations **1-40**.

In Section 2.3 we introduced 132 elementary codimension 1 strata in  $\mathcal{L}(M, T^*N, N)$ . From our analysis in Section 2.6 we have been able to glue them together, both over  $\mathbb{Z}$  and  $\mathbb{Z}_2$ , into respectively 57 and 47 big strata.

**Proof of Theorem 2.5.1.** Table 1 shows a basis of the space  $\mathcal{E}(M, T^*N, N; \mathbb{Q})$ .

In all tables in this chapter we are using dots for zero coefficients. The number

of basic elements (columns) in Table 1 is 42. All of them are linear equations in 57 unknown coefficients of the big strata. Hence the space  $\mathcal{D}(M, T^*N, N; \mathbb{Q})$  is 15-dimensional. Its basis is shown in Table 2. Lemma 2.4.1 listed thirteen of its elements counting the numbers of various isolated type singularities of the caustics, along with the fourteenth responsible for the Euler characteristic of the critical point set. The fifteenth was not too complicated to spot. This concludes our proof of Theorem 2.5.1.

**Proof of Theorem 2.5.3.** Similarly for the  $\mathbb{Z}_2$  case, Table 3 shows a basis of the space  $\mathcal{E}(M, T^*N, N; \mathbb{Z}_2)$ . This time we have 27 basic equations in 47 unknown coefficients of the big  $\mathbb{Z}_2$  strata. Therefore, the space  $\mathcal{D}(M, T^*N, N; \mathbb{Z}_2)$  is 20-dimensional. Its basis is shown in Table 4. The first fifteen elements are the *mod2* reduction of a basis of the space of integer discriminantal cycles listed in Corollary 2.5.2 and repeated in Table  $\mathbb{Z}$ . The last five elements are listed at the end of Remark 2.4.3. This concludes our proof of Theorem 2.5.3.



Table 1 cont.	18	18	18	18	19	19	20	22	22	23	23	23	23	27	27	27	27	28	28	29	29	35	
$TA_2^3$	.	.	.	.	.	.	.	.	.	.	.	.	.	.	.	.	.	.	.	.	.	.	.
$A_3^{\pm,+}A_2^2$	.	.	.	.	.	.	.	.	.	.	.	.	.	.	.	.	.	.	.	.	.	.	.
$A_3^{\pm,-}A_2^2$	.	.	.	.	.	.	.	.	.	.	.	.	.	.	.	.	.	.	.	.	.	.	.
$A_3^{2,e;+,+,+,+}$	.	.	.	.	.	.	.	.	.	.	.	.	.	.	.	.	.	.	.	.	.	.	.
$A_3^{2,e;+,+,+,-}$	.	.	.	.	.	.	.	.	.	.	.	.	.	.	.	.	.	1	1	.	.	.	1
$A_3^{2,e;+,+,-,+}$	.	.	.	.	.	.	.	.	.	.	.	.	.	.	.	.	.	.	.	.	.	.	.
$A_3^{2,e;+,+,-,-}$	.	.	.	.	.	.	.	.	.	.	.	.	.	.	.	.	.	-1	.	.	.	.	.
$A_3^{2,e;+,-,+,+}$	.	.	.	.	.	.	.	.	.	.	.	.	.	.	.	.	.	.	.	.	.	.	.
$A_3^{2,e;+,-,-,+}$	.	.	.	.	.	.	.	.	.	.	.	.	.	.	.	.	.	.	-1	.	.	.	.
$A_3^{2,e;+,-,-,-}$	.	.	.	.	.	.	.	.	.	.	.	.	.	.	.	.	.	.	.	.	.	.	.
$A_3^{2,e;-,-,+,+}$	.	.	.	.	.	.	.	.	.	.	.	.	.	.	.	.	.	.	.	.	.	.	.
$A_3^{2,e;-,-,+,+}$	.	.	.	.	.	.	.	.	.	.	.	.	.	.	.	.	.	.	.	.	.	.	.
$A_3^{2,e;-,-,-,-}$	.	.	.	.	.	.	.	.	.	.	.	.	.	.	.	.	.	.	.	.	.	.	-1
$A_3^{2,h;+,+,+,-}$	.	.	.	.	.	.	.	.	.	.	.	.	.	.	.	.	.	-2	2	1	-1	.	.
$A_3^{2,h;+,+,-,+}$	.	.	.	.	.	.	.	.	.	.	.	.	.	.	.	.	.	.	.	.	.	.	.
$A_3^{2,h;+,+,-,-}$	1	1	.	.	.	.	.	.	.	.	.	.	.	.	.	.	.	2	.	-1	.	.	.
$A_3^{2,h;+,-,-,+}$	.	.	1	1	.	.	.	.	.	.	.	.	.	.	.	.	.	.	2	.	-1	.	.
$A_3^{2,h;+,-,-,-}$	.	.	.	.	.	.	.	.	.	.	.	.	.	.	.	.	.	.	.	.	.	.	.
$A_3^{2,h;-,-,-,-}$	.	.	.	.	.	.	.	.	.	.	.	.	.	.	.	.	.	.	.	.	.	.	.
$A_4^+A_2$	.	.	.	.	.	.	.	.	.	.	.	.	.	.	2	2	.	.	.	.	.	.	2
$A_4^-A_2$	.	.	.	.	.	.	.	.	.	.	.	.	.	2	.	.	2	.	.	.	.	.	2
$TA_3^{+,+}A_2$	.	.	.	-2	.	.	.	2	.	.	-1	-1	.	.	.	.	.	.	.	.	.	-2	.
$TA_3^{+,-}A_2$	.	.	.	.	-2	.	.	2	.	.	-1	-1	.	.	.	.	.	.	.	.	.	-2	.
$TA_3^{-,+}A_2$	.	.	.	.	.	.	.	.	2	.	.	.	-1	-1	.	.	.	.	.	.	.	.	.
$TA_3^{-,-}A_2$	.	.	.	.	.	.	.	.	.	2	.	.	-1	-1	.	.	.	.	.	.	.	.	.
$A_5^{+,+,+}$	-1	.	.	1	.	.	.	.	.	.	.	.	.	.	.	.	.	.	.	.	.	.	.
$A_5^{+,+,-}$	.	-1	.	1	.	.	.	.	.	.	.	.	.	.	.	.	.	.	.	.	.	.	.
$A_5^{+,-,+}$	.	.	-1	.	1	.	.	.	.	.	.	.	.	.	.	.	.	.	.	.	.	.	.
$A_5^{+,-,-}$	.	.	.	-1	1	.	.	.	.	.	.	.	.	.	.	.	.	.	.	.	.	.	.
$A_5^{-,+,+}$	.	.	.	1	.	.	.	.	.	.	.	.	.	.	.	.	.	.	.	.	.	.	.
$A_5^{-,+,-}$	.	.	1	.	.	.	.	.	.	.	.	.	.	.	.	.	.	.	.	.	.	.	.
$A_5^{-,-,+}$	.	1	.	.	.	.	.	.	.	.	.	.	.	.	.	.	.	.	.	.	.	.	.
$A_5^{-,-,-}$	1	.	.	.	.	.	.	.	.	.	.	.	.	.	.	.	.	.	.	.	.	.	.
$A_4^{+,e/h}$	.	.	.	-2	.	.	.	.	-2	-2	.	.	.	.	.	.	.	.	.	.	.	.	-1
$A_4^{-,e/h}$	.	.	.	.	-2	.	.	-2	.	-2	.	.	.	.	.	.	.	.	.	.	.	.	1
$A_3^{+,+,q}$	.	.	.	.	.	1	.	1	1	.	.	.	.	.	.	.	.	.	.	.	.	.	.
$A_3^{+,-,q}$	.	.	.	.	.	.	.	1	1	.	.	.	.	.	.	.	.	.	.	.	.	.	.
$A_3^{-,+,q}$	.	.	.	.	.	.	.	.	.	1	1	.	.	.	.	.	.	.	.	.	.	.	.
$A_3^{-,-,q}$	.	.	.	.	.	-1	.	.	.	1	1	.	.	.	.	.	.	.	.	.	.	.	.
$D_{4,q}^{-,\pm,+}$	.	.	.	.	.	.	.	-1	.	-1	.	.	.	.	.	.	.	.	.	.	.	.	.
$D_{4,q}^{-,\pm,-}$	.	.	.	.	.	.	.	.	-1	-1	.	.	.	.	.	.	.	.	.	.	.	.	.
$D_{4,a/c}^{+,\pm,+}$	.	.	.	.	.	.	1	1	1	.	.	.	.	.	.	.	.	.	.	.	.	.	.
$D_{4,a/c}^{+,\pm,-}$	.	.	.	.	.	.	.	1	1	1	.	.	.	.	.	.	.	.	.	.	.	.	.
$D_{4,b}^{+,\pm,+}$	.	.	.	.	.	.	-1	.	.	.	.	.	.	.	.	.	.	.	.	.	.	.	.
$D_{4,b}^{+,\pm,-}$	.	.	.	.	.	.	.	-1	.	.	.	.	.	.	.	.	.	.	.	.	.	.	.
$D_5^{+,+}$	.	.	.	.	.	.	.	.	2	.	.	.	.	.	.	.	.	.	.	.	.	.	-1
$D_5^{+,-}$	.	.	.	.	.	.	.	.	.	2	.	.	.	.	.	.	.	.	.	.	.	.	.
$D_5^{-,+}$	.	.	.	.	.	.	.	.	.	.	2	.	.	.	.	.	.	.	.	.	.	.	1
$D_5^{-,-}$	.	.	.	.	.	.	.	.	.	.	.	2	.	.	.	.	.	.	.	.	.	.	.
$D_4^{-,+}A_2$	.	.	.	.	.	.	.	.	.	.	.	.	1	.	-1	.	.	-2	.	.	.	.	.
$D_4^{-,-}A_2$	.	.	.	.	.	.	.	.	.	.	.	.	.	1	.	-1	-2	.	.	.	.	.	.
$D_{4,2}^{+,+}A_2$	.	.	.	.	.	.	.	.	.	.	.	.	-1	.	.	.	.	.	.	.	.	.	-2
$D_{4,2}^{+,-}A_2$	.	.	.	.	.	.	.	.	.	.	.	.	.	-1	.	.	.	.	.	.	.	.	.
$D_{4,1}^{+,+}A_2$	.	.	.	.	.	.	.	.	.	.	.	.	.	.	.	.	.	.	.	.	.	.	2
$D_{4,1}^{+,-}A_2$	.	.	.	.	.	.	.	.	.	.	.	.	.	.	.	.	.	.	.	.	.	.	.
$D_{4,0}^{+,+}A_2$	.	.	.	.	.	.	.	.	.	.	.	.	.	.	.	1	.	.	.	.	.	.	.
$D_{4,0}^{+,-}A_2$	.	.	.	.	.	.	.	.	.	.	.	.	.	.	.	.	1	.	.	.	.	.	.

Table 2	$t$	$sw_{++}$	$sw_{+-}$	$sw_{-+}$	$sw_{--}$	$c_{++}$	$c_{+-}$	$c_{-+}$	$c_{--}$	$d_+^+$	$d_-^+$	$d_+^-$	$d_-^-$	$\chi$	15
$TA_2^3$	2	.	.	.	.	.	.	.	.	.	.	.	.	.	.
$A_3^\pm + A_2^2$	2	.	.	.	.	.	.	.	.	.	.	.	.	.	.
$A_3^\pm - A_2^2$	2	.	.	.	.	.	.	.	.	.	.	.	.	.	.
$A_3^{2,e;+,+,+}$	.	.	.	.	.	4	.	.	.	.	.	.	.	.	.
$A_3^{2,e;+,+,-}$	.	.	.	.	.	2	2	.	.	.	.	.	.	.	.
$A_3^{2,e;+,-,+}$	.	.	.	.	.	2	.	2	.	.	.	.	.	.	.
$A_3^{2,e;+,-,-}$	.	.	.	.	.	2	.	.	2	.	.	.	.	.	.
$A_3^{2,e;+,-,+}$	.	.	.	.	.	.	4	.	.	.	.	.	.	.	.
$A_3^{2,e;+,-,-}$	.	.	.	.	.	.	2	2	.	.	.	.	.	.	.
$A_3^{2,e;+,-,+}$	.	.	.	.	.	.	.	4	.	.	.	.	.	.	.
$A_3^{2,e;+,-,-}$	.	.	.	.	.	.	2	.	2	.	.	.	.	.	.
$A_3^{2,e;-,-,+}$	.	.	.	.	.	.	.	4	.	.	.	.	.	.	.
$A_3^{2,e;-,-,-}$	.	.	.	.	.	.	.	.	4	.	.	.	.	.	.
$A_3^{2,h;+,+,-}$	.	.	.	.	.	2	-2	.	.	.	.	.	.	.	.
$A_3^{2,h;+,-,+}$	.	.	.	.	.	2	.	-2	.	.	.	.	.	.	.
$A_3^{2,h;+,-,-}$	.	.	.	.	.	2	.	.	-2	.	.	.	.	.	.
$A_3^{2,h;+,-,+}$	.	.	.	.	.	.	2	-2	.	.	.	.	.	.	.
$A_3^{2,h;+,-,-}$	.	.	.	.	.	.	2	.	-2	.	.	.	.	.	.
$A_3^{2,h;-,-,+}$	.	.	.	.	.	.	.	2	-2	.	.	.	.	.	.
$A_4^+ A_2$	1	.	.	.	.	1	.	.	1	.	.	.	.	.	.
$A_4^- A_2$	1	.	.	.	.	.	1	1	.	.	.	.	.	.	.
$TA_3^+ + A_2$	.	.	.	.	.	2	.	.	.	.	.	.	.	.	.
$TA_3^+ - A_2$	.	.	.	.	.	.	2	.	.	.	.	.	.	.	.
$TA_3^- + A_2$	.	.	.	.	.	.	.	2	.	.	.	.	.	.	.
$TA_3^- - A_2$	.	.	.	.	.	.	.	.	2	.	.	.	.	.	.
$A_5^+,+,+$	.	.	.	.	2	2	.	.	.	.	.	.	.	.	.
$A_5^+,+,-$	.	2	.	.	.	2	.	.	.	.	.	.	.	.	.
$A_5^+,-,+$	.	.	.	2	.	.	2	.	.	.	.	.	.	.	.
$A_5^+,-,-$	.	.	2	.	.	.	2	.	.	.	.	.	.	.	.
$A_5^-,+,+$	.	.	2	.	.	.	.	2	.	.	.	.	.	.	.
$A_5^-,+,-$	.	.	.	2	.	.	.	2	.	.	.	.	.	.	.
$A_5^-,-,+$	.	2	.	.	.	.	.	.	2	.	.	.	.	.	.
$A_5^-,-,-$	.	.	.	.	2	.	.	.	2	.	.	.	.	.	.
$A_4^+,e/h$	.	1	.	.	1	.	.	.	.	.	.	.	.	.	.
$A_4^-,e/h$	.	.	1	1	.	.	.	.	.	.	.	.	.	.	.
$A_3^+,+,q$	.	.	.	.	.	.	.	.	.	.	.	.	.	1	1
$A_3^+,-,q$	.	.	.	.	.	.	.	.	.	.	.	.	.	1	-1
$A_3^-+,q$	.	.	.	.	.	.	.	.	.	.	.	.	.	1	-1
$A_3^-,-,q$	.	.	.	.	.	.	.	.	.	.	.	.	.	1	1
$D_{4,q}^-, \pm, +$	.	.	.	.	.	.	.	.	.	.	.	2	.	1	.
$D_{4,q}^-, \pm, -$	.	.	.	.	.	.	.	.	.	.	.	.	2	1	.
$D_{4,a/c}^+, \pm, +$	.	.	.	.	.	.	.	.	.	2	.	.	.	-1	.
$D_{4,a/c}^+, \pm, -$	.	.	.	.	.	.	.	.	.	.	2	.	.	-1	.
$D_{4,b}^+, \pm, +$	.	.	.	.	.	.	.	.	.	2	.	.	.	-1	.
$D_{4,b}^+, \pm, -$	.	.	.	.	.	.	.	.	.	.	2	.	.	-1	.
$D_5^+, +$	.	.	1	1	.	-2	.	.	.	-1	.	1	.	.	.
$D_5^+, -$	.	1	.	.	1	.	-2	.	.	.	-1	.	1	.	.
$D_5^-, +$	.	1	.	.	1	.	.	-2	.	-1	.	1	.	.	.
$D_5^-, -$	.	.	1	1	.	.	.	.	-2	.	-1	.	1	.	.
$D_4^-, + A_2$	.	.	.	.	.	3	.	-3	.	.	.	.	.	.	.
$D_4^-, - A_2$	.	.	.	.	.	.	3	.	-3	.	.	.	.	.	.
$D_{4,2}^+, + A_2$	2	.	.	.	.	1	.	-1	.	.	.	.	.	.	.
$D_{4,2}^+, - A_2$	2	.	.	.	.	.	1	.	-1	.	.	.	.	.	.
$D_{4,1}^+, + A_2$	.	.	.	.	.	1	.	-1	.	.	.	.	.	.	.
$D_{4,1}^+, - A_2$	.	.	.	.	.	.	1	.	-1	.	.	.	.	.	.
$D_{4,0}^+, + A_2$	-2	.	.	.	.	1	.	-1	.	.	.	.	.	.	.
$D_{4,0}^+, - A_2$	-2	.	.	.	.	.	1	.	-1	.	.	.	.	.	.

Table 3	15	16	17	17	17	18	18	20	20	22	22	23	23	27	27
$A_2^4$	.	1	.	.	.	.	.	.	.	.	.	.	.	.	.
$TA_2^2$	.	.	.	.	.	.	.	1	1	1	1	.	.	.	.
$TA_2^3$	1	.	.	.	.	.	.	.	.	.	.	.	.	.	.
$A_3^{\pm,+}A_2^2$	.	1	1	1	.	.	.	.	.	.	.	.	.	.	.
$A_3^{\pm,-}A_2^2$	.	1	.	.	1	.	.	.	.	.	.	.	.	.	.
$A_3^{2,e/h;+,+,+,+}$	.	.	1	.	.	.	.	.	.	.	.	.	.	.	.
$A_3^{2,e/h;+,+,+,-}$	.	.	.	.	.	.	.	.	.	.	.	.	.	.	.
$A_3^{2,e/h;+,+,-,+}$	.	.	.	.	.	.	.	.	.	.	.	.	.	.	.
$A_3^{2,e/h;+,+,-,-}$	.	.	1	.	1	1	.	.	.	.	.	.	.	.	.
$A_3^{2,e/h;+,-,+,-}$	.	.	.	.	.	.	.	.	.	.	.	.	.	.	.
$A_3^{2,e/h;+,-,-,+}$	.	.	.	.	.	.	.	1	.	.	.	.	.	.	.
$A_3^{2,e/h;+,-,-,-}$	.	.	.	.	.	.	.	.	.	.	.	.	.	.	.
$A_3^{2,e/h;-,-,+,-}$	.	.	.	.	.	.	.	.	.	.	.	.	.	.	.
$A_3^{2,e/h;-,-,-,-}$	.	.	.	.	1	.	.	.	.	.	.	.	.	.	.
$A_4^+A_2$	.	.	.	.	.	.	.	.	.	.	.	.	.	.	.
$A_4^-A_2$	.	.	.	.	.	.	.	.	.	.	.	.	.	.	.
$TA_3^{\pm,+}A_2$	1	.	.	.	.	.	.	.	.	.	.	.	.	1	1
$TA_3^{\pm,-}A_2$	1	.	.	.	.	.	.	.	.	.	.	.	.	1	1
$A_5^{+,\pm}$	.	.	.	.	.	1	.	.	.	.	.	.	.	.	.
$A_5^{-,\pm}$	.	.	.	.	.	.	1	.	.	.	.	.	.	.	.
$A_5^{+,\pm}$	.	.	.	.	.	.	1	.	.	.	.	.	.	.	.
$A_5^{-,\pm}$	.	.	.	.	.	1	.	.	.	.	.	.	.	.	.
$A_4^{+,e/h}$	.	.	.	.	.	.	.	.	.	.	.	.	.	.	.
$A_4^{-,e/h}$	.	.	.	.	.	.	.	.	.	.	.	.	.	.	.
$A_3^{+,-,q}$	.	.	.	.	.	.	.	1	.	.	.	1	1	.	.
$A_3^{-,-,q}$	.	.	.	.	.	.	.	.	1	.	.	1	1	.	.
$A_3^{-,+,-,q}$	.	.	.	.	.	.	.	.	1	.	.	.	.	.	.
$A_3^{-,-,-,q}$	.	.	.	.	.	.	.	1	.	.	.	.	.	.	.
$D_{4,q}^{-,\pm,+}$	.	.	.	.	.	.	.	.	.	.	.	1	.	.	.
$D_{4,q}^{-,\pm,-}$	.	.	.	.	.	.	.	.	.	.	.	.	1	.	.
$D_{4,q}^{+,\pm,+}$	.	.	.	.	.	.	.	.	.	1	.	1	.	.	.
$D_{4,a/c}^{+,\pm,-}$	.	.	.	.	.	.	.	.	.	.	1	.	1	.	.
$D_{4,b}^{+,\pm,+}$	.	.	.	.	.	.	.	.	.	1	.	.	.	.	.
$D_{4,b}^{+,\pm,-}$	.	.	.	.	.	.	.	.	.	.	1	.	.	.	.
$D_5^{+,+}$	.	.	.	.	.	.	.	.	.	.	.	.	.	.	.
$D_5^{+,-}$	.	.	.	.	.	.	.	.	.	.	.	.	.	.	.
$D_5^{-,+}$	.	.	.	.	.	.	.	.	.	.	.	.	.	.	.
$D_5^{-,-}$	.	.	.	.	.	.	.	.	.	.	.	.	.	.	.
$D_4^{-,+}A_2$	.	.	.	.	.	.	.	.	.	.	.	.	.	1	.
$D_4^{-,-}A_2$	.	.	.	.	.	.	.	.	.	.	.	.	.	.	1
$D_{4,2}^{+,+}A_2$	.	.	.	.	.	.	.	.	.	.	.	.	.	1	.
$D_{4,2}^{+,-}A_2$	.	.	.	.	.	.	.	.	.	.	.	.	.	.	1
$D_{4,1}^{+,+}A_2$	.	.	.	.	.	.	.	.	.	.	.	.	.	.	.
$D_{4,1}^{+,-}A_2$	.	.	.	.	.	.	.	.	.	.	.	.	.	.	.
$D_{4,0}^{+,+}A_2$	.	.	.	.	.	.	.	.	.	.	.	.	.	.	.
$D_{4,0}^{+,-}A_2$	.	.	.	.	.	.	.	.	.	.	.	.	.	.	.

Table 3 cont.	27	27	28	28	28	28	28	28	34	34	35	35
$A_2^4$	.	.	.	.	.	.	.	.	.	.	.	.
$TA_2^2$	.	.	.	.	.	.	.	.	.	.	.	.
$TA_2^3$	.	.	.	.	.	.	.	.	1	1	.	.
$A_3^{\pm,+}A_2^2$	.	.	.	.	.	.	.	.	.	.	.	.
$A_3^{\pm,-}A_2^2$	.	.	.	.	.	.	.	.	.	.	.	.
$A_3^{2,e/h;+,+,+,+}$	.	.	.	.	.	1	.	.	.	.	.	.
$A_3^{2,e/h;+,+,+,-}$	.	.	.	.	.	.	1	.	.	.	1	1
$A_3^{2,e/h;+,+,-,+}$	.	.	1	.	.	1	.	.	.	.	.	.
$A_3^{2,e/h;+,+,-,-}$	.	.	.	.	.	.	.	.	.	.	.	.
$A_3^{2,e/h;+,-,+,-}$	.	.	.	.	.	.	.	1	.	.	.	.
$A_3^{2,e/h;+,-,-,+}$	.	.	.	1	.	.	1	.	.	.	.	.
$A_3^{2,e/h;+,-,-,-}$	.	.	.	.	1	.	.	1	.	.	.	.
$A_3^{2,e/h;-,-,+,-}$	.	.	1	.	.	.	.	.	.	.	.	.
$A_3^{2,e/h;-,-,-,-}$	.	.	.	.	1	.	.	.	.	.	.	.
$A_4^+A_2$	.	.	.	.	.	.	.	.	.	.	.	.
$A_4^-A_2$	.	.	.	.	.	.	.	.	.	.	.	.
$TA_3^{\pm,+}A_2$	1	1	.	.	.	.	.	.	.	.	.	.
$TA_3^{\pm,-}A_2$	1	1	.	.	.	.	.	.	.	.	.	.
$A_5^{+,+,\pm}$	.	.	.	.	.	.	.	.	.	.	.	.
$A_5^{+,-,\pm}$	.	.	.	.	.	.	.	.	.	.	.	.
$A_5^{-,+,\pm}$	.	.	.	.	.	.	.	.	.	.	.	.
$A_5^{-,-,\pm}$	.	.	.	.	.	.	.	.	.	.	.	.
$A_4^{+,e/h}$	.	.	.	.	.	.	.	.	.	1	1	.
$A_4^{-,e/h}$	.	.	.	.	.	.	.	.	.	1	1	.
$A_3^{+,+,q}$	.	.	.	.	.	.	.	.	.	.	.	.
$A_3^{+,-,q}$	.	.	.	.	.	.	.	.	.	.	.	.
$A_3^{-,+,q}$	.	.	.	.	.	.	.	.	.	.	.	.
$A_3^{-,-,q}$	.	.	.	.	.	.	.	.	.	.	.	.
$D_{4,q}^{-,\pm,+}$	.	.	.	.	.	.	.	.	.	.	.	.
$D_{4,q}^{-,\pm,-}$	.	.	.	.	.	.	.	.	.	.	.	.
$D_{4,a/c}^{+,\pm,+}$	.	.	.	.	.	.	.	.	.	.	.	.
$D_{4,a/c}^{+,\pm,-}$	.	.	.	.	.	.	.	.	.	.	.	.
$D_{4,b}^{+,\pm,+}$	.	.	.	.	.	.	.	.	.	.	.	.
$D_{4,b}^{+,\pm,-}$	.	.	.	.	.	.	.	.	.	.	.	.
$D_5^{+,+}$	.	.	.	.	.	.	.	.	.	.	1	.
$D_5^{+,-}$	.	.	.	.	.	.	.	.	.	.	.	1
$D_5^{-,+}$	.	.	.	.	.	.	.	.	.	.	1	.
$D_5^{-,-}$	.	.	.	.	.	.	.	.	.	.	.	1
$D_4^{-,+}A_2$	1	.	.	.	.	.	.	.	.	.	.	.
$D_4^{-,-}A_2$	.	1	.	.	.	.	.	.	.	.	.	.
$D_{4,2}^{+,+}A_2$	.	.	.	.	.	.	.	.	.	.	.	.
$D_{4,2}^{+,-}A_2$	.	.	.	.	.	.	.	.	.	.	.	.
$D_{4,1}^{+,+}A_2$	.	.	.	.	.	.	.	.	1	.	.	.
$D_{4,1}^{+,-}A_2$	.	.	.	.	.	.	.	.	.	1	.	.
$D_{4,0}^{+,+}A_2$	1	.	.	.	.	.	.	.	1	.	.	.
$D_{4,0}^{+,-}A_2$	.	1	.	.	.	.	.	.	.	1	.	.

Table Z	$t$	$sw_{++}$	$sw_{+-}$	$c_{++}$	$c_{+-}$	$d_{+}^{+}$	$d_{-}^{+}$	$\chi$	15	$(sw_{++} + sw_{--})/2$	$(sw_{+-} + sw_{-+})/2$
$TA_2^3$	2	.	.	.	.	.	.	.	.	.	.
$A_3^{\pm,+} A_2^{\pm}$	2	.	.	.	.	.	.	.	.	.	.
$A_3^{\pm,-} A_2^{\pm}$	2	.	.	.	.	.	.	.	.	.	.
$A_3^{2,e;+,+,+,+}$	.	.	.	4	.	.	.	.	.	.	.
$A_3^{2,e;+,+,+,-}$	.	.	.	2	2	.	.	.	.	.	.
$A_3^{2,e;+,+,-,+}$	.	.	.	2	.	.	.	.	.	.	.
$A_3^{2,e;+,+,-,-}$	.	.	.	2	.	.	.	.	.	.	.
$A_3^{2,e;+,-,+,-}$	.	.	.	.	4	.	.	.	.	.	.
$A_3^{2,e;+,-,-,+}$	.	.	.	.	2	.	.	.	.	.	.
$A_3^{2,e;+,-,-,-}$	.	.	.	.	2	.	.	.	.	.	.
$A_3^{2,e;-,+,-,+}$	.	.	.	.	.	.	.	.	.	.	.
$A_3^{2,e;-,+,-,-}$	.	.	.	.	.	.	.	.	.	.	.
$A_3^{2,e;-,-,-,-}$	.	.	.	.	.	.	.	.	.	.	.
$A_3^{2,h;+,+,+,-}$	.	.	.	2	-2	.	.	.	.	.	.
$A_3^{2,h;+,+,-,+}$	.	.	.	2	.	.	.	.	.	.	.
$A_3^{2,h;+,+,-,-}$	.	.	.	2	.	.	.	.	.	.	.
$A_3^{2,h;+,-,-,+}$	.	.	.	.	2	.	.	.	.	.	.
$A_3^{2,h;+,-,-,-}$	.	.	.	.	2	.	.	.	.	.	.
$A_3^{2,h;-,-,+,-}$	.	.	.	.	.	.	.	.	.	.	.
$A_4^+ A_2$	1	.	.	1	.	.	.	.	.	.	.
$A_4^- A_2$	1	.	.	.	1	.	.	.	.	.	.
$TA_3^{+,+} A_2$	.	.	.	2	.	.	.	.	.	.	.
$TA_3^{+,-} A_2$	.	.	.	.	2	.	.	.	.	.	.
$TA_3^{-,+} A_2$	.	.	.	.	.	.	.	.	.	.	.
$TA_3^{-,-} A_2$	.	.	.	.	.	.	.	.	.	.	.
$A_5^{+,+,+}$	.	.	.	2	.	.	.	.	.	1	.
$A_5^{+,+,-}$	.	2	.	2	.	.	.	.	.	1	.
$A_5^{+,-,+}$	.	.	.	.	2	.	.	.	.	.	1
$A_5^{+,-,-}$	.	.	2	.	2	.	.	.	.	.	1
$A_5^{-,+,+}$	.	.	2	.	.	.	.	.	.	.	1
$A_5^{-,+,-}$	.	.	.	.	.	.	.	.	.	.	1
$A_5^{-,-,+}$	.	2	.	.	.	.	.	.	.	1	.
$A_5^{-,-,-}$	.	.	.	.	.	.	.	.	.	1	.
$A_4^{+,e/h}$	.	1	.	.	.	.	.	.	.	1	.
$A_4^{-,e/h}$	.	.	1	.	.	.	.	.	.	.	1
$A_3^{+,+,q}$	.	.	.	.	.	.	.	1	1	.	.
$A_3^{+,-,q}$	.	.	.	.	.	.	.	1	-1	.	.
$A_3^{-,+,q}$	.	.	.	.	.	.	.	1	-1	.	.
$A_3^{-,-,q}$	.	.	.	.	.	.	.	1	1	.	.
$D_{4,q}^{\pm,+}$	.	.	.	.	.	.	.	1	.	.	.
$D_{4,q}^{\pm,-}$	.	.	.	.	.	.	.	1	.	.	.
$D_{4,a/c}^{+, \pm,+}$	.	.	.	.	.	2	.	-1	.	.	.
$D_{4,a/c}^{+, \pm,-}$	.	.	.	.	.	.	2	-1	.	.	.
$D_{4,b}^{+, \pm,+}$	.	.	.	.	.	2	.	-1	.	.	.
$D_{4,b}^{+, \pm,-}$	.	.	.	.	.	.	2	-1	.	.	.
$D_5^{+,+}$	.	.	1	-2	.	-1	.	.	.	.	1
$D_5^{+,-}$	.	1	.	.	-2	.	-1	.	.	1	.
$D_5^{-,+}$	.	1	.	.	.	-1	.	.	.	1	.
$D_5^{-,-}$	.	.	1	.	.	.	-1	.	.	.	1
$D_4^{-,+} A_2$	.	.	.	3	.	.	.	.	.	.	.
$D_4^{-,-} A_2$	.	.	.	.	3	.	.	.	.	.	.
$D_{4,2}^{+,+} A_2$	2	.	.	1	.	.	.	.	.	.	.
$D_{4,2}^{+,-} A_2$	2	.	.	.	1	.	.	.	.	.	.
$D_{4,1}^{+,+} A_2$	.	.	.	1	.	.	.	.	.	.	.
$D_{4,1}^{+,-} A_2$	.	.	.	.	1	.	.	.	.	.	.
$D_{4,0}^{+,+} A_2$	-2	.	.	1	.	.	.	.	.	.	.
$D_{4,0}^{+,-} A_2$	-2	.	.	.	1	.	.	.	.	.	.



Table Z cont.	$(d_+^+ + d_-^-)/2$	$(t + c_{++} + c_{--})/2$	$(t + c_{+-} + c_{-+})/2$	$((d_+^+ + d_-^- + d_+^+ + d_-^-)/2) + \chi + 15)/2$
$TA_2^3$	.	1	1	.
$A_3^{\pm,+}A_2^2$	.	1	1	.
$A_3^{\pm,-}A_2^2$	.	1	1	.
$A_3^{2,e;+,+,+}$	.	2	.	.
$A_3^{2,e;+,+,-}$	.	1	1	.
$A_3^{2,e;+,-,+}$	.	2	.	.
$A_3^{2,e;+,-,-}$	.	1	1	.
$A_3^{2,e;+,-,-}$	.	.	2	.
$A_3^{2,e;+,-,-}$	.	1	1	.
$A_3^{2,e;+,-,-}$	.	.	2	.
$A_3^{2,e;+,-,-}$	.	2	.	.
$A_3^{2,e;+,-,-}$	.	1	1	.
$A_3^{2,e;+,-,-}$	.	.	2	.
$A_3^{2,e;+,-,-}$	.	2	.	.
$A_3^{2,e;+,-,-}$	.	1	1	.
$A_3^{2,e;+,-,-}$	.	.	2	.
$A_3^{2,h;+,+,-}$	.	1	-1	.
$A_3^{2,h;+,-,+}$	.	.	.	.
$A_3^{2,h;+,-,+}$	.	1	-1	.
$A_3^{2,h;+,-,+}$	.	-1	1	.
$A_3^{2,h;+,-,+}$	.	.	.	.
$A_3^{2,h;+,-,+}$	.	1	-1	.
$A_3^{2,h;+,-,+}$	.	.	.	.
$A_4^+A_2$	.	1	1	.
$A_4^-A_2$	.	1	1	.
$TA_3^{+,+}A_2$	.	1	.	.
$TA_3^{+,-}A_2$	.	.	1	.
$TA_3^{-,+}A_2$	.	1	.	.
$TA_3^{-,-}A_2$	.	.	1	.
$A_5^{+,+,+}$	.	1	.	.
$A_5^{+,+,-}$	.	1	.	.
$A_5^{+,-,+}$	.	.	1	.
$A_5^{+,-,-}$	.	.	1	.
$A_5^{-,+,+}$	.	1	.	.
$A_5^{-,+,-}$	.	1	.	.
$A_5^{-,-,+}$	.	.	1	.
$A_5^{-,-,-}$	.	.	1	.
$A_4^{+,e/h}$	.	.	.	.
$A_4^{-,e/h}$	.	.	.	.
$A_3^{+,+,q}$	.	.	.	1
$A_3^{+,-,q}$	.	.	.	.
$A_3^{-,+,q}$	.	.	.	.
$A_3^{-,-,q}$	.	.	.	1
$D_{4,q}^{\pm,+}$	1	.	.	1
$D_{4,q}^{\pm,-}$	.	.	.	1
$D_{4,a/c}^{\pm,+}$	1	.	.	.
$D_{4,a/c}^{\pm,-}$	.	.	.	.
$D_{4,b}^{\pm,+}$	1	.	.	.
$D_{4,b}^{\pm,-}$	.	.	.	.
$D_5^{+,+}$	.	-1	.	.
$D_5^{+,-}$	.	.	-1	.
$D_5^{-,+}$	.	-1	.	.
$D_5^{-,-}$	.	.	-1	.
$D_4^{-,+}A_2$	.	.	.	.
$D_4^{-,-}A_2$	.	.	.	.
$D_{4,2}^{+,+}A_2$	.	1	1	.
$D_{4,2}^{+,-}A_2$	.	1	1	.
$D_{4,1}^{+,+}A_2$	.	.	.	.
$D_{4,1}^{+,-}A_2$	.	.	.	.
$D_{4,0}^{+,+}A_2$	.	-1	-1	.
$D_{4,0}^{+,-}A_2$	.	-1	-1	.

Table 4	$t$	$sw_{++}$	$sw_{+-}$	$c_{++}$	$c_{+-}$	$d_+^+$	$d_-^+$	$\chi$	15	$(sw_{++} + sw_{--})/2$	$(sw_{+-} + sw_{-+})/2$
$A_2^4$	.	.	.	.	.	.	.	.	.	.	.
$TA_2^2$	.	.	.	.	.	.	.	.	.	.	.
$TA_2^3$	.	.	.	.	.	.	.	.	.	.	.
$A_3^{\pm,+}A_2^2$	.	.	.	.	.	.	.	.	.	.	.
$A_3^{\pm,-}A_2^2$	.	.	.	.	.	.	.	.	.	.	.
$A_3^{2,e/h;+,+,+,+}$	.	.	.	.	.	.	.	.	.	.	.
$A_3^{2,e/h;+,+,+,-}$	.	.	.	.	.	.	.	.	.	.	.
$A_3^{2,e/h;+,+,-,+}$	.	.	.	.	.	.	.	.	.	.	.
$A_3^{2,e/h;+,+,-,-}$	.	.	.	.	.	.	.	.	.	.	.
$A_3^{2,e/h;+,-,+,+}$	.	.	.	.	.	.	.	.	.	.	.
$A_3^{2,e/h;+,-,-,+}$	.	.	.	.	.	.	.	.	.	.	.
$A_3^{2,e/h;+,-,-,-}$	.	.	.	.	.	.	.	.	.	.	.
$A_3^{2,e/h;-,+,-,+}$	.	.	.	.	.	.	.	.	.	.	.
$A_3^{2,e/h;-,+,-,-}$	.	.	.	.	.	.	.	.	.	.	.
$A_3^{2,e/h;-,-,-,-}$	.	.	.	.	.	.	.	.	.	.	.
$A_4^+A_2$	1	.	.	1	.	.	.	.	.	.	.
$A_4^-A_2$	1	.	.	.	1	.	.	.	.	.	.
$TA_3^{\pm,+}A_2$	.	.	.	.	.	.	.	.	.	.	.
$TA_3^{\pm,-}A_2$	.	.	.	.	.	.	.	.	.	.	.
$A_5^{+,+,\pm}$	.	.	.	.	.	.	.	.	.	1	.
$A_5^{+,-,\pm}$	.	.	.	.	.	.	.	.	.	.	1
$A_5^{-,+,\pm}$	.	.	.	.	.	.	.	.	.	.	1
$A_5^{-,-,\pm}$	.	.	.	.	.	.	.	.	.	1	.
$A_4^{+,e/h}$	.	1	.	.	.	.	.	.	.	1	.
$A_4^{-,e/h}$	.	.	1	.	.	.	.	.	.	.	1
$A_3^{+,+,q}$	.	.	.	.	.	.	.	1	1	.	.
$A_3^{+,-,q}$	.	.	.	.	.	.	.	1	1	.	.
$A_3^{-,+ ,q}$	.	.	.	.	.	.	.	1	1	.	.
$A_3^{-,-,q}$	.	.	.	.	.	.	.	1	1	.	.
$D_{4,q}^{-,\pm,+}$	.	.	.	.	.	.	.	1	.	.	.
$D_{4,q}^{-,\pm,-}$	.	.	.	.	.	.	.	1	.	.	.
$D_{4,a/c}^{+,\pm,+}$	.	.	.	.	.	.	.	1	.	.	.
$D_{4,a/c}^{+,\pm,-}$	.	.	.	.	.	.	.	1	.	.	.
$D_{4,b}^{+,\pm,+}$	.	.	.	.	.	.	.	1	.	.	.
$D_{4,b}^{+,\pm,-}$	.	.	.	.	.	.	.	1	.	.	.
$D_5^{+,+}$	.	.	1	.	.	1	.	.	.	.	1
$D_5^{+,-}$	.	1	.	.	.	.	1	.	.	1	.
$D_5^{-,+}$	.	1	.	.	.	1	.	.	.	1	.
$D_5^{-,-}$	.	.	1	.	.	.	1	.	.	.	1
$D_4^{-,+}A_2$	.	.	.	1	.	.	.	.	.	.	.
$D_4^{-,-}A_2$	.	.	.	.	1	.	.	.	.	.	.
$D_{4,2}^{+,+}A_2$	.	.	.	1	.	.	.	.	.	.	.
$D_{4,2}^{+,-}A_2$	.	.	.	.	1	.	.	.	.	.	.
$D_{4,1}^{+,+}A_2$	.	.	.	1	.	.	.	.	.	.	.
$D_{4,1}^{+,-}A_2$	.	.	.	.	1	.	.	.	.	.	.
$D_{4,0}^{+,+}A_2$	.	.	.	1	.	.	.	.	.	.	.
$D_{4,0}^{+,-}A_2$	.	.	.	.	1	.	.	.	.	.	.

Table 4 cont.	$(d_+^+ + d_+^-)/2$	$(t + c_{+++} + c_{-+})/2$	$(t + c_{+-} + c_{--})/2$	$((d_+^+ + d_+^- + d_-^+ + d_-^-)/2) + \chi + 15)/2$	16	17	18	19	20
$A_2^4$	.	.	.	.	.	.	.	1	.
$TA_2^2$	.	.	.	.	1	.	.	.	.
$TA_2^3$	.	1	1	.	.	1	.	.	.
$A_3^{\pm,+} A_2^2$	.	1	1	.	.	.	.	.	.
$A_3^{\pm,-} A_2^2$	.	1	1	.	.	.	.	1	.
$A_3^{2,e/h;+,+,+,+}$	.	.	.	.	.	.	1	.	.
$A_3^{2,e/h;+,+,+,-}$	.	1	1	.	.	.	1	.	.
$A_3^{2,e/h;+,+,-,+}$	.	.	.	.	.	.	1	.	.
$A_3^{2,e/h;+,+,-,-}$	.	1	1	.	.	.	1	.	.
$A_3^{2,e/h;+,-,+,-}$	.	.	.	.	.	.	1	1	.
$A_3^{2,e/h;+,-,-,+}$	.	1	1	.	.	.	1	.	.
$A_3^{2,e/h;+,-,-,-}$	.	.	.	.	.	.	1	1	.
$A_3^{2,e/h;-,+,-,+}$	.	.	.	.	.	.	1	.	.
$A_3^{2,e/h;-,+,-,-}$	.	1	1	.	.	.	1	.	.
$A_3^{2,e/h;-,-,-,-}$	.	.	.	.	.	.	1	1	.
$A_4^+ A_2$	.	1	1	.	.	.	.	.	1
$A_4^- A_2$	.	1	1	.	.	.	.	.	.
$TA_3^{\pm,+} A_2$	.	1	.	.	.	.	.	.	.
$TA_3^{\pm,-} A_2$	.	.	1	.	.	1	.	.	.
$A_5^{+,+,\pm}$	.	1	.	.	.	.	.	.	.
$A_5^{+,-,\pm}$	.	.	1	.	.	.	.	.	.
$A_5^{-,+,\pm}$	.	1	.	.	.	.	1	.	.
$A_5^{-,-,\pm}$	.	.	1	.	.	.	1	.	.
$A_4^{+,e/h}$	.	.	.	.	.	.	.	.	.
$A_4^{-,e/h}$	.	.	.	.	.	.	.	.	.
$A_3^{+,-,q}$	.	.	.	.	1	.	.	.	.
$A_3^{-,+,-,q}$	.	.	.	.	.	1	.	.	.
$A_3^{-,-,-,q}$	.	.	.	.	1	1	.	.	.
$D_{4,q}^{-,\pm,+}$	1	.	.	.	1	.	.	.	.
$D_{4,q}^{-,\pm,-}$	.	.	.	.	1	.	.	.	.
$D_{4,a/c}^{+,\pm,+}$	1	.	.	.	.	.	.	.	.
$D_{4,a/c}^{+,\pm,-}$	.	.	.	.	.	.	.	.	.
$D_{4,b}^{+,\pm,+}$	1	.	.	.	.	1	.	.	.
$D_{4,b}^{+,\pm,-}$	.	.	.	.	.	1	.	.	.
$D_5^{+,+}$	.	1	.	.	.	.	.	.	.
$D_5^{+,-}$	.	.	1	.	.	.	.	.	.
$D_5^{-,+}$	.	1	.	.	.	.	.	.	.
$D_5^{-,-}$	.	.	1	.	.	.	.	.	.
$D_4^{-,+} A_2$	.	.	.	.	.	.	1	.	.
$D_4^{-,-} A_2$	.	.	.	.	.	.	1	.	.
$D_{4,2}^{+,+} A_2$	.	1	1	.	.	.	.	.	.
$D_{4,2}^{+,-} A_2$	.	1	1	.	.	.	.	.	.
$D_{4,1}^{+,+} A_2$	.	.	.	.	.	.	1	.	.
$D_{4,1}^{+,-} A_2$	.	.	.	.	.	.	1	.	.
$D_{4,0}^{+,+} A_2$	.	1	1	.	.	.	.	.	.
$D_{4,0}^{+,-} A_2$	.	1	1	.	.	.	.	.	.

# Chapter 4

## $D_6^+$ bifurcations

The aim of this chapter is to prove the  $D_6^+$  part of Theorem 2.6.2. Thus, we are going to derive cyclic equations **35-37**.

So, we now consider  $D_6^+$  bifurcations in detail. The main aim of this section is to understand the decorations of the strata that come from the  $D_6^+$  caustic,  $\mathcal{C}(D_6^+)$ . Since for our case we are considering the decoration  $s$  as well as  $\sigma$ , this chapter provides richer results than its parallel in [9], giving us 6 cyclic equations compared to 2.

Consider the  $\mathcal{R}_+$ -miniversal deformation of the  $D_6^+$  function singularity

$$\begin{aligned} F &= x^2y + \frac{1}{5}y^5 + \frac{1}{4}\alpha y^4 + \frac{1}{3}\beta y^3 + \frac{1}{2}\gamma y^2 + \delta y + \varepsilon x \\ &= x^2y + \varepsilon x + p(y) \end{aligned} \quad (8)$$

where  $\alpha, \beta, \gamma, \delta, \varepsilon \in \mathbb{R}$  are independent parameters.

Similar to Section 2.6.2.2 analysis of (8) yields the function

$$\Psi := y^2 p'(y) + \frac{\varepsilon^2}{4} = y^2(y^4 + \alpha y^3 + \beta y^2 + \gamma y + \delta) + \frac{\varepsilon^2}{4} \quad (9)$$

where we fix the weights of the variables as  $w_y = 1$ ,  $w_\alpha = 1$ ,  $w_\beta = 2$ ,  $w_\gamma = 3$ ,  $w_\delta = 4$  and  $w_\varepsilon = 3$ . Here, we use (9) to describe all degenerations in  $F$  in terms of those in  $\Psi$  (see Section 2.6.2.2 or [9] for the derivation of this function). This time the big caustic  $\mathcal{C}(D_6^+) \subset \mathbb{R}_{\alpha,\beta,\gamma,\delta,\varepsilon}^5$  corresponds to those polynomials  $\Psi$  which have either the root  $y = 0$  of multiplicity  $k > 2$  or a root  $y \neq 0$  of multiplicity  $k > 1$ . Again this results in  $\mathcal{C}(D_6^+)$  and its transversal sections having respectively  $D_k$  or  $A_k$  points. We should note we consider the  $D_3$  singularity as the  $A_3$  singularity at the origin  $x = y = 0$ .

Our task is now to analyse how we can represent  $\mathcal{C}(D_6^+)$  as a collection of 2-parameter bifurcations of 3-dimensional caustics. The corresponding bifurcation diagram in the parameter plane will be denoted  $\mathcal{B}(D_6^+)$ . In order to fulfill the task we study the generic map  $\pi : (\mathbb{R}_{\alpha,\beta,\gamma,\delta,\varepsilon}^5, \mathcal{C}(D_6^+)) \rightarrow \mathbb{R}^2$  by consideration of its two approximations by projections.

First we introduce the *straight projection* which is the principal part of the generic mapping  $\pi$ . It is defined as

$$\pi_s : (\mathbb{R}_{\alpha,\beta,\gamma,\delta,\varepsilon}^5) \rightarrow \mathbb{R}_{A,B}^2; (\alpha, \beta, \gamma, \delta, \varepsilon) \mapsto (A, B) = (\alpha, \beta).$$

Next is the *tilted projection* where we introduce terms of the next quasi-

homogeneous degree. This is

$$\pi_t : (\mathbb{R}_{\alpha,\beta,\gamma,\delta,\varepsilon}^5) \rightarrow \mathbb{R}_{A,B}^2; (\alpha, \beta, \gamma, \delta, \varepsilon) \mapsto (A, B) = (\alpha, \beta + C\gamma + E\varepsilon)$$

where  $C$  and  $E$  are arbitrary real coefficients.

In the rest of this chapter we analyse the contributions of different strata of  $\mathcal{C}(D_6^+)$  to the diagram  $\mathcal{B}_s(D_6^+)$  visible under the straight projection. If necessary we shall also analyse various tilted projections.

## 4.1 1-dimensional strata in $\mathcal{C}(D_6^+)$ and their straight projection

First we analyse the 1-dimensional strata of the  $D_6^+$  caustic and their straight projection. Here we introduce parametrisations of the strata in  $\mathcal{C}(D_6^+)$  based on the multiplicity options for the roots of  $\Psi$  that were mentioned before:

- $D_5$ :  $\Psi = y^5(y - u)$ ;
- $D_4A_2$ :  $\Psi = y^4(y - u)^2$ ;
- $D_3A_3$ :  $\Psi = y^3(y - u)^3$ ;
- $A_5$ :  $\Psi = (y - u)^5(y + \frac{u}{5})$ . However, the stratum is empty in  $\mathcal{C}(D_6^+)$  due to the positive sign of  $\varepsilon^2/4$  in (9);
- $A_4A_2$ :  $\Psi = (y - u)^4(y + \frac{u}{2})^2$ ;

- $A_3^2$ :  $\Psi = (y - u)^3(y + u)^3$  is also empty in  $\mathcal{C}(D_6^+)$  due to the same reason as before.

Here  $u \in \mathbb{R}$  and  $u \neq 0$ . In the last three cases the way the coefficients of  $u$  are chosen makes the coefficient of  $y$  in the expansion of  $\Psi$  zero.

In order to calculate the discriminantal strata in  $\mathcal{B}_s(D_6^+)$  we first equate the coefficients of the parametrisations above with those in (9) in order to find the strata in  $\mathcal{C}(D_6^+)$ . Then we obtain the discriminantal strata in  $\mathcal{B}_s(D_6^+)$  from the image of the map  $\pi_s$ ,  $(A, B) = (\alpha, \beta)$ . However, since these calculations have already been done in [9] we will just state the discriminantal strata.

The images of the 1-dimensional strata in  $\mathcal{B}_s(D_6^+)$  are:

- $D_5$ :  $B = 0$ ;
- $D_4A_2$ :  $A^2 = 4B$ ;
- $D_3A_3$ :  $A^2 = 3B$ ;
- $A_5$ : Empty in  $\mathcal{C}(D_6^+)$  and hence in  $\mathcal{B}_s(D_6^+)$ ;
- $A_4A_2$ :  $A^2 = 4B$ ;
- $A_3^2$ : Empty in  $\mathcal{C}(D_6^+)$  and hence in  $\mathcal{B}_s(D_6^+)$ .

All these strata are shown in Figure 52 below.

We find the decoration  $s$  of the  $D_5$  stratum by considering the principal part  $x^2y + \alpha y^4$  of (8) at the origin. When  $\alpha = A$  is positive we are on the right side of Figure 52 and so the right half-branch has decoration  $D_5^+$ . Similar

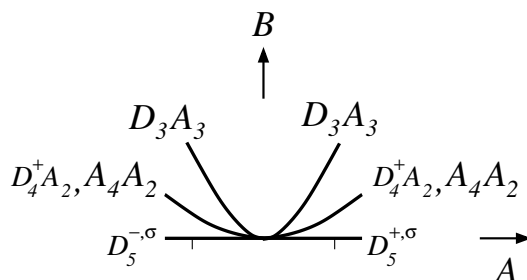


Figure 52: The part of  $\mathcal{B}_s(D_6^+)$  coming from the 1-dimensional strata of  $\mathcal{C}(D_6^+)$ .

analysis shows the left half-branch has decoration  $D_5^-$ . Now, the symmetry of the bifurcation diagram under the transformation

$$(A, B) \mapsto (-A, B)$$

lifts to the symmetry

$$(x, y, \alpha, \beta, \gamma, \delta, \varepsilon) \mapsto (x, -y, -\alpha, \beta, -\gamma, \delta, -\varepsilon), F \mapsto -F$$

of the family (8). This tells us that the source  $\mathbb{R}_{x,y,\gamma}^3$  and the target  $\mathbb{R}_{\gamma,\delta,\varepsilon}^3$  have the same orientations for both  $D_5$  half-branches, and so we choose them to have sign  $\sigma$ .

We now consider the co-orientation of the  $D_5$  stratum. When we cross the  $D_5$  stratum in the positive direction, as seen in Figure 13, we are changing the sign of the  $y^3$  coefficient (that is the coefficient  $\beta = B$ ) from positive to



negative. Therefore, when  $B$  is negative we are on the positive side of the  $D_5$  stratum. Hence, the  $D_5$  stratum in Figure 52 is co-oriented downwards.

Finally, the choice between plus and minus for the  $D_4^\pm A_2$  stratum is done by considering the principal part  $x^2y + \beta y^3$  of (8) at the origin. When the coefficient of  $y^3$  is positive we have  $D_4^+ A_2$ , and since  $\beta = B$  is always positive we have  $D_4^+ A_2$  for the whole of the stratum.

The decorations and co-orientations of the other strata in Figure 52 will be discussed later in Section 4.3 when we examine tilted projections of 2-dimensional strata in  $\mathcal{C}(D_6^+)$ .

## 4.2 2-dimensional strata in $\mathcal{C}(D_6^+)$ and their straight projection

We now parametrise the 2-dimensional strata in  $\mathcal{C}(D_6^+)$ :

- $A_4$ :  $\Psi = (y - u)^4(y^2 + vy + w)$  with  $w = \frac{uv}{4}$ ;
- $D_4$ :  $\Psi = y^4(y^2 + uy + v)$ ;
- $D_3A_2$ :  $\Psi = y^3(y - u)^2(y - v)$ ;
- $A_2^3$ :  $\Psi = (y^3 + uy^2 + v)^2$ ;
- $A_3A_2$ :  $\Psi = (y - u)^3(y - v)^2(y - w)$  with  $3vw + 2uw + uv = 0$ .

Here, the additional relations in the first and last cases exist due to the constraint of the coefficient of  $y$  in  $\Psi$  being zero.

Similar to Section 4.1 and following the calculations in [9] we state that the critical value sets of the map  $\pi_s$  on the strata from the previous list are:

- $A_4$ : the critical value set of the  $\pi_s$  on the stratum  $A_4 \subset \mathcal{C}(D_6^+)$  is the stratum  $A_4^{e/h} \subset \mathcal{B}_s(D_6^+)$  with the equation  $B = \frac{3}{8}A^2$ ;
- $D_4$ : here  $\pi_s$  maps the closure of the stratum  $D_4 \subset \mathcal{C}(D_6^+)$  isomorphically onto  $\mathbb{R}_{A,B}^2$  and hence its critical value set is empty. Therefore the strata  $D_{4,q}^\pm \subset \mathcal{B}_s(D_6^+)$  are empty;
- $D_3A_2$ : the stratum  $D_3A_2 \subset \mathcal{C}(D_6^+)$  is mapped by  $\pi_s$  onto  $\mathbb{R}_{A,B}^2$  so that ‘half’ of the plane is covered twice, while the other half is not covered at all. These halves are separated by the image of the cuspidal curve  $D_3A_3$  with the lower half being doubly covered (see Figure 52);
- $A_2^3$ : the whole stratum  $A_2^3 \subset \mathcal{C}(D_6^+)$  is sent by  $\pi_s$  to  $A^2 = 4B$ , that is, the stratum  $D_4A_2 \subset \mathcal{B}_s(D_6^+)$  (the same as  $A_4A_2$  under this projection);
- $A_3A_2$ : the stratum  $A_3A_2 \subset \mathcal{C}(D_6^+)$  is a surface that under the projection  $\pi_s$  has a double curve in its critical point set due to two  $A_3A_2$  points coming together. However, we see that  $\pi_s$  has no critical points on the open stratum  $A_3A_2 \subset \mathcal{C}(D_6^+)$ . Another result from [9] of particular interest is that the  $TA_3A_2$  strata coincide with the  $A_4A_2$  strata for the straight projection.

This means we now must consider the tilted projection of the  $A_2^3$  stratum since under the straight projection its whole image is 1-dimensional,

and, moreover, this image coincides with the strata  $D_4A_2$  and  $A_4A_2$  obtained earlier. Coincidence of the last two strata also confirms that the  $\pi_s$  is not sufficiently generic. Due to the reasons above the  $A_3A_2$  stratum will also be subject to tilting considerations.

## 4.3 Tilting the 2-dimensional strata

### 4.3.1 The $A_2^3$ stratum

We are considering the tilted projection of the stratum  $A_2^3 \subset \mathcal{C}(D_6^+)$  since its critical value set under  $\pi_s$  coincides with that of  $D_4A_2$  and  $A_4A_2$ .

Recall we parametrised the  $A_2^3$  stratum by  $\Psi = (y^3 + uy^2 + v)^2$ . Here, only those regions of the  $uv$ -plane in which the polynomial  $q = y^3 + uy^2 + v$  has three real roots correspond to real  $A_2^3$  points. In [9] it was found that this occurs when  $\Psi = y^4(y + u)^2$  and  $\Psi = (y + \frac{2u}{3})^4(y - \frac{u}{3})^2$  which are the  $D_4A_2$  and  $A_4A_2$  strata of  $\mathcal{C}(D_6^+)$ .

By equating the coefficients of the parametrised  $A_2^3$  stratum with (9) we obtain Figure 53 in 3-dimensions with  $\varepsilon = \pm 2v = \pm \gamma$ . Here the  $\alpha$ -axis is the  $D_4^+A_2$  stratum (not the  $D_4^-A_2$  stratum since the  $D_6^+$  caustic has  $A_2^3$  points next to it) and the two cubic curves are  $A_4A_2$ .

We now consider the possible images under the tilting map

$$\pi_t : (\mathbb{R}_{\alpha, \beta, \gamma, \delta, \varepsilon}^5) \rightarrow \mathbb{R}_{A, B}^2; (\alpha, \beta, \gamma, \delta, \varepsilon) \mapsto (A, B) = (\alpha, \beta + C\gamma + E\varepsilon)$$

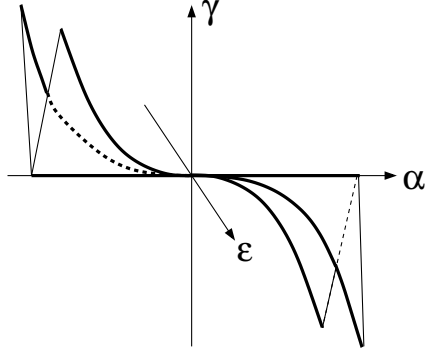


Figure 53: Projection of the  $A_2^3$  stratum of  $\mathcal{C}(D_6^+) \subset \mathbb{R}_{\alpha,\beta,\gamma,\delta,\varepsilon}^5$  to the  $\alpha\gamma\varepsilon$ -space. The image of the  $A_2^3$  consists of the regions of the planes  $\varepsilon = \pm\gamma$  between the  $D_4A_2$  line  $\gamma = 0$  and the  $A_4A_2$  curves  $\gamma = -\frac{4}{27}u^3$ .

for various values of arbitrary real coefficients  $C$  and  $E$ . The calculations of the discriminantal strata are found in [9] and so will not be repeated here. Our main area of interest is to see what happens to the two  $A_4A_2$  strata for different values of  $C$  and  $E$ . Topologically, when considering the tilted projections, we are roughly looking at the surface in Figure 53 from the  $\varepsilon$ -direction, the  $\gamma$ -direction or the  $-\varepsilon$ -direction which are shown respectively in Figures 54, 55 and 56.

In all three figures the co-orientation of the  $D_4^{+,\sigma}A_2$  stratum is to the right for reasons that will be explained at the end of this section. We leave the consideration of the decorations of the  $A_4A_2$  strata to Section 4.3.2.

In Figure 54 we co-orient the two  $A_4A_2$  strata towards the  $D_4^{+,\sigma}A_2$  stratum due to this being the region where the two triple points exist, as shown in Figure 53. Hence, we know the  $D_4^{+,\sigma}A_2$  stratum is of type  $D_{4,2}^{+,\sigma}A_2$  since

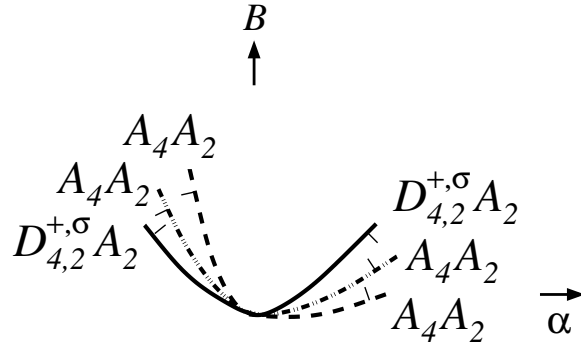


Figure 54: The bifurcation diagram coming from the tilted projection of the stratum  $A_2^3$  for  $(C, E) = (2, 1)$ . The  $D_4A_2$  and  $A_4A_2$  strata here split those in Figure 52.

crossing the stratum in the positive direction creates two triple points (as seen in Figures 14 and 15).

In Figure 55 the  $D_4^+A_2$  half-branches are of type  $D_{4,1}^{+,\sigma}A_2$  since there are triple points on either side due to the positions of the  $A_4A_2$  strata. The co-orientations of the  $A_4A_2$  strata are towards the  $D_{4,1}^{+,\sigma}A_2$  stratum.

Again, in Figure 56 the co-orientations of the  $A_4A_2$  strata are towards the  $D_4^{+,\sigma}A_2$  stratum due to this being the region where the two triple points exist. Hence, the  $D_4^{+,\sigma}A_2$  stratum is of type  $D_{4,0}^{+,\sigma}A_2$  since crossing the stratum in the positive direction loses two triple points (as seen in Figure 14).

We now explain why the  $D_4^{+,\sigma}A_2$  stratum is co-oriented to the right in Figures

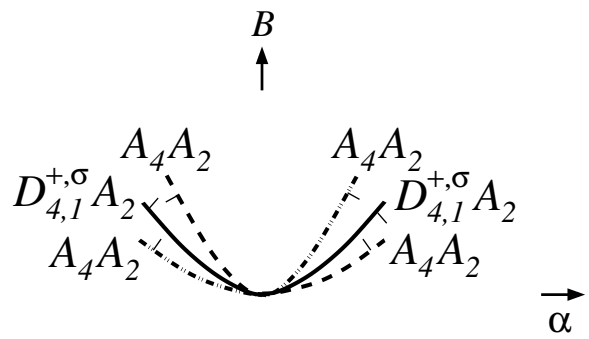


Figure 55: The bifurcation diagram coming from the tilted projection of  $A_2^3$  for  $(C, E) = (0, 1)$ .

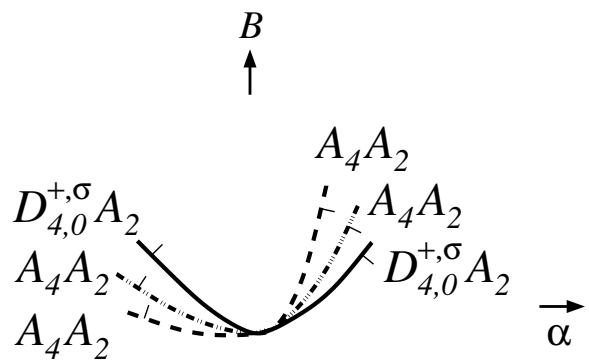


Figure 56: The bifurcation diagram coming from the tilted projection of the stratum  $A_2^3$  for  $(C, E) = (-2, -1)$ .

54, 55 and 56. Consider the  $uv$ -plane parametrising  $D_3A_2$ , that is,

$$\Psi = y^3(y + u)^2(y + v).$$

Comparing the coefficients of  $\Psi$  with those of (9) we have

$$\alpha = 2u + v$$

$$\beta = u^2 + 2uv$$

$$\gamma = u^2v.$$

Here, the  $u$ -axis parametrises  $D_4A_2$ , that is when  $v = 0$ , so that the positive direction of the  $u$ -axis corresponds to the orientation of the parabola shown in Figure 57.

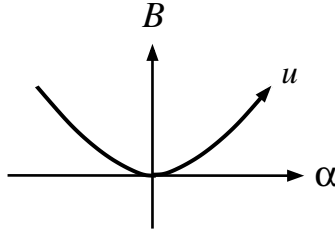


Figure 57:  $D_4A_2$  orientation in  $\mathbb{R}_{\alpha,B}^2$ .

We wish to co-orient the  $D_4A_2$  stratum towards the region with  $A_3^+A_2$  points since after a positive  $D_4A_2$  bifurcation there are  $A_3^+A_2$  points present, as seen in Figures 14 and 15. We know the sign of  $\gamma$  tells the  $D_3^+$  and  $D_3^-$  singularities apart: the sign being negative means we have  $D_3^+$ . Hence, the

region of  $D_3^+A_2$  (that is,  $A_3^+A_2$ ) points on the  $uv$ -plane is  $v < 0$ , except for the  $v$ -axis itself.

The determinant of the Jacobian of the map  $(u, v) \mapsto (\alpha, \beta)$  on the  $u$ -axis is

$$\left| \begin{array}{cc} 2 & 1 \\ 2u + 2v & 2u \end{array} \right|_{v=0} = \left| \begin{array}{cc} 2 & 1 \\ 2u & 2u \end{array} \right| = 2u.$$

Hence the map  $(u, v) \mapsto (\alpha, \beta)$  sends the orientation of the source plane to that of the target plane near the positive  $u$ -semi-axis, and reverses the orientation near the negative  $u$ -semi-axis. Therefore, the  $D_3^+A_2$  region  $v < 0$  which was on the right of the  $u$ -axis will be mapped to the right of the oriented parabola in Figure 57 when  $u > 0$ , and to the left of this parabola when  $u < 0$ .

### 4.3.2 The $A_3A_2$ stratum

In [9] the  $A_3A_2$  stratum was parametrised by  $\Psi = (y - u)^3(y - v)^2(y - w)$  where  $u, v, w$  were subject to the relations

$$q_1 = 3vw + 2uw + uv = 0 \quad \text{and} \quad q_2 = \varepsilon^2 - 4u^3v^2w = 0$$



and there were the following expressions for the coefficients of  $\Psi$

$$\begin{aligned}
\alpha &= -w - 2v - 3u \\
\beta &= 2vw + v^2 + 3uw + 6uv + 3u^2 \\
\gamma &= -v^2w - 6uvw - 3uw^2 - 3u^2w - 6u^2v - u^3 \\
\delta &= 3uv^2w + 6u^2vw + 3u^2v^2 + u^3w + 2u^3v
\end{aligned} \tag{10}$$

Like what was done in [9] we consider the  $A_3A_2$  stratum of  $\mathcal{C}(D_6^+) \subset \mathbb{R}_{\alpha,\beta,\gamma,\delta,\varepsilon}^5$  as parametrised by the surface  $S = \{q_1 = q_2 = 0\} \subset \mathbb{R}_{u,v,w,\varepsilon}^4$ , and look for critical points of  $\pi_t|_{A_3A_2}$  as critical points on  $S$  of  $\pi_t$  composed with the parametrisation map, that is, of

$$(u, v, w, \varepsilon) \mapsto (\alpha, \beta, \gamma, \delta, \varepsilon) \mapsto (A, B) = (\alpha, \beta + C\gamma + E\varepsilon),$$

where  $C$  and  $E$  are arbitrary real constants.

In order to visualise the discriminantal strata for  $D_6^+$  we start with the projection  $S' \subset \mathbb{R}_{u,w,\varepsilon}^3$  of our surface  $S$  paramtrising the closure of the stratum  $A_3A_2 \subset \mathcal{C}(D_6^+)$ . Here,  $S$  projects onto  $S'$  bijectively due to the conditions  $q_1 = 0$  and  $q_2 = 0$ . We see that  $S'$  has no points with  $uw < 0$ , covers the  $uw > 0$  region twice and contains the  $u$ - and  $w$ -axes, as shown in Figure 58.

According to [9], the following strata of  $\mathcal{C}(D_6^+)$  and critical curves show up on  $S'$  in Figure 58:

- $D_5$ ,  $u = v = 0 = \varepsilon$ , the  $w$ -axis;

- $D_3A_3$ ,  $v = w = 0 = \varepsilon$ , the  $u$ -axis;
- $A_4A_2$ ,  $u = w$ ;
- $TA_3A_2$ , the pre-images of the  $TA_3A_2$  strata of  $\mathcal{B}_t(D_6^+)$ .

As stated previously the  $TA_3A_2$  strata coincide with the  $A_4A_2$  strata for the straight projection. However in the tilted projection the  $TA_3A_2$  have quadratic tangency on  $S'$  with  $A_4A_2$  (the sides depend on the signs of  $(C \pm E)$ ).

We will now provide illustrations for the various cases. Firstly, Figure 58 illustrates the situation for when  $C = 2$  and  $E = 1$ .

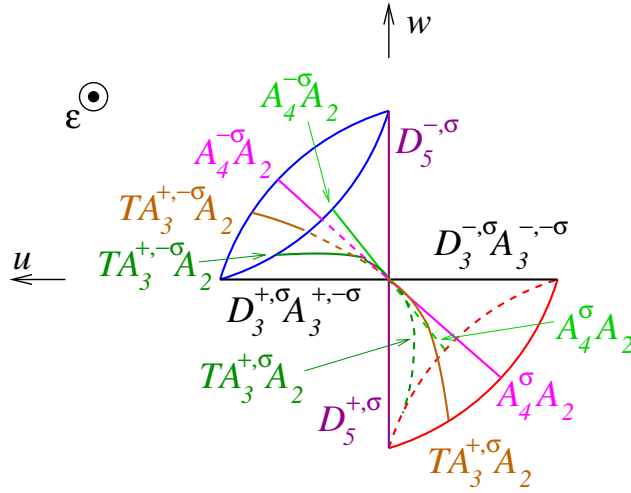


Figure 58: The strata on the surface  $S' \subset \mathbb{R}_{u,w,\varepsilon}^3$  parametrising the strata in the closure of the stratum  $A_3A_2$  in  $\mathcal{B}_t(D_6^+)$  when  $C = 2$  and  $E = 1$ .

Let us now find the decorations of strata in Figure 58 in detail. The decorations of  $D_5$  can be calculated from work previously done in Figure 52.

Since for  $D_5$  we have  $u = 0$ ,  $v = 0$  and  $w \neq 0$  we have  $\Psi = y^5(y - w)$ . This gives us  $A = -w$ . Hence, the positive  $A$ -semi-axis in Figure 52 is the negative  $w$ -semi-axis in Figure 58. The same holds for the other half of the  $D_5$  stratum.

Next we have the  $D_3A_3$  stratum which is the  $u$ -axis. We have  $\Psi = y^3(y - u)^3$ , which corresponds in (8) to the principal part  $x^2y - u^3y^2$  at the origin. From this we can see the sign  $s$  decorating  $D_3$  will be the sign of the coefficient of  $-y^2$ , which is the sign of  $u$ . Hence for positive  $u$  we have  $D_3^+A_3$  and for negative  $u$  we have  $D_3^-A_3$ . We also know the degree  $\sigma$  of  $D_3$  will be the same as for  $D_5$  from Figure 13. Therefore both  $D_3A_3$  half-branches have decoration  $D_3^\sigma$ . The sign  $s$  and degree  $\sigma$  of  $A_3$  in  $D_3A_3$  will be explained later.

It is now possible to find the decorations of all the other strata. We shall start from the negative  $w$ -ray, at  $D_5^{+,\sigma}$  and travel up to the negative  $u$ -ray,  $D_3^{-,\sigma}A_3$ , following the red path as shown in Figure 58.

According to the  $D_5$  transition in Figure 13 two  $A_3A_2$  points merging at  $D_5^{+,\sigma}$  are  $A_3^{+,\sigma}A_2$ . Therefore both  $TA_3A_2$  strata next to the  $D_5^{+,\sigma}$  in Figure 58 are  $TA_3^{+,\sigma}A_2$ . Next as we carry on, we will arrive at swallowtail and smooth sheet intersections. As we move through these strata, our  $A_3^{+,\sigma}$  points switch signs to  $A_3^{-,-\sigma}$ , hence giving the strata the decoration  $A_4^\sigma A_2$ . Finally we will arrive at  $D_3^{-,-\sigma}A_3^{-,-\sigma}$  since our  $A_3$  point has decorations  $(-, -\sigma)$ .

It is possible to repeat the process with the blue path shown in the upper

left octant in Figure 58. However, a quicker way is to look at the symmetry

$$(u, v, w) \mapsto (-u, -v, -w). \quad (11)$$

This transformation lifts to the symmetry

$$(x, y, \alpha, \beta, \gamma, \delta, \varepsilon) \mapsto (x, -y, -\alpha, \beta, -\gamma, \delta, -\varepsilon), F \mapsto -F$$

of the family (8). This tells us that the source  $\mathbb{R}_{x,y,\gamma}^3$  and the target  $\mathbb{R}_{\gamma,\delta,\varepsilon}^3$  have the same orientations and so  $\sigma$  is preserved. However, due to  $F \mapsto -F$  the sign  $s$  changes.

We now explain how the surface  $S' \subset \mathbb{R}_{u,w,\varepsilon}^3$  is mapped, via the stratum  $A_3A_2 \subset \mathcal{C}(D_6^+)$  by  $\pi_t$  to the  $AB$ -plane. Consider, for example, its quarter  $S'_+$  within the octant where all the  $u, w, \varepsilon$  are non-negative. According to (10) the boundary of  $S'_+$  formed by the positive  $w$ - and  $u$ -rays is mapped to respectively the negative  $A$ -ray and the left half of the parabola  $D_3A_3$  in Figure 59. The image of  $S'_+$  covers the small sector of the  $AB$ -plane between these two branches, and the only singularities this covering has are folds along the  $A_4A_2$  and  $TA_3A_2$  curves on  $S'_+$ . These folds give us the two strata of  $\mathcal{B}_t(D_6^+)$  shown in Figure 59. Similar considerations for the other quarters of  $S'$  explain the rest of the strata in Figure 59. The strata there are co-oriented to the sides on which the folding of  $S'$  has more pre-images.

The previous strata calculated from tilting the  $A_2^3$  stratum for  $(C, E) = (2, 1)$  (see Figure 54) are also contained in Figure 59. Of course, it then

follows that the co-orientations of the  $A_4A_2$  strata (towards the nearest  $D_4A_2$  branches) are already known from Section 4.3.1.

Now, the decorations of the  $A_4^{e/h}$  strata in Figure 59 can be calculated by balancing the increments of the numbers of swallowtail points generated by crossing the  $D_5^{-,\sigma}$  and  $D_5^{+,\sigma}$  strata.

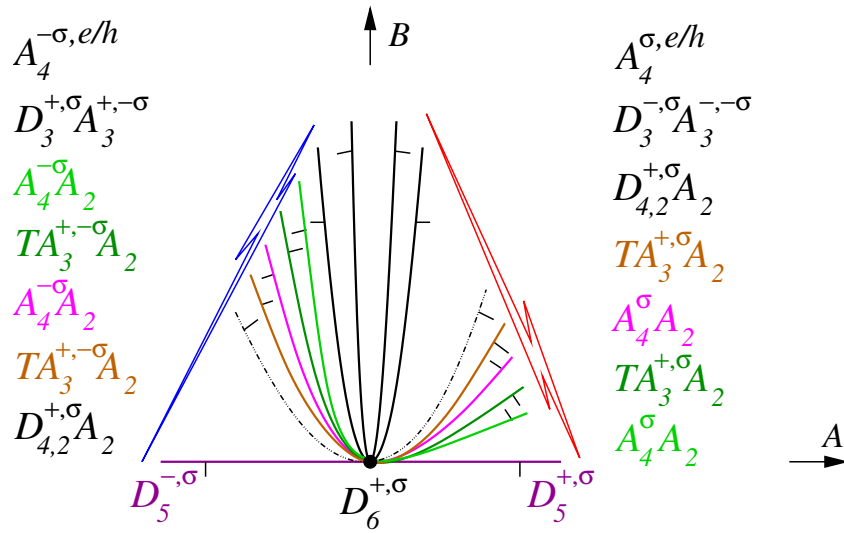


Figure 59: Part of the bifurcation diagram  $\mathcal{B}_t(D_6^+)$  when  $C = 2$  and  $E = 1$ . Positions of the  $A_4A_2$  and  $D_4A_2$  curves follow Figure 54.

It was proved in [9] that the higher dimensional strata of the  $D_6^+$  caustic do not contribute to the bifurcation diagrams. Therefore, Figure 59 yields the cyclic equation

$$\begin{aligned}
 \mathbf{35.} \quad & a_3^{2,e;+,\sigma;+,-\sigma} - a_3^{2,e;-, \sigma;-, -\sigma} + 2a_4^{-\sigma}a_2 + 2a_4^{\sigma}a_2 - 2ta_3^{+,-\sigma}a_2 - 2ta_3^{+,\sigma}a_2 - \\
 & 2d_{4,2}^{+,\sigma}a_2 + a_4^{-\sigma,e/h} - a_4^{\sigma,e/h} + d_5^{-,\sigma} - d_5^{+,\sigma} = 0
 \end{aligned}$$

where we consider the  $D_3A_3$  strata as  $A_3^2$ . Here we detect this stratum is elliptic by comparing our normal form  $F$  to the normal forms in Section 2.3.1.1.

The next topologically different option for the strata on the surface  $S'$  may be achieved by taking  $C = 1$  and  $E = 2$  which is illustrated in Figure 60.

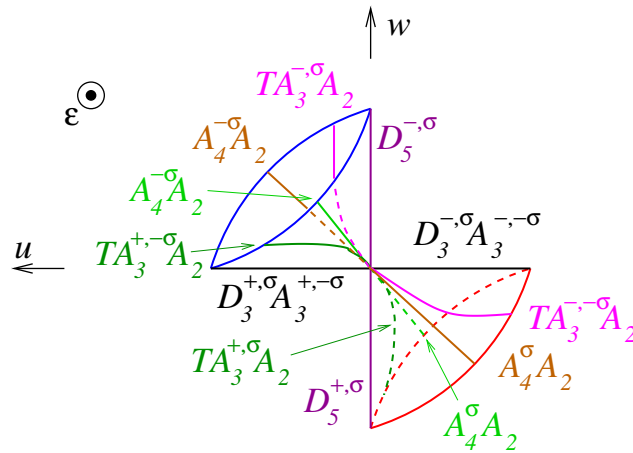


Figure 60: The surface  $S'$  for  $C = 1$  and  $E = 2$ .

The strata in Figure 60 have:

- The same positions and decorations of the  $D_5$ ,  $D_3A_3$  and  $A_4A_2$  strata as in Figure 58;
- One of the two  $TA_3A_2$  strata in each octant change position relative to the  $A_4A_2$  stratum compared to Figure 58. Due to this switch the moved  $TA_3A_2$  strata change their signs  $s$  and  $\sigma$ .

Now, the surface  $S'$  is mapped via  $\pi_t$  down to the  $AB$ -plane creating

$\mathcal{B}_t(D_6^+)$  shown in Figure 61. This time the previous strata calculated from tilting the  $A_2^3$  stratum for  $(C, E) = (0, 1)$  (see Figure 55) are also contained in the figure.

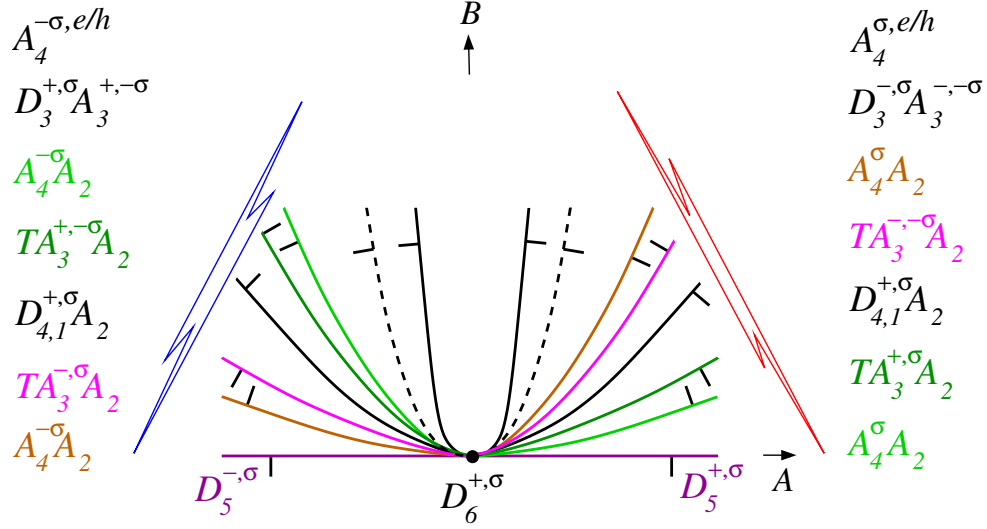


Figure 61: The bifurcation diagram  $\mathcal{B}_t(D_6^+)$  when  $C = 1$  and  $E = 2$ , with the contribution from Figure 55.

Again, strata are co-oriented to the sides on which the folding has more pre-images. Figure 61 yields the cyclic equation

$$\begin{aligned}
 \mathbf{36.} \quad & a_3^{2,e;+, \sigma;+, -\sigma} - a_3^{2,e;-,\sigma;-,-\sigma} - ta_3^{+,-\sigma} a_2 - ta_3^{+,\sigma} a_2 + ta_3^{-,\sigma} a_2 + ta_3^{-,-\sigma} a_2 - \\
 & 2d_{4,1}^{+,\sigma} a_2 + a_4^{-\sigma, e/h} - a_4^{\sigma, e/h} + d_5^{-,\sigma} - d_5^{+,\sigma} = 0.
 \end{aligned}$$

The last topologically different option for the strata on the surface  $S'$  may be achieved by taking  $C = -2$  and  $E = -2$  which is illustrated in Figure 62.

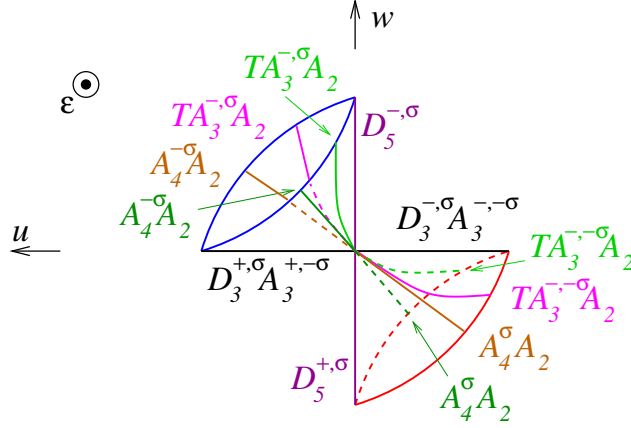


Figure 62: The surface  $S'$  for  $C = -2$  and  $E = -1$ .

Here the strata in Figure 62 have:

- The same positions and decorations of the  $D_5$ ,  $D_3A_3$  and  $A_4A_2$  strata as in Figure 58 and 60;
- Both  $TA_3A_2$  strata in each octant change position relative to the  $A_4A_2$  stratum compared to Figure 58. Due to this move both decorations  $s$  and  $\sigma$  of  $TA_3A_2$  change.

The surface  $S'$  is mapped via  $\pi_t$  down to the  $AB$ -plane creating  $\mathcal{B}_t(D_6^+)$  shown in Figure 63. This time the previous strata calculated from tilting the  $A_2^3$  stratum for  $(C, E) = (-2, -1)$  (see Figure 56) are contained in the figure.

Now, Figure 63 yields the cyclic equation

$$\begin{aligned}
 \mathbf{37.} \quad & a_3^{2,e;+,σ;+,-σ} - a_3^{2,e;-,\sigma;-,-\sigma} - 2a_4^{-\sigma}a_2 - 2a_4^{\sigma}a_2 + 2ta_3^{-,\sigma}a_2 + 2ta_3^{-,-\sigma}a_2 - \\
 & 2d_{4,0}^{+,\sigma}a_2 + a_4^{-\sigma,e/h} - a_4^{\sigma,e/h} + d_5^{-,\sigma} - d_5^{+,\sigma} = 0.
 \end{aligned}$$



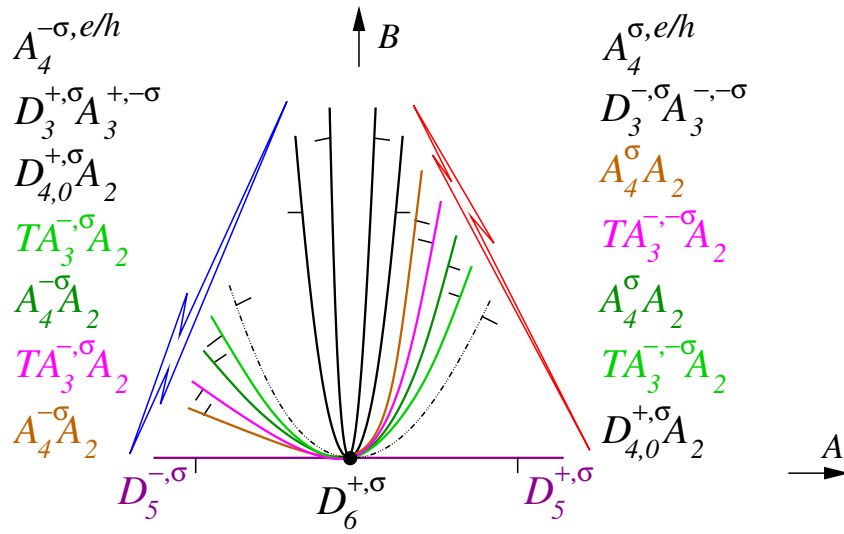


Figure 63: The bifurcation diagram  $\mathcal{B}_t(D_6^+)$  when  $C = -2$  and  $E = -1$ , with the contribution from Figure 56.

This concludes our proof of the  $D_6^+$  part of Theorem 2.6.2.

# Chapter 5

## $D_6^-$ bifurcations

We now turn our attention to proving the  $D_6^-$  part of Theorem 2.6.2, that is, deriving equation **38**.

Similar to Chapter 4, we consider  $D_6^-$  bifurcations and obtain the decorations of the strata that come from the  $D_6^-$  caustic,  $\mathcal{C}(D_6^-)$ . This time the  $\mathcal{R}_+$ -miniversal deformation of the  $D_6^-$  function singularity is

$$\begin{aligned} F &= -x^2y + \frac{1}{5}y^5 + \frac{1}{4}\alpha y^4 + \frac{1}{3}\beta y^3 + \frac{1}{2}\gamma y^2 + \delta y + \varepsilon x \\ &= -x^2y + \varepsilon x + p(y) \end{aligned} \tag{12}$$

where  $\alpha, \beta, \gamma, \delta, \varepsilon \in \mathbb{R}$  are independent parameters. Here, this family only differs from the  $D_6^+$  family by the sign of the  $x^2y$  term.

Like in Section 4 analysis of (12) yields the function

$$\Psi := y^2 p'(y) - \frac{\varepsilon^2}{4} = y^2(y^4 + \alpha y^3 + \beta y^2 + \gamma y + \delta) - \frac{\varepsilon^2}{4} \quad (13)$$

which we use to describe all degenerations in  $F$ . We should notice that this  $\Psi$  only differs from the one in the  $D_6^+$  case by the sign of the  $\varepsilon^2$  term.

## 5.1 1-dimensional strata in $\mathcal{C}(D_6^-)$ and their straight projection

We now analyse the 1-dimensional strata of  $\mathcal{C}(D_6^-)$  and their straight projection. We introduce the parametrisations of the strata in  $\mathcal{C}(D_6^-)$  based on the multiplicity options for the roots of  $\Psi$  from Section 4:

- $D_5$  with  $\Psi = y^5(y - u)$ ;
- $D_4A_2$  with  $\Psi = y^4(y - u)^2$ ;
- $D_3A_3$  with  $\Psi = y^3(y - u)^3$ ;
- $A_5$  with  $\Psi = (y - u)^5(y + \frac{u}{5})$ ;
- $A_4A_2$  with  $\Psi = (y - u)^4(y + \frac{u}{2})^2$ . However, the stratum is empty in  $\mathcal{C}(D_6^-)$  due to the negative sign of  $\varepsilon^2/4$  in (13);
- $A_3^2$  with  $\Psi = (y - u)^3(y + u)^3$  and  $\varepsilon^2 = 4u^6$ .

Here  $u \in \mathbb{R}$  and  $u \neq 0$ . Again, in the last three cases the way the coefficients of  $u$  are chosen makes the coefficient of  $y$  in the expansion of  $\Psi$  zero.

The images of these strata under the mapping

$$\pi_s : (\mathbb{R}_{\alpha,\beta,\gamma,\delta,\varepsilon}^5) \rightarrow \mathbb{R}_{A,B}^2; (\alpha, \beta, \gamma, \delta, \varepsilon) \mapsto (A, B) = (\alpha, \beta)$$

are listed below and shown in Figure 64:

- $D_5$ :  $B = 0$ ;
- $D_4A_2$ :  $A^2 = 4B$ ;
- $D_3A_3$ :  $A^2 = 3B$ ;
- $2A_5$ :  $64B = 25A^2$ . Here, the stratum is doubled in the  $\varepsilon$ -direction in  $\mathcal{C}(D_6^-)$ ;
- $A_4A_2$ : Empty in  $\mathcal{C}(D_6^-)$  and hence in  $\mathcal{B}_s(D_6^-)$ ;
- $2A_3^2$ :  $A = 0$ ,  $B \leq 0$ . Again, the stratum is doubled in the  $\varepsilon$ -direction in  $\mathcal{C}(D_6^-)$ .

From  $\Psi$  we immediately see that all our observations done in Section 4.1 about the decorations of the  $D_5$  stratum as well as the degree signs  $\sigma$  of the  $D_{\geq 3}$  strata stay true for  $D_6^-$ . Hence, in Figure 64 the decorations of the  $D_5$  stratum are inherited from the  $D_6^+$  case due to the expressions (8) and (12) only differing by the sign of the  $\varepsilon^2$  term. Since  $\varepsilon$  equals zero in the stratification of  $D_5$  this change of sign has no affect between the two cases.

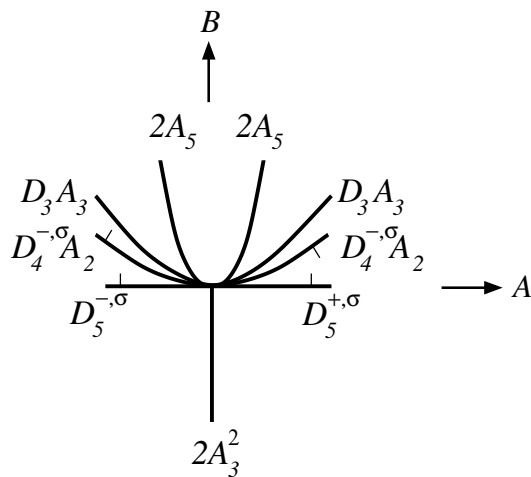


Figure 64: The part of  $\mathcal{B}_s(D_6^-)$  coming from the 1-dimensional strata of  $\mathcal{C}(D_6^-)$ .

We now turn our attention to the co-orientation of the  $D_5$  stratum. For the  $D_6^-$  case, when we cross the  $D_5$  stratum in the positive direction, as seen in Figure 13, we are changing the sign of the  $y^3$  coefficient (that is the coefficient  $\beta = B$ ) from negative to positive. Therefore, the  $D_5$  stratum in Figure 64 is co-oriented upwards.

The choice between plus and minus for the  $D_4^\pm A_2$  stratum is done by considering the principal part  $-x^2 y + \beta y^3$  of (12) at the origin. When the coefficient of  $y^3$  is positive we have  $D_4^- A_2$  and since  $\beta = B$  is always positive we have  $D_4^- A_2$  for the whole of the stratum. Again, its co-orientation is inherited from the  $D_6^+$  case.

The decorations and co-orientations of the other strata in Figure 64 will be discussed later in Section 5.2 when we examine the straight projections of

2-dimensional strata in  $\mathcal{C}(D_6^-)$ .

## 5.2 2-dimensional strata in $\mathcal{C}(D_6^-)$ and their straight projection

We now parametrise the 2-dimensional strata in  $\mathcal{C}(D_6^-)$ :

- $A_4$ :  $\Psi = (y - u)^4(y^2 + vy + \frac{uv}{4})$  with  $\varepsilon^2 + u^5v = 0$ ;
- $D_4$ :  $\Psi = y^4(y^2 + uy + v)$ ;
- $D_3A_2$ :  $\Psi = y^3(y - u)^2(y - v)$ ;
- $A_2^3$ :  $\Psi = (y^3 + uy^2 + v)^2$ ;
- $A_3A_2$ :  $\Psi = (y - u)^3(y - v)^2(y - w)$  with  $3vw + 2uw + uv = 0$ .

The critical value sets of the map  $\pi_s$  on the strata from this list are (see Figure 65):

- $A_4$ : this is very similar with the  $D_6^+$  situation except  $u$  and  $v$  now have opposite signs to each other. Here, the critical value set of the  $\pi_s$  on the stratum  $A_4 \subset \mathcal{C}(D_6^-)$  is the stratum  $A_4^{e/h} \subset \mathcal{B}_s(D_6^-)$  with the equation  $B = \frac{3}{8}A^2$ . Respectively, the decoration of  $A_4^{e/h}$  will follow from the analysis of the decorations of  $A_4$  which will be done later in this section;

- $D_4$ : There is no difference with the  $D_6^+$  situation. That is,  $\pi_s$  maps the closure of the stratum  $D_4 \subset \mathcal{C}(D_6^-)$  isomorphically onto  $\mathbb{R}_{A,B}^2$  and hence its critical value set is empty. Therefore the strata  $D_{4,q}^\pm \subset \mathcal{B}_s(D_6^-)$  are empty;
- $D_3A_2$ : similarly to the  $D_6^+$  case, the stratum  $D_3A_2 \subset \mathcal{C}(D_6^-)$  is mapped by  $\pi_s$  onto  $\mathbb{R}_{A,B}^2$  so that ‘half’ of the plane is covered twice, while the other half is not covered at all. These halves are separated by the image of the cuspidal curve  $D_3A_3$  with the lower half being doubly covered;
- $A_2^3$ : empty in  $\mathcal{C}(D_6^-)$  and hence in  $\mathcal{B}_s(D_6^-)$ ;
- $A_3A_2$ : the stratum  $A_3A_2 \subset \mathcal{C}(D_6^-)$  is mapped by  $\pi_s$  so that there are no critical points on the open stratum  $A_3A_2 \subset \mathcal{C}(D_6^-)$ . Moreover, according to [9], such critical points will not appear even when we consider a generic projection instead of  $\pi_s$ . Therefore, the  $TA_3A_2$  stratum in our planar bifurcation diagrams of  $D_6^-$  is empty, and there is no need to consider tilted projections of  $A_3A_2 \subset \mathcal{C}(D_6^-)$  like we did for the  $D_6^+$  case.

The bifurcation diagram produced from the straight projection of the strata in  $\mathcal{C}(D_6^-)$  is shown in Figure 65. We remark that there is no need to consider tilted projections for the  $D_6^-$  case, unlike in  $D_6^+$ . This is due to the images of all strata being different which confirms that  $\pi_s$  is sufficiently generic.

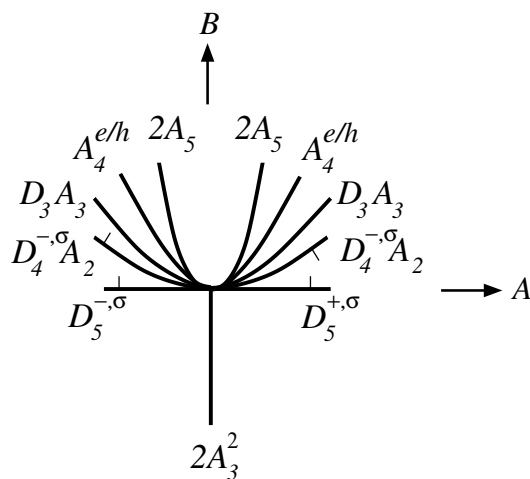


Figure 65: The part of  $\mathcal{B}_s(D_6^-)$  coming from the 1-dimensional strata of  $\mathcal{C}(D_6^-)$  and  $A_4$ .

We now analyse the decorations and co-orientations of the strata in detail.

$A_4$ : Consider the surface  $V = \{\varepsilon^2 + u^5v = 0\} \subset \mathbb{R}_{u,v,\varepsilon}^3$  that parametrises the stratum  $A_4 \subset \mathcal{C}(D_6^-)$  which is then projected down to the  $AB$ -plane by  $\pi_s$ . According to [9], the following strata of  $\mathcal{C}(D_6^-)$  and critical curves show up on  $V$ , as illustrated in Figure 66:

- $A_4^{e/h}$ :  $v = 0$ , the  $u$ -axis;
- $D_5$ :  $u = 0$ , the  $v$ -axis;
- $A_5$ :  $v = -\frac{4u}{5}$ .



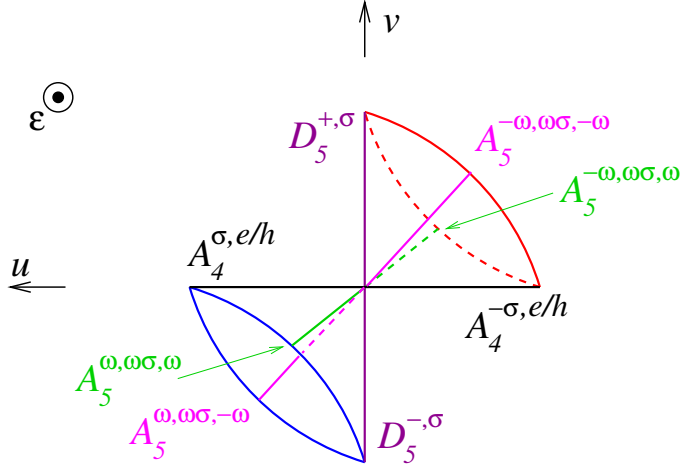


Figure 66: The strata on the surface  $V \subset \mathbb{R}_{u,v,\epsilon}^3$  parametrising the strata in the closure of the stratum  $A_4$  in  $\mathcal{C}(D_6^-)$ .

We examine the decorations of the strata in Figure 66. For  $D_5$  we have  $u = 0$  and therefore  $\Psi = y^5(y + v)$ . This gives us  $A = v$ . Hence, the positive  $A$ -semi-axis,  $D_5^{+, \sigma}$ , in Figure 64 is the positive  $v$ -semi-axis in Figure 66. The same holds for the other half of the  $D_5$  stratum.

We will now start at the negative  $v$ -ray,  $D_5^{-, \sigma}$ , and follow the blue path up to the positive  $u$ -ray in order to determine the decorations of all the other strata.

According to the  $D_5$  transition in Figure 13 the two swallowtail points created at  $D_5^{-, \sigma}$  have decorations  $A_4^{+, \sigma}$  and  $A_4^{-, -\sigma}$ . Next, we are able to determine the decorations in the two  $A_5$  strata in Figure 66 by considering the symmetry

$$(u, v, \epsilon) \mapsto (u, v, -\epsilon). \quad (14)$$

This transformation lifts to the symmetry

$$(x, y, \alpha, \beta, \gamma, \delta, \varepsilon) \mapsto (-x, y, \alpha, \beta, \gamma, \delta, -\varepsilon), \quad F \mapsto F$$

of the family (12). This tells us that both the source  $\mathbb{R}_{x,y,\gamma}^3$  and the target  $\mathbb{R}_{\gamma,\delta,\varepsilon}^3$  change their orientation and so  $\sigma$  is preserved. However, the change of orientation of the target changes the writhe decoration. Due to  $F \mapsto F$  the sign  $s$  stays the same. Therefore the  $A_5$  strata will have the same decorations  $s$  and  $\sigma$  but different signs of the writhe. Now recall from Section 2.3.1.1 the relation  $writhe \cdot (t, \tau) = (-s, -\sigma)$  for the decorations of the  $(t, \tau)$ -swallowtails born in the  $A_5^{s,\sigma,\omega}$  bifurcation. From this we see that the  $A_4^{-,-\sigma}$  point mentioned before is born from an  $A_5^{\omega,\omega\sigma,\omega}$  bifurcation. Likewise, the  $A_4^{+,\sigma}$  point is born from  $A_5^{\omega,\omega\sigma,-\omega}$ . Now, on the parametrising surface  $V$  in Figure 66 we have the same kind of  $A_4$  points on either side of the  $A_5$  strata. Hence, the  $A_4^{e/h}$  stratum has decoration  $A_4^{\sigma,e/h}$ .

Similarly, we can repeat this process with the red path shown and find the decorations of strata in the upper right octant of Figure 66. However, analysing the symmetry as we did in (11), Section 4.3.2, provides the same results quicker.

Now, the surface  $V$  in Figure 66 is mapped via  $\pi_s$  down to the  $AB$ -plane creating  $\mathcal{B}_s(D_6^-)$  in Figure 67.

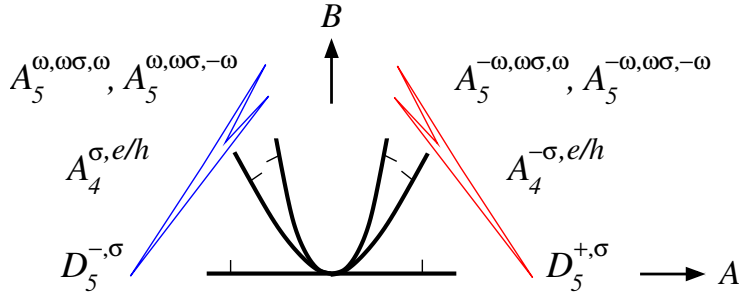


Figure 67: The bifurcation diagram  $\mathcal{B}_s(D_6^-)$  for the surface  $V$ .

In Figure 67 we know the  $D_5$  stratum is co-oriented upwards from previous considerations in Section 5.1. All the other strata are co-oriented towards the creation of swallowtail points.

$A_3A_2$ : Take  $\Psi = (y - u)^3(y - v)^2(y - w)$  with  $u, v, w$  subject to the relations

$$q_1 = 3vw + 2uw + uv = 0 \quad \text{and} \quad q_2 = e^2 + 4u^3v^2w = 0,$$

and with the expressions for the coefficients of  $\Psi$  the same as equations (10).

Like in [9] we consider the  $A_3A_2$  stratum of  $\mathcal{C}(D_6^-) \subset \mathbb{R}_{\alpha, \beta, \gamma, \delta, \varepsilon}^5$  as parametrised by the surface  $S = \{q_1 = q_2 = 0\} \subset \mathbb{R}_{u, v, w, \varepsilon}^4$ , and look for critical points of  $\pi_s|_{A_3A_2}$  as critical points on  $S$  of  $\pi_s$  composed with the parametrisation map, that is, of

$$(u, v, w, \varepsilon) \mapsto (\alpha, \beta, \gamma, \delta, \varepsilon) \mapsto (A, B).$$

It should be recalled that since there are no  $TA_3A_2$  strata mapped under the straight projection there is no need to consider tilted projections of  $A_3A_2 \subset \mathcal{C}(D_6^-)$  like we did for the  $D_6^+$  case.

We have that

- $D_3A_3$ :  $v, w = 0$ , the  $u$ -axis;
- $D_5$ :  $u, v = 0$ , the  $w$ -axis;
- $D_4A_2$ :  $u, w = 0$ , the  $v$ -axis;
- $A_5$ :  $u = v$ .

The equation  $q_1 = 0$  defines a cone  $C$  in the  $uvw$ -space which contains all three coordinate axes, and the rest of  $C$  is situated in the six coordinate octants (those in which not all of the three coordinates are of the same signs). The equation  $q_2 = 0$  defines a double cover of those four of these six parts of  $C$  where  $uw < 0$ . Out of these four:

- 1) the pieces  $\{u > 0, v > 0, w < 0\}$  and  $\{u < 0, v < 0, w > 0\}$  project injectively onto the  $w = 0$  plane, and therefore are parametrised by the 1st and 3rd quadrants of the  $uv$ -plane;
- 2) the pieces  $\{u < 0, v > 0, w > 0\}$  and  $\{u > 0, v < 0, w < 0\}$  project injectively onto the  $u = 0$  plane, and therefore are parametrised by the 1st and 3rd quadrants of the  $vw$ -plane.

We denote the corresponding closures of the double covers of these two pairs of regions by  $S_1$  and  $S_2$ , and consider them as surfaces in  $\mathbb{R}_{u,v,\varepsilon}^3$  and  $\mathbb{R}_{v,w,\varepsilon}^3$  respectively. These two surfaces should be joined along the  $v$ -axis to represent the surface  $S = \{q_1 = q_2 = 0\}$  in  $\mathbb{R}_{u,v,w,\varepsilon}^4$ . We depict  $S_1$  in Figure 68 and  $S_2$  in Figure 70.

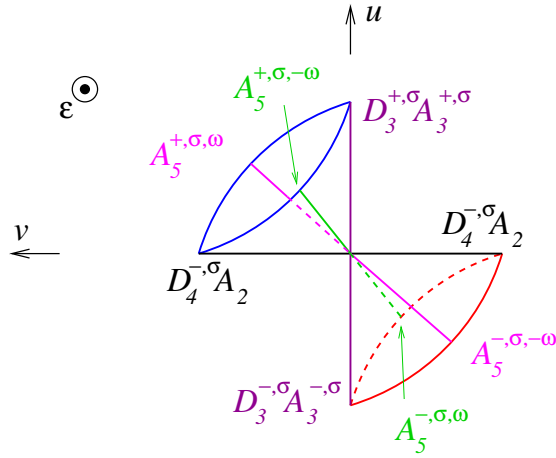


Figure 68: The surface  $S_1$  over the  $uv$ -plane.

In Figure 68 the degree signs  $\sigma$  in  $D_4^\sigma A_2$  and  $D_3^\sigma A_3$  are inherited from the  $D_6^+$  case. We also know the choice between plus and minus for the  $D_4^\pm A_2$  stratum from previous considerations in Section 5.1.

Next we have the  $D_3 A_3$  stratum which is the  $u$ -axis. Here  $\Psi = y^3(y - u)^3$ , which corresponds in (12) to the principal part  $-x^2 y - u^3 y^2$  at the origin. The sign  $s$  decorating  $D_3$  will be the sign of the coefficient of  $-y^2$ , which corresponds to the sign of  $u$ . Hence we have  $D_3^+ A_3$  for positive  $u$  and  $D_3^- A_3$  for negative  $u$ . The sign  $s$  and degree  $\sigma$  of  $A_3$  in  $D_3 A_3$  will be found later.

We now find the decorations of the other strata. We start from the positive  $v$ -ray, at  $D_4^{-,\sigma}A_2$  and travel up to the positive  $u$ -ray,  $D_3^{+,\sigma}A_3$ , following the blue path as shown in Figure 68. We know from the positive  $D_4^{-,\sigma}A_2$  transition in Figure 14 that  $A_3^{+,\sigma}A_2$  points are created after the bifurcation. Using this and applying the symmetry (14) we determine our  $A_5$  strata have decorations  $A_5^{+,\sigma,\omega}$  and  $A_5^{+,\sigma,-\omega}$ . As we move through these strata, our  $A_3^{+,\sigma}$  points keep their decorations. Finally we arrive at  $D_3^{+,\sigma}A_3^{+,\sigma}$  since our  $A_3$  point has decorations  $(+,\sigma)$ .

We now remark that comparing the decorations of the  $A_5$  strata in Figures 66 and 68 tells us that the writhe  $\omega = +$ . Hence, we set  $\omega = +$  in the rest of the bifurcation diagrams in this section and in the overall cyclic equation.

The surface  $S_1$  from Figure 68 that parametrised  $A_3A_2$  is mapped via  $\pi_s$  down to the  $AB$ -plane creating the part of  $\mathcal{B}_s(D_6^-)$  in Figure 69.

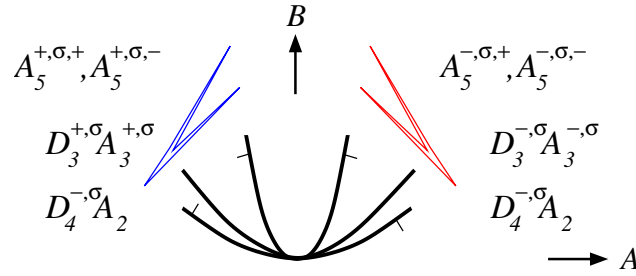


Figure 69: The bifurcation diagram  $\mathcal{B}_s(D_6^-)$  for the surface  $S_1$ .

In Figure 69 the co-orientation of the  $D_3A_3$  stratum will be determined later.

Similarly, we will now examine the decorations of the strata on the surface

$S_2$  in Figure 70.

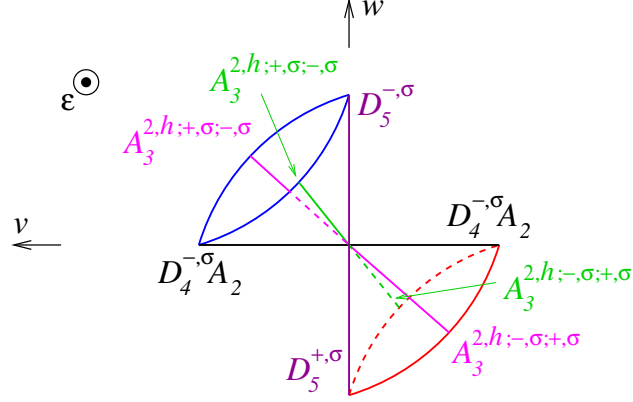


Figure 70: The surface  $S_2$  over the  $vw$ -plane. The  $A_3$  decorations of the  $A_3A_2$  points from the blue half of the surface are  $(-, \sigma)$ , and from the red are  $(+, \sigma)$ .

In Figure 70 the  $D_4^{-, \sigma} A_2$  stratum is the  $v$ -axis. We can also show that the positive  $A$ -semi-axis,  $D_5^{s, \sigma}$ , in Figure 64 is the negative  $w$ -semi-axis in Figure 70. The opposite also holds for the other half of the  $D_5$  stratum.

In order to find the decorations of the  $A_3^2$  strata we first show how the surface  $S_2$  is mapped via  $\pi_s$  down to the  $AB$ -plane, creating  $\mathcal{B}_s(D_6^-)$  in Figure 71.

Now, according to the  $D_4^{-, \sigma} A_2$  transition in Figure 15,  $A_3^{-, \sigma} A_2$  points occur before the bifurcation and  $A_3^{+, \sigma} A_2$  points occur afterwards. Therefore, due to the co-orientation of the  $D_4^{-, \sigma} A_2$  stratum in the  $AB$ -plane we have that the  $A_3$  decorations of the  $A_3A_2$  points from the blue half of the surface in Figure 70 are  $(-, \sigma)$ , and from the red are  $(+, \sigma)$ . We also know that the  $A_3^2$  strata are hyperbolic since there are  $A_3A_2$  points before and after the bifurcation.

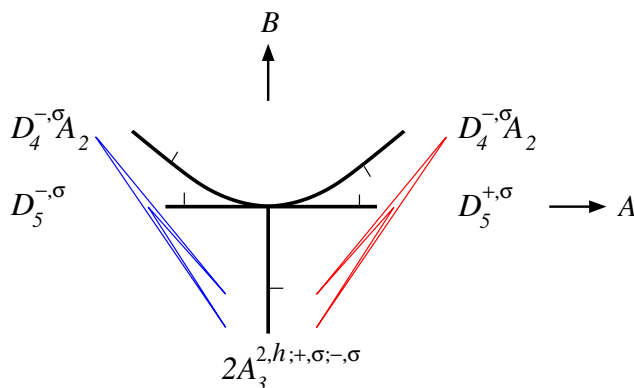


Figure 71: The bifurcation diagram  $\mathcal{B}_s(D_6^-)$  for the surface  $S_2$ .

Finally, the decorations  $s$  and  $\sigma$  of the two hyperbolic cuspidal edges meeting are found from the blue folding meeting the red one at their vertices on the negative  $B$ -ray in Figure 71. At each of these two junctions, two  $A_3$  points participate:  $A_3^{-,\sigma}$  from the left and  $A_3^{+,\sigma}$  from the right.

$D_3A_2$ : Take  $\Psi = y^3(y - u)^2(y - v)$ . The strata of  $\mathcal{C}(D_6^-)$  that occur on the  $uv$ -plane parametrising  $D_3A_2$  are

- $D_5$ :  $u = 0$ , the  $v$ -axis;
- $D_4A_2$ :  $v = 0$ , the  $u$ -axis;
- $D_3A_3$ :  $u = v$ ,

where Figure 72 provides the illustration.



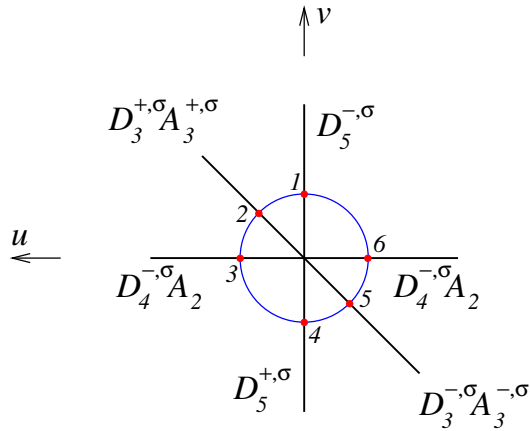


Figure 72: Strata of  $\mathcal{C}(D_6^-)$  that occur on the  $uv$ -plane parametrising  $D_3A_2$ .

All the decorations of strata in Figure 72 have been considered in other cases and so we will not repeat explanations for them here.

The  $uv$ -plane that parametrised  $D_3A_2$  in Figure 72 is mapped via  $\pi_s$  down to the  $AB$ -plane creating  $\mathcal{B}_s(D_6^-)$  in Figure 73.

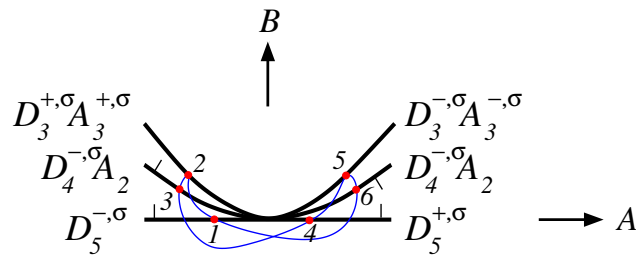


Figure 73: The bifurcation diagram  $\mathcal{B}_s(D_6^-)$ .

In order to determine the co-orientation of the  $D_3A_3$  stratum in Figure 73 we consider it as  $A_3^2$ . We know from Figures 69 and 73 that there must be

$A_3A_2$  points either side of the  $A_3^2$  stratum and so it is hyperbolic. Finally for  $D_3^{+, \sigma} A_3^{+, \sigma}$  we have  $A_3^{2, h; +, \sigma; +, \sigma}$ , which is non-co-orientable. The same is true for the  $D_3^{-, \sigma} A_3^{-, \sigma}$  stratum.

### 5.3 Complete bifurcation diagram for $D_6^-$

We now combine all the strata for  $D_6^-$  into one complete bifurcation diagram, Figure 74.

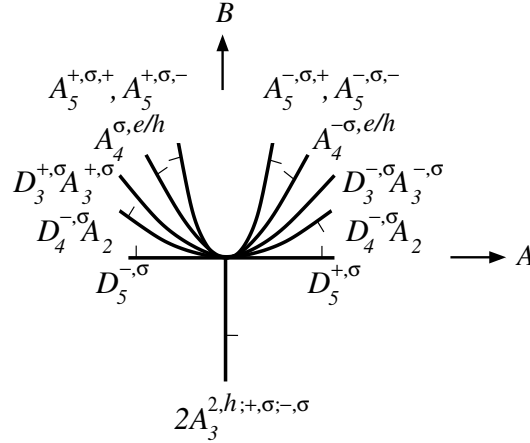


Figure 74: The complete bifurcation diagram  $\mathcal{B}_s(D_6^-)$ .

This yields the cyclic equation for  $D_6^-$

$$\begin{aligned}
 \mathbf{38.} \quad & d_5^{+, \sigma} - d_5^{-, \sigma} + a_4^{-, \sigma, e/h} - a_4^{\sigma, e/h} + a_5^{+, \sigma, +} + a_5^{+, \sigma, -} - a_5^{-, \sigma, +} - a_5^{-, \sigma, -} - \\
 & 2d_4^{-, \sigma} a_2 + 2a_3^{2, h; +, \sigma; -, \sigma} + [a_3^{2, h; +, \sigma; +, \sigma}] + [a_3^{2, h; -, \sigma; -, \sigma}] = 0.
 \end{aligned}$$

This concludes our proof of the  $D_6^-$  part of Theorem 2.6.2.

# Chapter 6

## $E_6$ bifurcations

We are now proving the  $E_6$  part of Theorem 2.6.2, that is, deriving cyclic equations **39** and **40**. Our aim is to understand the decorations of the strata that come from the  $E_6$  caustic,  $\mathcal{C}(E_6)$ .

Since for our setting we are considering the decoration  $s$  as well as  $\sigma$ , we have two types of  $E_6$  bifurcations to consider compared to one in the parallel case in [9] (see [4]). We introduce them by considering the  $\mathcal{R}_+$ -miniversal deformation of the  $E_6^s$  isolated function singularity

$$F = s\left(\frac{1}{3}x^3 + \alpha xy^2 + \beta xy + \gamma x + \frac{1}{4}y^4 + \frac{1}{2}\delta y^2 + \varepsilon y\right) \quad (15)$$

where  $\alpha, \beta, \gamma, \delta, \varepsilon \in \mathbb{R}$  are independent parameters. This family is quasi-homogeneous, and we fix the weights of the variables as

$$w_x = 4, \quad w_y = 3, \quad w_\alpha = 2, \quad w_\beta = 5, \quad w_\gamma = 8, \quad w_\delta = 6, \quad w_\varepsilon = 9.$$

Similar to Chapters 4 and 5 we analyse how we can represent  $\mathcal{C}(E_6^s)$  as a collection of 2-parameter bifurcations of caustics in three dimensions. The corresponding bifurcation diagram in the parameter plane will be denoted by  $\mathcal{B}(E_6^s)$ . Again, our method is to study successive approximations of the generic map

$$\pi : (\mathbb{R}_{\alpha,\beta,\gamma,\delta,\varepsilon}^5, \mathcal{C}(E_6^s)) \rightarrow \mathbb{R}^2.$$

This time taking the lowest weight part of such  $\pi$  gives us the straight projection

$$\pi_0 : (\mathbb{R}_{\alpha,\beta,\gamma,\delta,\varepsilon}^5) \rightarrow \mathbb{R}_{A,B}^2; (\alpha, \beta, \gamma, \delta, \varepsilon) \mapsto (A, B) = (\alpha, \beta).$$

The tilted projections are denoted by  $\pi_k$  where  $k$  is how much higher the weights of the additional monomials participating in the maps may be comparing with the weights of the components of the principal part  $\pi_0$ . For example the projection

$$\pi_1 : (\mathbb{R}_{\alpha,\beta,\gamma,\delta,\varepsilon}^5) \rightarrow \mathbb{R}_{A,B}^2; (\alpha, \beta, \gamma, \delta, \varepsilon) \mapsto (\alpha, \beta + d\delta)$$

depends on one extra real parameter  $d \neq 0$ .

The bifurcation diagrams  $\mathcal{B}_k(E_6^s)$  produced from the  $\pi_k$  projections serve as successive approximations to the bifurcation diagram  $\mathcal{B}(E_6^s)$  of the generic map  $\pi$ . We remark that once certain strata of the  $\mathcal{B}(E_6^s)$  appear in a sufficiently generic way in certain  $\mathcal{B}_k(E_6^s)$ , their contributions to the cyclic equa-

tions stay the same for higher  $k$ .

**Lemma 6.0.1.** *It is not necessary to consider co-orientations of strata in  $\mathcal{C}(E_6^s)$ .*

*Proof.* Recall the equation and solution spaces over  $\mathbb{Q}$  from Section 3. The rank of the solution space over  $\mathbb{Q}$ , shown in Table 2, is 15. For 14 of its generators we know invariants whose derivatives they are. Therefore, they satisfy any cyclic equation over the integers we may be able to obtain from  $E_6^\pm$  bifurcations. The fifteenth generator is a linear combination of the  $A_3^q$  strata which, according to Section 5.3 of [9], do not appear in  $\mathcal{B}(E_6^\pm)$ . Therefore, this last generator also satisfies any possible  $E_6^\pm$  cyclic equation. On the other hand, Table 1 is a table of 32 linearly independent cyclic equations in 47 unknowns, and its equations have been obtained without any  $E_6$  considerations. Thus, any  $E_6^\pm$  integer cyclic equation must be a rational linear combination of the Table 1 equations.  $\square$

Hence, we will only be considering *mod*2 coefficients for  $E_6^s$ .

According to [9], Chapter 5, all contributions to  $\mathcal{B}(E_6^s)$  are from the closures of the  $A_3$  and  $A_2^3$  strata. Therefore, we consider the closures of these strata in detail for the rest of this chapter. We remark that in the closure of the  $A_3$  stratum particular attention is required for the  $A_4$ ,  $D_4$  and  $A_3A_2$  strata. Since there are two types of  $E_6$  bifurcation we will first turn our attention to the  $E_6^+$  case, and the  $E_6^-$  equations will easily follow from that.

## 6.1 $E_6^+$ bifurcations

### 6.1.1 Stratification of $\mathcal{C}(E_6^+)$

For the  $D_6^\pm$  cases in Chapters 4 and 5 we managed to describe all degenerations in the versal families in terms of the new families of functions in just one variable. There, various strata of the caustics corresponded to real roots of  $\Psi$  of various multiplicities. However, this approach cannot be used for the  $E_6^+$  case. In [9] the parametrisations of the strata in  $\mathcal{C}(E_6)$  were constructed by using the general singularity theory approach to finding adjacencies of a uni-germ of an isolated function singularity  $Z$  to various (multi-)singularities  $Y$ . However, since our main task is to understand the decorations of the strata that come from  $\mathcal{C}(E_6^+)$  and not to calculate the discriminantal strata themselves we borrow the parametrisations of strata from [9].

#### 6.1.1.1 The $A_3$ stratum in $\mathcal{C}(E_6^+)$

The closure of the 3-dimensional stratum  $A_3 \subset \mathcal{C}(E_6^+)$  can be parametrised by the base  $\mathbb{R}_{u,v,w}^3$  of the family of functions

$$G = \frac{1}{3}x^3 + ux^2 + vx^2y + wxy^2 + \frac{1}{4}y^4$$

introduced in [9] and shown in Figure 75.

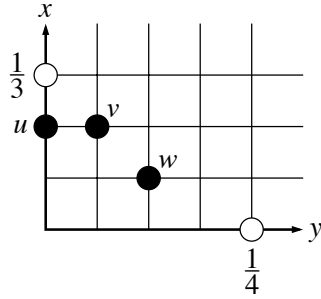


Figure 75: The function family  $G$  parametrising the stratum  $A_3 \subset \mathcal{C}(E_6^+)$ .

The parametrisation of the  $A_3$  stratum obtained in [9] is:

$$\begin{aligned}
 \alpha &= -v^2 + w & (16) \\
 \beta &= \frac{4}{3}v^5 - 2uv + 2w^2v - \frac{10}{3}v^3w \\
 \gamma &= -u^2 + v^2w^3 - 2uv^2w - \frac{7}{3}v^4w^2 + \frac{4}{3}uv^4 + \frac{16}{9}v^6w - \frac{4}{9}v^8 \\
 \delta &= -2uw - 3w^2v^2 + 4v^4w - \frac{4}{3}v^6 + 4uv^2 \\
 \varepsilon &= -\frac{8}{3}v^7w - 2w^2uv + \frac{16}{27}v^9 + 2u^2v - 2w^3v^3 + \frac{16}{3}uv^3w \\
 &\quad -\frac{8}{3}uv^5 + 4v^5w^2
 \end{aligned}$$

#### 6.1.1.1.1 2-dimensional strata in the closure of the $A_3$ stratum in $\mathcal{C}(E_6^+)$

The parametrisation (16) includes parametrisations of three of the 2-dimensional strata in  $\mathcal{C}(E_6^+)$  (the other 2-dimensional strata will show up later). Their parametrisations are listed below:

2-dimensional strata	Parametrisations of the strata in $\mathcal{C}(E_6^+)$
$D_4$ ( $u = 0$ )	$\alpha = v$ $\beta = -2uv$ $\gamma = u^2v$ $\delta = -3u^2$ $\varepsilon = 2u^3$
$A_4$ ( $u = w^2$ )	$\alpha = -v^2 + w$ $\beta = \frac{4}{3}v^5 - \frac{10}{3}v^3w$ $\gamma = -w^3v^2 - w^4 + \frac{16}{9}v^6w - v^4w^2 - \frac{4}{9}v^8$ $\delta = -\frac{4}{3}v^6 + 4v^4w + v^2w^2 - 2w^3$ $\varepsilon = \frac{2}{27}v(8v^8 - 36v^6w + 18v^4w^2 + 45v^2w^3)$

According to [9], we find the stratum  $A_3A_2$  within the parameter space of (16), as the surface

$$\begin{aligned}
& -12w^2uv^2 - 16v^6u - 40v^2w^4 - 9v^6w^2 - 16uw^3 + 33v^4w^3 \\
& + 27v^2u^2 + 42v^4wu + 16w^5 = 0.
\end{aligned} \tag{17}$$



**6.1.1.1.2 1-dimensional strata in the closure of the  $A_3$  stratum in  $\mathcal{C}(E_6^+)$**

According to [9], there are six 1-dimensional strata (one of them has two components) within the parametrisation (16):

1-dimensional strata	Parametrisations of the strata in $\mathcal{C}(E_6^+)$
$A_5$	$\alpha = w$ $\beta = 0$ $\gamma = -w^4$ $\delta = -2w^3$ $\varepsilon = 0$
$D_5$ $(u = w = 0)$	$\alpha = -v^2$ $\beta = \frac{4}{3}v^5$ $\gamma = -\frac{4}{9}v^8$ $\delta = -\frac{4}{3}v^6$ $\varepsilon = \frac{16}{27}v^9$
$D_5$ $(u = 0, w = \frac{3}{4}v^2)$	$\alpha = -\frac{1}{4}v^2$ $\beta = -\frac{1}{24}v^5$ $\gamma = -\frac{1}{576}v^8$ $\delta = -\frac{1}{48}v^6$ $\varepsilon = -\frac{1}{864}v^9$

1-dimensional strata	Parametrisations of the strata in $\mathcal{C}(E_6^+)$
$D_4A_2$ $(w = v^2, u = 0)$	$\alpha = 0$ $\beta = 0$ $\gamma = 0$ $\delta = -\frac{1}{3}v^6$ $\varepsilon = -\frac{2}{27}v^9$
$A_4A_2$ $(u = w^2, w = \frac{1}{2}v^2(3 + \sqrt{5}))$	$\alpha = \frac{1}{2}(1 + \sqrt{5})v^2$ $\beta = -\frac{1}{3}(11 + 5\sqrt{5})v^5$ $\gamma = -\frac{8}{9}(38 + 17\sqrt{5})v^8$ $\delta = -\frac{1}{6}(59 + 27\sqrt{5})v^6$ $\varepsilon = \frac{2}{27}(422 + 189\sqrt{5})v^9$
$A_4A_2$ $(u = w^2, w = \frac{1}{2}v^2(3 - \sqrt{5}))$	$\alpha = \frac{1}{2}(1 - \sqrt{5})v^2$ $\beta = -\frac{1}{3}(11 - 5\sqrt{5})v^5$ $\gamma = -\frac{8}{9}(38 - 17\sqrt{5})v^8$ $\delta = -\frac{1}{6}(59 - 27\sqrt{5})v^6$ $\varepsilon = \frac{2}{27}(422 - 189\sqrt{5})v^9$
$A_3^2$	$\alpha = 0$ $\beta = 0$ $\gamma = -u^2$ $\delta = 0$ $\varepsilon = 0$

### 6.1.1.2 The $A_2^3$ stratum in $\mathcal{C}(E_6^+)$

According to [9], the 2-dimensional stratum  $A_2^3 \subset \mathcal{C}(E_6^+)$  has two components.

The first of them is obtained from the family of functions

$$G = \frac{1}{3} + vy^2 + wy^3 + \frac{1}{4}y^4$$

shown in Figure 76. The co-ordinate change  $y := y + w$  transforms it to a

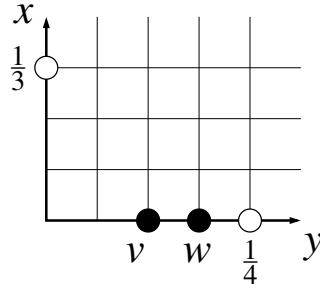


Figure 76: The function family  $G$  parametrising the stratum  $A_2^3 \subset \mathcal{C}(E_6^+)$ .

subfamily of the family (15) setting the parameters of the latter to be

$$\alpha = 0 \tag{18}$$

$$\beta = 0$$

$$\gamma = 0$$

$$\delta = 2v - 3w^2$$

$$\varepsilon = 2w^3 - 2vw.$$

Here, the image of this parametrisation is the  $4\delta^3 + 27\varepsilon^2 \leq 0$  region of the  $\delta\varepsilon$ -plane in  $\mathbb{R}_{\alpha,\beta,\gamma,\delta,\varepsilon}^5$ . The boundary  $4\delta^3 + 27\varepsilon^2 = 0$  of the image is the  $D_4A_2$  stratum.

As for the second  $A_2^3$  component, MAPLE calculations in [9] showed that its image under the projection to  $\mathbb{R}_{\alpha,\beta,\delta}^3$  satisfies the equation

$$3\beta^2 + 4\alpha^2\delta + 4\alpha^5 = 0.$$

We will depict this surface and the strata contained in it later in Section 6.1.3.

### 6.1.2 The closure of the $A_3$ stratum in $\mathcal{C}(E_6^+)$

We now visualise the closure of the  $A_3$  stratum in Figure 77. We should note that in order to make the diagram less complicated, some of the 1-dimensional strata are not shown as curves but are represented by their endpoints on the boundary of the cube.

We explain the decorations of the strata in Figure 77. We know from Figure 75 that the  $D_4$  stratum is on the  $u = 0$  plane. Now, looking at the principal part shown in Figure 75 for  $u \neq 0$  we can collect the square to give  $u(x + \frac{w}{2u}y^2)^2 + (\frac{1}{4} - \frac{w^2}{4u})y^4$ . Therefore, if  $w \neq 0$  and  $u$  is very small the coefficient of  $y^4$  has the sign of  $(-u)$ , which means we have  $A_3^{-,\sigma}$  points for  $u > 0$  and  $A_3^{+,\sigma}$  points for  $u < 0$ . Here we are setting the second decoration of  $A_3$  to be  $\sigma$ .

The decoration of  $D_4^+$  in  $D_4A_2$ , indicating that  $D_4$  is a purse, is due to

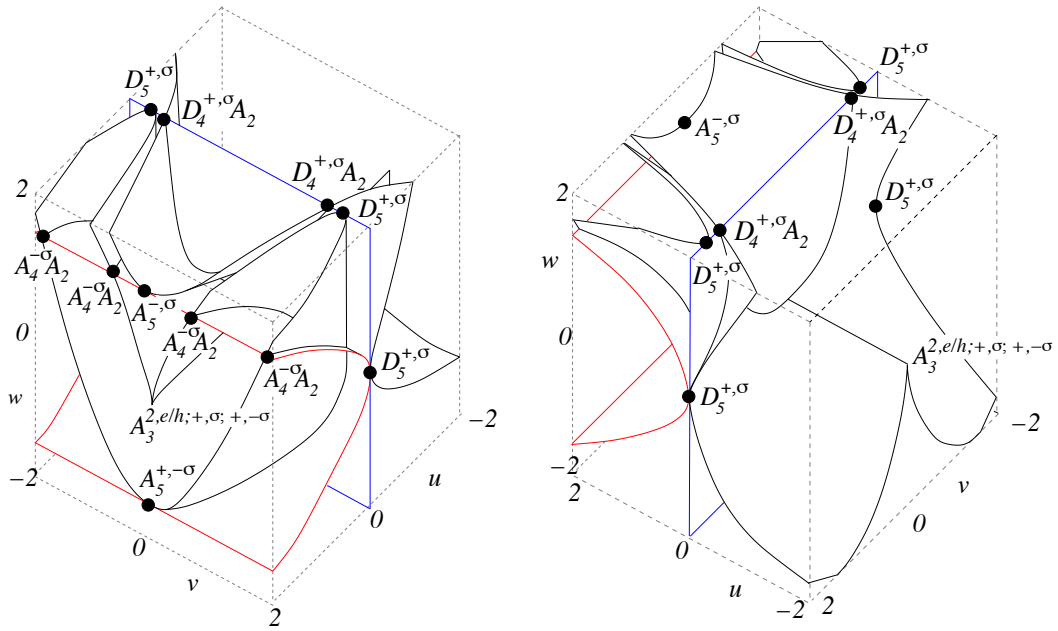


Figure 77: Two views of the  $\mathbb{R}^3_{u,v,w}$  parametrising the stratum  $A_3 \subset \mathcal{C}(E_6^+)$ . The 2-dimensional strata are:  $D_4 = \{u = 0\}$ ,  $A_4 = \{u = w^2\}$  and  $A_3 A_2$  from (17).

[9], Section 5.3.1. The decoration  $\sigma$  in  $D_4^+$  is due to the previous choice of  $\sigma$ . However, we do not know if the points are of type  $D_{4,0}^{+,\sigma} A_2$ ,  $D_{4,1}^{+,\sigma} A_2$ , or  $D_{4,2}^{+,\sigma} A_2$ . This will be found in the tilted projection section later and for now we just omit the second lower decoration.

One of the  $D_5$  strata is on the  $v$ -axis, when the principal part of the  $D_5$  normal form at the origin is  $vx^2y + \frac{y^4}{4}$ . Here, the  $s$ -decoration of  $D_5$  is the sign of the coefficient of  $y^4$  and therefore we have  $D_5^{+,\sigma}$ . Again, the  $\sigma$  decoration is inherited from the neighbouring  $D_4^{+,\sigma}$  points. Since the other  $D_5$  stratum has the same image under (16) we know both  $D_5$  strata must have the same decorations.

Now, the  $A_4$  stratum is on the  $w^2 = u$  surface. In order to be consistent with previous considerations notice that the  $0 < u < w^2$  region contains  $A_3^{-,\sigma}$  points. Therefore for  $u > w^2$  we have  $A_3^{+,-\sigma}$ . Hence, we know from Section 2.3.1.2, Figure 12, that the  $A_4 A_2$  points have decoration  $A_4^{-\sigma} A_2$  where the decoration is the product of the signs  $s$  and  $\sigma$  due to equations 5 and 6.

The decorations  $s$  and  $\sigma$  of the  $A_5$  singularities are inherited from those of the  $A_3$  points in the neighbouring  $A_3 A_2$  strata. That is, of the  $A_3$  points in the regions just above the  $A_5$  points in Figure 77, left. Therefore, we have  $A_5^{-,\sigma}$  for  $w > 0$  and  $A_5^{+,-\sigma}$  for  $w < 0$ . We should note we are omitting the decoration  $\omega$  from our  $A_5$  strata due to equations 18 and 19 gluing up certain strata over  $\mathbb{Z}_2$ .

Finally, we consider the decorations of the  $A_3^2$  stratum. We know from [9], Section 5.3.4, that the stratum is  $A_3^{2,h}$ . However, according to equation 14

we have glued up the elliptic and hyperbolic cases over  $\mathbb{Z}_2$ . In the  $u > w^2$  region we have  $A_3^{+,-\sigma}$  points and for  $u < 0$  we have  $A_3^{+,\sigma}$  points. Therefore, we see from Section 2.3.1.2, Figure 12, that the stratum must be decorated as  $A_3^{2,e/h;+,\sigma:+,-\sigma}$ .

### 6.1.2.1 The straight projection of the $A_3$ stratum

We now analyse the straight projection of the 1-dimensional strata of  $\mathcal{C}(E_6^+)$  listed in Section 6.1.1.1.2. We obtain the discriminantal strata in  $\mathcal{B}_0(E_6^+)$  from the images of the map

$$\pi_0 : (\mathbb{R}_{\alpha,\beta,\gamma,\delta,\varepsilon}^5) \rightarrow \mathbb{R}_{A,B}^2; (\alpha, \beta, \gamma, \delta, \varepsilon) \mapsto (A, B) = (\alpha, \beta),$$

which are listed below and depicted in Figure 78:

- $A_5$ :  $B = 0$ ;
- $D_5$ :  $9B^2 = -16A^5$  (both  $D_5$  strata in  $\mathcal{C}(E_6^+)$  are mapped to this stratum in  $\mathcal{B}_0(E_6^+)$ );
- $A_4A_2$ :  $9B^2 = (22 + 10\sqrt{5})A^5$  (the dashed curve in Figure 78);
- $A_4A_2$ :  $9B^2 = (22 - 10\sqrt{5})A^5$ ;
- $D_4A_2$ : the origin  $A = B = 0$ ;
- $A_3^2$ : again, the origin  $A = B = 0$ .

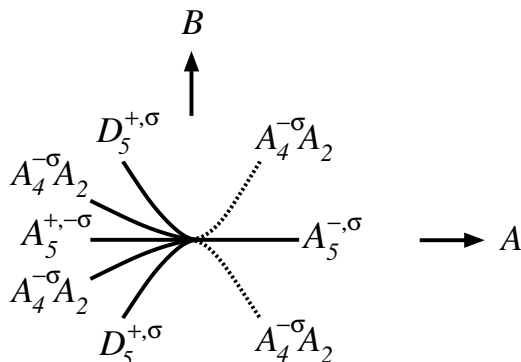


Figure 78: The strata of  $\mathcal{B}_0(E_6^+)$  coming from the 1-dimensional strata of  $\mathcal{C}(E_6^+)$ .

The decorations of the  $D_5^{+, \sigma}$  and  $A_4^{-\sigma} A_2$  strata in Figure 78 are inherited from Figure 77. We also know the  $A_5$  singularities occur when  $A = \alpha = w$  from Section 6.1.1. Therefore, it is apparent from Figure 77 that for the positive  $A$ -ray in Figure 78 we have  $A_5^{-, \sigma}$  and for the negative  $A$ -ray we have  $A_5^{+, -\sigma}$ .

It is visible from Figure 78 that the  $D_5^{+, \sigma}$  and  $A_4^{-\sigma} A_2$  strata do not contribute to the  $E_6^+$  cyclic equations since we are working *mod*2. Therefore, the contribution of 1-dimensional strata from the closure of the  $A_3$  stratum under the straight projection to any  $E_6^+$  cyclic equation is

$$a_5^{+, -\sigma} + a_5^{-, \sigma}.$$

According to equations 14 and 18 this is equal to  $a_3^{2, e/h; +, -\sigma; -, \sigma}$  over  $\mathbb{Z}_2$ .

Hence, we have the result:



**Lemma 6.1.1.** *The contribution of the closure of 1-dimensional strata from the closure of the stratum  $A_3 \subset \mathcal{C}(E_6^+)$  under the straight projection to any  $E_6^+$  cyclic equation over  $\mathbb{Z}_2$  is  $a_3^{2,e/h;+,-\sigma;-\sigma}$ .*

### 6.1.2.2 Tilted projections of strata in the closure of the $A_3$ stratum

We now turn our attention to tilted projections of some strata contained in the closure of the  $A_3$  stratum. It is necessary to consider tilted projections since some of the 1-dimensional strata in Section 6.1.2, such as  $D_4A_2$  and  $A_3^2$  behave poorly under  $\pi_0$  and are mapped by it just to the origin  $A = B = 0$ . This shows that the projection  $\pi_0$  was not sufficiently generic. Moreover, it was noticed in [9] that the straight projection was not sufficient to understand what happens with 2-dimensional strata. Hence we now consider tilted projections for the closures of the  $A_4$ ,  $D_4$  and  $A_3A_2$  strata like in [9].

Like in Section 6.1.2, we assume that in the space  $\mathbb{R}_{u,v,w}^3$  of Figure 77 parametrising the closure of the stratum  $A_3 \subset \mathcal{C}(E_6^+)$ , the region  $u < 0$  corresponds to  $A_3^{+,\sigma}$  points, the region  $0 < u < w^2$  corresponds to  $A_3^{-,\sigma}$  points and the  $u > w^2$  region corresponds to  $A_3^{+,-\sigma}$ . This setting implies that all  $D_4^\pm$  points are  $D_4^{\pm,\sigma}$ , and all  $D_5$  bifurcations are  $D_5^{+,\sigma}$ .

### 6.1.2.2.1 The $A_4$ stratum in $\mathcal{C}(E_6^+)$

Recall from Section 6.1.1.1.1 that a parametrisation of the 2-dimensional stratum  $A_4 \subset \mathcal{C}(E_6^+)$  is:

$$\begin{aligned}\alpha &= -v^2 + w \\ \beta &= \frac{4}{3}v^5 - \frac{10}{3}v^3w \\ \gamma &= -w^3v^2 - w^4 + \frac{16}{9}v^6w - v^4w^2 - \frac{4}{9}v^8 \\ \delta &= -\frac{4}{3}v^6 + 4v^4w + v^2w^2 - 2w^3 \\ \varepsilon &= \frac{2}{27}v(8v^8 - 36v^6w + 18v^4w^2 + 45v^2w^3)\end{aligned}$$

It is convenient to denote this parametrisation  $p_{A_4}$ . From [9] we know we are required to approximate the generic map  $\pi$  by

$$\pi_3 : (\mathbb{R}_{\alpha,\beta,\gamma,\delta,\varepsilon}^5) \rightarrow \mathbb{R}_{A,B}^2; (\alpha, \beta, \gamma, \delta, \varepsilon) \mapsto (A, B) = (\alpha, \beta + d\delta + g\gamma)$$

in order to see all relevant discriminantal strata in  $\mathcal{B}(E_6^+)$ . Therefore we obtain the composition map

$$\pi_3 \circ p_{A_4} : (\mathbb{R}_{v,w}^2) \rightarrow \mathbb{R}_{A,B}^2; (v, w) \mapsto (A, B) = (\alpha, \beta + d\delta + g\gamma).$$

The critical point set of  $\pi_3$  is

$$vw \left( v + d(w - 2v^2) + g \left( w^2 + wv^2 - \frac{2}{3}v^4 \right) \right) = 0$$

where the factors correspond in  $\mathcal{C}(E_6^+)$  to the  $A_5$ ,  $D_5$  and  $A_4^{e/h}$  strata. Now, the discriminantal strata in  $\mathcal{B}_3(E_6^+)$  are obtained from the images of the composition map  $\pi_3 \circ p_{A_4}$  and are borrowed from [9]:

- $A_5$ :  $B = -2dA^3 - gA^4$ ;
- $D_5$ :  $B^2 \sim -\frac{16}{9}A^5$ ;
- $A_4^{e/h}$ :  $B = -2dA^3 - (g + \frac{5}{3}d^3)A^4$ .

We now have the choice to set  $d$  to be positive or negative. If we set  $d$  to be positive, the map  $\pi_3 \circ p_{A_4}$  folds the  $vw$ -plane like in Figure 79. As was shown in [9], Section 5.3.2, if we consider changing  $d$  to be negative then Figure 79, right, is reflected in the horizontal axis with all the strata decorations following their half-branches, with the only change being the decoration  $\omega$  in the  $A_5$  strata becomes  $-\omega$ . However, since we are working over  $\mathbb{Z}_2$  we do not take the writhe decoration  $\omega$  into consideration for our case. Therefore the  $d < 0$  option yields the same cyclic equation.

The decorations of the  $D_5$  and  $A_5$  strata in Figure 79 follow Figure 77. From previous considerations in Section 6.1.2 we know we have  $A_3$  points of type  $A_3^{-,\sigma}$  and  $A_3^{+,-\sigma}$  either side of the  $A_4$  stratum when we consider it as a surface in  $\mathbb{R}_{u,v,w}^3$  (see Figure 77). Therefore, the  $A_4^{e/h}$  strata in Figure 79 are  $A_4^{-\sigma,e/h}$ .

We see from Figure 79 that the  $D_5^{+,\sigma}$  and  $A_4^{-\sigma,e/h}$  strata do not contribute to the  $E_6^+$  cyclic equations since we are working *mod*2. Therefore, the contri-

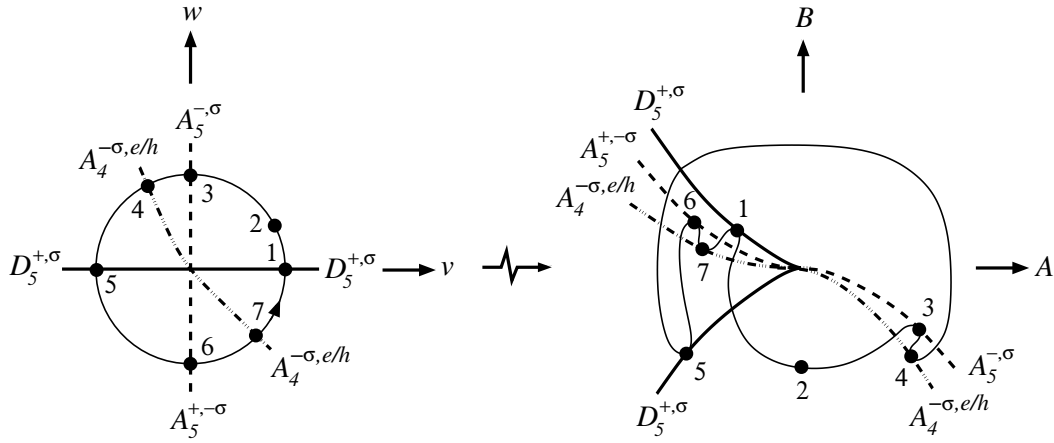


Figure 79: The folding of the  $vw$ -plane by  $\pi_3 \circ p_{A_4}$  when  $d > 0$ , producing part of  $\mathcal{B}_3(E_6^+)$  on the right.

tribution of the  $A_4$  closure to any  $\text{mod}2$   $E_6^+$  cyclic equation is

$$a_5^{+,-\sigma} + a_5^{-,\sigma}.$$

**Lemma 6.1.2.** *The contribution of the closure of the  $A_4$  stratum to any  $E_6^+$  cyclic equation over  $\mathbb{Z}_2$  is the same as the contribution of all 1-dimensional strata from the closure of the  $A_3$  stratum under the straight projection, considered in Section 6.1.2.*

#### 6.1.2.2.2 The $D_4$ stratum in $\mathcal{C}(E_6^+)$

We now recall a relation between two parametrisations of the  $D_4 \subset \mathcal{C}(E_6^+)$  used in [9]. The parametrisations are illustrated in Figure 80. The first, non-injective, is that by the plane  $u = 0$  from Figure 77, and the second is a

natural injective version. These two function families are related by the pleat map

$$(s, t) = \left( w - v^2, \frac{2}{3}v^3 - vw \right). \quad (19)$$

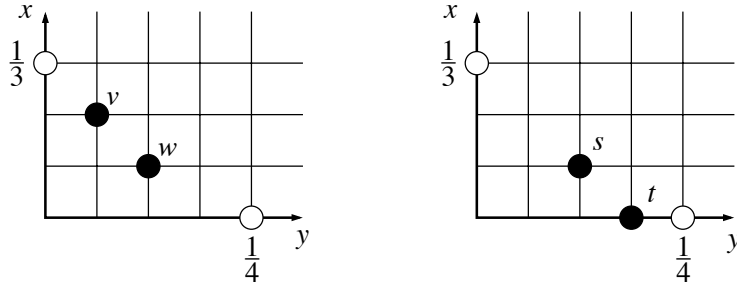


Figure 80: Two function families parametrising the stratum  $D_4 \subset \mathcal{C}(E_6^+)$ .

We obtain a parametrisation of the  $D_4$  stratum in terms of  $s$  and  $t$  by taking the function family in Figure 80, right, and eliminating the  $y^3$  term by the co-ordinate change  $y := y + t$ . Comparing the coefficients of the result to (15) we obtain:

$$\begin{aligned} \alpha &= s \\ \beta &= -2st \\ \gamma &= st^2 \\ \delta &= -3t^2 \\ \varepsilon &= 2t^3 \end{aligned}$$

We denote this parametrisation  $p_{D_4}$ .

Now, for the closure of the  $D_4$  stratum it is sufficient to consider the tilted projection

$$\pi_1 : (\mathbb{R}_{\alpha,\beta,\gamma,\delta,\varepsilon}^5) \rightarrow \mathbb{R}_{A,B}^2; (\alpha, \beta, \gamma, \delta, \varepsilon) \mapsto (A, B) = (\alpha, \beta + d\delta)$$

in order to detect all the strata. Hence, we obtain the composition map

$$\pi_1 \circ p_{D_4} : (s, t) \mapsto (A, B) = (\alpha, \beta + d\delta) = (s, -2st - 3dt^2).$$

This composition is a fold map. Its critical point set  $D_{4,q}^+$  is  $s+3dt = 0$  and we show it in Figure 81 (cf. [9]). We also show there how the strata contained in the closure of the  $D_4$  stratum are mapped by (19) from the  $vw$ -plane to the  $st$ -plane if  $d > 0$ . All the decorations of the  $D_4$  and  $D_5$  singularities follow Figure 77. We should note that in Figure 81 we see how the two  $D_5$  strata from the  $vw$ -plane are mapped to one stratum in the  $st$ -plane.

The discriminantal strata in  $\mathcal{B}_1(E_6^+)$  delivered by the critical values of the map  $\pi_1 \circ p_{D_4}$  are shown in Figure 82.

MAPLE calculations show that both half-branches of the  $D_{4,q}^{+,\pm,\sigma}$  strata are of type  $D_{4,a}^{+,\pm,\sigma}$ . We are using here the big stratum  $D_{4,a}^{+,\pm,\sigma}$  obtained in Section 2.6.2.1. The second lower decorations in  $D_4^{+,\sigma} A_2$  follow from [9], Section 5.3.1.

We see from Figure 82 that the  $D_5$  and  $D_{4,q}$  strata do not contribute to any  $E_6^+$  cyclic equation *mod*2. Hence, we have the result:

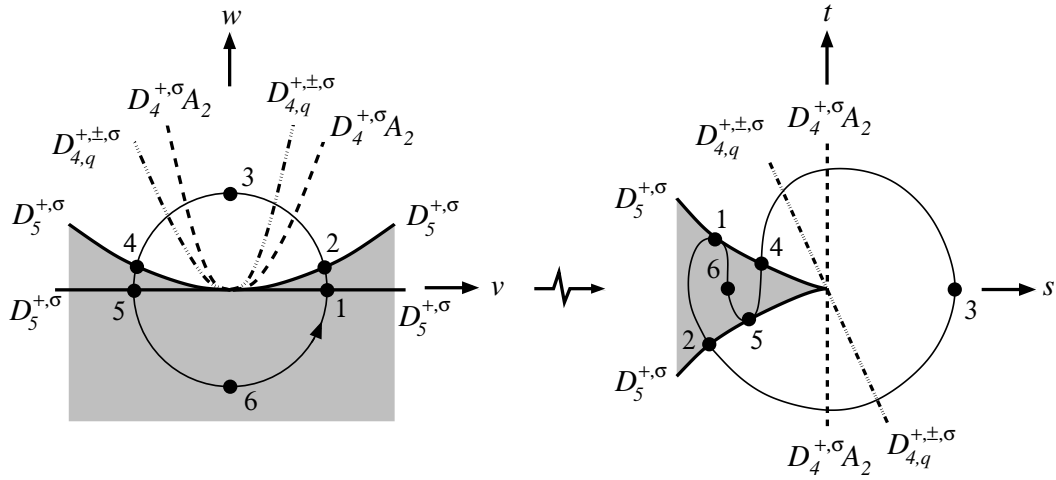


Figure 81: Mapping  $\mathbb{R}_{v,w}^2$  to  $\mathbb{R}_{s,t}^2$  for  $d > 0$ . The shaded regions represent  $D_4^{-, \sigma}$  points and the non-shaded regions  $D_4^{+, \sigma}$ .

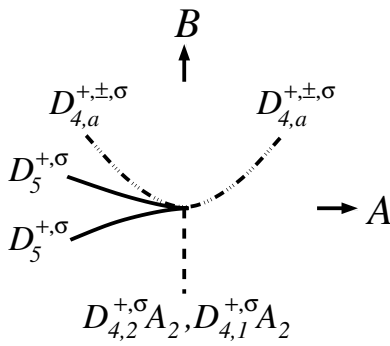


Figure 82: The part of  $\mathcal{B}_1(E_6^+)$  coming from the closure of the stratum  $D_4 \subset \mathcal{C}(E_6^+)$ .

**Lemma 6.1.3.** *The contribution of the closure of the stratum  $D_4 \subset \mathcal{C}(E_6^+)$  to any  $E_6^+$  cyclic equation over  $\mathbb{Z}_2$  is*

$$d_{4,1}^{+,\sigma} a_2 + d_{4,2}^{+,\sigma} a_2.$$

### 6.1.2.2.3 The $A_3A_2$ stratum in $\mathcal{C}(E_6^+)$

Recall (17) from Section 6.1.1.1.1, that is, the equation of the  $A_3A_2$  surface is

$$\begin{aligned} -12w^2uv^2 - 16v^6u - 40v^2w^4 - 9v^6w^2 - 16uw^3 + 33v^4w^3 + 27v^2u^2 \\ + 42v^4wu + 16w^5 = 0. \end{aligned}$$

To understand the contribution of this surface to the critical value set of the generic map  $\pi$ , we first approximate  $\pi$  by the tilted projection of the lowest weight:

$$\pi_1 : (\alpha, \beta, \gamma, \delta, \varepsilon) \mapsto (A, B) = (\alpha, \beta + d\delta)$$

where the parameters  $\alpha, \beta, \delta$  are given by (16).

Here, we are looking for  $TA_3A_2$  strata as critical values of  $\pi_1$  on the open  $A_3A_2$  stratum. The corresponding critical points have been detected in [9] and are described by the following formulas:

- i)  $v = -2dw + 5d^3w^2 - \frac{133}{4}d^5w^3 + \dots$ ,  $u = \frac{4w}{27d^2} + \frac{5w^2}{27} - \frac{229}{108}d^2w^3 + \dots$
- ii)  $v = -6dw + 27d^3w^2 - \frac{8667}{4}d^5w^3 + \dots$ ,  $u = w^2 - \frac{225}{4}d^2w^3 + \dots$
- iii)  $w = v^2 - 2dv^3 + 9d^2v^4 + \dots$ ,  $u = -dv^5 + 8d^2v^6 + \dots$



These strata emerge respectively from the  $A_3^2$ ,  $A_5$  and  $D_4A_2$  strata in Figure 77. The six  $TA_3A_2$  half-branches are represented by the grey circles in Figure 83 for  $d > 0$ .

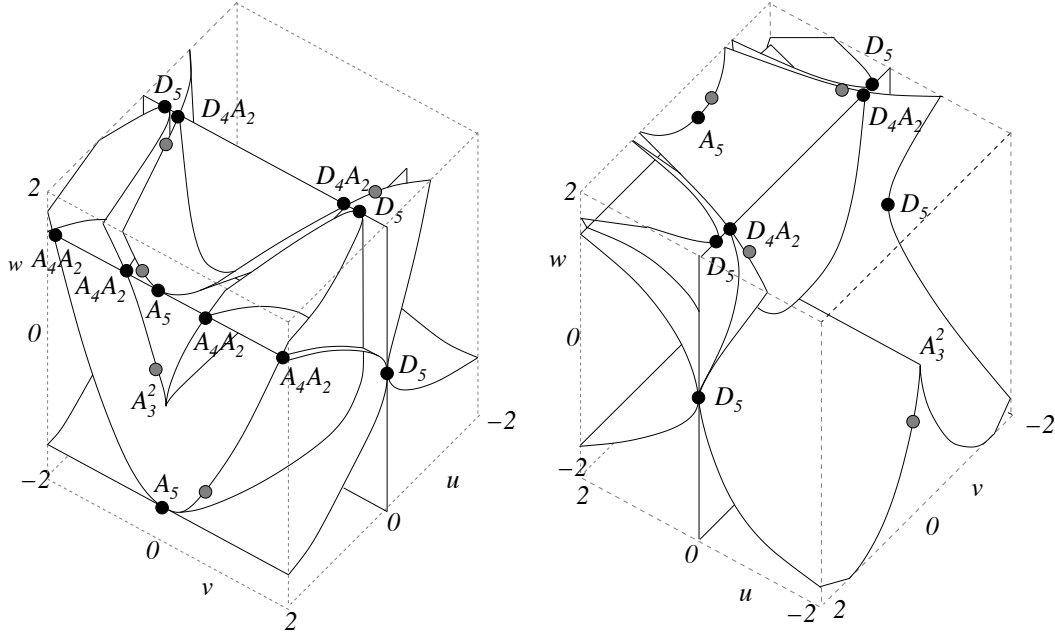


Figure 83: The  $\mathbb{R}_{u,v,w}^3$  parametrising the stratum  $A_3 \subset \mathcal{C}(E_6^+)$  with the emerging  $TA_3A_2$  strata denoted by grey circles for  $d > 0$ . The grey circles will be reflected in the  $v = 0$  plane for  $d < 0$ .

Recall that in Figure 77 the region  $u < 0$  corresponds to  $A_3^{+,\sigma}$  points, the region  $0 < u < w^2$  corresponds to  $A_3^{-,\sigma}$  points and the  $u > w^2$  region corresponds to  $A_3^{+,-\sigma}$ . This implies that two of the half-branches in Figure 83 are  $TA_3^{+,\sigma}A_2$ , two are  $TA_3^{-,\sigma}A_2$  and the final two are  $TA_3^{+,-\sigma}A_2$ . Coming in pairs, these strata do not contribute to any  $\text{mod}2 E_6^+$  cyclic equation.

Next, we approximate the generic map  $\pi$  by the tilted projection

$$\pi_3 : (\mathbb{R}_{\alpha,\beta,\gamma,\delta,\varepsilon}^5) \rightarrow \mathbb{R}_{A,B}^2; (\alpha, \beta, \gamma, \delta, \varepsilon) \mapsto (A, B) = (\alpha, \beta + d\delta + g\gamma)$$

where the parameters  $\alpha, \beta, \delta$  are given by (16). Here our aim is to understand the  $A_3^2$  stratum in  $\mathcal{B}(E_6^+)$ .

Recall that the  $A_3^2$  stratum in Figure 77 corresponds to the  $u$ -axis in  $\mathbb{R}_{u,v,w}^3$ . Also recall from Section 6.1.1.2 that a parametrisation of the  $A_3^2$  stratum is:

$$\begin{aligned} \alpha &= 0 \\ \beta &= 0 \\ \gamma &= -u^2 \\ \delta &= 0 \\ \varepsilon &= 0. \end{aligned}$$

So, its  $\pi_3$ -image is the stratum  $A_3^2 \subset \mathcal{B}_3(E_6^+)$  with equation  $(A, B) = (0, -gu^2)$ . This is depicted in Figure 84.

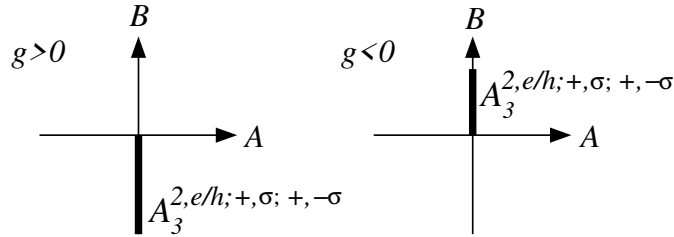


Figure 84: The stratum  $A_3^2 \subset \mathcal{B}_3(E_6^+)$ .

The decorations of the  $A_3^2$  bifurcation follow from Figure 77, Section 6.1.2. Therefore, our  $A_3^2$  stratum is  $A_3^{2,e/h;+,\sigma;+,-\sigma}$ .

**Lemma 6.1.4.** *The contribution of the closure of the stratum  $A_3A_2 \subset \mathcal{C}(E_6^+)$  to any mod2  $E_6^+$  cyclic equation over  $\mathbb{Z}_2$  is  $a_3^{2,e/h;+,\sigma;+,-\sigma}$ .*

### 6.1.3 The closure of the $A_2^3$ stratum in $\mathcal{C}(E_6^+)$

Recall from Section 6.1.1.2 that the  $A_2^3$  stratum has two components. The image of the projection of the first  $A_2^3$  component is the  $4\delta^3 + 27\varepsilon^2 < 0$  region of the  $\delta\varepsilon$ -plane in  $\mathbb{R}_{\alpha,\beta,\gamma,\delta,\varepsilon}^5$  and is bounded by the  $D_4A_2$  stratum. The image of the projection of the second  $A_2^3$  component is the part of the surface  $3\beta^2 + 4\alpha^2\delta + 4\alpha^5 = 0$  which is shown in bold in Figure 85. We also show part of the image of the projection of both  $A_2^3$  components to  $\mathbb{R}_{\alpha,\beta,\delta,\varepsilon}^4$  in Figure 86.

The surface in Figure 85 is a Whitney umbrella. Only its highlighted part corresponds to genuine triple points of the caustic whilst the remaining part is due to a pair of points in a triplet being complex.

In Figure 86 we can see the image of the first parametrisation of  $A_2^3$  which is the region on the  $\delta\varepsilon$ -plane bounded by the  $D_4A_2$  half-branches.

Now, the decorations of the  $D_4A_2$  strata in Figure 86 follow from previous considerations in Section 6.1.2.2.2. For a mod2 cyclic equation, we do not need to consider any projection to the discriminantal plane: we just need to know the numbers of half-branches of the strata, and this information is contained in Figure 86.

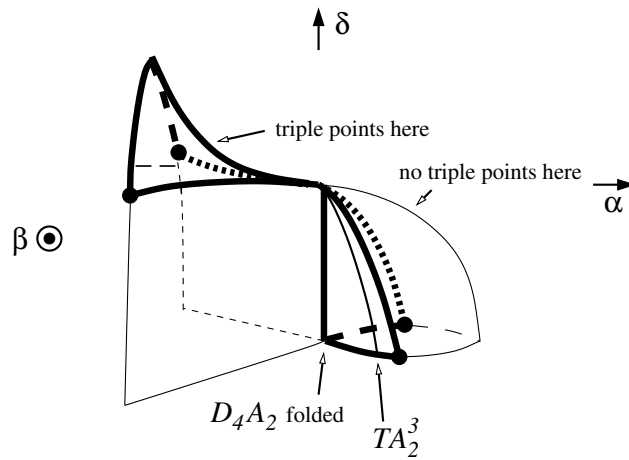


Figure 85: The image of the projection of the stratum  $A_2^3 \subset \mathcal{C}(E_6^+)$  to  $\mathbb{R}_{\alpha, \beta, \delta}^3$ . The black discs mark the  $A_4 A_2$  half-branches in  $\mathcal{C}(E_6^+)$ . Here we are not concerned about their decorations since the  $A_4 A_2$  strata have already been considered in Section 6.1.2. These  $A_4 A_2$  strata bound the regions of triple points.

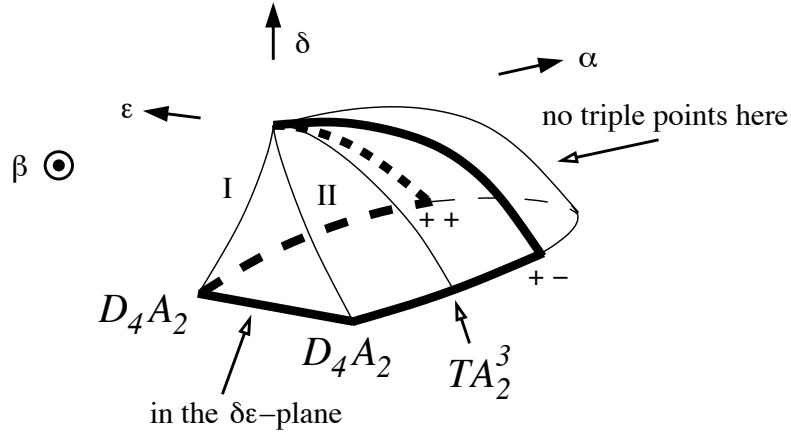


Figure 86: The result of the introduction of an extra parameter  $\varepsilon$ , in the  $\alpha \geq 0$  part of Figure 85.

We know direct from Figure 86 that the contribution of the  $A_2^3$  closure to any  $E_6^+$  cyclic equation is

$$d_{4,1}^{+,\sigma} a_2 + ta_2^3 + d_{4,2}^{+,\sigma} a_2$$

which is zero due to equation **34** when in the  $\mathbb{Z}_2$  setting.

**Lemma 6.1.5.** *The total contribution of the closure of the stratum  $D_4 \subset \mathcal{C}(E_6^+)$  considered in Lemma 6.1.3 and of the closure of the stratum  $A_2^3 \subset \mathcal{C}(E_6^+)$  to any  $E_6^+$  cyclic equation over  $\mathbb{Z}_2$  is zero.*

### 6.1.4 The $E_6^+$ cyclic equation

MAPLE calculations in [9] show that the generic mapping  $\pi$  has no critical points on the open strata  $A_2^2$  and  $A_3$  of  $\mathcal{C}(E_6^+)$ . Therefore the strata  $TA_2^2$  and  $A_3^q$  in  $\mathcal{B}(E_6^+)$  are empty.

Summing up the results from Lemmas 6.1.1, 6.1.2, 6.1.3, 6.1.4 and 6.1.5 we obtain a cyclic equation for  $E_6^+$  over  $\mathbb{Z}_2$ ,

$$\mathbf{39.} \quad a_3^{2,e/h;+,\sigma;+,-\sigma} + a_3^{2,e/h;+,-\sigma;-\sigma} = 0.$$

## 6.2 $E_6^-$ equations

We now consider the cyclic equation that comes from  $\mathcal{C}(E_6^-)$ . Due to (15) the only difference between the  $E_6^+$  and  $E_6^-$  cyclic equations is that all the terms switch their  $s$ -decorations to the opposite. Hence modifying equation **39** we obtain the following  $E_6^-$  cyclic equation over  $\mathbb{Z}_2$ ,

$$\mathbf{40.} \quad a_3^{2,e/h;-\sigma;-\sigma} + a_3^{2,e/h;-\sigma;+\sigma} = 0.$$

This concludes our proof of the  $E_6$  part of Theorem 2.6.2.

## Chapter 7

# Geometric interpretations of additional mod2 discriminantal cycles

In Remark 2.4.3 we introduced five basic *mod2* linear combinations  $I'_{16}, \dots, I'_{20}$  of the codimension 1 strata. According to Theorem 2.5.3, they generate the space of *mod2* discriminantal cycles with the help of the *mod2* reduction of the basis of the space of integer discriminantal cycles.

We will now show that certain linear combinations involving non-trivially these five discriminantal cycles (and some of the other fifteen) are dual to invariants having an integral geometric interpretation when we assume the target manifold  $N$  is  $\mathbb{R}^3$ . So, we devote this chapter to construction of four such local invariants.

The five *mod2* discriminantal cycles in question are:

$$\begin{aligned}
I'_{16} & : TA_2^2 + A_3^{-,+;q} + A_3^{-,-;q} + D_{4,b}^{+,+} + D_{4,b}^{+,-} \\
I'_{17} & : TA_2^3 + TA_3^{\pm,-} A_2 + D_4^{-,+} A_2 + D_4^{-,-} A_2 + D_{4,1}^{+,+} A_2 + D_{4,1}^{+,-} A_2 \\
I'_{18} & : A_3^{2,e/h;+,+;+,+} + A_3^{2,e/h;+,+;+,-} + A_3^{2,e/h;+,+;-,+} + A_3^{2,e/h;+,+;-, -} \\
& \quad + A_3^{2,e/h;+,-;+,-} + A_3^{2,e/h;+,-;-,+} + A_3^{2,e/h;+,-;-,-} + A_3^{2,e/h;-,+;+,-} \\
& \quad + A_3^{2,e/h;-,+;-,-} + A_3^{2,e/h;-,-;-,-} + A_5^{-,+;\pm} + A_5^{-,-;\pm} \\
I'_{19} & : A_2^4 + A_3^{\pm,-} A_2^2 + A_3^{2,e/h;+,-;+,-} + A_3^{2,e/h;+,-;-,-} + A_3^{2,e/h;-,-;-,-} \\
I'_{20} & : A_4^+ A_2.
\end{aligned}$$

Three of the interpretations of the *mod2* cycles that we found are based on the number of components and the self-linking number of one of three framed links constructed from the cuspidal edge and self-intersection locus of  $\mathcal{C}$ . In this chapter we are using two standard symbols:  $\odot$  for the framing directed towards the reader and  $\otimes$  for the framing looking away from the reader. We will depict the cuspidal edges in the diagrams by solid black lines, and the framing by red dashed lines. We show the self-intersection locus of caustics by a dashed black line. If the framing of a link component is blackboard, then we will not show the framing.

The fourth interpretation of a *mod2* cycle is a sum of the *mod2* degrees of swallowtail points of a caustic.

We will also consider a fifth local invariant, the *mod2* linking number of the two framed links constructed from the cuspidal edges and self-intersection locus of  $\mathcal{C}$ . However, the derivative of this invariant turns out to be a linear



combination of the derivatives of already known invariants.

In our proof of each theorem in this chapter about a particular invariant  $I$ , our aim will be to check that the increments  $x_i$  of the invariant across the strata  $X_i$  in our standard expression of the derivative  $I' = \sum x_i X_i$  are exactly those claimed in the theorem.

## 7.1 The number of components and self-linking of the cuspidal edge ( $I_{fe}$ )

A *mod2* invariant combining the number of components and the self-linking of the cuspidal edge of the critical value set of an ordinary generic map of a 3-manifold to  $\mathbb{R}^3$  was introduced in [10]. We will now define its analogue in a generic Lagrangian situation which involves an additional step due to the stable presence of  $D_4$  points.

Like in [10] we start with a construction of a framed link from cuspidal edges of  $\mathcal{C}$ . The way we introduce the framing at a regular point of a cuspidal edge depends only on the sign  $\sigma$  of the edge and is illustrated by the transversal sections shown in Figure 87.

The sign  $s$  will play no role in this construction. However, for the sake of continuity, we shall still keep the decoration in the bifurcations. Near swallowtails, we smoothen the cuspidal edge and join the framings along the two branches by adding a half-twist of the sign coinciding with the sign  $\sigma$  of the swallowtail. We also smoothen the cuspidal edges at  $D_4^\pm$  points to obtain

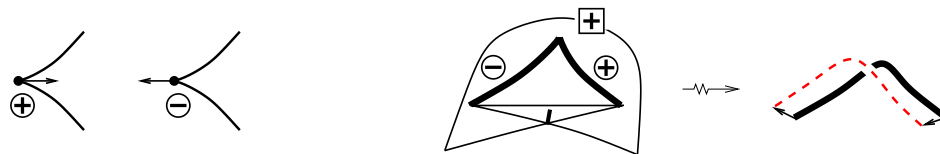


Figure 87: Making a framed link from the cuspidal edges. Here the decorations correspond to  $\sigma$  only.

the framed links shown in Figure 88.

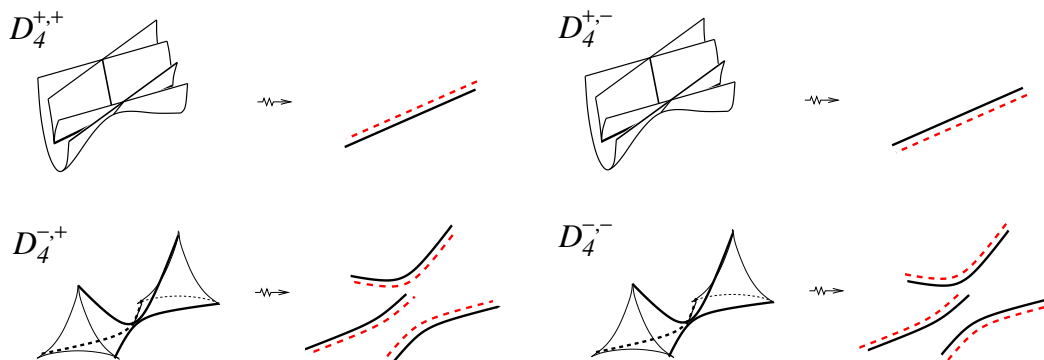


Figure 88: Framed link at  $D_4^{\pm, \sigma}$ .

We arbitrarily orient our framed link, and calculate its writhe  $w$  as the algebraic number of crossings of the cores of the components in the link diagram obtained plus the sum of the algebraic numbers of full rotations done by the framing of each of the components around its own core. Since the number of crossings of two different components in a link diagram is even, the quantity  $w \bmod 4$  does not depend on the orientations of the components. We denote the number of components of our link by  $n$ .

**Theorem 7.1.1.** *The mod2 invariant  $I_{fe} = n + w/2$  is local. It is dual to the cycle*




$$A_3^{2,e/h} + A_3^q + A_4^{e/h} + A_5^{\pm,-,\pm} + D_5.$$

We note that omission of an index means summation along all possible values of this index. Also, we are not concerned if the quantity  $(w/2) \bmod 2$  is integer or half-integer since its increments are integer which is sufficient for our considerations.



Recalling the expressions for our 20 basic discriminantal cycles from Table 4, we have

$$I'_{fe} = I'_{15} + I'_{18} + I'_{sw_{++}} + I'_{(sw_{+-}+sw_{-+})/2}.$$

In order to prove Theorem 7.1.1 as well as the other theorems in this chapter we first introduce a few useful definitions and results. Following the terminology used for the Kauffman bracket polynomial in [17] we introduce

**Definition 7.1.2.** *For ribbon links, we call the replacement of a crossing  with  the A-move, and its replacement with  the B-move. All three fragments are assumed to be blackboard ribbons.*

**Lemma 7.1.3. (AB Lemma).** *The move A changes the quantity  $(n + w/2) \bmod 2$  by  $1/2$  and the move B by  $-1/2$ .*

**Definition 7.1.4.** *For ribbon links, we call the replacement of a crossing  with  the C-move. It is the result of the two-step compositions  $(-A)B$  and  $(-B)A$ . Again, the fragments are assumed to be blackboard ribbons.*

The AB Lemma implies

**Lemma 7.1.5. (C Lemma).** *The C-move changes the quantity  $(n+w/2) \bmod 2$  by 1.*

**Proof of Lemma 7.1.3 (AB Lemma).** In order to prove Lemma 7.1.3 (AB Lemma) we first examine the A-move, which is shown in Figure 89.

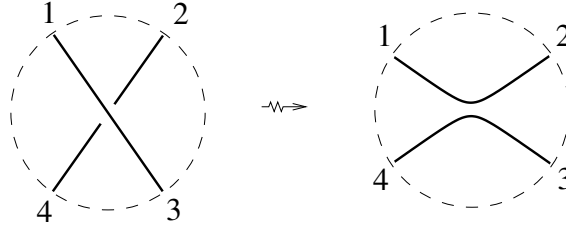


Figure 89: A-move.

The rest of the link diagram is outside the disk and connects points 1, 2, 3 and 4 by arcs which we will call *external*. These are shown in blue in the later diagrams. We show the external arcs in a simplified way as they can actually have crossings with one another as well as with other link components. We have several combinatorial cases.

- Assume the external arcs are 14 and 23 (see Figure 90). Then the move preserves the number of the components. Assume the orientations of the only components involved are as in Figure 90. We see the external arc 14 has been reversed. We can show this does not effect  $(w/2) \bmod 2$  outside the disk by closing the external arcs with chords 14 and 23 as depicted

in Figure 91. The modified link diagrams in Figure 91 differ only by the reorientation of the left component and we know reorientation of a link component does not effect  $(w/2) \bmod 2$ . So, the only contribution to the increment of  $(w/2) \bmod 2$  comes from inside the disk. Finally, we see the writhe inside the disk increases by 1. Hence,  $(w/2) \bmod 2$  increases by  $1/2$  and so, the quantity  $(n + w/2) \bmod 2$  changes by  $1/2$ .

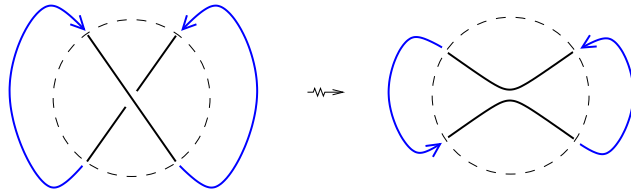


Figure 90: The A-move with external arcs 14 and 23.

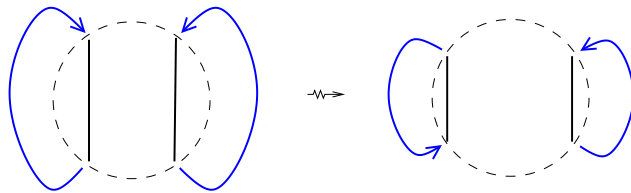


Figure 91: Closing the external arcs 14 and 23.

- Assume the external arcs are 12 and 34 (see Figure 92). The move produces two components from one. We choose orientation of the initial component, and orient the final ones so that the external arcs keep their orientations. We see the writhe inside the disk decreases by 1, so  $(w/2) \bmod 2$  changes by  $-1/2$ . Hence, the quantity  $(n + w/2) \bmod 2$

changes by  $1/2$ .

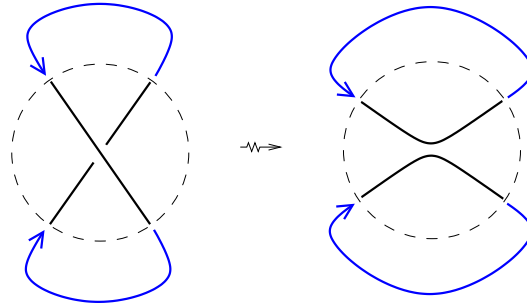


Figure 92: The A-move with external arcs 12 and 34.

- Assume the external arcs are 13 and 24 (see Figure 93). The move produces one component from two. This time we choose an orientation of the final component, and orient the two initial so that the external arcs keep their orientations. We see the writhe inside the disk decreases by 1, so  $(w/2) \bmod 2$  changes by  $-1/2$ . Hence, the quantity  $(n + w/2) \bmod 2$  changes by  $1/2$ .

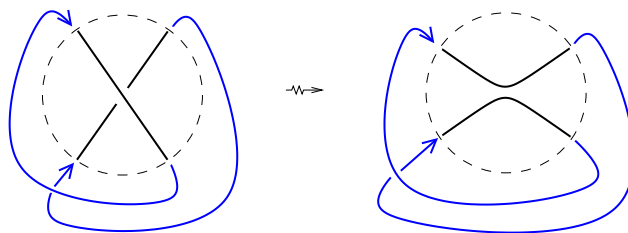


Figure 93: The A-move with external arcs 13 and 24.

Thus the A-move always changes the  $(n + w/2) \bmod 2$  by  $1/2 \bmod 2$ .

Now, the B-move is the change crossing followed by the A-move. At the first step here  $\Delta(n + w/2) = \Delta(w/2) = 1 \pmod{2}$ , and at the second  $\Delta(n + w/2) = 1/2$ . Hence the total increment is  $3/2 = -1/2 \pmod{2}$ , as claimed.  $\square$

**Corollary 7.1.6. (Six ends Corollary).** *Consider a local transformation of a link shown in Figure 94, where the fragments are assumed to be blackboard ribbons. The transformation changes the quantity  $(n + w/2) \pmod{2}$  by one.*

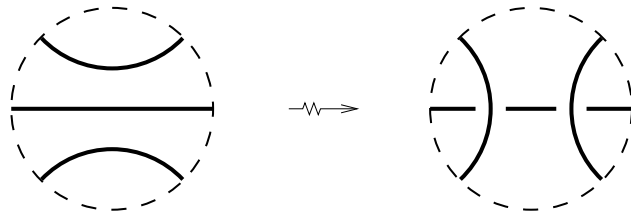


Figure 94: The six ends move.

**Proof of Corollary 7.1.6. (Six ends Corollary).** Figure 95 represents the move of Figure 94 as a sequences of the elementary moves. By the AB and C Lemmas, the quantity  $(n + w/2) \pmod{2}$  changes by 1.

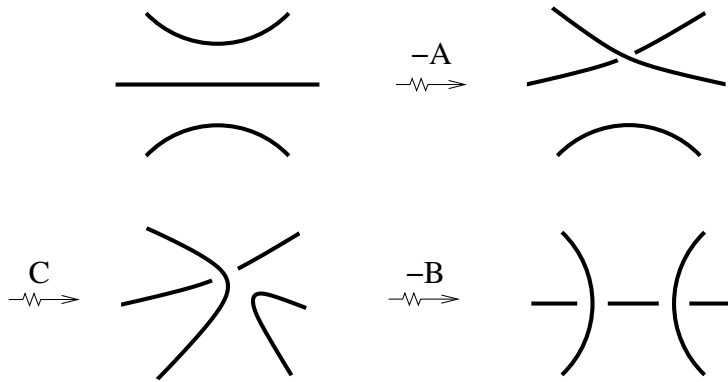


Figure 95: Decomposition of the six ends move.

□

**Corollary 7.1.7. (Eight ends Corollary).** *Consider a local transformation of a link shown in Figure 96, where the fragments are assumed to be blackboard ribbons. The transformation does not change the quantity  $(n + w/2) \bmod 2$ .*

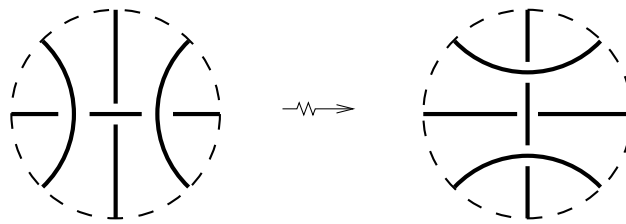


Figure 96: The eight ends move.

**Proof of Corollary 7.1.7. (Eight ends Corollary).** Figure 97 represents the move of Figure 96 as a sequences of the elementary moves. By the AB and C Lemmas, the quantity  $(n + w/2) \bmod 2$  does not change.



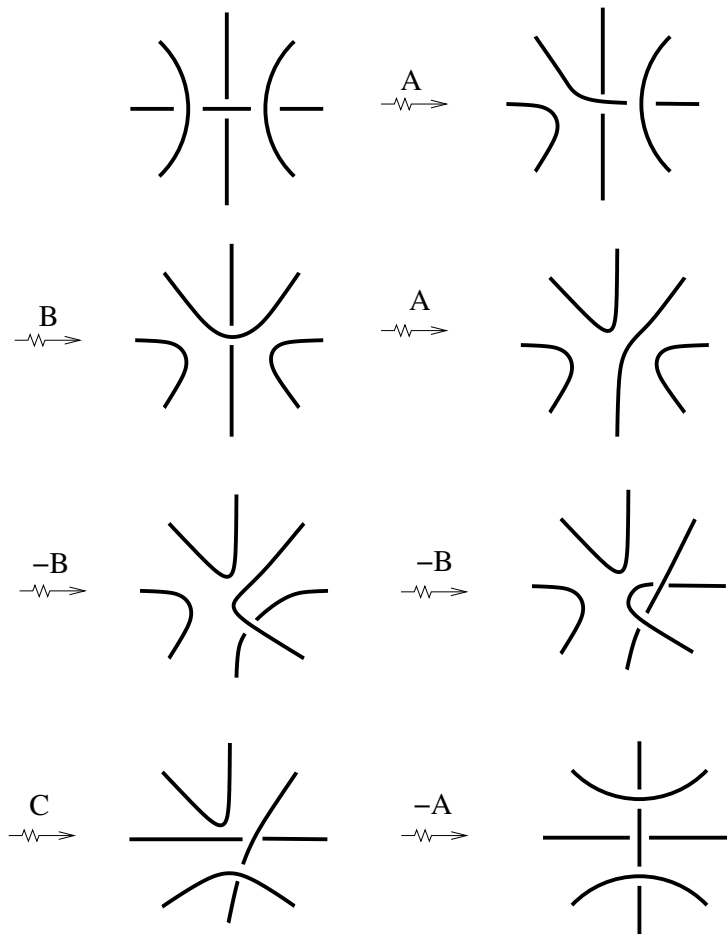


Figure 97: Decomposition of the eight ends move.

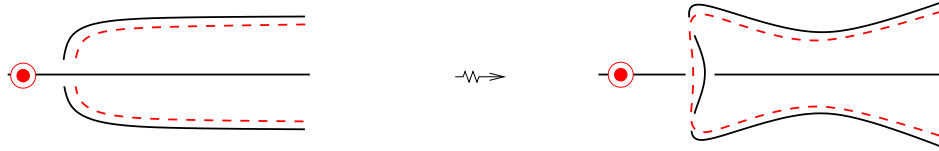
□

The result of Lemma 7.1.5 (C Lemma) will help us to prove Theorem 7.1.1. The results from Corollaries 7.1.6 and 7.1.7 will be used later, for study of other link invariants.

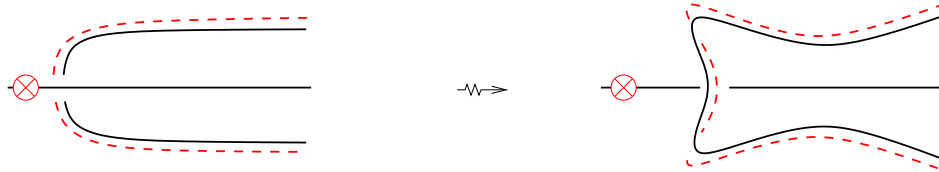
**Proof of Theorem 7.1.1.** In all the bifurcations considered below, the orientations of all surviving local link components are the same before and after the transition. It is obvious that the following bifurcations from Figures 11, 12 and 13 contribute increment 1 to the invariant  $I_{fe}$ :

- $A_3^{2,e/h}$ :  $\Delta n = 0$ ,  $\Delta w/2 = 1$ ;
- $A_3^{s,\sigma,+,+}$ :  $\Delta n = 1$ ,  $\Delta w/2 = 0$ ;
- $A_3^{s,\sigma,+,-}$ : according to the C Lemma;
- $A_3^{s,\sigma,-,-}$ :  $\Delta n = 1$ ,  $\Delta w/2 = 0$ ;
- $A_4^c$ :  $\Delta n = 1$ ,  $\Delta w/2 = 0$ ;
- $A_4^h$ : according to the C Lemma;
- $A_5^{s,\sigma,\omega}$ :  $\Delta n = 0$ . In general for  $A_5^{s,\sigma,\omega}$  we have  $\Delta w = \omega - \omega\sigma = \omega(1 - \sigma)$ , since two swallowtails are created with the sign opposite to  $\omega$ , each contributing  $-\omega\sigma/2$  to the change in writhe. Hence when  $\sigma = -$ ,  $\Delta w \bmod 4 = 2$  and  $\Delta w/2 = 1$ . Therefore,  $a_5^{s,-,\pm} = 1$ . Similarly for  $A_5^{s,+,\pm}$ ,  $\Delta w \bmod 4 = 0$ ,  $\Delta w/2 = 0 \implies a_5^{s,+,\pm} = 0$ ;
- $D_5^{s,+}$ :  $\Delta n = 0$ ,  $\Delta w/2 = 1$ . After the bifurcation two swallowtails are created, of opposite signs, that is,  $\sigma$  and  $-\sigma$ . These swallowtails produce half twists of opposite signs, so they do not contribute to any change in writhe. However, we see that the only local crossing involved in the

bifurcation switches during the transition, thus changing the writhe by  $\pm 2$ . Hence  $d_5^{s,+} = 1$ ;



- $D_5^{s,-}$ :  $\Delta n = 0$ ,  $\Delta w/2 = 1$ . Analysis similar to  $D_5^{s,+}$  tells us the swallow-tails do not contribute to the writhe change. And again, the only local crossing involved in the bifurcation switches during the transition, thus changing the writhe by  $\pm 2$ . Hence  $d_5^{s,-} = 1$ .



The  $D_{4,a/b/c}^{+,s,\sigma}$  and  $D_{4,q}^{-,s,\sigma}$  bifurcations do not contribute to  $I_{fe}$  since the framed links before and after the transitions are clearly isotopic (cf. Figures 13 and 88). It is obvious why all other bifurcations do not contribute and hence, no explanation for them is given.  $\square$

## 7.2 Framed link formed by positive cuspidal edges and self-intersection lines ( $I_{dc^+}$ )

In [1] Aicardi introduced two *mod*2 invariants combining the number of components and the self-linking of self-intersection sets and cuspidal edges of the critical value set of an ordinary generic map of a 3-manifold to  $\mathbb{R}^3$ . Like in Section 7.1 we now define their analogue in a generic Lagrangian situation. We also adjust Aicardi's treatment of triple points.

Following [1] we first look at the framed link  $L_+$  formed from positive cuspidal edges ( $\sigma = +$ ) and self-intersection lines. The way this link is constructed is as follows.

- Framing the edges  $A_3^{s,+}$  stays as it was in Section 7.1 (Figure 98).

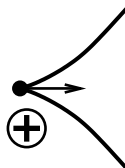


Figure 98: Framing of  $A_3^{s,+}$ .

- The framing of  $A_2^2$  segments is defined as shown in Figure 99.

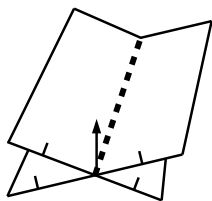


Figure 99: Framing of  $A_2^2$ .

We now postulate the behaviour of  $L_+$  near points of isolated singularity types.

- The link  $L_+$  at an  $A_3^{s,+}A_2$  junction is shown in Figure 100. At  $A_3^{s,-}A_2$ , the link will of course not include the edge component.

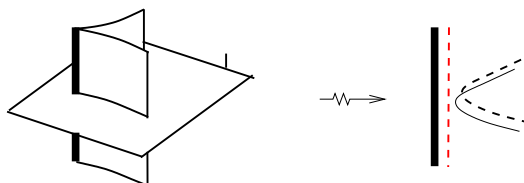


Figure 100:  $L_+$  at  $A_3^{s,+}A_2$  points.

- The link  $L_+$  at a  $\sigma = +$  swallowtail is shown in Figure 101. This is a junction of the self intersection and edge parts. The local writhe of the framing is  $1/4$ . At a  $\sigma = -$  swallowtail the fragment shown in Figure 101 should be reflected from the right to the left, and the local writhe of the framing will be  $-1/4$ .

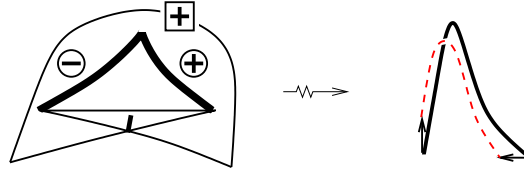


Figure 101:  $L_+$  at  $A_4^{s,+}$ .

- Unlike what was done in [1], we now postulate the way to canonically resolve triple points so that  $L_+$  would be a genuine link. For this, we think about a caustic being locally an arrangement of three coordinate planes of an orthogonal system of coordinates. See Figure 102, left. We assume that the coorientations of these planes are given by the standard unit vectors  $i, j, k$  so that taking them exactly in this order we get the right orientation of  $\mathbb{R}^3$ . The  $i$ -,  $j$ - and  $k$ -self-intersection lines are framed respectively by the vectors  $j+k, k+i$  and  $i+j$ . We deform these lines (off the planes) slightly and continuously near the origin, and keeping their framings unchanged. Namely, we move the  $i$ -  $j$ - and  $k$ -lines respectively in the directions of the vectors  $k-j, i-k$  and  $j-i$ . The general rule here is that each of these vectors is the cross-product (framing of the plane perpendicular to the line) $\times$ (framing of the line). For example  $i \times (j+k) = k-j$ . The result of the whole local deformation of the cores is shown in Figure 102, right.

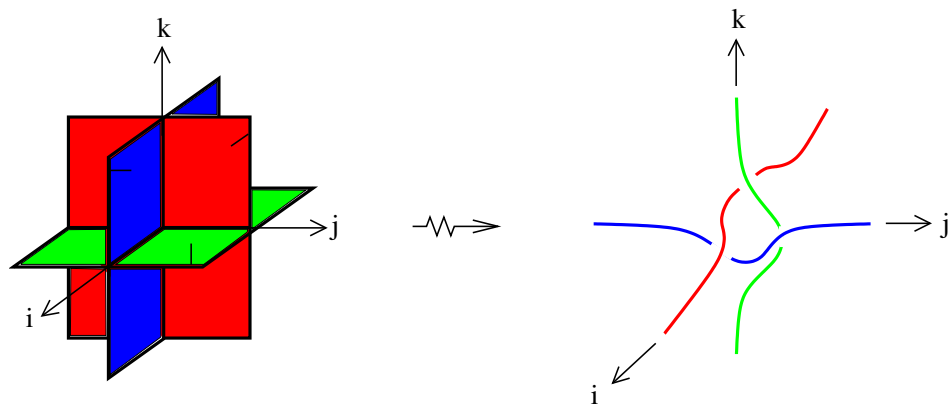


Figure 102: Resolution of a triple point  $A_2^3$ .

**Remark 7.2.1.** *Figure 102 shows that if each of the three local self-intersection branches is oriented in the direction of the co-orientation of its transversal  $A_2$  sheet, then the signs of the crossings after the resolution are  $+, +, +$ . Therefore, if we orient exactly one of the branches in the opposite way, the signs become  $+, -, -$ . Reversing the orientation of exactly two branches gives us also  $+, -, -$ . And reversing all three we have  $+, +, +$ .*

- We now look at the  $L_+$  near  $D_4^\pm$  points. We smooth out the  $D_4^-$  point as shown in Figure 103. Hence,  $L_+$  of  $D_4^{-,+}$  is shown in Figure 104. The contribution of  $D_4^{-,-}$  to our framed link is empty, since we have there no positive cuspidal edges or self-intersections.

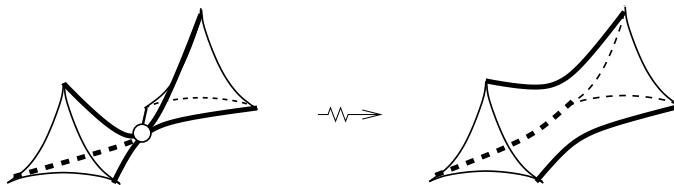


Figure 103: Smoothing of a  $D_4^-$  point.

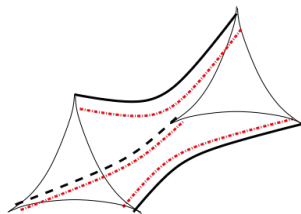


Figure 104:  $L_+$  at  $D_4^{-,+}$ .

- The rule for smoothing the  $L_+$  at  $D_4^{+,+}$  points is shown in Figure 105. The framed link  $L_+$  for  $D_4^{+,-}$  is similar to  $D_4^{+,+}$  but with the cuspidal edge component removed.

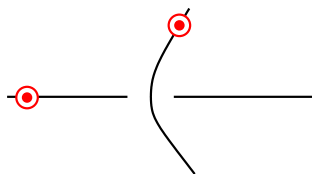


Figure 105:  $L_+$  at  $D_4^{+,+}$ .



We now introduce the new invariant,

$$I_{dc^+} = n^+ + \frac{(w^+ + t)}{2}$$

where  $n^+$  is the number of components of the link  $L_+$ ,  $w^+$  is the writhe of  $L_+$  and  $t$  is the number of triple points of the caustic.

**Theorem 7.2.2.** *The mod2 invariant  $I_{dc^+}$  is dual to the cycle*

$$\begin{aligned} &A_2^4 + TA_2^2 + A_3^{\pm,+}A_2^2 + TA_3A_2 + A_3^{2,e/h;\pm,+;\pm,-} + A_3^{2,e/h;\pm,-;\pm,-} + A_4^{\pm,e/h} \\ &+ A_5^{\pm,-,\pm} + A_3^{\pm,+q} + D_{4,a/c}^{+,\pm,\pm}. \end{aligned}$$

We should note that due to working *mod2* we have the symmetry  $A_3^{2,e/h;s,\sigma;s',\sigma'} = A_3^{2,e/h;s',\sigma';s,\sigma}$ . Hence in Theorem 7.2.2,  $A_3^{2,e/h;\pm,+;\pm,-}$  is a sum of eight elementary strata while  $A_3^{2,e/h;\pm,-;\pm,-}$  is a sum of six. The same also applies for the theorems later in this chapter.

Recalling the expressions for our 20 basic discriminantal cycles from Table 4, we have

$$\begin{aligned} I'_{dc^+} = &I'_{15} + I'_{16} + I'_{17} + I'_{19} + I'_{\chi} + I'_{d_{\pm}^+} + I'_{c_{++}} + I'_{c_{+-}} + I'_{(sw_{++}+sw_{--})/2} \\ &+ I'_{(sw_{+-}+sw_{-+})/2} + I'_{(t+c_{++}+c_{-+})/2} + I'_{(((d_{-}^++d_{-}^-)/2)+((d_{+}^++d_{+}^-)/2)+\chi+15)/2}. \end{aligned}$$

**Proof of Theorem 7.2.2.**

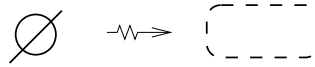
We first consider bifurcations where contributions of triple points are zero.

- $D_{4,a}^+$  (line 2 of Figure 13):

$$D_{4,a}^{+,s,+}: \Delta w^+ / 2 = 0, \Delta n^+ = 1 \implies d_{4,a}^{+,s,+} = 1;$$



$$D_{4,a}^{+,s,-}: \Delta w^+ / 2 = 0, \Delta n^+ = 1 \implies d_{4,a}^{+,s,-} = 1;$$

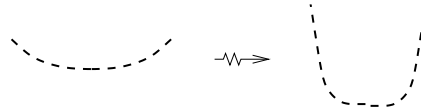


- $D_{4,b}^+$  (line 3 of Figure 13):

$$D_{4,b}^{+,s,+}: \Delta w^+ / 2 = 0, \Delta n^+ = 0 \implies d_{4,b}^{+,s,+} = 0;$$

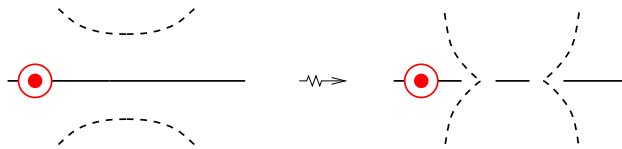


$$D_{4,b}^{+,s,-}: \Delta w^+ / 2 = 0, \Delta n^+ = 0 \implies d_{4,b}^{+,s,-} = 0;$$

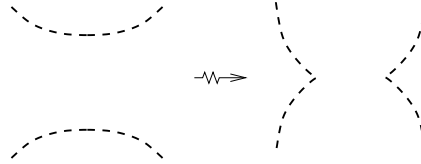


- $D_{4,c}^+$  (line 4 of Figure 13):

$D_{4,c}^{+,s,+}$ : Due to the Six ends Corollary, transforming the left link to the right one changes the quantity  $(n + w/2) \bmod 2$  by 1  $\implies d_{4,c}^{+,s,+} = 1$ ;



$D_{4,c}^{+,s,-}$ : We know directly from the C Lemma that the transformation of the link changes the quantity  $(n + w/2) \bmod 2$  by 1  $\implies d_{4,c}^{+,s,-} = 1$ ;



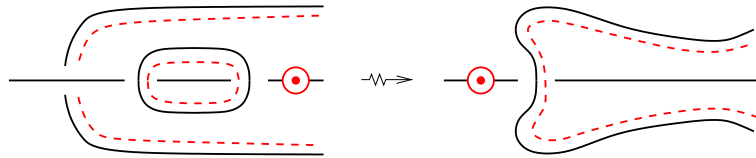
- $D_{4,q}^-$  (line 1 of Figure 13):

$D_{4,q}^{-,s,+}$ : Its link contribution is the same as in the case of  $I_{fe}$ . Hence  $d_{4,q}^{-,s,+} = 0$ ;

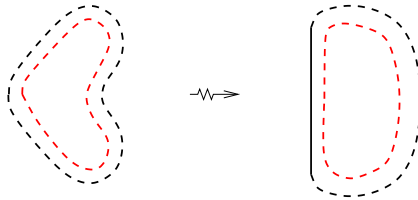
$D_{4,q}^{-,s,-}$ : Its link contribution is empty  $\implies d_{4,q}^{-,s,-} = 0$ ;

- $D_5$  (line 5 of Figure 13):

$D_5^{s,+}$ :  $\Delta w^+ / 2 = 1 \bmod 2$ ,  $\Delta n^+ = 1 \implies d_5^{s,+} = 0$ ;

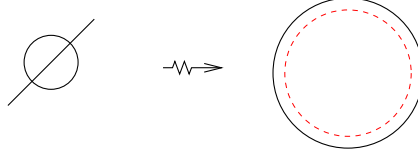


$D_5^{s,-}$ :  $\Delta w^+ / 2 = 0$ ,  $\Delta n^+ = 0 \implies d_5^{s,-} = 0$ ;

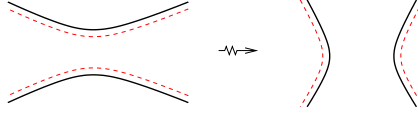


- $A_3^q$  (lines 1, 2 and 3 of Figure 11):

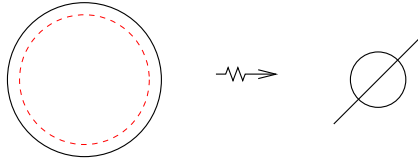
$$A_3^{s,+,+}: \Delta w^+/2 = 0, \Delta n^+ = 1 \implies a_3^{s,+,+} = 1;$$



$$A_3^{s,+,-}: \text{According to the C Lemma } a_3^{s,+,-} = 1;$$



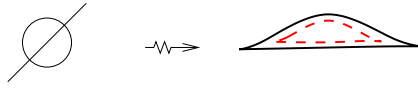
$$A_3^{s,-,-}: \Delta w^+/2 = 0, \Delta n^+ = 1 \implies a_3^{s,-,-} = 1;$$



$A_3^{s,-,+}$ ,  $A_3^{s,-,-}$  and  $A_3^{s,-,-}$ : We have no local components in the framed link before and after the bifurcation. Therefore,

$$a_3^{s,-,+} = a_3^{s,-,-} = a_3^{s,-,-} = 0;$$

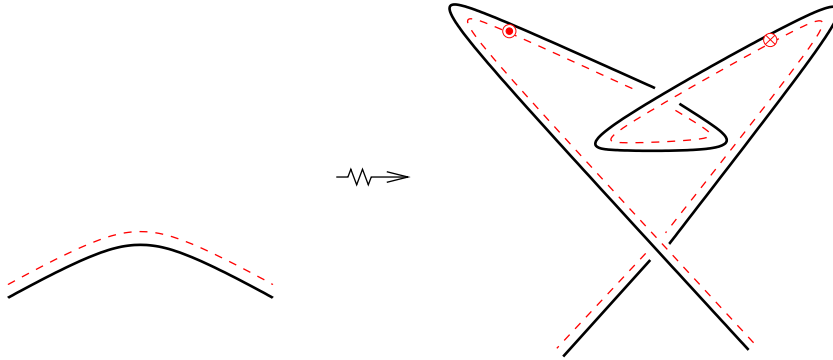
- $A_4^{\varepsilon,\varepsilon}$  (line 4 of Figure 11): At the bifurcation, two swallowtails of opposite signs,  $\sigma$  and  $-\sigma$ , are created, hence with the total zero contribution to the writhe. However,  $\Delta(n^+) = 1$ . Therefore,  $a_4^{\varepsilon,\varepsilon} = 1$ ;



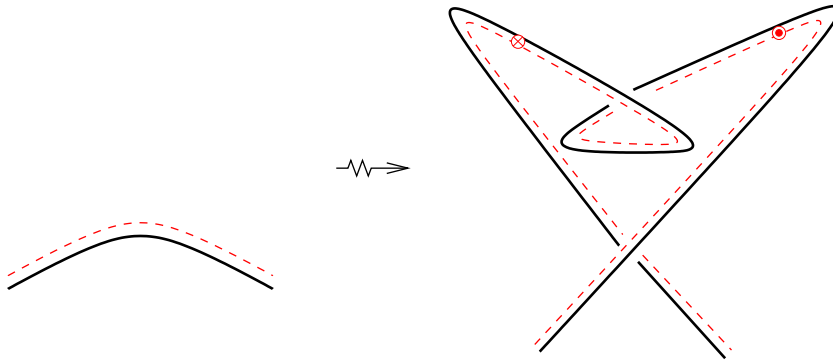
- $A_4^{\varepsilon, h}$  (line 5 of Figure 11): Similar to  $L_+$  of  $A_3^{s, +, +, -}$ . Hence, the C Lemma implies  $a_4^{\varepsilon, h} = 1$ ;

- $A_5$  (line 6 of Figure 11):

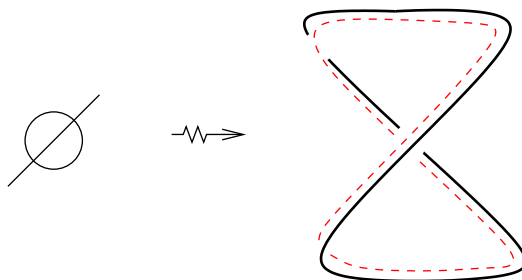
$A_5^{s, +, +}$ : We have  $\Delta w^+ / 2 = 0$ ,  $\Delta n^+ = 0 \implies a_5^{s, +, +} = 0$ .



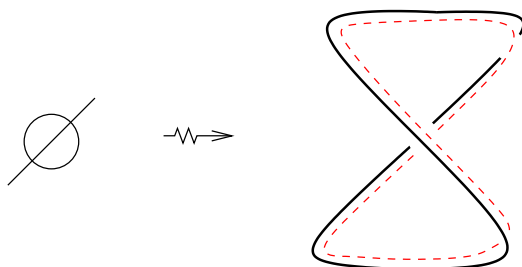
$A_5^{s, +, -}$ : The link transition is the mirror image of the previous one, hence  $a_5^{s, +, -} = 0$ .



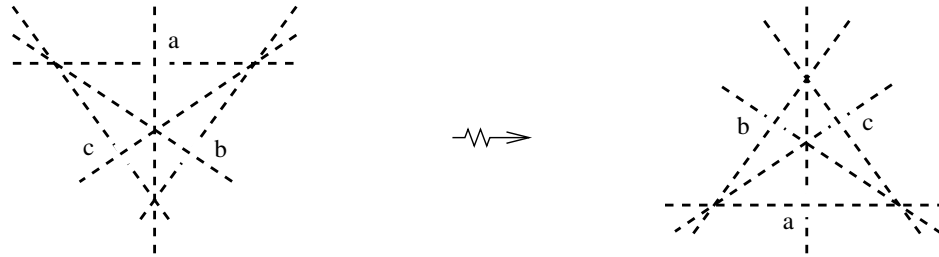
$$A_5^{s,-,+}: \Delta w^+ / 2 = 0, \Delta n^+ = 1 \implies a_5^{s,-,+} = 1.$$



$$A_5^{s,-,-}: \Delta w^+ / 2 = 0, \Delta n^+ = 1 \implies a_5^{s,-,-} = 1.$$



- $A_2^4$  (line 1 of Figure 12): Here, in the ‘big’ triangle the ‘medians’ go (at the crossings  $a, b, c$ ) above its sides before the bifurcation and under after. We do not need to consider the triple points resolved, since any triplet of sheets meet after the bifurcation the same way as before. Hence, the resolution of each triple point stays the same. We see,  $\Delta w^+ / 2 = 1 \text{ mod } 2$  due to the changes at the crossings  $a, b$  and  $c$ , and  $\Delta n^+ = 0$ . Hence,  $a_2^4 = 1$ ;



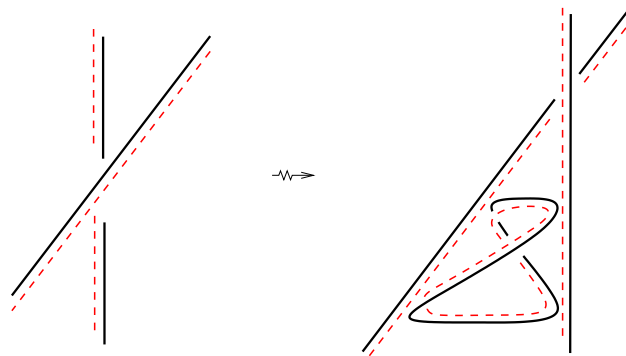
- $TA_2^{2,e}$  (line 3, left of Figure 12):  $\Delta w^+ / 2 = 0, \Delta n^+ = 1 \implies ta_2^{2,e} = 1$ ;



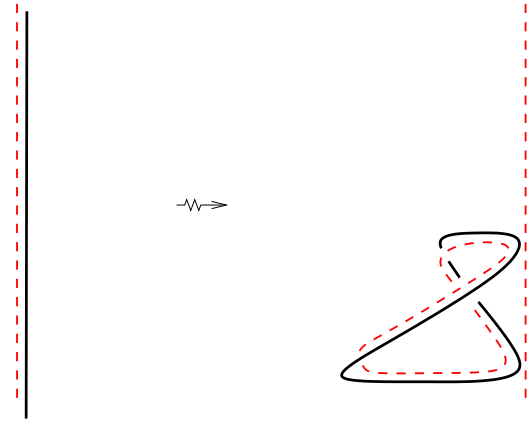
- $TA_2^{2,h}$  (line 3, right of Figure 12): Its link is similar to  $L_+$  of  $D_{4,c}^{+,s,-}$ . The C Lemma implies  $ta_2^{2,h} = 1$ ;

- $A_3^{2,e}$  (line 5 of Figure 12):

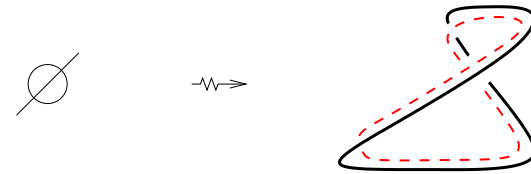
$A_3^{2,e;s,+,s',+}$ : We have  $\Delta n^+ = 1$ . It is obvious that  $\Delta w^+ / 2 = 1$  due to the change of the edge crossing and the newborn component of  $L^+$  having writhe 0. Therefore,  $a_3^{2,e;s,+,s',+} = 0$ ;



$$A_3^{2,e;s,+,s',-}: \Delta n^+ = 1, \Delta w^+/2 = 0 \implies a_3^{2,e;s,+,s',-} = 1;$$

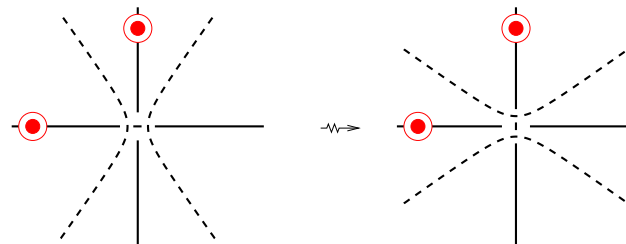


$$A_3^{2,e;s,-;s',-}: \Delta n^+ = 1, \Delta w^+/2 = 0 \implies a_3^{2,e;s,-;s',-} = 1;$$



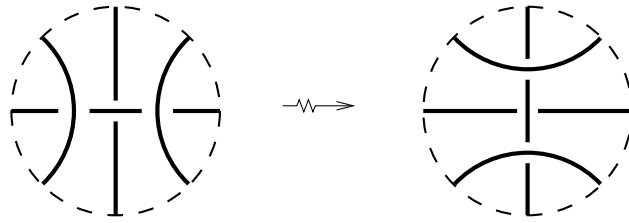
- $A_3^{2,h}$  (line 6, left of Figure 12):

$A_3^{2,h;s,+,s',+}$ : Here we are looking at the bifurcation from inside the cuspidal edge surfaces.

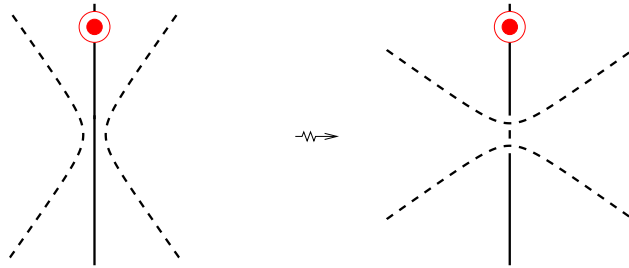




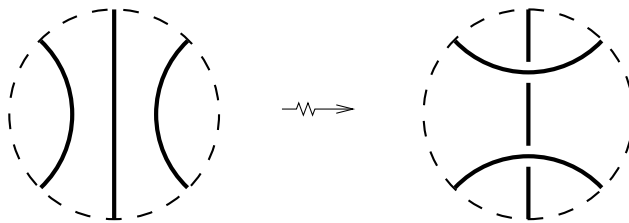
A simplified version of the link contribution is shown below. Applying the Eight ends Corollary we know transforming the left diagram to the right one does not change the quantity  $(n+w/2) \bmod 2 \implies a_3^{2,h;s,+,s',+} = 0$ ;



$A_3^{2,h;s,+,s',-}$ :



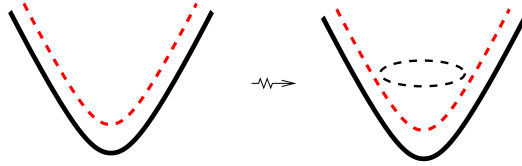
A simplified version of the link contribution is shown below. From the Six ends Corollary we know transforming the left link fragment to the right one changes the quantity  $(n+w/2) \bmod 2$  by 1  $\implies a_3^{2,h;s,+,s',-} = 1$ ;



$A_3^{2,h;s,-;s',-}$ : The local transformation of  $L_+$  here is similar to that for  $D_{4,c}^{+,s,-}$ . By the C Lemma  $a_3^{2,h;s,-;s',-} = 1$ ;

- $TA_3A_2^e$  (line 7, left of Figure 12):

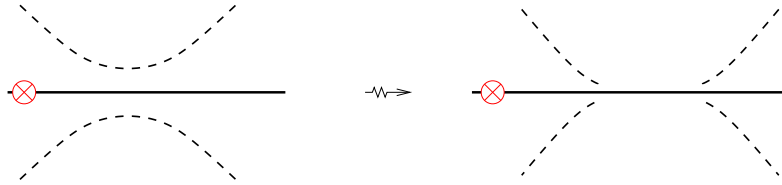
$$TA_3^{s,+}A_2^e: \Delta w^+/2 = 0, \Delta n^+ = 1 \implies ta_3^{s,+}A_2^e = 1;$$



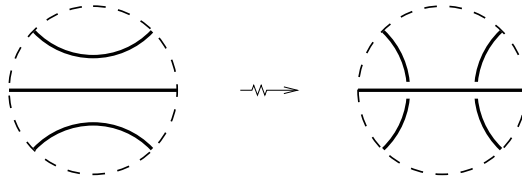
$TA_3^{s,-}A_2^e$ : The local framed link transformation is that of  $TA_3^{s,+}A_2^e$  with the cuspidal edge removed.  $\Delta w^+/2 = 0, \Delta n^+ = 1 \implies ta_3^{s,-}A_2^e = 1$ ;

- $TA_3A_2^h$  (line 7, right of Figure 12):

$$TA_3^{s,+}A_2^h:$$



A simplified version of the link contribution is shown below. We should note this is the same as Figure 94 viewed from the back. Hence the Six ends Collary shows  $ta_3^{s,+}A_2^h = 1$ ;

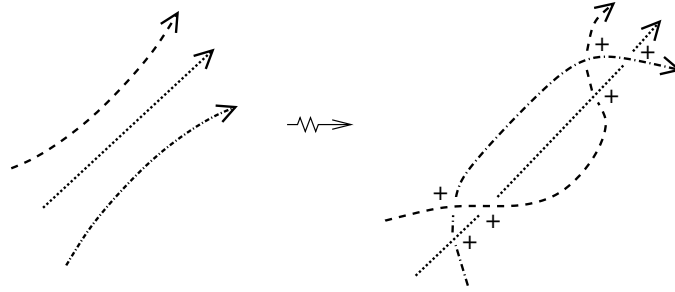


$TA_3^{s,-}A_2^h$ : Its link contribution is similar to  $TA_3^{s,+}A_2^h$  but with the removal of the cuspidal edge. The C Lemma implies  $ta_3^{s,-}a_2^h = 1$ ;

We now consider bifurcations with contributions from triple points.

- $TA_2^3$  (line 2 of Figure 12): We consider the four options of how the sheets are co-oriented separately.

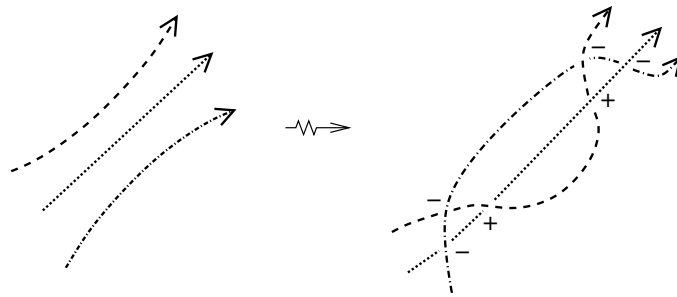
$TA_2^{3,0}$ : This is when all three  $A_2$  sheets are co-oriented ‘inside the bubble’ after the bifurcation. The framed link with the triple points resolved is shown below. We assign arbitrary directions to the branches and we should note that changing the orientation of any branch does not effect the *mod*4 increment of the local writhe. We see  $\Delta w^+ = 6$  and  $\Delta t = 2$ . So, we have  $\Delta(w^+ + t)/2 = 0 \text{ mod } 2$  and  $\Delta n^+ = 0$ . Hence  $ta_2^{3,0} = 0$ .



**Alternative explanation:** We assume that all the  $A_2$  sheets are co-oriented inside the bubble. Therefore the orientations of all self-intersection branches are consistent with the co-orientations of the sheets at the lower triple point, and are opposite to the co-orientations of the sheets at the upper triple point. So, we have three positive crossings instead of

each triple point (see Remark 7.2.1) giving us  $\Delta w^+ = 6$ . Since  $\Delta t = 2$  we have  $\Delta(w^+ + t)/2 = 0 \pmod{2}$  and  $\Delta n^+ = 0$ . Thus  $ta_2^{3,0} = 0$ .

$TA_2^{3,1}$ : Here the co-orientation of the  $A_2$  sheets are exactly as in Figure 12.  $\Delta w^+ = -2$  and  $\Delta t = 2$ . So, we have  $\Delta(w^+ + t)/2 = 0 \pmod{2}$  and  $\Delta n^+ = 0$ . Hence  $ta_2^{3,1} = 0$ .



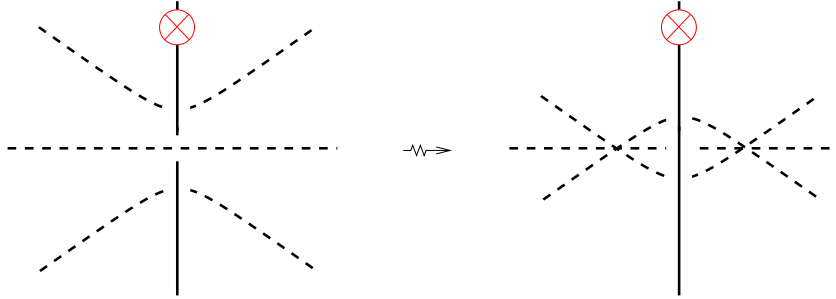
**Alternative explanation:** Comparing with the  $TA_2^{3,0}$  case, for  $TA_2^{3,1}$  we are now changing the co-orientation of one of the sheets but still keeping the orientations of the branches. According to Remark 7.2.1, this provides one positive and two negative crossings instead of each of the triple points, giving us  $\Delta w^+ = -2$ . Since  $\Delta t = 2$  we have  $\Delta(w^+ + t)/2 = 0 \pmod{2}$ . Together with  $\Delta n^+ = 0$  this implies that  $ta_2^{3,1} = 0$ .

$TA_2^{3,2}$ : Its link contribution will be the same as  $TA_2^{3,1}$ .

$TA_2^{3,3}$ : Its link contribution will be the same as  $TA_2^{3,0}$ .

- $A_3A_2^2$  (line 4 of Figure 12):

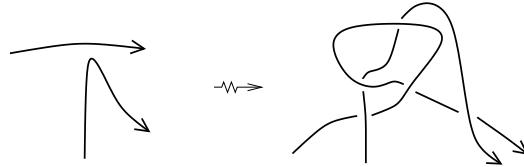
$A_3^{s,+}A_2^{2,0}$ ,  $A_3^{s,+}A_2^{2,1}$  and  $A_3^{s,+}A_2^{2,2}$ : We see there that the  $A_2^2$  part of  $L_+$  (with the triple points not resolved) bifurcates exactly the same way as in the  $TA_2^3$  cases. Therefore for this part on its own,  $\Delta w^+ = 2 \bmod 4$  and  $\Delta t = 2$ . Hence, in total,  $\Delta n^+ = 0$  and  $\Delta(w^+ + t)/2 = 1$  due to the change of the crossing of the cuspidal edge with the meeting line of the two  $A_2$  sheets. Hence,  $a_3^{s,+}a_2^{2,0} = a_3^{s,+}a_2^{2,1} = a_3^{s,+}a_2^{2,2} = 1$ ;



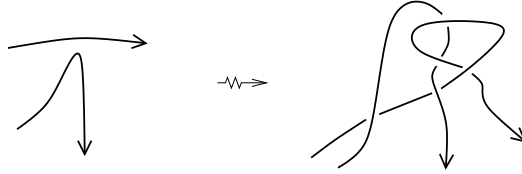
$A_3^{s,-}A_2^{2,0}$ ,  $A_3^{s,-}A_2^{2,1}$  and  $A_3^{s,-}A_2^{2,2}$ : Respectively, their framed links will be the same as  $A_3^{s,+}A_2^{2,0}$ ,  $A_3^{s,+}A_2^{2,1}$  and  $A_3^{s,+}A_2^{2,2}$  but with the removal of the cuspidal edge. Therefore,  $a_3^{s,-}a_2^{2,0} = a_3^{s,-}a_2^{2,1} = a_3^{s,-}a_2^{2,2} = 0$ ;

- $A_4A_2$  (line 6, right of Figure 12):

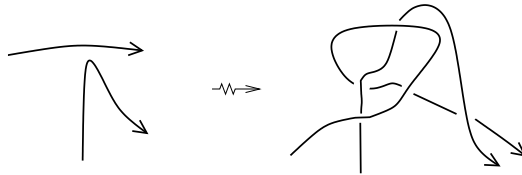
$A_4^{s,+}A_2^1$ :  $\Delta w^+ = -1$ ,  $\Delta t = 1$ . Hence,  $\Delta(w^+ + t)/2 = 0$  and  $\Delta n^+ = 0$   
 $\implies a_4^{s,+}a_2^1 = 0$ ;



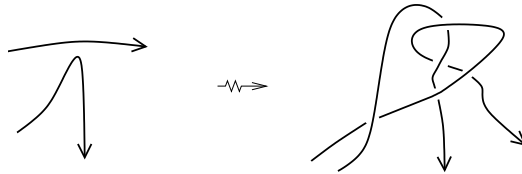
$A_4^{s,-} A_2^1$ :  $\Delta w^+ = -1$ ,  $\Delta t = 1$ . Hence,  $\Delta(w^+ + t)/2 = 0$  and  $\Delta n^+ = 0$   
 $\implies a_4^{s,-} a_2^1 = 0$ ;



$A_4^{s,+} A_2^0$ :  $\Delta w^+ = -1$ ,  $\Delta t = 1$ . Hence,  $\Delta(w^+ + t)/2 = 0$  and  $\Delta n^+ = 0$   
 $\implies a_4^{s,+} a_2^0 = 0$ ;

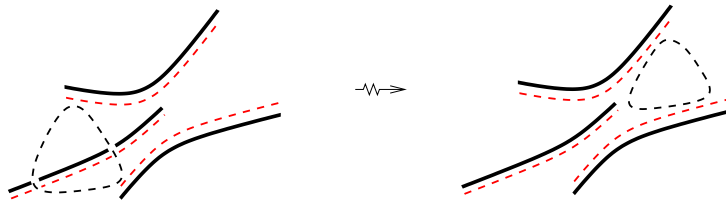


$A_4^{s,-} A_2^0$ :  $\Delta w^+ = -1$ ,  $\Delta t = 1$ . Hence,  $\Delta(w^+ + t)/2 = 0$  and  $\Delta n^+ = 0$   
 $\implies a_4^{s,-} a_2^0 = 0$ ;



- $D_4^- A_2$  (lines 1 and 2 of Figure 14):

$D_4^{-,+} A_2^\pm$ :  $\Delta w^+ / 2 = 0$ ,  $\Delta n^+ = 0 \implies d_4^{-,+} a_2^\pm = 0$ ;



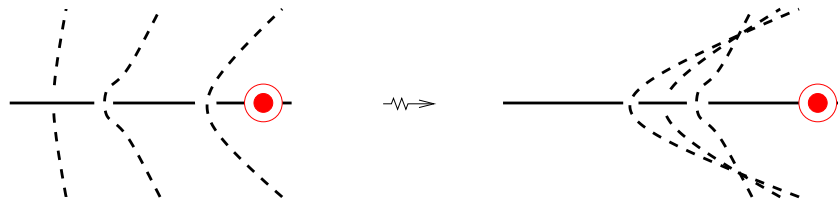
$D_4^{-,-} A_2^\pm$ : Its framed link contribution will be similar to  $L_+$  of  $D_4^{-,+} A_2^\pm$  but it will have the cuspidal edges removed. So we have  $\Delta w^+ / 2 = 0$  and  $\Delta n^+ = 0 \implies d_4^{-,-} a_2^\pm = 0$ ;

- $D_{4,2}^+ A_2$  (line 5 of Figure 14 and line 1 of Figure 15):

$D_{4,2}^{+,-} A_2^+, D_{4,2}^{+,-} A_2^-$ : Respectively, the transition of the fragments of the framed links are the same as  $TA_2^{3,0}$  and  $TA_2^{3,1}$  and so the increment of the invariant is the same. Hence,  $d_{4,2}^{+,-} a_2^+ = d_{4,2}^{+,-} a_2^- = 0$ ;

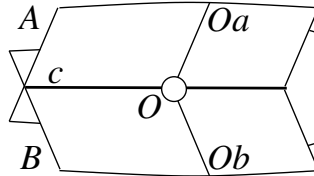


$D_{4,2}^{+,+} A_2^+, D_{4,2}^{+,+} A_2^-$ : We should notice that the transition differs from  $D_{4,2}^{+,-} A_2^+$  and  $D_{4,2}^{+,-} A_2^-$  by only the presence of the straight edge component which switches its crossings with two of the other local branches. Since each switch means changing the total writhe by  $\pm 2$ , the *mod 4* effect of the two switches is 0. Hence  $d_{4,2}^{+,+} a_2^+ = d_{4,2}^{+,+} a_2^- = 0$ ;



- $D_{4,1}^+ A_2$  (lines 2, 3, 4, and 5 of Figure 15):

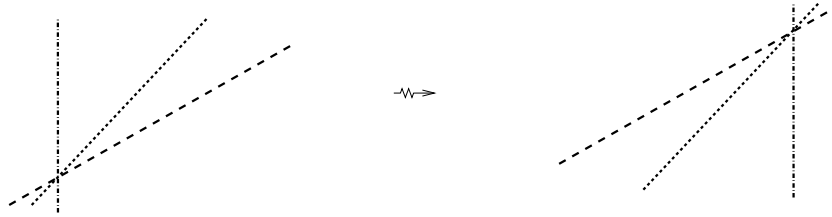
$D_{4,1}^{+,-} A_2$ : Recall we have  $D_{4,1}^{+,-} A_2 = D_{4,l}^{+,-} A_2 + D_{4,r}^{+,-} A_2$ . In all the  $D_4^+ A_2$ -left or -right cases, from the  $L_+$ -bifurcational point of view, the purse may be kind of opened up and replaced by a pair of planes  $A$  and  $B$  which are nearly horizontal but still meet transversally along a line which we shall call  $c$ . The planes are co-oriented upwards. The  $D_4^+$  point is then represented by some point  $O \in c$ . The cuspidal edge of the purse corresponds then to two rays emanating from  $O$  perpendicular to  $c$ : ray  $Oa$  in the upper half of plane  $A$ , and ray  $Ob$  in the upper half of plane  $B$ . This is illustrated below. The way we postulated the resolutions of  $L_+$  near  $D_4^+$  points corresponds to joining  $Oa$  and  $Ob$  in one smooth curve passing under  $c$ .



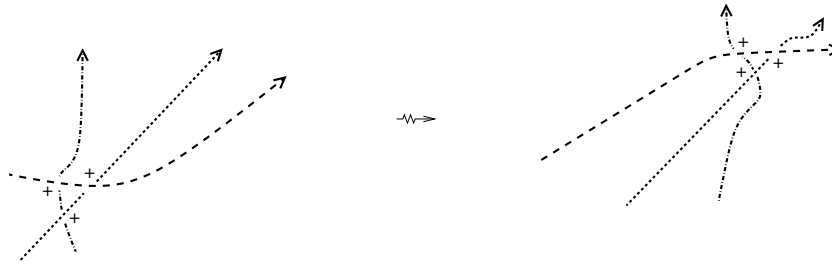
Now a smooth  $A_2$  sheet  $C$  moves into this configuration in a generic way, that is, transversally to  $c$ ,  $Oa$  and  $Ob$ . Then we see that the pre- and post-bifurcation resolutions of the triple points coincide. This yields the zero-jump conclusion in the cases not involving the cuspidal edge. If the edge participates in the link, then the additional argument similar to that used in the  $D_{4,2}^{+,+} A_2$  cases works to yield the same. As examples, we consider  $D_{4,l}^{+,-} A_2^+$  and  $D_{4,l}^{+,+} A_2^+$  in detail.



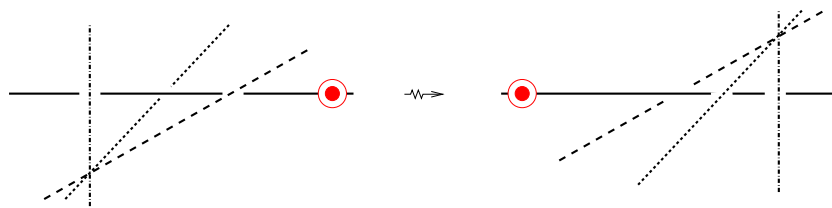
$D_{4,l}^{+,-} A_2^+$ :



We resolve the triple points to give the illustration below. We see the resolutions of the triple points coincide.  $\Delta w^+ = 0$ ,  $\Delta t = 0$ . So we have  $\Delta(w^+ + t)/2 = 0$  and  $\Delta n^+ = 0$ . Hence  $d_{4,1}^{+,-} a_2^+ = 0$ .



$D_{4,l}^{+,+} A_2^+$ :



The transition differs from  $D_{4,l}^{+,-} A_2^+$  by only the presence of the straight edge component which switches its crossings with two of the other local branches. Since each switch means changing the total writhe by  $\pm 2$ , the  $\text{mod} 4$  effect of the two switches is 0. Hence  $d_{4,l}^{+,+} a_2^+ = 0$ .

- $D_{4,0}^+ A_2$  (lines 3 and 4 of Figure 14):

$D_{4,0}^{+,+} A_2^\pm$ : Since we are not considering the  $s$ -decorations in the invariants, we can consider the  $D_{4,0}^{+,+} A_2^\pm$  transition to be the opposite to  $D_{4,2}^{+,+} A_2^\pm$ . Hence, since  $d_{4,2}^{+,+} a_2^\pm = 0$  we have  $d_{4,0}^{+,+} a_2^\pm = 0$ ;

$D_{4,0}^{+,-} A_2^\pm$ : Using the same logic as above, we can consider  $D_{4,0}^{+,-} A_2^\pm$  to be the opposite to  $D_{4,2}^{+,-} A_2^\pm$ . Hence, since  $d_{4,2}^{+,-} a_2^\pm = 0$  we have  $d_{4,0}^{+,-} a_2^\pm = 0$ .

□

### 7.3 Framing negative cuspidal edges and self-intersection lines ( $I_{dc^-}$ )

Following [1] we look at the framed link  $L_-$  formed by negative cuspidal edges ( $\sigma = -$ ) and self-intersection lines. Its construction details are as follows.

- Framing along edges  $A_3^{s,-}$  is shown in Figure 106.

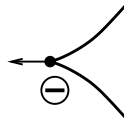


Figure 106: Framing along  $A_3^{s,-}$ .

- The framing of  $A_2^2$  segments is shown in Figure 107.

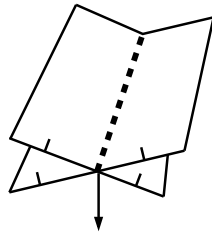


Figure 107: Framing of  $A_2^2$ .

We now postulate the behaviour of  $L_-$  near points of isolated singularity types.

- The link  $L_-$  at an  $A_3^{s,-}A_2$  junction is shown in Figure 108. At  $A_3^{s,+}A_2$ , the link will of course not include the edge component.

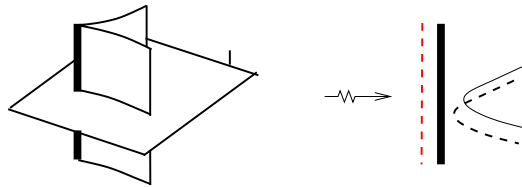


Figure 108:  $L_-$  at  $A_3^{s,-}A_2$  points.

- The link  $L_-$  at a  $\sigma = +$  swallowtail is shown in Figure 109. The local writhe of the framing here is  $-1/4$ . At a  $\sigma = -$  swallowtail we define the  $L_-$  via the reflection of Figure 109, that is, in this case the local writhe is  $+1/4$ .

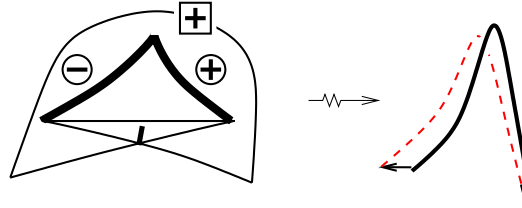


Figure 109:  $L_-$  at a swallowtail  $A_4^{s,+}$ .

- We resolve triple points the same way as this was done in  $L_+$  (Figure 102), with the only difference that the local framing is now opposite to the one we had that time. (In the cross-product interpretation of the deformations of the branches we are now still using the framing  $L_+$ ).
- We now look at the  $L_-$  near  $D_4^\pm$  points. We smooth out the  $D_4^-$  point as we did for the  $L_+$  case in Figure 103.  $L_-$  of  $D_4^{-,-}$  is similar to  $L_+$  of  $D_4^{-,+}$ , shown in Figure 104, with the only difference being that the framing is outside the pyramid. Of course, the contribution of  $D_4^{-,+}$  to our framed link is empty.
- $L_-$  of  $D_4^{+,-}$  is similar to  $L_+$  of  $D_4^{+,+}$ , shown in Figure 105, with the only difference being that the framing will now face away from the reader. The  $L_-$  framing for  $D_4^{+,+}$  is similar to  $D_4^{+,-}$  but with the cuspidal edge component removed.

We introduce the invariant,

$$I_{dc^-} = n^- + \frac{(w^- + t)}{2}$$

where  $n^-$  is the number of components of the link  $L_-$ ,  $w^-$  is the writhe of  $L_-$  and  $t$  is the number of triple points of the caustic.

**Theorem 7.3.1.** *The mod2 invariant  $I_{dc^-}$  is dual to the cycle*

$$\begin{aligned} &A_2^4 + TA_2^2 + A_3^{\pm,-}A_2^2 + TA_3A_2 + A_3^{2,e/h;\pm,+;\pm,+} + A_3^{2,e/h;\pm,+;\pm,-} + A_4^{\pm,e/h} \\ &+ A_5^{\pm,+;\pm} + A_3^{\pm,-,q} + D_{4,a/c}^{+,\pm,\pm}. \end{aligned}$$

Recalling the expressions for our 20 basic discriminantal cycles from Table 4, we have

$$\begin{aligned} I'_{dc^-} = &I'_{16} + I'_{18} + I'_{19} + I'_{\chi} + I'_{sw_{++}} + I'_{(sw_{+-}+sw_{-+})/2} + I'_{(t+c_{++}+c_{-+})/2} \\ &+ I'_{(t+c_{+-}+c_{--})/2} + I'_{(((d_+^++d_-^+)/2)+((d_+^++d_-^+)/2)+\chi+15)/2}. \end{aligned}$$

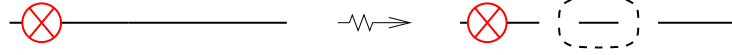
**Proof of Theorem 7.3.1.**

Again, we first consider bifurcations where contributions of triple points are zero.

- $D_{4,a}^+$  (line 2 of Figure 13):

$$D_{4,a}^{+,s,+}: \text{ Its } L_- \text{ is the same as } L_+ \text{ of } D_{4,a}^{+,s,-} \implies d_{4,a}^{+,s,+} = 1;$$

$$D_{4,a}^{+,s,-}: \Delta w^-/2 = 0, \Delta n^- = 1 \implies d_{4,a}^{+,s,-} = 1;$$



- $D_{4,b}^+$  (line 3 of Figure 13):

$$D_{4,b}^{+,s,+}: \text{Same as } L_+ \text{ of } D_{4,b}^{+,s,-} \implies d_{4,b}^{+,s,+} = 0;$$

$D_{4,b}^{+,s,-}$ : Its contribution to  $L_-$  is the same as the contribution of  $D_{4,b}^{+,s,+}$  to  $L_+$  with the only difference being that the framing of the cuspidal edge will be in the direction away from the reader. Hence,  $d_{4,b}^{+,s,-} = 0$ ;

- $D_{4,c}^+$  (line 4 of Figure 13):

$$D_{4,c}^{+,s,+}: \text{Its contribution to } L_- \text{ is the same as that of } D_{4,c}^{+,s,-} \text{ to } L_+ \implies d_{4,c}^{+,s,+} = 1;$$

$D_{4,c}^{+,s,-}$ : Similar to  $L_+$  of  $D_{4,c}^{+,s,+}$  with the framing of the cuspidal edge directed away from the reader. Hence,  $d_{4,c}^{+,s,-} = 1$ ;

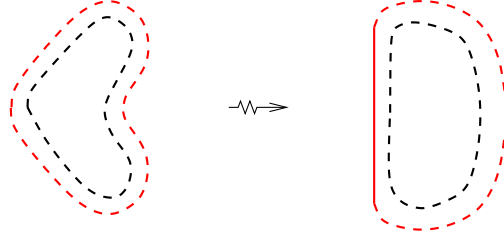
- $D_{4,q}^-$  (line 1 of Figure 13):

$$D_{4,q}^{-,s,+}: \text{Its link contribution is empty} \implies d_{4,q}^{-,s,+} = 0;$$

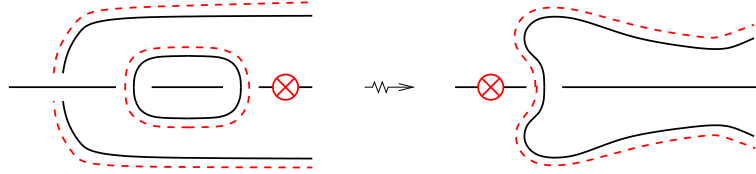
$D_{4,q}^{-,s,-}$ : Its framed link is the same as its contribution to  $I_{fe}$ . Hence,  $d_{4,q}^{-,s,-} = 0$ ;

- $D_5$  (line 5 of Figure 13):

$$D_5^{s,+}: \Delta w^-/2 = 0, \Delta n^- = 0 \implies d_5^{s,+} = 0;$$



$$D_5^{s,-}: \Delta w^-/2 = 1 \pmod{2}, \Delta n^- = 1 \implies d_5^{s,-} = 0;$$



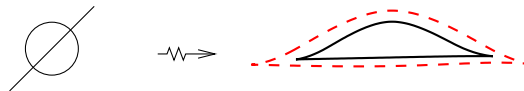
- $A_3^q$  (lines 1, 2 and 3 of Figure 11):

$A_3^{s,+,+,+}$ ,  $A_3^{s,+,+,-}$  and  $A_3^{s,+,-,-}$ : It is obvious that  $L_-$  does not have local components at the corresponding bifurcations. Therefore,

$$a_3^{s,+,+,+} = a_3^{s,+,+,-} = a_3^{s,+,-,-} = 0;$$

$A_3^{s,-,+,+}$ ,  $A_3^{s,-,+,-}$  and  $A_3^{s,-,-,-}$ : Respectively, their contributions to  $L_-$  are similar to the contributions of  $A_3^{s,+,+,+}$ ,  $A_3^{s,+,+,-}$  and  $A_3^{s,+,-,-}$  to  $L_+$ , with the only difference being that the framing is now in the opposite direction. Hence,  $a_3^{s,-,+,+} = a_3^{s,-,+,-} = a_3^{s,-,-,-} = 1$ ;

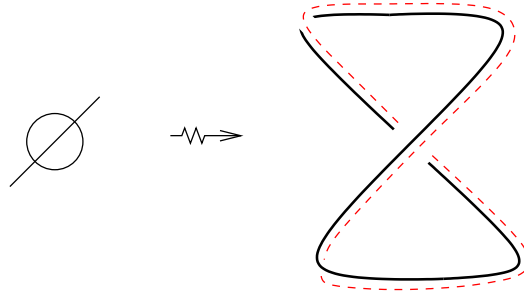
- $A_4^{\varepsilon,e}$  (line 4 of Figure 11):  $\Delta w^-/2 = 0, \Delta n^- = 1 \implies a_4^{\varepsilon,e} = 1$ ;



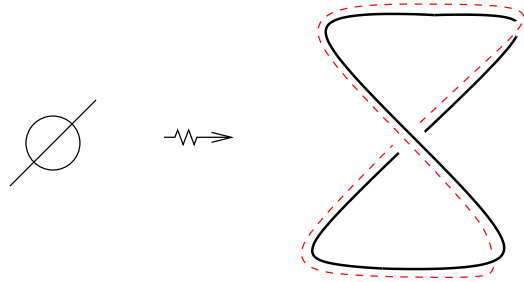
- $A_4^{\varepsilon, h}$  (line 5 of Figure 11): Similar to  $L_+$  of  $A_3^{s, +, +, -}$ . Hence, the C Lemma implies  $a_4^{\varepsilon, h} = 1$ ;

- $A_5$  (line 6 of Figure 11):

$$A_5^{s, +, +}: \Delta w^- / 2 = 0, \Delta n^- = 1 \implies a_5^{s, +, +} = 1.$$

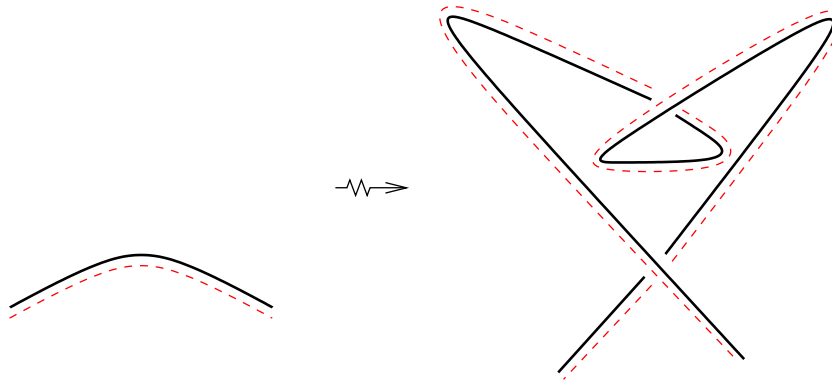


$$A_5^{s, +, -}: \Delta w^- / 2 = 0 \text{ and } \Delta n^- = 1 \implies a_5^{s, +, -} = 1.$$

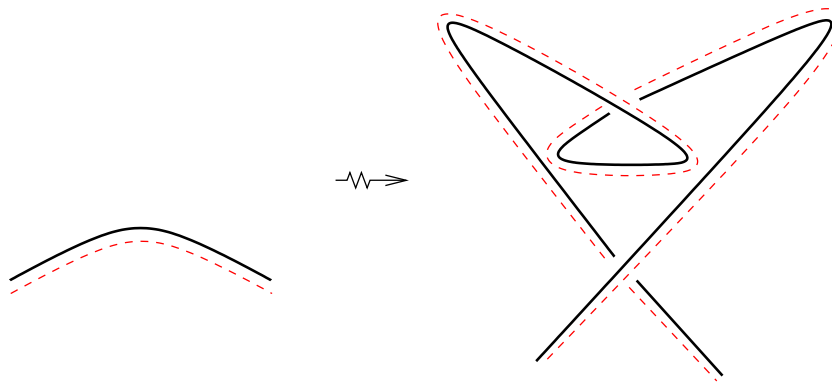


$$A_5^{s, -, +}: \Delta w^- / 2 = 0, \Delta n^- = 0 \implies a_5^{s, -, +} = 0.$$





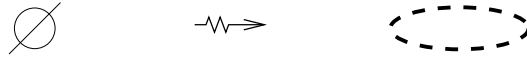
$$A_5^{s,-,-}: \Delta w^-/2 = 0, \Delta n^- = 0 \implies a_5^{s,-,-} = 0.$$



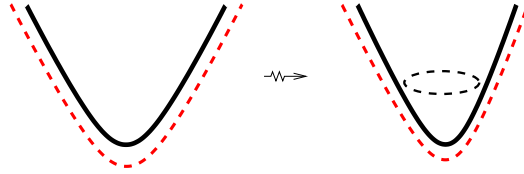
- $A_2^4$  (line 1 of Figure 12): Its contribution to  $L_-$  is exactly the same as its contribution to  $L_+$ . Therefore  $a_2^4 = 1$ ;
- $TA_2^{2,e}$  (line 3, left of Figure 12): Its contribution to  $L_-$  is similar to  $L_+$  with the only difference being the framing looking in the opposite direction. Hence,  $\Delta w^-/2 = 0, \Delta n^- = 1 \implies ta_2^{2,e} = 1$ ;
- $TA_2^{2,h}$  (line 3, right of Figure 12): Its link contribution is similar to  $L_+$  of  $D_{4,c}^{+,s,-}$ . Applying the C Lemma we have  $ta_2^{2,h} = 1$ ;

- $A_3^{2,e;s,\sigma;s',\sigma'}$  and  $A_3^{2,h;s,\sigma;s',\sigma'}$  (lines 5 and 6 of Figure 12): The contributions of  $A_3^{2,e;s,\sigma;s',\sigma'}$  to  $I_{dc^-}$  and of  $A_3^{2,e;s,-\sigma;s',-\sigma'}$  to  $I_{dc^+}$  coincide. The same holds for the hyperbolic case;
- $TA_3A_2^e$  (line 7, left of Figure 12):

$$TA_3^{s,+}A_2^e: \Delta w^-/2 = 0, \Delta n^- = 1 \implies ta_3^{s,+}a_2^e = 1;$$



$$TA_3^{s,-}A_2^e: \Delta w^-/2 = 0, \Delta n^- = 1 \implies ta_3^{s,-}a_2^e = 1;$$



- $TA_3A_2^h$  (line 7, right of Figure 12):

$$TA_3^{s,+}A_2^h: \text{Similar to } L_+ \text{ of } TA_3^{s,-}A_2^h. \text{ Hence } ta_3^{s,+}a_2^h = 1;$$

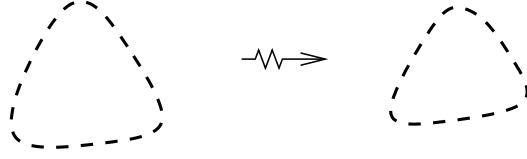
$$TA_3^{s,-}A_2^h: \text{Similar to } L_+ \text{ of } TA_3^{s,+}A_2^h. \text{ Hence } ta_3^{s,-}a_2^h = 1;$$

We now consider bifurcations with contributions from triple points.

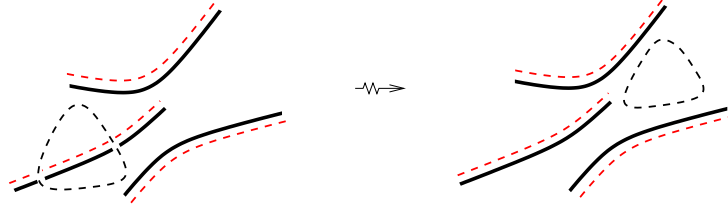
- $TA_2^3$  (line 2 of Figure 12): Its contribution to  $L_-$  will be the same as its contribution to  $L_+$ , provided we co-orient the three  $A_2$  sheets in the opposite direction to what was done for the  $L_+$  case. Hence  $ta_2^3 = 0$ ;
- $A_3^{s,\sigma}A_2^2$  (line 4 of Figure 12): The contributions of  $A_3^{s,\sigma}A_2^2$  to  $L_-$  coincide with those of  $A_3^{s,-\sigma}A_2^2$  to  $L_+$ . Hence,  $a_3^{s,+}a_2^2 = 0$  and  $a_3^{s,-}a_2^2 = 1$ ;

- $A_4^{s,\sigma} A_2$  (line 6, right of Figure 12): Contributions of  $A_4^{s,\sigma} A_2$  to  $L_-$  are the same as those of  $A_4^{s,-\sigma} A_2$  to  $L_+$ . Hence,  $a_4^{s,\sigma} a_2 = 0$ ;
- $D_4^- A_2$  (lines 1 and 2 of Figure 14):

$$D_4^{-,+} A_2^\pm: \Delta w^- / 2 = 0, \Delta n^- = 0 \implies d_4^{-,+} a_2^\pm = 0;$$



$$D_4^{-,-} A_2^\pm: \Delta w^- / 2 = 0, \Delta n^- = 0 \implies d_4^{-,-} a_2^\pm = 0;$$



- $D_{4,2/1/0}^{+,\sigma} A_2^\pm$  (lines 3 – 5 of Figure 14 and 1 – 5 of Figure 15): The contributions of  $D_{4,2/1/0}^{+,\sigma} A_2^\pm$  to  $L_-$  are the same as that of  $D_{4,2/1/0}^{+,-\sigma} A_2^\pm$  to  $L_+$ . Hence,  $d_{4,2/1/0}^{+,\sigma} a_2^\pm = 0$ .

□

## 7.4 Linking invariant ( $I_\lambda$ )

The linking number of two oriented links  $A$  and  $B$  in  $\mathbb{R}^3$  is the sum of the crossing numbers in their link diagram over all crossings where  $A$  passes over  $B$ . The roles of  $A$  and  $B$  may be swapped here to get the same result.

If links  $A$  and  $B$  are not oriented then the crossings lose their signs, and we are left with the *mod2 linking number* which is equal to the parity of the number of crossings in the link diagram at which  $A$  passes over  $B$  (equivalently,  $B$  over  $A$ ). We are now going to study this number for the links related to the links  $L_+$  and  $L_-$  considered each on its own in the two previous sections.

Namely, we denote  $L_{+,\varepsilon}$  the link obtained from  $L_+$  by displacing each point a small positive distance  $\varepsilon$  in the direction of the framing of  $L_+$  at that point, and similarly  $L_{-,\varepsilon}$  the link obtained from  $L_-$  by displacing each point  $\varepsilon$  in the direction of the framing of  $L_-$  at that point. Denote by  $\lambda$  the *mod2* linking number  $\langle L_{+,\varepsilon}, L_{-,\varepsilon} \rangle$  and for consistency with previous notation we call the new invariant  $I_\lambda$ . We will depict  $L_{+,\varepsilon}$  by a solid black line and  $L_{-,\varepsilon}$  by a solid red line.

**Theorem 7.4.1.** *The mod2 invariant  $I_\lambda$  is dual to the cycle*

$$A_3^{\pm,\pm} A_2^2 + A_4^{\pm,\pm} A_2 + A_3^{2,\varepsilon/h;\pm,+\pm,-} + A_5^{\pm,+\pm}.$$

Recalling the expressions for our 20 basic discriminantal cycles from Table 4, we have

$$\begin{aligned} I'_\lambda = & I'_{17} + I'_{d_-^+} + I'_{c_{++}} + I'_{c_{+-}} + I'_{(t+c_{+-}+c_{--})/2} + I'_t + I'_{sw_{++}} + I'_{sw_{+-}} \\ & + I'_{(sw_{++}+sw_{--})/2} + I'_{(sw_{+-}+sw_{-+})/2}. \end{aligned}$$

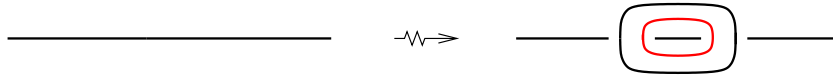
**Proof of Theorem 7.4.1.**

To understand the contributions of various strata to the invariant  $I_\lambda$ , we now check how the parity of numbers of crossings of one of the links over the other changes under the bifurcations. For each stratum  $X_i$  below, the corresponding increment  $x_i$  is  $\Delta\lambda$ .

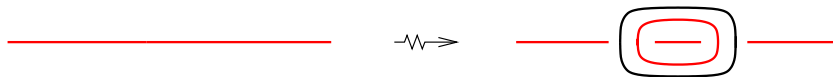
We use the symbol  $\otimes$  in the illustrations of this proof to indicate the direction of the shift of the link component, unlike earlier where it denoted the direction of the framing.

- $D_{4,a}^+$  (line 2 of Figure 13):

$$D_{4,a}^{+,s,+}: \Delta\lambda = 0;$$

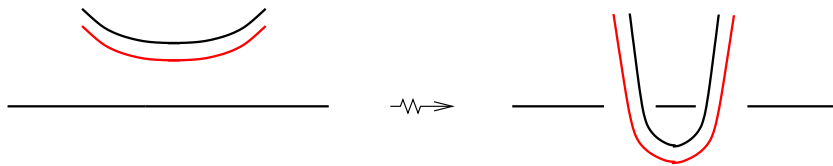


$$D_{4,a}^{+,s,-}: \Delta\lambda = 0;$$

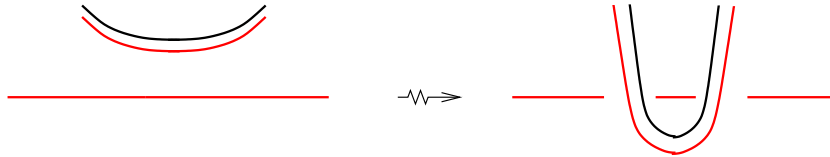


- $D_{4,b}^+$  (line 3 of Figure 13):

$$D_{4,b}^{+,s,+}: \Delta\lambda = 0;$$

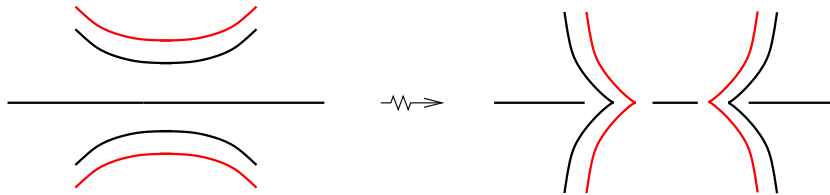


$D_{4,b}^{+,s,-}$ :  $\Delta\lambda = 0$ ;

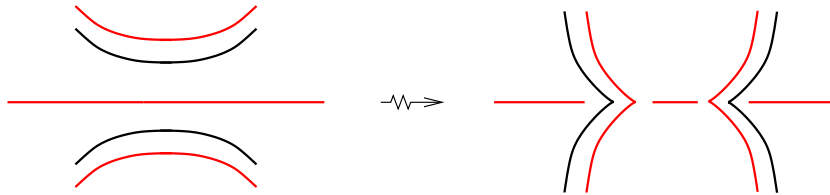


- $D_{4,c}^+$  (line 4 of Figure 13):

$D_{4,c}^{+,s,+}$ :  $\Delta\lambda = 0$ ;



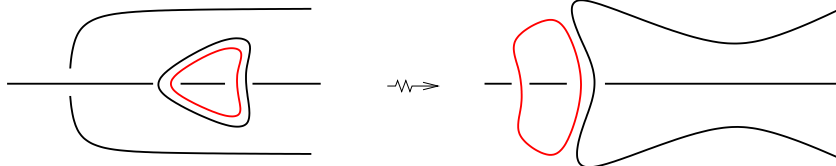
$D_{4,c}^{+,s,-}$ :  $\Delta\lambda = 0$ ;



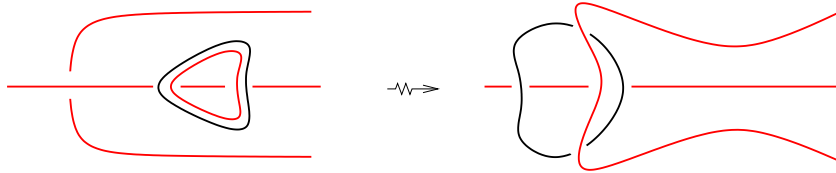
- $D_{4,q}^{-,s,\sigma}$  (line 1 of Figure 13): Only one of the two links, namely  $L_{\sigma,\varepsilon}$  shows up locally. Hence,  $d_{4,q}^{-,s,\sigma} = 0$ ;

- $D_5$  (line 5 of Figure 13):

$$D_5^{s,+}: \Delta\lambda = 0;$$

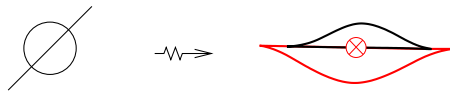


$$D_5^{s,-}: \Delta\lambda = 0;$$

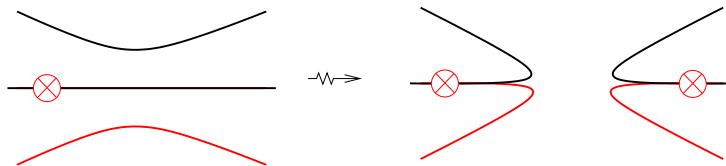


- $A_3^{s,\sigma,q}$  (lines 1, 2 and 3 of Figure 11): In all the  $A_3^{s,\sigma,q}$  bifurcations, only the  $L_{\sigma,\varepsilon}$  link shows up locally. Hence,  $a_3^{s,\sigma,q} = 0$ ;

- $A_4^{\varepsilon,e}$  (line 4 of Figure 11):  $\Delta\lambda = 0$ ;

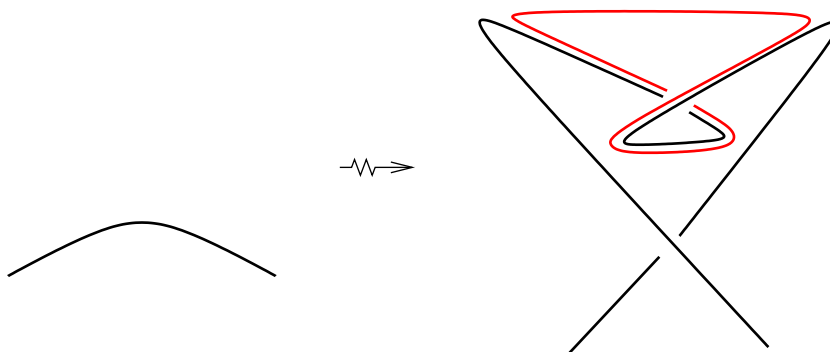


- $A_4^{\varepsilon,h}$  (line 5 of Figure 11):  $\Delta\lambda = 0$ ;

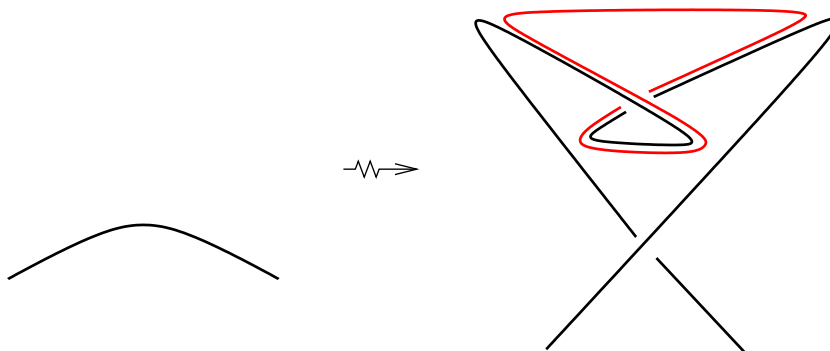


- $A_5$  (line 6 of Figure 11):

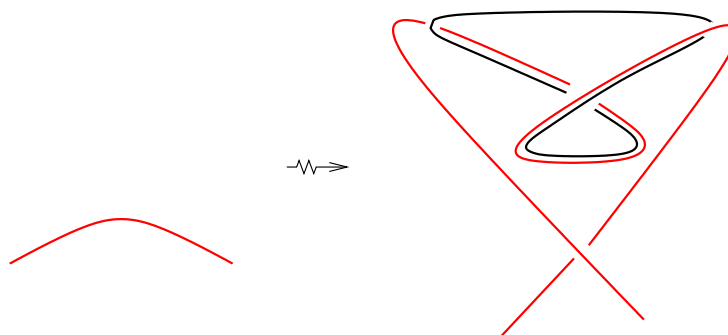
$$A_5^{s,+,+}: \Delta\lambda = 1;$$



$$A_5^{s,+,-}: \Delta\lambda = 1;$$

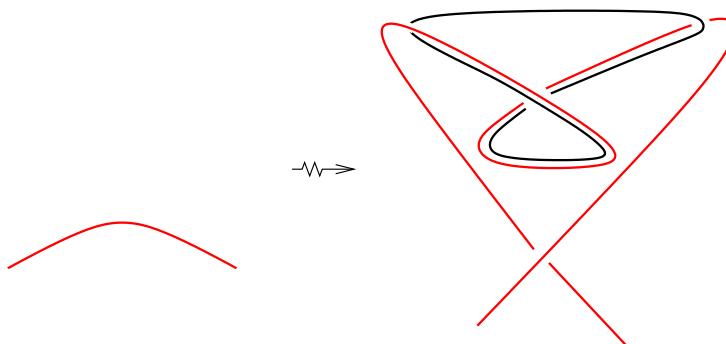


$$A_5^{s,-,+}: \Delta\lambda = 0;$$

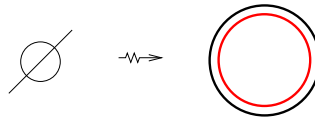




$$A_5^{s,-,-}: \Delta\lambda = 0;$$

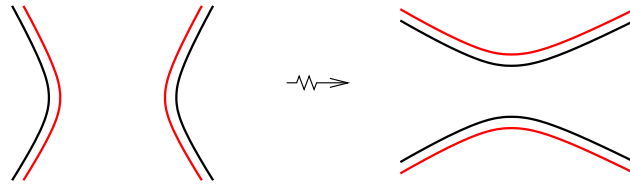


- $A_2^4$  (line 1 of Figure 12): As was explained in the  $A_2^4$  item from Section 7.2 we know the resolution of each triple point stays the same, since any triplet of sheets meet after the bifurcation the same way as before. Hence, there will be no contribution to the change in the linking number from the triple points. In addition, we have three double crossings (points a, b and c). Here each double crossing provides exactly one occasion of, say, the red going over the black. So, since we have three occasions of that before the bifurcation and still three after, there is no parity change in the linking number which implies  $a_2^4 = 0$ ;
- $TA_2^{2,e}$  (line 3, left of Figure 12):  $\Delta\lambda = 0$ . Below we illustrate the case of  $TA_2^{2,e,2}$  or  $TA_2^{2,e,1}$  with the parabolic  $A_2$  sheet co-oriented outwards. If  $TA_2^{2,e,0}$  or  $TA_2^{2,e,1}$  with the parabolic  $A_2$  sheet co-oriented inwards was considered, the colours would swap in the figure but our conclusion would yield the same result.



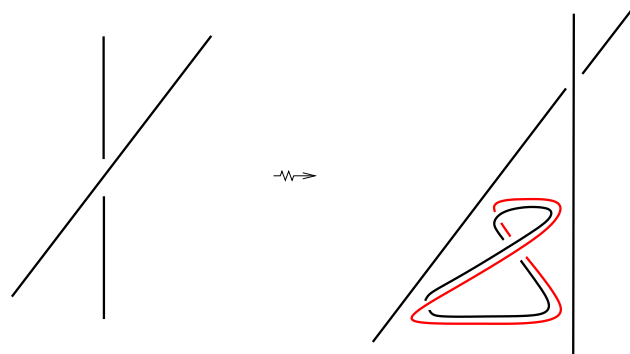
- $TA_2^{2,h}$  (line 3, right of Figure 12): Consider  $TA_2^{2,h,0}$ . Here,  $\Delta\lambda = 0$ .

Similarly,  $ta_2^{2,h,1} = 0$ ;

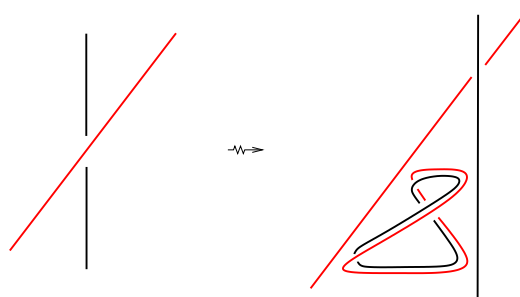


- $A_3^{2,e}$  (line 5 of Figure 12):

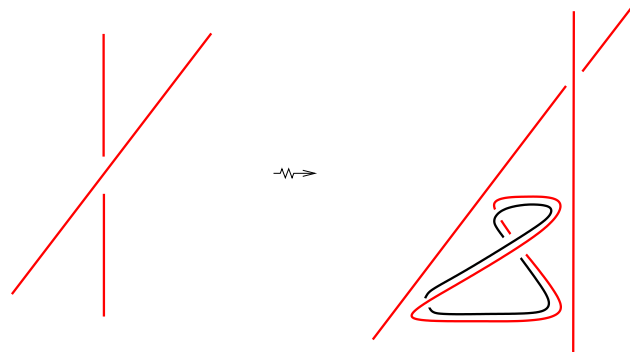
$A_3^{2,e;s,+,s',+}$ :  $\Delta\lambda = 0$ ;



$A_3^{2,e;s,+,s',-}$ :  $\Delta\lambda = 1$ ;

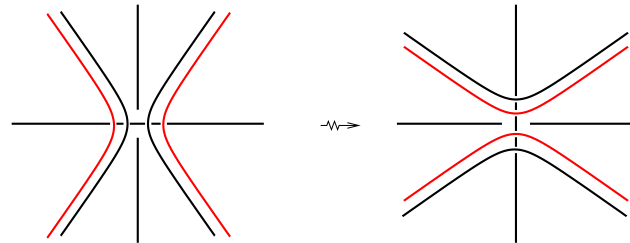


$$A_3^{2,e;s,-;s',-}: \Delta\lambda = 0;$$

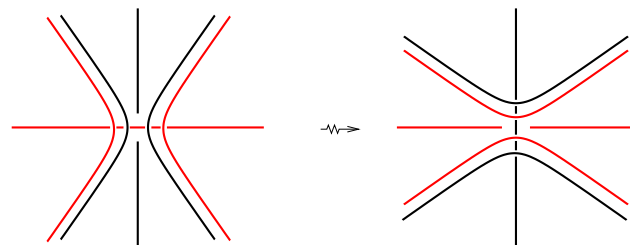


- $A_3^{2,h}$  (line 6, left of Figure 12): Here we are looking at the bifurcation from inside the edge surfaces.

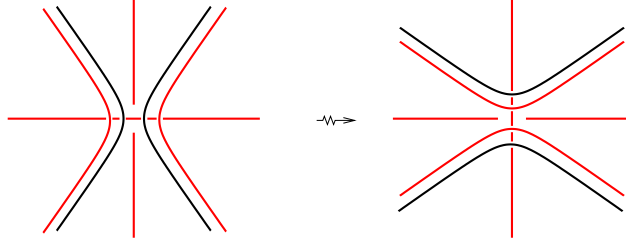
$$A_3^{2,h;s,+,s',+}: \Delta\lambda = 0;$$



$$A_3^{2,h;s,+,s',-}: \Delta\lambda = 1;$$

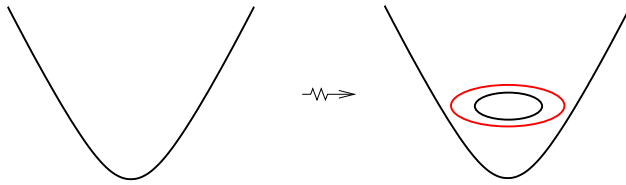


$$A_3^{2,h;s,-;s',-}: \Delta\lambda = 0;$$



- $TA_3A_2^e$  (line 7, left of Figure 12):

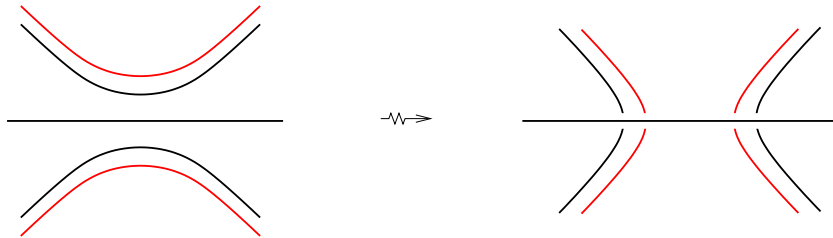
$$TA_3^{s,+}A_2^e: \Delta\lambda = 0;$$



$TA_3^{s,-}A_2^e$ : Its links are similar to the links of  $TA_3^{s,+}A_2^e$  with the only difference being the cuspidal edge is red. Hence,  $ta_3^{s,-}a_2^e = 0$ ;

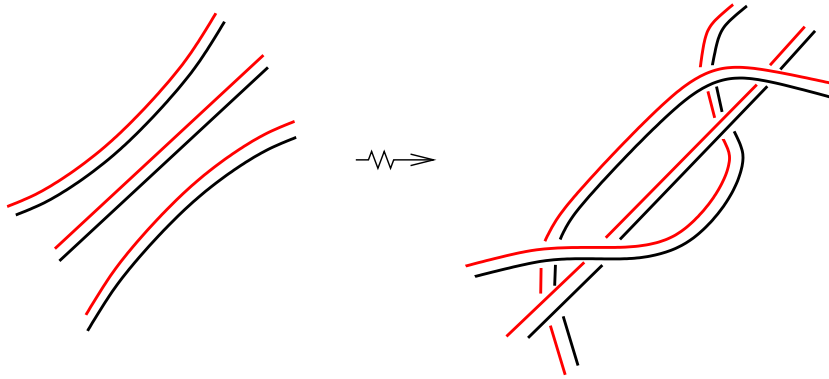
- $TA_3A_2^h$  (line 7, right of Figure 12):

$$TA_3^{s,+}A_2^h: \Delta\lambda = 0;$$



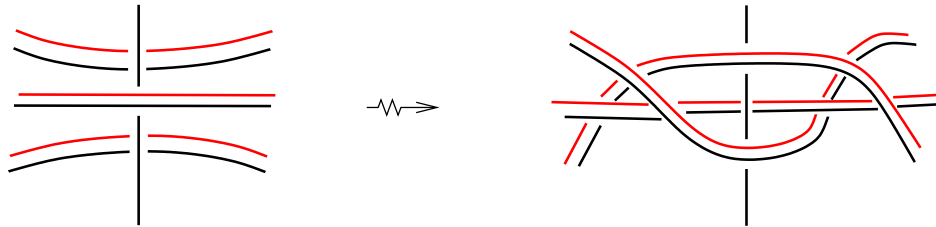
$TA_3^{s,-}A_2^h$ : Its links are similar to the links of  $TA_3^{s,+}A_2^h$  but the horizontal cuspidal edge is red. Hence,  $ta_3^{s,-}a_2^h = 0$ ;

- $TA_2^3$  (line 2 of Figure 12): Before the bifurcation we have no triple points on the self-intersection locus, and afterwards we have two. Resolving the two triple points, we obtain six double crossings of the  $L_{\pm,\varepsilon}$ , and at each of these six we have  $L_{+,\varepsilon}$  crossing over  $L_{-,\varepsilon}$  exactly once. Hence,  $\Delta\lambda = 0$ . As an example, we show the links of  $TA_2^{3,0}$  below;



- $A_3A_2^2$  (line 4 of Figure 12):

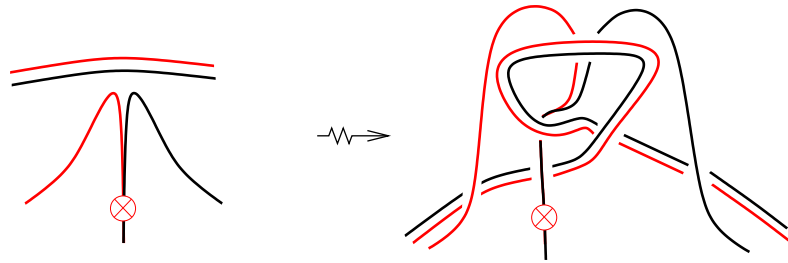
$A_3^{s,+}A_2^2$ : We should notice that the transition  $A_3^{s,+}A_2^2$  differs from  $TA_2^3$  by only the presence of a straight edge component which switches its crossings with all of the other local branches. We know  $TA_2^3$  does not change the linking number but switching three crossings changes the linking number by  $1 \pmod{2}$ . Therefore,  $\Delta\lambda = 1$ . For example,  $A_3^{s,+}A_2^{2,0}$  is shown below;



$A_3^{s,-} A_2^2$ : The links are similar to  $A_3^{s,+} A_2^2$  with the colour of the vertical cuspidal edge swapped from black to red. Hence,  $a_3^{s,-} a_2^2 = 1$ ;

- $A_4 A_2$  (line 6, right of Figure 12):

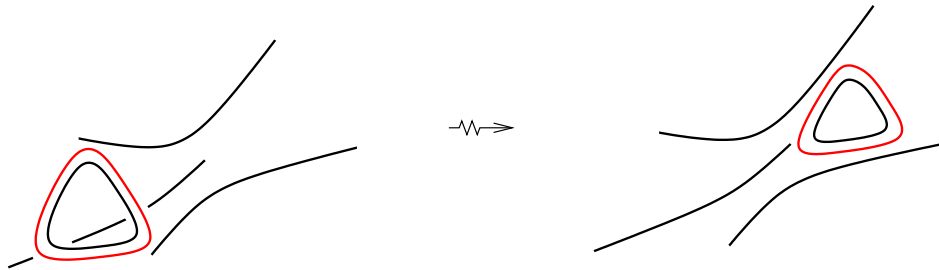
$A_4^{s,+} A_2$ : For example, consider  $A_4^{s,+} A_2^1$ . Here, like for the  $A_4^{s,+} A_2^0$  case, we have four double crossings and two single crossings of alternate colours. Therefore,  $\Delta\lambda = 1$ ;



$A_4^{s,-} A_2$ : Again, we have four double crossings and two single crossings of alternate colours. Therefore,  $a_4^{s,-} a_2 = 1$ ;

- $D_4^- A_2$  (lines 1 and 2 of Figure 14):

$D_4^{-,+} A_2^\pm$ :  $\Delta\lambda = 0$ ;

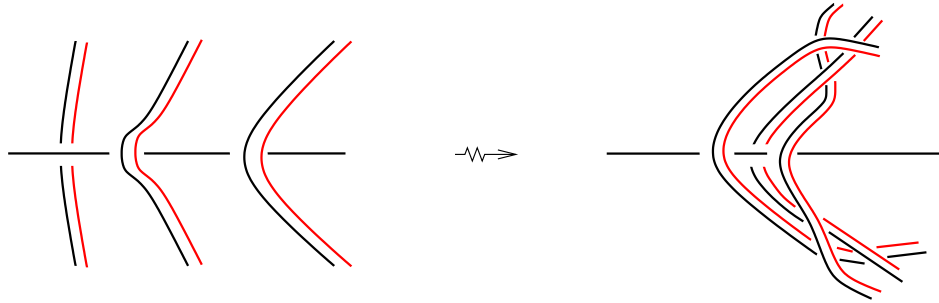


$D_4^{-,-}A_2^\pm$ : Similar to  $D_4^{-,+}A_2^\pm$  but with all the cuspidal edges now red.

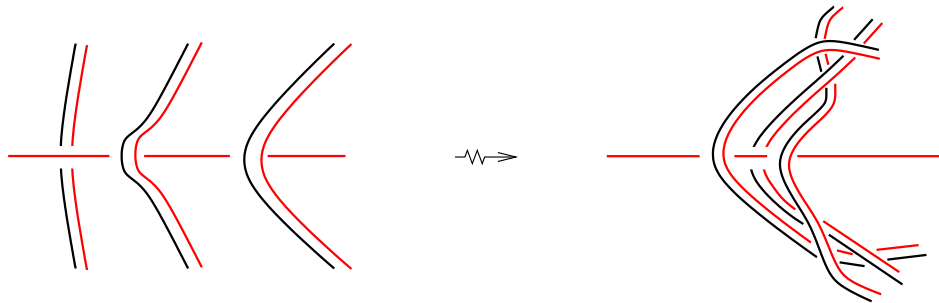
Therefore,  $d_4^{-,-}a_2^\pm = 0$ ;

- $D_{4,2}^+A_2$  (line 5 of Figure 14 and line 1 of Figure 15):

$D_{4,2}^{+,+}A_2$ : Similar to the transition  $A_3^{s,+}A_2^2$  where a straight edge component switches its crossings with two of the other local branches. Hence,  $d_{4,2}^{+,+}a_2 = 0$ . For example, the  $D_{4,2}^{+,+}A_2^+$  transition is shown below;

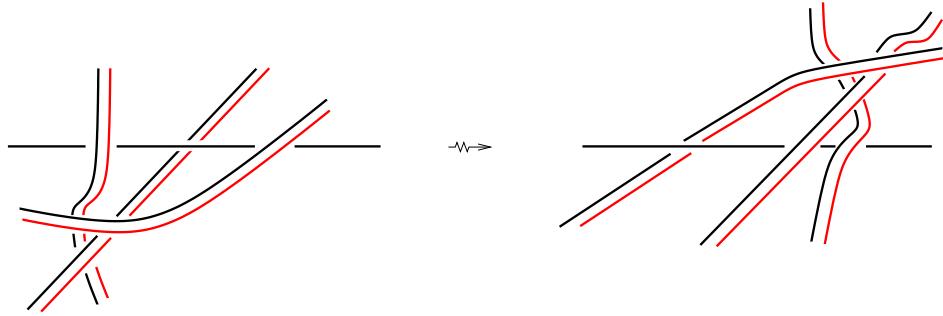


$D_{4,2}^{+,-}A_2$ : The links are similar to the  $D_{4,2}^{+,+}A_2$  cases, except the change of colour of the horizontal branch. Hence,  $d_{4,2}^{+,-}a_2 = 0$ . The  $D_{4,2}^{+,-}A_2^+$  transition is shown as an example below;



- $D_{4,1}^+ A_2$  (lines 2, 3, 4, and 5 of Figure 15):

$D_{4,1}^{+,+} A_2^\pm$ : As was explained in Section 7.2 we know that the pre- and post-bifurcation resolutions of the triple points coincide for  $D_{4,1}^{+,+} A_2$ . In addition, two of the three crossings of the edge with the local branches of  $L_{-, \varepsilon}$  change during the bifurcation. Therefore,  $d_{4,1}^{+,+} a_2^\pm = 0$ . For example, the  $D_{4,l}^{+,+} A_2^+$  transition is shown below;



$D_{4,1}^{+,-} A_2^\pm$ : Similar to the  $D_{4,1}^{+,+} A_2^\pm$  case, except the change of colour of the horizontal branch. Hence  $d_{4,1}^{+,-} a_2^\pm = 0$ ;

- $D_{4,0}^+ A_2$  (lines 3 and 4 of Figure 14):

$D_{4,0}^{+,+} A_2^\pm$ : Since we are not considering the  $s$ -decorations in the invariants, we can consider this move to be the opposite of the move  $D_{4,2}^{+,+} A_2^\pm$ . Therefore, since  $d_{4,2}^{+,+} a_2^\pm = 0$  this implies  $d_{4,0}^{+,+} a_2^\pm = 0$ ;

$D_{4,0}^{+,-} A_2^\pm$ : Using the same logic as above, we consider  $D_{4,0}^{+,-} A_2^\pm$  to be opposite to  $D_{4,2}^{+,-} A_2^\pm$ . Hence,  $d_{4,0}^{+,-} a_2^\pm = 0$ .

□



## 7.5 *mod2* degrees of generic singularities in $\mathbb{R}^3$

Our final geometric interpretation of a *mod2* discriminantal cycle is based on the *mod2* degrees of generic singularities in  $\mathbb{R}^3$ .

We define the *mod2* degree of a non-caustical point in  $\mathbb{R}^3$  as the *mod2* degree of the radial projection map of the caustic onto a sphere centred at that point. This depends only on the connected component of the complement to the caustic.

We introduce *mod2* degrees of  $A_3A_2$ ,  $A_4$ ,  $D_4$ , and triple points, and check if any summation of these is a local invariant. We let  $P$  be a point of a generic singularity and  $P'$  be the perturbation of  $P$ . Then we set  $deg_2(P) := deg_2(P')$ .

- $A_3^{s,\sigma}A_2$ , Figure 110: The point  $P'$  is inside the cuspidal edge, and on the side of the  $A_2$  sheet that is consistent with its co-orientation.

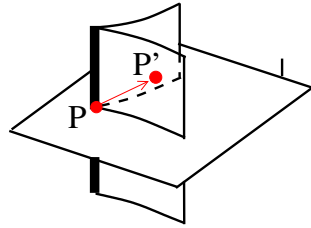


Figure 110: The *mod2* degree of an  $A_3A_2$  point.

- $A_4^{s,\sigma}$ , Figure 111: The point  $P'$  is contained inside the pyramid.

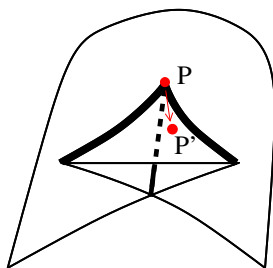


Figure 111: The *mod2* degree of a swallowtail point.

- $D_4^{+,\sigma}$ , Figure 112: The point  $P'$  is inside the purse.

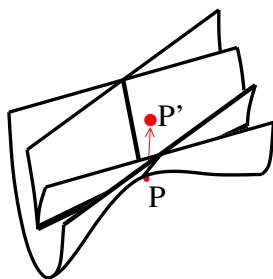


Figure 112: The *mod2* degree of a  $D_4^{+,\sigma}$  point.

- $D_4^{-,\sigma}$ , Figure 113: The point  $P'$  is outside the pyramid.

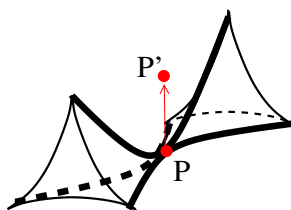


Figure 113: The *mod2* degree of a  $D_4^{-,\sigma}$  point.

- Triple points, Figure 114: The point  $P'$  is inside the octant into which all three  $A_2$  sheets are co-oriented.

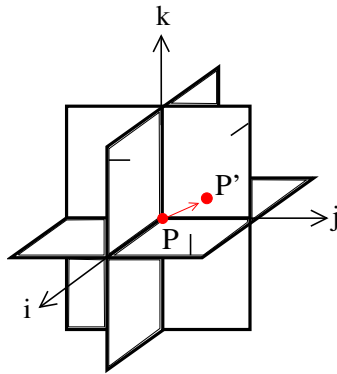


Figure 114: The  $\text{mod}2$  degree of a triple point.

We would like to understand which linear combinations of sums of the degrees of all points of particular types may be local invariants. For this, we will now check how these particular sums change during all our elementary 1-parameter bifurcations. Our method will be as follows. Consider the complement to the caustic. We assign the  $\text{mod}2$  degree  $d$  to one of its connected components, denoted by  $U$ , which survives (at least partially) during the transition. The degree of any component  $U'$  differs from  $d$  by the parity of the number of times a generic path from  $U$  to  $U'$  meets the caustic. Say for example we know a swallowtail point has degree  $d$  before passing through a smooth  $A_2$  sheet, then we know afterwards the same point will have degree  $d + 1$ . Hence, it is possible to give all our components degrees, before and after the bifurcation. From this we calculate the change in parity of the sums of the degrees.

Table 5 shows the change in the sums of the degrees of all generic isolated singular points in our bifurcations obtained by direct inspection of Figures 11,

12, 13, 14 and 15. We do not provide all the details of the calculation. Table 5 allows us to detect one local invariant which is not a linear combination of invariants for which we already know their geometric sense. For this invariant we will give all the details of the *mod*2 degree calculations.

Table 5	$A_3^{+,+}$	$A_3^{+,-}$	$A_3^{-,+}$	$A_3^{-,-}$	$A_2^2$	$A_4^{+,+}$	$A_4^{+,-}$	$A_4^{-,+}$	$A_4^{-,-}$	$D_4^{+,+}$	$D_4^{+,-}$	$D_4^{-,+}$	$D_4^{-,-}$	$A_3^{+,+}A_2$	$A_3^{+,-}A_2$	$A_3^{-,+}A_2$	$A_3^{-,-}A_2$	$t$
$A_2^4$	.	.	.	.	.	.	.	.	.	.	.	.	.	.	.	.	.	.
$TA_2^2$	.	.	.	.	.	.	.	.	.	.	.	.	.	.	.	.	.	.
$TA_2^3$	.	.	.	.	1	.	.	.	.	.	.	.	.	.	.	.	.	.
$A_3^{\pm,+}A_2^2$	.	.	.	.	1	.	.	.	.	.	.	.	.	.	.	.	.	.
$A_3^{\pm,-}A_2^2$	.	.	.	.	1	.	.	.	.	.	.	.	.	.	.	.	.	.
$A_3^{2,e/h;+,+,+,+}$	.	.	.	.	.	.	.	.	.	.	.	.	.	.	.	.	.	.
$A_3^{2,e/h;+,+,+,-}$	1	1	.	.	.	.	.	.	.	.	.	.	.	.	.	.	.	.
$A_3^{2,e/h;+,+,-,+}$	1	.	1	.	.	.	.	.	.	.	.	.	.	.	.	.	.	.
$A_3^{2,e/h;+,+,-,-}$	1	.	.	1	.	.	.	.	.	.	.	.	.	.	.	.	.	.
$A_3^{2,e/h;+,-,+,-}$	.	.	.	.	.	.	.	.	.	.	.	.	.	.	.	.	.	.
$A_3^{2,e/h;+,-,-,+}$	.	1	1	.	.	.	.	.	.	.	.	.	.	.	.	.	.	.
$A_3^{2,e/h;+,-,-,-}$	.	1	.	1	.	.	.	.	.	.	.	.	.	.	.	.	.	.
$A_3^{2,e/h;-,+,-,+}$	.	.	.	.	.	.	.	.	.	.	.	.	.	.	.	.	.	.
$A_3^{2,e/h;-,+,-,-}$	.	.	1	1	.	.	.	.	.	.	.	.	.	.	.	.	.	.
$A_3^{2,e/h;-,-,-,-}$	.	.	.	.	.	.	.	.	.	.	.	.	.	.	.	.	.	.
$A_4^{+,+}A_2^1$	$d+1$	.	.	$d+1$	$d$	1	.	.	.	.	.	.	.	$d$	.	.	$d$	$d$
$A_4^{+,+}A_2^0$	$d+1$	.	.	$d+1$	$d$	1	.	.	.	.	.	.	.	$d+1$	.	.	$d+1$	$d+1$
$A_4^{+,-}A_2^1$	.	$d+1$	$d+1$	.	$d$	.	1	.	.	.	.	.	.	.	$d$	$d$	.	$d$
$A_4^{+,-}A_2^0$	.	$d+1$	$d+1$	.	$d$	.	1	.	.	.	.	.	.	$d+1$	$d+1$	.	$d+1$	.
$A_4^{-,+}A_2^1$	.	$d+1$	$d+1$	.	$d$	.	.	1	.	.	.	.	.	.	$d$	$d$	.	$d$
$A_4^{-,+}A_2^0$	.	$d+1$	$d+1$	.	$d$	.	.	1	.	.	.	.	.	$d+1$	$d+1$	.	$d+1$	.
$A_4^{-,-}A_2^1$	$d+1$	.	.	$d+1$	$d$	.	.	1	.	.	.	.	.	$d$	.	.	$d$	$d$
$A_4^{-,-}A_2^0$	$d+1$	.	.	$d+1$	$d$	.	.	1	.	.	.	.	.	$d+1$	.	.	$d+1$	$d+1$
$TA_3^{+,+}A_2$	1	.	.	.	.	.	.	.	.	.	.	.	.	.	.	.	.	.
$TA_3^{+,-}A_2$	.	1	.	.	.	.	.	.	.	.	.	.	.	.	.	.	.	.
$TA_3^{-,+}A_2$	.	.	1	.	.	.	.	.	.	.	.	.	.	.	.	.	.	.
$TA_3^{-,-}A_2$	.	.	.	1	.	.	.	.	.	.	.	.	.	.	.	.	.	.
$A_5^{+,+,\pm}$	$d$	.	.	$d+1$	$d+1$	.	.	.	.	.	.	.	.	.	.	.	.	.
$A_5^{+,-,\pm}$	.	$d$	$d+1$	.	$d+1$	.	.	.	.	.	.	.	.	.	.	.	.	.
$A_5^{-,+\pm}$	.	$d+1$	$d$	.	$d+1$	.	.	.	.	.	.	.	.	.	.	.	.	.
$A_5^{-,-,\pm}$	$d+1$	.	.	$d$	$d+1$	.	.	.	.	.	.	.	.	.	.	.	.	.
$A_4^{+,e/h}$	$d$	.	.	$d$	$d$	$d$	.	$d$	.	.	.	.	.	.	.	.	.	.
$A_4^{-,e/h}$	.	$d$	$d$	.	$d$	.	$d$	$d$	.	.	.	.	.	.	.	.	.	.
$A_3^{+,+,q}$	.	.	.	.	.	.	.	.	.	.	.	.	.	.	.	.	.	.
$A_3^{+,-,q}$	.	.	.	.	.	.	.	.	.	.	.	.	.	.	.	.	.	.
$A_3^{-,+,q}$	.	.	.	.	.	.	.	.	.	.	.	.	.	.	.	.	.	.
$A_3^{-,-,q}$	.	.	.	.	.	.	.	.	.	.	.	.	.	.	.	.	.	.
$D_{4,q}^{\pm,+}$	$d$	.	$d$	.	.	.	.	.	.	.	.	.	.	.	.	.	.	.
$D_{4,q}^{\pm,-}$	.	$d$	.	$d$	.	.	.	.	.	.	.	.	.	.	.	.	.	.
$D_{4,\alpha/c}^{\pm,+}$	$d$	.	$d$	.	.	.	.	.	.	.	.	.	.	.	.	.	.	.
$D_{4,\alpha/c}^{\pm,-}$	.	$d$	.	$d$	.	.	.	.	.	.	.	.	.	.	.	.	.	.
$D_{4,b}^{\pm,+}$	$d$	.	$d$	.	.	.	.	.	.	.	.	.	.	.	.	.	.	.
$D_{4,b}^{\pm,-}$	.	$d$	.	$d$	.	.	.	.	.	.	.	.	.	.	.	.	.	.
$D_5^{+,+}$	$d+1$	$d$	.	.	.	$d$	$d$	.	$d$	.	$d+1$	.	.	.	.	.	.	.
$D_5^{+,-}$	$d$	$d+1$	.	.	.	$d$	.	.	$d$	.	$d$	.	$d+1$	.	.	.	.	.
$D_5^{-,+}$	.	.	$d+1$	$d$	.	$d$	.	.	$d$	$d$	.	$d+1$	.	.	.	.	.	.
$D_5^{-,-}$	.	.	$d$	$d+1$	.	.	$d$	$d$	.	.	$d$	.	$d+1$	.	.	.	.	.
$D_4^{-,+}A_2^+$	$d+1$	.	$d$	.	.	.	.	.	.	.	.	1	.	$d$	.	$d$	.	.
$D_4^{-,-}A_2^+$	.	$d+1$	.	$d$	.	.	.	.	.	.	.	.	1	.	$d$	.	$d$	.
$D_{4,2}^{+,+}A_2^+$	$d+1$	.	$d$	.	.	.	.	.	.	1	.	.	.	$d$	.	$d$	.	.
$D_{4,2}^{+,-}A_2^+$	.	$d+1$	.	$d$	.	.	.	.	.	.	1	.	.	.	$d$	.	$d$	.
$D_{4,1}^{+,+}A_2^+$	$d+1$	.	$d$	.	1	.	.	.	.	1	.	.	.	$d$	.	$d$	.	.
$D_{4,1}^{+,-}A_2^+$	.	$d+1$	.	$d$	1	.	.	.	.	.	1	.	.	.	$d$	.	$d$	.
$D_{4,0}^{+,+}A_2^+$	$d+1$	.	$d$	.	.	.	.	.	.	1	.	.	.	$d$	.	$d$	.	.
$D_{4,0}^{+,-}A_2^+$	.	$d+1$	.	$d$	.	.	.	.	.	.	1	.	.	.	$d$	.	$d$	.
$D_4^{-,+}A_2^-$	$d+1$	.	$d$	.	.	.	.	.	.	.	.	1	.	$d+1$	.	$d+1$	.	.
$D_4^{-,-}A_2^-$	.	$d+1$	.	$d$	.	.	.	.	.	.	.	.	1	.	$d+1$	.	$d+1$	.
$D_{4,2}^{+,+}A_2^-$	$d+1$	.	$d$	.	.	.	.	.	.	1	.	.	.	$d+1$	.	$d+1$	.	.
$D_{4,2}^{+,-}A_2^-$	.	$d+1$	.	$d$	.	.	.	.	.	.	1	.	.	.	$d+1$	.	$d+1$	.
$D_{4,1}^{+,+}A_2^-$	$d+1$	.	$d$	.	1	.	.	.	.	1	.	.	.	$d+1$	.	$d+1$	.	.
$D_{4,1}^{+,-}A_2^-$	.	$d+1$	.	$d$	1	.	.	.	.	.	1	.	.	.	$d+1$	.	$d+1$	.
$D_{4,0}^{+,+}A_2^-$	$d+1$	.	$d$	.	.	.	.	.	.	1	.	.	.	$d+1$	.	$d+1$	.	.
$D_{4,0}^{+,-}A_2^-$	.	$d+1$	.	$d$	.	.	.	.	.	.	1	.	.	.	$d+1$	.	$d+1$	.

Using Table 5, we are able to find new invariants by adding a combination of columns together, provided all  $d$ 's cancel out. We find eight invariants which are listed below as well as their expressions as linear combinations of earlier invariants, up to an additive constant:

- $\deg_2(A_3^{+,+} A_2 \cup A_3^{-,+} A_2 \cup \text{triple points}) = \emptyset;$
- $\deg_2(A_3^{+,+} A_2 \cup A_3^{+,-} A_2 \cup A_3^{-,+} A_2 \cup A_3^{-,-} A_2) = \emptyset;$
- $\deg_2(A_4^{+,+} \cup A_4^{-,-}) = I_{20};$
- $\deg_2(A_4^{+,+} \cup A_4^{+,-} \cup A_4^{-,+} \cup A_4^{-,-}) = t;$
- $\deg_2(D_4^{+,+} \cup D_4^{-,+}) = d_+^+ + c_{++} + I_{20};$
- $\deg_2(D_4^{+,+} \cup D_4^{+,-} \cup D_4^{-,+} \cup D_4^{-,-}) = c_{++} + c_{+-} + d_+^+ + d_-^+ + t;$
- $\deg_2(A_3^{+,+} \cup A_3^{+,-} \cup A_3^{-,+} \cup A_3^{-,-}) = (t + c_{++} + c_{-+})/2 + (t + c_{+-} + c_{--})/2 + c_{++} + c_{+-} + t;$
- $\deg_2(A_3^{+,+} \cup A_3^{-,+} \cup A_2^2 \cup D_4^{+,+} \cup D_4^{+,-}) = (t + c_{++} + c_{-+})/2 + c_{++} + I_{20}.$

Hence the invariant  $\deg_2(A_4^{+,+} \cup A_4^{-,-})$  is an integral geometric interpretation of the discriminantal cycle  $I'_{20}$ . We will now give a detailed proof of this.

**Theorem 7.5.1.** *The mod2 invariant  $\deg_2(A_4^{+,+} \cup A_4^{-,-})$  is dual to the cycle*

$$A_4^{+,+} A_2 + A_4^{-,-} A_2.$$

Recalling the expressions for our earlier invariants, we see that the linear combination in the theorem states that, up to an additive constant,

$$\deg_2(A_4^{+,+} \cup A_4^{-,-}) = I_{20}.$$

**Proof of Theorem 7.5.1.**

To calculate the increments of the sum of *mod2* degrees of  $A_4^{+,+}$  and  $A_4^{-,-}$  points, we will consider all bifurcations from Section 2.3 that contain them. See Figures 11, 12 and 13.

The following bifurcations do not contribute to the invariant since two points of  $A_4^{+,+}$  or  $A_4^{-,-}$  are born with the same *mod2* degrees which implies  $\Delta \deg_2(A_4^{+,+} \cup A_4^{-,-}) = 0 \text{ mod } 2$ :

- $A_4^{+,e/h}$ : an  $A_4^{+,+}$  and  $A_4^{-,-}$  point;
- $A_5^{+,+,+}$ : two  $A_4^{-,-}$  points;
- $A_5^{+,+,-}$ : two  $A_4^{+,+}$  points;
- $A_5^{-,-,+}$ : two  $A_4^{+,+}$  points;
- $A_5^{-,-,-}$ : two  $A_4^{-,-}$  points;
- $D_5^{+,-}$ : an  $A_4^{+,+}$  and  $A_4^{-,-}$  point;
- $D_5^{-,+}$ : an  $A_4^{+,+}$  and  $A_4^{-,-}$  point.

The following two bifurcations contribute increment 1 to the invariant:

- $A_4^{+,+} A_2$ :  $\Delta deg_2(A_4^{+,+}) = 1$  and  $\Delta deg_2(A_4^{-,-}) = 0 \implies \Delta deg_2(A_4^{+,+} + A_4^{-,-}) = 1$ ;
- $A_4^{-,-} A_2$ :  $\Delta deg_2(A_4^{+,+}) = 0$  and  $\Delta deg_2(A_4^{-,-}) = 1 \implies \Delta deg_2(A_4^{+,+} + A_4^{-,-}) = 1$ .

□

## 7.6 Summary of the extra *mod2* invariants

We now summarise our results from this chapter.

Our aim was to construct *mod2* local invariants which are defined path-independently and are not reductions of integer invariants. Papers [10] and [1] suggested to involve (self-)linking numbers of certain framed links in the target. This was our reason to take  $N = \mathbb{R}^3$  as the simplest manifold where such numbers are well-defined. As usual, we have been looking for invariants up to an arbitrary choice of additive constants for connected components of the space of our Lagrangian maps.

The *mod2* reduction of the space  $\mathcal{D}(M, T^*N, N; \mathbb{Z})$  of integer discriminantal cycles is a codimension 5 subspace in its  $\mathbb{Z}_2$  analogue  $\mathcal{D}(M, T^*N, N; \mathbb{Z}_2)$ . Therefore, the ultimate goal was to construct five *mod2* invariants whose derivatives are linearly independent modulo this subspace.

We have managed to construct five invariants of the kind we wanted:  $I_{fe}$ ,  $I_{dc^+}$ ,  $I_{dc^-}$ ,  $I_\lambda$ ,  $deg_2(A_4^{+,+} \cup A_4^{-,-})$ . However, as it may be easily seen from our expressions of their derivatives in terms of the *mod2* basis from Table 4,



their span modulo the above subspace is just 4-dimensional: the  $I_\lambda$  may be excluded without any affect on the span.

Bearing in mind that there is one integer discriminantal cycle,  $I'_{15}$ , still waiting for its realisation as a derivative of an integer path-independent invariant, we have the following statements about the dimensions of the spaces of local invariants.

**Corollary 7.6.1.** *The space of integer local invariants of Lagrangian maps between two oriented 3-manifolds has dimension either 14 or 15.*

**Corollary 7.6.2.** *For  $N = \mathbb{R}^3$ , the space of mod2 local invariants of Lagrangian maps between two oriented 3-manifolds has dimension at least 18 and at most 20.*

It actually does not matter in these corollaries which particular Lagrangian fibration  $E \rightarrow N$  is used in the maps.

**Remark 7.6.3.** *The four mod2 invariants  $I_{fe}$ ,  $I_{dc+}$ ,  $I_{dc-}$  and  $I_\lambda$  do not depend on our  $s$ -decoration of the caustic strata and of the bifurcations. Therefore, they are well-defined in the special setting used by Gallagher. This was briefly mentioned in the introduction to [9], without any details given.*

# Chapter 8

## Non-oriented source or target

Recall that throughout this thesis we have been considering the space  $\mathcal{L}(M, T^*N, N)$  of all Lagrangian maps  $M \looparrowright T^*N \rightarrow N$  between fixed oriented 3-manifolds. In this chapter we obtain similar classification results, both over  $\mathbb{Q}$  and  $\mathbb{Z}_2$ , assuming at least one of the 3-manifolds is either non-oriented or non-orientable. We use the subscript *no* to denote a non-orientable manifold. First we consider the case of a non-oriented source and then a non-oriented target.

Recall from Section 2.5 the notation  $\mathcal{D}(M, T^*N, N; \mathbb{K})$  to be the space of discriminantal cycles in  $\mathcal{L}(M, T^*N, N)$  with coefficients  $\mathbb{K} = \mathbb{Q}, \mathbb{Z}, \mathbb{Z}_2$ . We also recall from Section 3 the notation  $\mathcal{E}(M, T^*N, N; \mathbb{K})$  for the space spanned by all equations in  $\mathcal{L}(M, T^*N, N)$  provided by the 2-parameter bifurcation families.

## 8.1 Non-oriented source

Consider the space of all Lagrangian maps between fixed 3-manifolds, a non-oriented source manifold  $M_{no}$ , and an oriented target manifold  $N$ . In this setting we cannot differentiate between the signs  $\sigma = \pm$ , that is, the local degree  $\pm 1$  of the Lagrangian map. This means elementary codimension 1 strata in  $\mathcal{L}(M, T^*N, N)$  differing only by the sign  $\sigma$  are glued together. For example, gluing together the  $A_5$  strata with opposite  $\sigma$  decorations creates the big stratum  $A_5^{s,\pm,\omega} = A_5^{s,+,\omega} + A_5^{s,-,\omega}$ . We should also note that due to equations 5 and 6 from Section 2.6.1.1 we now have the big stratum  $A_4^{\pm,\pm}A_2 = A_4^{+,+}A_2 + A_4^{+,-}A_2 + A_4^{-,+}A_2 + A_4^{-,-}A_2$ . Here we denote any new big strata by replacing the decoration  $\sigma$  with  $\pm$ . This reduces the number of codimension 1 strata from the oriented source and target case, shown in Table 1 over  $\mathbb{Z}$  and Table 3 over  $\mathbb{Z}_2$ , to 25 over  $\mathbb{Z}$  and 23 over  $\mathbb{Z}_2$  in  $\mathcal{L}(M_{no}, T^*N, N)$ .

**Theorem 8.1.1.** *The space  $\mathcal{D}(M_{no}, T^*N, N; \mathbb{Q})$  has rank 8. It is spanned by the discriminantal cycles*

$$I'_t, \quad I'_{sw_+}, \quad I'_{sw_-}, \quad I'_{c_+}, \quad I'_{c_-}, \quad I'_{d^+}, \quad I'_{d^-}, \quad I'_\chi.$$

Here, the discriminantal cycles are either taken straight from Lemma 2.4.1 or are the sums of its discriminantal cycles only differing in the decoration  $\sigma$ . Therefore, we now omit the decoration  $\sigma$  in the notation of the discriminantal cycles. The signs of the subscripts correspond to the  $s$ -decorations and the

signs of the superscripts denote the type of  $D_4$  points. For example, the third discriminantal cycle shown is  $I'_{sw_-}$  which is the sum of the cycles  $I'_{sw_-,+}$  and  $I'_{sw_-,-}$  from Lemma 2.4.1 and is the derivative of the number of  $s = -$  swallowtails.

Here and for the rest of this chapter we are considering our invariants up to a choice of additive constants of connected components of the space of Lagrangian maps. Hence, passing from discriminantal cycles to invariants we have the following result:

**Corollary 8.1.2.** *The space of rational local invariants of  $\mathcal{L}(M_{no}, T^*N, N)$  is spanned by*

$$I_t, \quad I_{sw_+}, \quad I_{sw_-}, \quad I_{c_+}, \quad I_{c_-}, \quad I_{d^+}, \quad I_{d^-}, \quad I_\chi.$$

**Proof of Theorem 8.1.1.**

Table 6 shows a basis of the space  $\mathcal{E}(M_{no}, T^*N, N; \mathbb{Q})$ . It is obtained by modifying Table 1 in Section 3. Here we glue up the codimension 1 strata differing only by the decoration  $\sigma$  to create the bigger strata. For example, say we are introducing the bigger stratum  $Z = X + Y$ . In each of the cyclic equations, which are the columns of Table 1, the entries of rows  $X$  and  $Y$  are added up and declared the row  $Z$ . We then reduce the system of thus obtained linear equations to a system of linearly independent equations. This is done by moving in the table from the left to the right and omitting every column which is a linear combination of the columns to its left.

The rank of the Table 6 matrix is 17, that is,  $\mathcal{E}(M_{no}, T^*N, N; \mathbb{Q})$  is 17-dimensional. Now, since we have 25 codimension 1 big strata in  $\mathcal{L}(M_{no}, T^*N, N)$ , the space  $\mathcal{D}(M_{no}, T^*N, N; \mathbb{Q})$  must be 8-dimensional, and its basis is shown in Table 7. This concludes our proof of Theorem 8.1.1.

Table 6	13	14	14	14	14	15	18	18	19	20	22	23	23	27	27	28	29
$TA_2^3$	2	.	.	.	.	1	.	.	.	.	.	.	.	.	.	.	.
$A_3^{\pm,\pm}A_2^2$	-2	.	.	.	.	.	.	.	.	.	.	.	.	.	.	.	.
$A_3^{2,e;+,\pm;+,\pm}$	.	1	.	.	.	.	.	.	.	.	.	.	.	.	.	1	.
$A_3^{2,e;+,\pm;-,\pm}$	.	.	1	1	.	.	.	.	.	.	.	.	.	.	.	-1	.
$A_3^{2,e;-,\pm;-,\pm}$	.	.	.	.	1	.	.	.	.	.	.	.	.	.	.	.	.
$A_3^{2,h;+,\pm;-,\pm}$	.	.	1	-1	.	.	1	1	.	.	.	.	.	.	.	2	-1
$A_4^{\pm,\pm}A_2$	.	.	.	.	.	-2	.	.	.	.	.	.	.	2	2	.	.
$TA_3^{+,\pm}A_2$	.	-2	-2	.	.	1	.	-2	.	.	2	.	-2	.	.	.	.
$TA_3^{-,\pm}A_2$	.	.	.	-2	-2	1	.	.	.	.	.	.	2	.	-2	.	.
$A_5^{+,\pm,+}$	.	.	.	.	.	.	-1	.	1	.	.	.	.	.	.	.	.
$A_5^{+,\pm,-}$	.	.	.	.	.	.	.	-1	1	.	.	.	.	.	.	.	.
$A_5^{-,\pm,+}$	.	.	.	.	.	.	.	1	.	.	.	.	.	.	.	.	.
$A_5^{-,\pm,-}$	.	.	.	.	.	.	1	.	.	.	.	.	.	.	.	.	.
$A_4^{\pm,e/h}$	.	.	.	.	.	.	.	-2	.	.	-2	-2	.	.	.	.	.
$A_3^{+,\pm,q}$	.	.	.	.	.	.	.	.	.	1	.	2	.	.	.	.	.
$A_3^{-,\pm,q}$	.	.	.	.	.	.	.	.	-1	.	.	2	.	.	.	.	.
$D_{4,q}^{-,\pm,\pm}$	.	.	.	.	.	.	.	.	.	.	-1	-1	.	.	.	.	.
$D_{4,a/c}^{+,\pm,\pm}$	.	.	.	.	.	.	.	.	.	1	1	1	.	.	.	.	.
$D_{4,b}^{+,\pm,\pm}$	.	.	.	.	.	.	.	.	.	-1	.	.	.	.	.	.	.
$D_5^{+,\pm}$	.	.	.	.	.	.	.	.	.	.	.	2	.	.	.	.	.
$D_5^{-,\pm}$	.	.	.	.	.	.	.	.	.	.	.	.	2	.	.	.	.
$D_4^{-,\pm}A_2$	.	.	.	.	.	.	.	.	.	.	.	.	.	1	-1	-2	.
$D_{4,2}^{+,\pm}A_2$	.	.	.	.	.	.	.	.	.	.	.	.	.	-1	.	.	.
$D_{4,1}^{+,\pm}A_2$	.	.	.	.	.	.	.	.	.	.	.	.	.	.	.	.	2
$D_{4,0}^{+,\pm}A_2$	.	.	.	.	.	.	.	.	.	.	.	.	.	.	1	.	.

Table 7	$t$	$sw_+$	$sw_-$	$c_+$	$c_-$	$d^+$	$d^-$	$\chi$
$TA_2^3$	2	.	.	.	.	.	.	.
$A_3^{\pm,\pm}A_2^2$	2	.	.	.	.	.	.	.
$A_3^{2,e;+,\pm;+,\pm}$	.	.	.	4	.	.	.	.
$A_3^{2,e;+,\pm;-, \pm}$	.	.	.	2	2	.	.	.
$A_3^{2,e;-, \pm;-, \pm}$	.	.	.	.	4	.	.	.
$A_3^{2,h;+,\pm;-, \pm}$	.	.	.	2	-2	.	.	.
$A_4^{\pm,\pm}A_2$	1	.	.	1	1	.	.	.
$TA_3^{+,\pm}A_2$	.	.	.	2	.	.	.	.
$TA_3^{-,\pm}A_2$	.	.	.	.	2	.	.	.
$A_5^{+,\pm,+}$	.	.	2	2	.	.	.	.
$A_5^{+,\pm,-}$	.	2	.	2	.	.	.	.
$A_5^{-,\pm,+}$	.	2	.	.	2	.	.	.
$A_5^{-,\pm,-}$	.	.	2	.	2	.	.	.
$A_4^{\pm,e/h}$	.	1	1	.	.	.	.	.
$A_3^{+,\pm,q}$	.	.	.	.	.	.	.	1
$A_3^{-,\pm,q}$	.	.	.	.	.	.	.	1
$D_{4,q}^{-,\pm,\pm}$	.	.	.	.	.	.	2	1
$D_{4,a/c}^{+,\pm,\pm}$	.	.	.	.	.	2	.	-1
$D_{4,b}^{+,\pm,\pm}$	.	.	.	.	.	2	.	-1
$D_5^{+,\pm}$	.	1	1	-2	.	-1	1	.
$D_5^{-,\pm}$	.	1	1	.	-2	-1	1	.
$D_4^{-,\pm}A_2$	.	.	.	3	-3	.	.	.
$D_{4,2}^{+,\pm}A_2$	2	.	.	1	-1	.	.	.
$D_{4,1}^{+,\pm}A_2$	.	.	.	1	-1	.	.	.
$D_{4,0}^{+,\pm}A_2$	-2	.	.	1	-1	.	.	.

**Corollary 8.1.3.** *For generators of  $\mathcal{D}(M_{no}, T^*N, N; \mathbb{Z})$  one can take*

$$I'_t, \quad I'_{sw_+}, \quad I'_{c_+}, \quad I'_{d^+}, \quad I'_\chi, \quad I'_{(d^++d^-)/2}, \quad I'_{(sw_++sw_-)/2}, \quad I'_{(c_++c_-)/2}.$$

Here, the discriminantal cycles are taken straight from Remark 2.4.2 or are the sums of its cycles.

**Corollary 8.1.4.** *The space of integer local invariants of  $\mathcal{L}(M_{no}, T^*N, N)$  is spanned by*

$$I_t, \quad I_{sw_+}, \quad I_{c_+}, \quad I_{d^+}, \quad I_\chi, \quad I_{(d^++d^-)/2}, \quad I_{(sw_++sw_-)/2}, \quad I_{(c_++c_-)/2}.$$

We now consider the  $\mathbb{Z}_2$  analogue to Theorem 8.1.1.

**Theorem 8.1.5.** *The space  $\mathcal{D}(M_{no}, T^*N, N; \mathbb{Z}_2)$  has rank 10. It is spanned by the discriminantal cycles*

$$I'_t, \quad I'_{sw_+}, \quad I'_{c_+}, \quad I'_{d^+}, \quad I'_\chi, \quad I'_{(d^++d^-)/2}, \quad I'_{(sw_++sw_-)/2}, \quad I'_{(c_++c_-)/2}, \quad I'_{16}, \quad I'_{18}.$$

This time the discriminantal cycles are taken straight from Remark 2.4.3 or are the sums of its discriminantal cycles.

**Proof of Theorem 8.1.5.**

We obtain a basis of the space  $\mathcal{E}(M_{no}, T^*N, N; \mathbb{Z}_2)$  by modifying Table 3 using the same method that was used for the  $\mathbb{Q}$  case. The result is shown in Table 8.



Here,  $\mathcal{E}(M_{no}, T^*N, N; \mathbb{Z}_2)$  is 13-dimensional. Since in  $\mathcal{L}(M_{no}, T^*N, N)$  there are 23 codimension 1 big strata,  $\mathcal{D}(M_{no}, T^*N, N; \mathbb{Z}_2)$  has dimension 10. Its basis is shown in Table 9. This concludes our proof of Theorem 8.1.5.

Table 8	15	16	17	17	18	20	22	23	27	27	28	34	35
$A_2^4$	.	1	.	.	.	.	.	.	.	.	.	.	.
$TA_2^2$	.	.	.	.	.	1	1	.	.	.	.	.	.
$TA_2^3$	1	.	.	.	.	.	.	.	.	.	.	1	.
$A_3^{\pm, \pm} A_2^2$	.	.	1	1	.	.	.	.	.	.	.	.	.
$A_3^{2, e/h; +, \pm; +, \pm}$	.	.	1	.	.	.	.	.	.	.	.	.	1
$A_3^{2, e/h; +, \pm; -, \pm}$	.	.	1	1	1	.	.	.	.	.	1	.	.
$A_3^{2, e/h; -, \pm; -, \pm}$	.	.	.	1	.	.	.	.	.	.	1	.	1
$A_4^{\pm, \pm} A_2$	.	.	.	.	.	.	.	.	.	.	.	.	.
$TA_3^{\pm, \pm} A_2$	.	.	.	.	.	.	.	.	.	.	.	.	.
$A_5^{+, \pm, \pm}$	.	.	.	.	1	.	.	.	.	.	.	.	.
$A_5^{-, \pm, \pm}$	.	.	.	.	1	.	.	.	.	.	.	.	.
$A_4^{\pm, e/h}$	.	.	.	.	.	.	.	.	.	.	.	.	.
$A_3^{+, \pm, q}$	.	.	.	.	.	1	.	.	.	.	.	.	.
$A_3^{-, \pm, q}$	.	.	.	.	.	1	.	.	.	.	.	.	.
$D_{4, q}^{-, \pm, \pm}$	.	.	.	.	.	.	.	1	.	.	.	.	.
$D_{4, a/c}^{+, \pm, \pm}$	.	.	.	.	.	.	1	1	.	.	.	.	.
$D_{4, b}^{+, \pm, \pm}$	.	.	.	.	.	.	1	.	.	.	.	.	.
$D_5^{+, \pm}$	.	.	.	.	.	.	.	.	.	.	.	.	1
$D_5^{-, \pm}$	.	.	.	.	.	.	.	.	.	.	.	.	1
$D_4^{-, \pm} A_2$	.	.	.	.	.	.	.	.	1	1	.	.	.
$D_{4, 2}^{+, \pm} A_2$	.	.	.	.	.	.	.	.	1	.	.	.	.
$D_{4, 1}^{+, \pm} A_2$	.	.	.	.	.	.	.	.	.	.	.	1	.
$D_{4, 0}^{+, \pm} A_2$	.	.	.	.	.	.	.	.	.	1	.	1	.

Table 9	$t$	$sw_+$	$c_+$	$d^+$	$\chi$	$(d^+ + d^-)/2$	$(sw_+ + sw_-)/2$	$(c_+ + c_-)/2$	16	18
$A_2^4$	.	.	.	.	.	.	.	.	.	.
$TA_2^2$	.	.	.	.	.	.	.	.	1	.
$TA_2^3$	.	.	.	.	.	.	.	.	.	.
$A_3^{\pm,\pm}A_2^2$	.	.	.	.	.	.	.	.	.	.
$A_3^{2,e/h;+,\pm;+,\pm}$	.	.	.	.	.	.	.	.	.	1
$A_3^{2,e/h;+,\pm;-\,\pm}$	.	.	.	.	.	.	.	.	.	1
$A_3^{2,e/h;-\,\pm;-\,\pm}$	.	.	.	.	.	.	.	.	.	1
$A_4^{\pm,\pm}A_2$	1	.	1	.	.	.	.	1	.	.
$TA_3^{\pm,\pm}A_2$	.	.	.	.	.	.	.	1	.	.
$A_5^{+,\pm,\pm}$	.	.	.	.	.	.	1	1	.	.
$A_5^{-,\pm,\pm}$	.	.	.	.	.	.	1	1	.	1
$A_4^{\pm,e/h}$	.	1	.	.	.	.	1	.	.	.
$A_3^{+,\pm,q}$	.	.	.	.	1	.	.	.	.	.
$A_3^{-,\pm,q}$	.	.	.	.	1	.	.	.	1	.
$D_{4,q}^{-,\pm,\pm}$	.	.	.	.	1	1	.	.	.	.
$D_{4,a/c}^{+,\pm,\pm}$	.	.	.	.	1	1	.	.	.	.
$D_{4,b}^{+,\pm,\pm}$	.	.	.	.	1	1	.	.	1	.
$D_5^{+,\pm}$	.	1	.	1	.	.	1	1	.	.
$D_5^{-,\pm}$	.	1	.	1	.	.	1	1	.	.
$D_4^{-,\pm}A_2$	.	.	1	.	.	.	.	.	.	.
$D_{4,2}^{+,\pm}A_2$	.	.	1	.	.	.	.	.	.	.
$D_{4,1}^{+,\pm}A_2$	.	.	1	.	.	.	.	.	.	.
$D_{4,0}^{+,\pm}A_2$	.	.	1	.	.	.	.	.	.	.

## 8.2 Non-oriented target

Similarly, we now consider the space of all Lagrangian maps between fixed 3-manifolds, a source manifold  $M$  which is either oriented or non-oriented and a non-oriented target manifold  $N_{no}$ . Here, we are not making any assumptions about the orientability of the source manifold since both options provide the same results when the target manifold is non-oriented.

Like for the non-oriented source case, we cannot differentiate between the signs  $\sigma = \pm$ . Again, this means elementary codimension 1 strata in  $\mathcal{L}(M, T^*N, N)$  differing only by the sign  $\sigma$  are glued together. In addition we cannot use left or right rotations in the target space. Therefore, all swallowtails become of one kind. As well,  $A_5$  transitions with the same  $s$  decoration but opposite writhe decorations are glued up, creating the big stratum  $A_5^{s, \pm, \pm} = A_5^{s, +, +} + A_5^{s, +, -} + A_5^{s, -, +} + A_5^{s, -, -}$ . In order to be consistent with previous notation we replace the glued up decorations with  $\pm$  where necessary. This further reduces the number of codimension 1 strata from the non-oriented source case to 23 both over  $\mathbb{Z}$  and  $\mathbb{Z}_2$  in  $\mathcal{L}(M, T^*N, N_{no})$ .

**Theorem 8.2.1.** *The space  $\mathcal{D}(M, T^*N, N_{no}; \mathbb{Q})$  has rank 7. It is spanned by the discriminantal cycles*

$$I'_t, \quad I'_{sw}, \quad I'_{c+}, \quad I'_{c-}, \quad I'_{d+}, \quad I'_{d-}, \quad I'_\chi.$$

Similar to the non-oriented source case over  $\mathbb{Q}$ , the discriminantal cycles

are either taken straight from Lemma 2.4.1 or are the sums of the Lemma's discriminantal cycles.

**Corollary 8.2.2.** *The space of rational local invariants of  $\mathcal{L}(M, T^*N, N_{no})$  is spanned by*

$$I_t, \quad I_{sw}, \quad I_{c_+}, \quad I_{c_-}, \quad I_{d^+}, \quad I_{d^-}, \quad I_\chi.$$

**Proof of Theorem 8.2.1.**

A basis of the space  $\mathcal{E}(M, T^*N, N_{no}; \mathbb{Q})$  is shown in Table 10. It is obtained from modifying Table 6 like we did for the non-oriented source case over  $\mathbb{Q}$ . However, this time we include the big strata  $A_5^{s, \pm, \pm} = A_5^{s, +, +} + A_5^{s, +, -} + A_5^{s, -, +} + A_5^{s, -, -}$ .

Here  $\mathcal{E}(M, T^*N, N_{no}; \mathbb{Q})$  is 16-dimensional. Since in  $\mathcal{L}(M, T^*N, N_{no})$  we have 23 codimension 1 big strata,  $\mathcal{D}(M, T^*N, N_{no}; \mathbb{Q})$  must be 7-dimensional. Its basis is shown in Table 11. This concludes our proof of Theorem 8.2.1.

Table 10	13	14	14	14	14	15	18	19	20	22	23	23	27	27	28	29
$TA_2^3$	2	.	.	.	.	1	.	.	.	.	.	.	.	.	.	.
$A_3^{\pm, \pm} A_2^2$	-2	.	.	.	.	.	.	.	.	.	.	.	.	.	.	.
$A_3^{2, e; +, \pm; +, \pm}$	.	1	.	.	.	.	.	.	.	.	.	.	.	.	1	.
$A_3^{2, e; +, \pm; -, \pm}$	.	.	1	1	.	.	.	.	.	.	.	.	.	.	-1	.
$A_3^{2, e; -, \pm; -, \pm}$	.	.	.	.	1	.	.	.	.	.	.	.	.	.	.	.
$A_3^{2, h; +, \pm; -, \pm}$	.	.	1	-1	.	.	1	.	.	.	.	.	.	.	2	-1
$A_4^{\pm, \pm} A_2$	.	.	.	.	.	-2	.	.	.	.	.	.	2	2	.	.
$TA_3^{+, \pm} A_2$	.	-2	-2	.	.	1	.	-2	.	.	2	.	-2	.	.	.
$TA_3^{-, \pm} A_2$	.	.	.	-2	-2	1	.	.	.	.	.	2	.	-2	.	.
$A_5^{+, \pm, \pm}$	.	.	.	.	.	.	-1	2	.	.	.	.	.	.	.	.
$A_5^{-, \pm, \pm}$	.	.	.	.	.	.	1	.	.	.	.	.	.	.	.	.
$A_4^{\pm, e/h}$	.	.	.	.	.	.	.	-2	.	.	-2	-2	.	.	.	.
$A_3^{+, \pm, q}$	.	.	.	.	.	.	.	.	1	.	2	.	.	.	.	.
$A_3^{-, \pm, q}$	.	.	.	.	.	.	.	.	-1	.	.	2	.	.	.	.
$D_{4, q}^{-, \pm, \pm}$	.	.	.	.	.	.	.	.	.	.	-1	-1	.	.	.	.
$D_{4, a/c}^{+, \pm, \pm}$	.	.	.	.	.	.	.	.	.	1	1	1	.	.	.	.
$D_{4, b}^{+, \pm, \pm}$	.	.	.	.	.	.	.	.	.	-1	.	.	.	.	.	.
$D_5^{+, \pm}$	.	.	.	.	.	.	.	.	.	.	2	.	.	.	.	.
$D_5^{-, \pm}$	.	.	.	.	.	.	.	.	.	.	.	2	.	.	.	.
$D_4^{-, \pm} A_2$	.	.	.	.	.	.	.	.	.	.	.	.	1	-1	-2	.
$D_{4, 2}^{+, \pm} A_2$	.	.	.	.	.	.	.	.	.	.	.	.	-1	.	.	.
$D_{4, 1}^{+, \pm} A_2$	.	.	.	.	.	.	.	.	.	.	.	.	.	.	.	2
$D_{4, 0}^{+, \pm} A_2$	.	.	.	.	.	.	.	.	.	.	.	.	.	1	.	.

Table 11	$t$	$sw$	$c_+$	$c_-$	$d^+$	$d^-$	$\chi$
$TA_2^3$	2	.	.	.	.	.	.
$A_3^{\pm, \pm} A_2^2$	2	.	.	.	.	.	.
$A_3^{2, e; +, \pm; +, \pm}$	.	.	4	.	.	.	.
$A_3^{2, e; +, \pm; -, \pm}$	.	.	2	2	.	.	.
$A_3^{2, e; -, \pm; -, \pm}$	.	.	.	4	.	.	.
$A_3^{2, h; +, \pm; -, \pm}$	.	.	2	-2	.	.	.
$A_4^{\pm, \pm} A_2$	1	.	1	1	.	.	.
$TA_3^{+, \pm} A_2$	.	.	2	.	.	.	.
$TA_3^{-, \pm} A_2$	.	.	.	2	.	.	.
$A_5^{+, \pm, \pm}$	.	2	2	.	.	.	.
$A_5^{-, \pm, \pm}$	.	2	.	2	.	.	.
$A_4^{\pm, e/h}$	.	2	.	.	.	.	.
$A_3^{+, \pm, q}$	.	.	.	.	.	.	1
$A_3^{-, \pm, q}$	.	.	.	.	.	.	1
$D_{4, q}^{-, \pm, \pm}$	.	.	.	.	.	2	1
$D_{4, a/c}^{+, \pm, \pm}$	.	.	.	.	2	.	-1
$D_{4, b}^{+, \pm, \pm}$	.	.	.	.	2	.	-1
$D_5^{+, \pm}$	.	2	-2	.	-1	1	.
$D_5^{-, \pm}$	.	2	.	-2	-1	1	.
$D_4^{-, \pm} A_2$	.	.	3	-3	.	.	.
$D_{4, 2}^{+, \pm} A_2$	2	.	1	-1	.	.	.
$D_{4, 1}^{+, \pm} A_2$	.	.	1	-1	.	.	.
$D_{4, 0}^{+, \pm} A_2$	-2	.	1	-1	.	.	.

**Corollary 8.2.3.** *For generators of  $\mathcal{D}(M, T^*N, N_{no}; \mathbb{Z})$  one can take*

$$I'_t, \quad I'_{c_+}, \quad I'_{d^+}, \quad I'_\chi, \quad I'_{(d^++d^-)/2}, \quad I'_{sw/2}, \quad I'_{(c_++c_-)/2}.$$

Here, the discriminantal cycles are taken straight from Corollary 8.1.3.

**Corollary 8.2.4.** *The space of integer local invariants of  $\mathcal{L}(M, T^*N, N_{no})$  is spanned by*

$$I_t, \quad I_{c_+}, \quad I_{d^+}, \quad I_\chi, \quad I_{(d^++d^-)/2}, \quad I_{sw/2}, \quad I_{(c_++c_-)/2}.$$

We now consider the  $\mathbb{Z}_2$  analogue of Theorem 8.2.1.

**Theorem 8.2.5.** *The space  $\mathcal{D}(M, T^*N, N_{no}; \mathbb{Z}_2)$  has rank 10. It is spanned by the discriminantal cycles*

$$I'_t, \quad I'_{c_+}, \quad I'_{d^+}, \quad I'_\chi, \quad I'_{(d^++d^-)/2}, \quad I'_{sw/2}, \quad I'_{(c_++c_-)/2}, \quad I'_{16}, \quad I'_{18}$$

and the extra basic discriminantal cycle

$$I'_{21} = A_5^{+,\pm,\pm} + A_5^{-,\pm,\pm}.$$

This time the discriminantal cycles are taken straight from Theorem 8.1.5.

It is possible to give a geometric interpretation of the basic discriminantal cycle  $I'_{21}$  direct from Table 9, that is  $\mathcal{D}(M_{no}, T^*N, N; \mathbb{Z}_2)$ . In our case we know the target manifold  $N_{no}$  is non-oriented and so, we don't know its the orientation. Let's now assume that  $N_{no}$  is not oriented but orientable and fix an orientation, for example the right one. We see from Table 9 that  $I_{sw_+} + I_{(sw_++sw_-)/2} = I_{21}$ . Hence, the invariant  $I_{(sw_--sw_+)/2}$  is an integral geometric interpretation of the basic discriminantal cycle  $I'_{21}$ . We should note if

we change the orientation of the target, the sign  $\pm$  of the swallowtails swap but since we are working *mod*2 it does not change the result.

**Proof of Theorem 8.2.5.**

A basis of the space  $\mathcal{E}(M, T^*N, N_{no}; \mathbb{Z}_2)$  is shown in Table 12 and was obtained by modifying Table 8 by including the big strata  $A_5^{s,\pm,\pm} = A_5^{s,+,+} + A_5^{s,+,-} + A_5^{s,-,+} + A_5^{s,-,-}$ .

Since in  $\mathcal{L}(M, T^*N, N_{no})$  we have 23 codimension 1 big strata the space  $\mathcal{D}(M, T^*N, N_{no}; \mathbb{Z}_2)$  must be 10-dimensional, and its basis is shown in Table 13. This concludes our proof of Theorem 8.2.5.



Table 12	15	16	17	17	18	20	22	23	27	27	28	34	35
$A_2^4$	.	1	.	.	.	.	.	.	.	.	.	.	.
$TA_2^2$	.	.	.	.	.	1	1	.	.	.	.	.	.
$TA_2^3$	1	.	.	.	.	.	.	.	.	.	.	1	.
$A_3^{\pm,\pm}A_2^2$	.	.	1	1	.	.	.	.	.	.	.	.	.
$A_3^{2,e/h;+,\pm;+,\pm}$	.	.	1	.	.	.	.	.	.	.	.	.	1
$A_3^{2,e/h;+,\pm;-\,\pm}$	.	.	1	1	1	.	.	.	.	.	1	.	.
$A_3^{2,e/h;-\,\pm;-\,\pm}$	.	.	.	1	.	.	.	.	.	.	1	.	1
$A_4^{\pm,\pm}A_2$	.	.	.	.	.	.	.	.	.	.	.	.	.
$TA_3^{\pm,\pm}A_2$	.	.	.	.	.	.	.	.	.	.	.	.	.
$A_5^{+,\pm,\pm}$	.	.	.	.	1	.	.	.	.	.	.	.	.
$A_5^{-,\pm,\pm}$	.	.	.	.	1	.	.	.	.	.	.	.	.
$A_4^{\pm,e/h}$	.	.	.	.	.	.	.	.	.	.	.	.	.
$A_3^{+,\pm,q}$	.	.	.	.	.	1	.	.	.	.	.	.	.
$A_3^{-,\pm,q}$	.	.	.	.	.	1	.	.	.	.	.	.	.
$D_{4,q}^{-,\pm,\pm}$	.	.	.	.	.	.	.	1	.	.	.	.	.
$D_{4,a/c}^{+,\pm,\pm}$	.	.	.	.	.	.	1	1	.	.	.	.	.
$D_{4,b}^{+,\pm,\pm}$	.	.	.	.	.	.	1	.	.	.	.	.	.
$D_5^{+,\pm}$	.	.	.	.	.	.	.	.	.	.	.	.	1
$D_5^{-,\pm}$	.	.	.	.	.	.	.	.	.	.	.	.	1
$D_4^{-,\pm}A_2$	.	.	.	.	.	.	.	.	1	1	.	.	.
$D_{4,2}^{+,\pm}A_2$	.	.	.	.	.	.	.	.	1	.	.	.	.
$D_{4,1}^{+,\pm}A_2$	.	.	.	.	.	.	.	.	.	.	.	1	.
$D_{4,0}^{+,\pm}A_2$	.	.	.	.	.	.	.	.	.	1	.	1	.

Table 13	$t$	$c_+$	$d^+$	$\chi$	$(d^+ + d^-)/2$	$sw/2$	$(c_+ + c_-)/2$	16	18	21
$A_2^4$	.	.	.	.	.	.	.	.	.	.
$TA_2^2$	.	.	.	.	.	.	.	1	.	.
$TA_2^3$	.	.	.	.	.	.	.	.	.	.
$A_3^{\pm,\pm}A_2^2$	.	.	.	.	.	.	.	.	.	.
$A_3^{2,e/h;+,\pm;+,\pm}$	.	.	.	.	.	.	.	.	1	.
$A_3^{2,e/h;+,\pm;-, \pm}$	.	.	.	.	.	.	.	.	1	.
$A_3^{2,e/h;-, \pm;-, \pm}$	.	.	.	.	.	.	.	.	1	.
$A_4^{\pm,\pm}A_2$	1	1	.	.	.	.	1	.	.	.
$TA_3^{\pm,\pm}A_2$	.	.	.	.	.	.	1	.	.	.
$A_5^{+,\pm,\pm}$	.	.	.	.	.	1	1	.	.	1
$A_5^{-,\pm,\pm}$	.	.	.	.	.	1	1	.	1	1
$A_4^{\pm,e/h}$	.	.	.	.	.	1	.	.	.	.
$A_3^{+,\pm,q}$	.	.	.	1	.	.	.	.	.	.
$A_3^{-,\pm,q}$	.	.	.	1	.	.	.	1	.	.
$D_{4,q}^{-,\pm,\pm}$	.	.	.	1	1	.	.	.	.	.
$D_{4,a/c}^{+,\pm,\pm}$	.	.	.	1	1	.	.	.	.	.
$D_{4,b}^{+,\pm,\pm}$	.	.	.	1	1	.	.	1	.	.
$D_5^{+,\pm}$	.	.	1	.	.	1	1	.	.	.
$D_5^{-,\pm}$	.	.	1	.	.	1	1	.	.	.
$D_4^{-,\pm}A_2$	.	1	.	.	.	.	.	.	.	.
$D_{4,2}^{+,\pm}A_2$	.	1	.	.	.	.	.	.	.	.
$D_{4,1}^{+,\pm}A_2$	.	1	.	.	.	.	.	.	.	.
$D_{4,0}^{+,\pm}A_2$	.	1	.	.	.	.	.	.	.	.

# List of Figures

1	Singularities of generic caustics in $\mathbb{R}^2$ . . . . .	10
2	Local singularities of the critical value sets. The encircled values $\sigma = \pm$ indicate the local degree $\pm 1$ of a map at the cuspidal edge. The boxed signs are the definitions of the signs of the swallowtail points. . . . .	13
3	Making a framed link from cuspidal edges from [10]. . . . .	15
4	The top row shows $A_2^2$ , $A_2^3$ , $A_3^\sigma$ and $A_3^\sigma A_2$ singularities of generic caustics. The middle row shows the two different types of $A_4^\sigma$ singularities whilst the bottom row depicts $D_4^+$ (purse) and $D_4^-$ (pyramid) singularities. . . . .	18
5	Examples of 1-parameter bifurcations from [9]. . . . .	20
6	A codimension 2 degeneration involving a swallowtail and a smooth $A_2$ sheet from [9]. At the most degenerate moment, the sheet is tangent to the self-intersection line at the swallowtail point. . . . .	21

7	Transversal section of a discriminantal stratum of codimension 2 in $\Omega$ . . . . .	29
8	The $A_2^2$ , $A_2^3$ , $A_3^{s,\sigma}$ and $A_3^{s,\sigma} A_2$ stable singularities of generic caustics. . . . .	35
9	$A_4^{s,\sigma}$ singularities. . . . .	36
10	The $D_4^{\pm,\sigma}$ caustics in $\mathbb{R}^3$ , the purse and pyramid. . . . .	36
11	Positive moves in generic 1-parameter bifurcations of caustics of corank 1 maps. . . . .	40
12	Positive moves in generic 1-parameter families of corank 1 multi-germs of caustics. . . . .	42
13	Positive moves in generic 1-parameter bifurcations of uni-germ caustics near corank 2 points of the maps. . . . .	45
14	Positive moves in generic 1-parameter bifurcations of multi-germ caustics involving corank 2 points of the maps. . . . .	48
15	More positive moves in generic 1-parameter bifurcations of multi-germ caustics involving corank 2 points of the maps. . . . .	49
16	Bifurcation diagram of the families $SA_2$ obtained from interaction of a smooth $A_2$ sheet with a codimension 1 bifurcation $S$ . . . . .	57
17	A $TA_3^{s,\sigma} A_2^{e,1}$ bifurcation interacting with a smooth $A_2$ sheet. . . . .	59
18	An $A_5^{s,\sigma,-}$ bifurcation interacting with a smooth $A_2$ sheet. . . . .	61

19	Bifurcations obtained from interaction of a smooth $A_2$ sheet with $A_5^{s,\sigma,-}$ . . . . .	61
20	Bifurcation diagram of a cubic analogue of the $A_4^{\varepsilon,e}$ bifurcation. . . . .	63
21	Codimension 2 degeneration due to special position of a cuspidal edge with respect to the tangent plane at an edge point. . . . .	65
22	$\Gamma$ and $C$ interacting for various values of $\alpha$ and $\beta$ in the projected $xy$ -plane. . . . .	65
23	Codimension 2 degeneration of a swallowtail interacting with a cuspidal edge. . . . .	68
24	Codimension 2 degenerations of a swallowtail interacting with a smooth sheet and the transversal intersection of two smooth sheets. . . . .	69
25	Discriminants of the families $\frac{1}{7}x^7 + \frac{1}{5}(\lambda_1 \pm w + \alpha v)x^5 + \frac{1}{4}\lambda_2 x^4 + \frac{1}{3}wx^3 + \frac{1}{2}vx^2 + ux, \quad \alpha \in \mathbb{R};$ $s(\frac{1}{6}x^6 + \frac{1}{4}wx^4 + \frac{1}{3}(\pm w^2 + \lambda_1 w + \lambda_2)x^3 + \frac{1}{2}vx^2 + ux);$ $\frac{1}{5}x^5 + \frac{1}{3}vx^3 + \frac{1}{2}(\pm v^2 + \lambda_1 v + \lambda_2 \pm w^2)x^2 + ux.$ . . . . .	72
26	Bifurcations diagrams of the cubic analogues of the quadratic $D_4^\pm$ singularities. . . . .	76
27	Bifurcation diagrams for the sign choices of the coefficient of $\beta$ in (5). . . . .	79
28	The $D_5$ and $D_{4,q}$ strata. . . . .	83

29	The $A_4$ surface in $\mathbb{R}_{\alpha,\beta,\delta,r,t}^5$ . Its edge is the $D_5$ stratum. Projection to $\mathbb{R}_{r,t}^2$ provides the bifurcational strata. . . . .	85
30	The $TA_3A_2$ stratum. . . . .	86
31	The $TD_3A_2$ stratum. . . . .	87
32	The $A_3^q$ and $D_{4,q}^\pm$ strata. . . . .	89
33	$y(3y^2 + 2\alpha y + \psi) = 0$ and $15y^2 + 8\alpha y + 3\psi = 0$ below the $A_3^{*,*,+,-}$ half-branch. . . . .	90
34	$y(3y^2 + 2\alpha y + \psi) = 0$ and $15y^2 + 8\alpha y + 3\psi = 0$ above the $A_3^{*,*,+,-}$ half-branch. . . . .	90
35	$y(3y^2 + 2\alpha y + \psi) = 0$ and $15y^2 + 8\alpha y + 3\psi = 0$ above the $A_3^{*,*,+,+}$ half-branch. . . . .	91
36	$y(3y^2 + 2\alpha y + \psi) = 0$ and $15y^2 + 8\alpha y + 3\psi = 0$ below the $A_3^{*,*,+,+}$ half-branch. . . . .	91
37	$y(3y^2 + 2\alpha y + \psi) = 0$ and $15y^2 + 8\alpha y + 3\psi = 0$ below the $A_3^{*,*,+,-}$ half-branch. . . . .	92
38	$y(3y^2 + 2\alpha y + \psi) = 0$ and $15y^2 + 8\alpha y + 3\psi = 0$ at the $A_3^{*,*,+,-}$ half-branch. . . . .	92
39	$y(3y^2 + 2\alpha y + \psi) = 0$ and $15y^2 + 8\alpha y + 3\psi = 0$ above the $A_3^{*,*,+,-}$ half-branch. . . . .	93
40	$y(3y^2 + 2\alpha y + \psi) = 0$ and $15y^2 + 8\alpha y + 3\psi = 0$ above the $A_3^{*,*,-,-}$ half-branch. . . . .	94
41	$y(3y^2 + 2\alpha y + \psi) = 0$ and $15y^2 + 8\alpha y + 3\psi = 0$ at the $A_3^{*,*,-,-}$ half-branch. . . . .	94

42	$y(3y^2 + 2\alpha y + \psi) = 0$ and $15y^2 + 8\alpha y + 3\psi = 0$ below the $A_3^{*,*, -, -}$ half-branch. . . . .	95
43	The bifurcation diagrams for $SA_2$ where $S = D_{4,q}^\pm$ . . . . .	97
44	Bifurcation diagram of passing a smooth $A_2$ sheet through $D_5^{s,\sigma}$ . . . . .	98
45	Bifurcation diagrams for a cuspidal edge surface interacting with a pyramid. . . . .	101
46	Bifurcations of a cuspidal surface interacting with a purse. . . . .	103
47	Bifurcations of a pair of transversal $A_2$ sheets with a pyramid. . . . .	104
48	Three examples of bifurcations of a pair of transversal sheets with a purse out of up to a possible sixteen. . . . .	106
49	Bifurcations of a pyramid and a smooth $A_2$ sheet of a caustic tangent to the cuspidal edge of the pyramid at the $D_4^-$ point. . . . .	107
50	Bifurcations of a purse and a smooth $A_2$ sheet of a caustic tangent to the cuspidal edge of the purse at the $D_4^+$ point. . . . .	108
51	Bifurcation diagrams of an $A_2$ sheet of a caustic tangent to a self-intersection ray of a purse at its $D_4^+$ point. . . . .	109
52	The part of $\mathcal{B}_s(D_6^+)$ coming from the 1-dimensional strata of $\mathcal{C}(D_6^+)$ . . . . .	127
53	Projection of the $A_2^3$ stratum of $\mathcal{C}(D_6^+) \subset \mathbb{R}_{\alpha,\beta,\gamma,\delta,\varepsilon}^5$ to the $\alpha\gamma\varepsilon$ -space. The image of the $A_2^3$ consists of the regions of the planes $\varepsilon = \pm\gamma$ between the $D_4A_2$ line $\gamma = 0$ and the $A_4A_2$ curves $\gamma = -\frac{4}{27}u^3$ . . . . .	131

54	The bifurcation diagram coming from the tilted projection of the stratum $A_2^3$ for $(C, E) = (2, 1)$ . The $D_4A_2$ and $A_4A_2$ strata here split those in Figure 52. . . . .	132
55	The bifurcation diagram coming from the tilted projection of $A_2^3$ for $(C, E) = (0, 1)$ . . . . .	133
56	The bifurcation diagram coming from the tilted projection of the stratum $A_2^3$ for $(C, E) = (-2, -1)$ . . . . .	133
57	$D_4A_2$ orientation in $\mathbb{R}_{\alpha, B}^2$ . . . . .	134
58	The strata on the surface $S' \subset \mathbb{R}_{u, w, \varepsilon}^3$ parametrising the strata in the closure of the stratum $A_3A_2$ in $\mathcal{B}_t(D_6^+)$ when $C = 2$ and $E = 1$ . . . . .	137
59	Part of the bifurcation diagram $\mathcal{B}_t(D_6^+)$ when $C = 2$ and $E = 1$ . Positions of the $A_4A_2$ and $D_4A_2$ curves follow Figure 54. . . . .	140
60	The surface $S'$ for $C = 1$ and $E = 2$ . . . . .	141
61	The bifurcation diagram $\mathcal{B}_t(D_6^+)$ when $C = 1$ and $E = 2$ , with the contribution from Figure 55. . . . .	142
62	The surface $S'$ for $C = -2$ and $E = -1$ . . . . .	143
63	The bifurcation diagram $\mathcal{B}_t(D_6^+)$ when $C = -2$ and $E = -1$ , with the contribution from Figure 56. . . . .	144
64	The part of $\mathcal{B}_s(D_6^-)$ coming from the 1-dimensional strata of $\mathcal{C}(D_6^-)$ . . . . .	148



65	The part of $\mathcal{B}_s(D_6^-)$ coming from the 1-dimensional strata of $\mathcal{C}(D_6^-)$ and $A_4$ . . . . .	151
66	The strata on the surface $V \subset \mathbb{R}_{u,v,\varepsilon}^3$ parametrising the strata in the closure of the stratum $A_4$ in $\mathcal{C}(D_6^-)$ . . . . .	152
67	The bifurcation diagram $\mathcal{B}_s(D_6^-)$ for the surface $V$ . . . . .	154
68	The surface $S_1$ over the $uv$ -plane. . . . .	156
69	The bifurcation diagram $\mathcal{B}_s(D_6^-)$ for the surface $S_1$ . . . . .	157
70	The surface $S_2$ over the $vw$ -plane. The $A_3$ decorations of the $A_3A_2$ points from the blue half of the surface are $(-, \sigma)$ , and from the red are $(+, \sigma)$ . . . . .	158
71	The bifurcation diagram $\mathcal{B}_s(D_6^-)$ for the surface $S_2$ . . . . .	159
72	Strata of $\mathcal{C}(D_6^-)$ that occur on the $uv$ -plane parametrising $D_3A_2$ . . . . .	160
73	The bifurcation diagram $\mathcal{B}_s(D_6^-)$ . . . . .	160
74	The complete bifurcation diagram $\mathcal{B}_s(D_6^-)$ . . . . .	161
75	The function family $G$ parametrising the stratum $A_3 \subset \mathcal{C}(E_6^+)$ . . . . .	166
76	The function family $G$ parametrising the stratum $A_2^3 \subset \mathcal{C}(E_6^+)$ . . . . .	170
77	Two views of the $\mathbb{R}_{u,v,w}^3$ parametrising the stratum $A_3 \subset \mathcal{C}(E_6^+)$ . The 2-dimensional strata are: $D_4 = \{u = 0\}$ , $A_4 = \{u = w^2\}$ and $A_3A_2$ from (17). . . . .	172
78	The strata of $\mathcal{B}_0(E_6^+)$ coming from the 1-dimensional strata of $\mathcal{C}(E_6^+)$ . . . . .	175

79	The folding of the $vw$ -plane by $\pi_3 \circ p_{A_4}$ when $d > 0$ , producing part of $\mathcal{B}_3(E_6^+)$ on the right. . . . .	179
80	Two function families parametrising the stratum $D_4 \subset \mathcal{C}(E_6^+)$ . . . . .	180
81	Mapping $\mathbb{R}_{v,w}^2$ to $\mathbb{R}_{s,t}^2$ for $d > 0$ . The shaded regions represent $D_4^{-,\sigma}$ points and the non-shaded regions $D_4^{+,\sigma}$ . . . . .	182
82	The part of $\mathcal{B}_1(E_6^+)$ coming from the closure of the stratum $D_4 \subset \mathcal{C}(E_6^+)$ . . . . .	182
83	The $\mathbb{R}_{u,v,w}^3$ parametrising the stratum $A_3 \subset \mathcal{C}(E_6^+)$ with the emerging $TA_3A_2$ strata denoted by grey circles for $d > 0$ . The grey circles will be reflected in the $v = 0$ plane for $d < 0$ . . . . .	184
84	The stratum $A_3^2 \subset \mathcal{B}_3(E_6^+)$ . . . . .	185
85	The image of the projection of the stratum $A_2^3 \subset \mathcal{C}(E_6^+)$ to $\mathbb{R}_{\alpha,\beta,\delta}^3$ . The black discs mark the $A_4A_2$ half-branches in $\mathcal{C}(E_6^+)$ . Here we are not concerned about their decorations since the $A_4A_2$ strata have already been considered in Section 6.1.2. These $A_4A_2$ strata bound the regions of triple points. . . . .	187
86	The result of the introduction of an extra parameter $\varepsilon$ , in the $\alpha \geq 0$ part of Figure 85. . . . .	188
87	Making a framed link from the cuspidal edges. Here the decorations correspond to $\sigma$ only. . . . .	193
88	Framed link at $D_4^{\pm,\sigma}$ . . . . .	193
89	A-move. . . . .	195

90	The A-move with external arcs 14 and 23. . . . .	196
91	Closing the external arcs 14 and 23. . . . .	196
92	The A-move with external arcs 12 and 34. . . . .	197
93	The A-move with external arcs 13 and 24. . . . .	197
94	The six ends move. . . . .	198
95	Decomposition of the six ends move. . . . .	199
96	The eight ends move. . . . .	199
97	Decomposition of the eight ends move. . . . .	200
98	Framing of $A_3^{s,+}$ . . . . .	203
99	Framing of $A_2^2$ . . . . .	204
100	$L_+$ at $A_3^{s,+}A_2$ points. . . . .	204
101	$L_+$ at $A_4^{s,+}$ . . . . .	205
102	Resolution of a triple point $A_2^3$ . . . . .	206
103	Smoothing of a $D_4^-$ point. . . . .	207
104	$L_+$ at $D_4^{-,+}$ . . . . .	207
105	$L_+$ at $D_4^{+,+}$ . . . . .	207
106	Framing along $A_3^{s,-}$ . . . . .	225
107	Framing of $A_2^2$ . . . . .	226
108	$L_-$ at $A_3^{s,-}A_2$ points. . . . .	226
109	$L_-$ at a swallowtail $A_4^{s,+}$ . . . . .	227
110	The <i>mod</i> 2 degree of an $A_3A_2$ point. . . . .	248
111	The <i>mod</i> 2 degree of a swallowtail point. . . . .	249
112	The <i>mod</i> 2 degree of a $D_4^{+,\sigma}$ point. . . . .	249

113	The <i>mod</i> 2 degree of a $D_4^{-,\sigma}$ point. . . . .	249
114	The <i>mod</i> 2 degree of a triple point. . . . .	250

# Bibliography

- [1] F. Aicardi, ‘On Mod2 Local Invariants of Maps Between 3-Manifolds’, ResearchGate publication 259189520, 1–8.
- [2] S. Alsaeed, *Local invariants of fronts in 3-manifolds*, Ph. D. Thesis, University of Liverpool, 2014.
- [3] V. I. Arnold, S. M. Gusein-Zade and A. N. Varchenko, *Singularities of differentiable maps. Vol. I. The classification of critical points, caustics and wave fronts*, Monographs in Mathematics **82**, Birkhäuser Boston, Boston, MA, 1985, xi+382 pp.
- [4] V. I. Arnold, *Singularities of caustics and wave fronts*, Mathematics and its Applications (Soviet Series) **62**, Kluwer, Dordrecht, 1990, xiv+259 pp.
- [5] V. I. Arnold, ‘Plane curves, their invariants, perestroikas and classifications’. With an appendix by F. Aicardi, *Advances in Soviet Mathematics* **21**, Singularities and bifurcations, American Mathematical Society, Providence, RI, 1994, 33–91.

- [6] V. I. Arnold, *Topological invariants of plane curves and caustics*, University Lecture Series **5**, American Mathematical Society, Providence, RI, 1994, viii+60 pp.
- [7] V. I. Arnold, ‘Invarianty i perestroiki ploskih frontov’, Osobennosti gladkikh otobrazheniy s dopolnitel’nyimi strukturami, *Trudy Mat. Inst. Steklov.* **209** (1995) 14–64. English translation: ‘Invariants and perestroikas of wave fronts on the plane’, Singularities of smooth mappings with additional structures, *Proc. Steklov Inst. Math.* **209** (1995) 11–56.
- [8] S. Chmutov, S. Duzhin and J. Mostovoy, *Introduction to Vassiliev Knot Invariants*, Cambridge University Press, Cambridge, 2012, xvi+504 pp.
- [9] K. Gallagher, *Invariants of Lagrangian Mappings*, Ph. D. Thesis, University of Liverpool, 2016.
- [10] V. Goryunov, ‘Local invariants of maps between 3-manifolds’. *Journal of Topology* **6**, London Mathematical Society, (2013), 757–776.
- [11] V. Goryunov and S. Alsaeed, ‘Local invariants of framed fronts in 3-manifolds’, *Arnold Mathematical Journal*, **1** (2015), no. 3, 211–232.
- [12] V. Goryunov, and K. Gallagher, ‘On Planar Caustics’, *Journal of Knot Theory and Ramifications* **25** (2016), no. 12, 1642004, 1–24.
- [13] V. Goryunov, ‘Local invariants of mappings of surfaces into three-space’, *The Arnold-Gelfand mathematical seminars. Geometry and singularity*

- theory* (eds V. I. Arnold, I. M. Gelfand, V. S. Retakh and M. Smirnov), Birkhäuser Boston, Boston, MA, 1997, 223–255.
- [14] V. Goryunov, ‘Vassiliev type invariants in Arnold’s  $J^+$ -theory of plane curves without direct self-tangencies’, *Topology* **37** (1998), no. 3, 603–620.
- [15] A. B. Merkov, ‘On the classification of ornaments’, Singularities and bifurcations, *Advances in Soviet Mathematics* **21**, Amer. Math. Soc., Providence, RI, 1994, 199–211.
- [16] T. Ohmoto and F. Aicardi, ‘First order local invariants of apparent contours’, *Topology* **45** (2006) no. 1, 27–45.
- [17] V. V. Prasolov and A. B. Sossinsky, *Knots, Links, Braids and 3-Manifolds: An Introduction to the New Invariants in Low-dimensional Topology*, Translations of Mathematical Monographs **154**, American Mathematical Society, Providence, RI, 1997, viii+239 pp.
- [18] V. A. Vassiliev, ‘Cohomology of knot spaces’, Theory of singularities and its applications, *Advances in Soviet Mathematics* **1**, American Mathematical Society, Providence, RI, 1994, 225–262.
- [19] V. A. Vassiliev, ‘Invariants of ornaments’, Singularities and bifurcations, *Advances in Soviet Mathematics* **21**, Amer. Math. Soc., Providence, RI, 1994, 225–262.
- [20] H. Whitney, ‘On regular closed curves in the plane’, *Compositio Math.* **4** (1936), 276–284.

- [21] M. Yamamoto, ‘First order semi-local invariants of stable maps of 3-manifolds into the plane’, Proc. London Math. Soc. (3) **92** (2006) 471–504.
- [22] V. M. Zakalyukin, ‘Reconstructions of fronts and caustics depending on a parameter, and versality of mappings’. *Current problems in mathematics*, vol. 22, 56–93, Itogi Nauki i Tekhniki, Akad. Nauk SSSR, VINITI, Moscow, 1983 (Russian). English translation: *Journal of Soviet Mathematics* **27** (1984) no.3, 2713–2735.